Interaction of radioelements (Ra, U) with diatoms

Yihua He

COLLEGE DOCTORAL PAYS DE LA LOIRE
ED MATIERE,MOLECULES MATERIAUX ET GEOSCIENCES

IMT Atlantique
Bretagne-Pays de la Loire
École Mines-Télécom

THÈSE DE DOCTORAT

DE
Ecole Nationale Supérieure Mines-Télécom Atlantique

Bretagne Pays de la Loire - IMT Atlantique

ECOLEDOCTORALEN°596

Matière,Molécules,Matériaux et Géosciences

Spécialité :Chimie Analytique et Radiochimie

Par
Yihua HE

Interaction des radioéléments (U, Ra) avec les diatomées

Thèse présentée et soutenue à SUBATECH, Nantes, le 19 Décembre 2023
Unité de recherche : SUBATECH – UMR 6457
Numéro National de Thèse (NNT) : 2023IMTA0376

Rapporteurs avant soutenance :

Dr. Mirella DEL NERO	Chargée de recherche, Institut Pluridisciplinaire Hubert Curien
Pr. Mohamed Larbi MERROUN	Professeur, Université de Granada

Composition du Jury :

Président :	Pr. Abdesselam ABDELOUAS	Professeur, IMT Atlantique
Examinateurs :	Pr. Olivier CLARISSE	Professeur, Université de Moncton
	Pr. Dominic LARIVIERE	Professeur, Université Laval
	Dr. Mirella DEL NERO	Chargée de recherche, IPHC
	Pr. Mohamed Larbi MERROUN	Professeur, Université de Granada
Dir. de thèse :	Dr. Gilles MONTAVON	Directeur de recherche, SUBATECH
Encadrant de thèse :	Dr. Olivier PERON	Maître de conférence, SUBATECH
Co-encadrant de thèse :	Dr. Susanne SACHS	Docteur en chimie, HZDR

Invité(s)
Pr. Benoît SCHOEFS Professeur, Le Mans Université

Résumé du manuscrit « Interaction des radioéléments (U, Ra) avec les diatomées »

Par HE Yihua

Thèse présentée et soutenue à Nantes, le 19 Décembre 2023

Unité de recherche : SUBATECH – UMR 6457

Les diatomées sont un type de microalgues unicellulaires appartenant au groupe des Bacillariophyta. Elles comptent parmi les organismes les plus abondants et les plus divers (environ 2000 espèces existantes (Guiry, 2012)) sur Terre et peuvent être trouvées dans divers environnements aquatiques, notamment les océans, les lacs, les rivières et même les surfaces humides. Les diatomées sont des producteurs primaires et contribuent de manière significative à la production annuelle d'oxygène. Ces micro-organismes jouent également un rôle essentiel dans les cycles biogéochimiques mondiaux, tels que le cycle du carbone (C), le cycle de la silice et le cycle de l'urée. En outre, les diatomées sont cruciales pour les écosystèmes de la Terre et ont une importance écologique et géologique considérable. Ces dernières années, les diatomées ont fait l'objet de recherches dans divers domaines scientifiques (Lopez et al., 2005). En écologie, par exemple, elles sont souvent considérées comme des bioindicateurs pour évaluer la qualité de l'eau et la santé environnementale en raison de leur sensibilité aux changements dans leur environnement, tels que la disponibilité des nutriments, le pH, la température et le stress métallique (Necchi Jr, 2016).

Les bactéries sont souvent les voisines des diatomées dans leur milieu de vie, et certaines d'entre elles peuvent même se trouver à la surface des diatomées. Les relations entre les diatomées et les bactéries sont complexes et font l'objet d'une attention croissante dans la recherche écologique. L'interaction entre les diatomées (ou les algues en général) et les bactéries implique divers mécanismes tels que l'échange de nutriments, la transduction de signaux et le transfert de gènes (Kouzuma et Watanabe, 2015). Parmi les nombreuses interactions entre les diatomées et les bactéries, la relation mutuellement bénéfique, également appelée interaction synergique, a fait l'objet de diverses études dans la littérature (Amin et al., 2012 ; Seymour et al., 2017). On pense que les diatomées libèrent des exsudats et des substances polymériques extracellulaires (EPS) qui peuvent servir de source d'énergie et de carbone pour les bactéries vivant en symbiose. À leur tour,

les bactéries peuvent reminéraliser ces composés organiques, en les décomposant en formes inorganiques qui peuvent être facilement absorbées par les diatomées. Les bactéries peuvent également produire de l'EPS qui facilite l'agrégation des cellules des diatomées et entraîne la formation de biofilms. Il est donc important de prendre en compte à la fois les diatomées et les bactéries associées vivant en symbiose dans ce travail afin de se rapprocher le plus possible des conditions *in natura*.

La structure de la communauté microbienne est d'une importance vitale dans les études écologiques puisqu'elle peut indiquer la santé écologique des environnements aquatiques. Diverses études soulignent les changements de la structure de la communauté microbienne causés par la pollution aux pesticides, aux métaux lourds ou au drainage minier acide (AMD) (Méndez-García et al., 2015 ; Muturi et al., 2017 ; Yin et al., 2015). En général, la diversité et l'abondance de la communauté microbienne sont affectées négativement par les facteurs mentionnés ci-dessus. Il est également démontré que certaines espèces de diatomées ou de bactéries sensibles seront progressivement remplacées par des espèces plus résistantes qui tolèrent les métaux lourds ou le stress dû à l'acidité, par exemple.

Au cours des dernières décennies, plusieurs chercheurs se sont intéressés à l'impact écologique des activités minières humaines (Salomons, 1995). En fait, les activités minières peuvent entraîner des perturbations significatives du sol et de l'environnement aquatique. L'un des impacts écologiques les plus préoccupants des activités minières est l'AMD. Il se produit lorsque des minéraux sulfurés tels que la pyrite (FeS_2), présents dans les roches extraites ou les résidus, entrent en contact avec l'air et l'eau en raison des activités minières. L'oxydation des sulfures conduit à la formation d'acide sulfurique dans l'eau, ce qui abaisse le pH des milieux environnants et entraîne plusieurs conséquences. L'un des problèmes les plus préoccupants est l'effet de lixiviation des métaux, où certains métaux lourds, tels que le cuivre (Cu), le zinc (Zn), le plomb (Pb), le cadmium (Cd), etc.

Dans le cas des activités d'extraction de l'uranium (U), l'AMD augmentera la mobilité de U puisque U se trouve généralement dans l'état d'oxydation hexavalent (+6) (sous la forme de l'ion uranyle(VI), UO_2^{2+}) dans des conditions acides et oxydantes et qu'il devient plus mobile dans

l'environnement. Par conséquent, l'AMD peut faciliter le transport et la migration de U dans le sol et l'eau. L'acidité et la présence de U ou d'autres métaux lourds peuvent dégrader considérablement les écosystèmes terrestres et aquatiques et réduire la biodiversité. En raison de la radioactivité, certaines matières radioactives naturelles (NORM), dont U, ont un impact radiologique supplémentaire sur l'écosystème. Elles soulèvent davantage de préoccupations écologiques, en particulier lorsque les NORM pénètrent dans la chaîne alimentaire.

Pour évaluer l'impact écologique des activités minières de U sur les micro-organismes vivants, plusieurs chercheurs se concentrent sur les diatomées ou les bactéries en tant que bioindicateurs et analysent la structure de leur communauté autour de certaines régions touchées par l'exploitation minière de U (Herlory et al., 2013 ; Sutcliffe et al., 2017). Il existe plusieurs études qui examinent spécifiquement les interactions des bactéries U dans un contexte environnemental plus général, c'est-à-dire dans des eaux enrichies en U ou des sols contaminés (Tableau I-1 du chapitre 1). Pour cela, différentes techniques microscopiques et spectroscopiques ont été employées pour élucider les mécanismes d'interaction et étudier la spéciation de U au niveau moléculaire.

Bien que la recherche axée sur l'interaction entre les radionucléides et les organismes vivants (tels que les cellules végétales, les algues et les bactéries en monoculture) ait prospéré au cours des dernières décennies, les mécanismes sous-jacents restent relativement peu clairs, en particulier dans un système plus complexe et plus réaliste, par exemple un système symbiotique diatomées-bactéries. Pour mieux comprendre les effets potentiels des radionucléides sur la communauté microbienne, il est nécessaire d'approfondir les interactions potentielles. D'importantes lacunes persistent dans les connaissances, qui empêchent une évaluation complète et précise de l'impact écologique des radionucléides sur les micro-organismes vivants.

Dans ce contexte, plusieurs projets de recherche ont été lancés en France dans le cadre de la ZATU (la Zone Atelier Territoires Uranifères), qui est devenue membre du réseau français des Zones Ateliers (ZA) depuis 2015 et a été reconduite comme l'un des observatoires de recherche socio-écologique à long terme (LTSER) par l'Institut de l'Écologie et de l'Environnement du CNRS (Centre National de la Recherche Scientifique). Parmi tous les projets de recherche menés

dans le cadre de la ZATU, les sources minérales radioactives font l'objet d'une attention particulière car elles représentent des écosystèmes insulaires dans lesquels les rayonnements ionisants exercent une influence sur la diversité et la composition des communautés microbiennes. Lancé en 2019, le projet TIRAMISU (biodiversiTy In RAdioactive MIneral Springs of the Auvergne region) vise à élucider les interactions complexes entre les radionucléides et les microorganismes qui vivent dans ces sources minérales naturellement radioactives.

Le projet TIRAMISU est le fruit d'une collaboration entre biologistes, écologistes, physiciens et radiochimistes, qui poursuivent collectivement quatre objectifs principaux :

1. Identification et caractérisation radiologique des sources radioactives naturelles.
2. Analyse des communautés microbiennes en termes de diversité et de structure.
3. Étude de l'interaction entre les radionucléides et les micro-organismes.
4. Mise en œuvre d'une analyse multiparamétrique basée sur les données observées et la modélisation des doses de rayonnement reçues par les organismes habitant des compartiments distincts à proximité des sources (c'est-à-dire l'eau, les sédiments et les interfaces).

Avec le soutien de la boîte à outils de simulation Monte Carlo GATE (GEANT4 Application for Tomographic Emission), le projet TIRAMISU vise à intégrer des données biologiques, chimiques et radiologiques pour évaluer les doses reçues et prédire les dommages causés par la radioactivité à l'acide désoxyribonucléique (ADN) des diatomées et des bactéries vivant dans les sources minérales étudiées. Pour augmenter la précision de la simulation, il est donc crucial d'étudier la localisation des radionucléides tels que U au niveau cellulaire, c'est-à-dire d'étudier l'adsorption en surface et le comportement d'incorporation intracellulaire. Il est également nécessaire d'obtenir des paramètres chimiques relatifs tels que le coefficient de distribution K_d.

Contribuant à ce projet structurel, les principaux objectifs de ce travail sont les suivants :

1. Caractérisation de la bio-association U, Ra dans un système symbiotique

diatomées-bactéries en distinguant l'adsorption et l'incorporation : étude de la cinétique d'adsorption, détermination du coefficient de distribution et étude du comportement de rétention en fonction du temps (en fonction des phases de croissance).

2. Localisation de U au niveau de la cellule à l'aide de diverses techniques microscopiques.
3. Étude de la spéciation de U à l'aide de différentes techniques spectroscopiques.
4. Étude de la contribution potentielle des bactéries aux interactions globales entre les diatomées et les radionucléides étudiés.

Le chapitre 1 présente un état des lieux général sur un large éventail de sujets, allant des généralités sur les diatomées et les bactéries (partie I) aux interactions des métaux lourds (y compris U et Ra) avec les diatomées et les bactéries (partie II). Dans la première partie, deux groupes microbiens omniprésents dans la nature, à savoir les diatomées et les bactéries, sont présentés en détail. On les trouve dans un large éventail d'écosystèmes différents sur Terre et ils jouent un rôle extrêmement important. Divers aspects des diatomées et des bactéries sont élucidés, tels que la taxonomie, la morphologie, le cycle de vie, la reproduction et les différents rôles qu'elles jouent dans les écosystèmes. À ce jour, leur évolution s'est avérée extrêmement fructueuse sur Terre. En outre, les mécanismes d'interaction entre ces deux groupes de micro-organismes sont examinés. Il est démontré que les relations entre les diatomées et les bactéries sont complexes et diverses, par exemple des relations mutuellement bénéfiques ou compétitives. Leurs interactions complexes sont à l'origine de la diversité des écosystèmes naturels. À la fin de la première partie, l'importance écologique des diatomées et des bactéries est mentionnée. En effet, elles jouent un rôle important dans l'évaluation de la santé des écosystèmes et de nombreuses études les ont considérées comme des bioindicateurs pour étudier l'impact écologique des pollutions (métaux lourds, pesticides, effluents industriels, etc.) sur les écosystèmes. Outre la surveillance des changements dans l'état des écosystèmes, les diatomées et les bactéries (et plus généralement les micro-organismes) peuvent également être utilisées pour la bioremédiation. L'utilisation de micro-organismes dans la biorestauration s'est avérée être une approche efficace, respectueuse de l'environnement et rentable. La capacité des diatomées et des bactéries à adsorber efficacement les métaux lourds a conduit à leur utilisation généralisée dans le post-traitement des eaux usées industrielles ou la décontamination des sites contaminés par les métaux lourds.

Dans la partie II, divers sujets pertinents sont abordés autour de deux radioéléments, U et Ra, tels que leurs propriétés physico-chimiques, l'histoire de leur découverte, leur transport dans l'environnement, leur biotoxicité et leur impact sur l'écosystème. Il est mentionné que les micro-organismes jouent un rôle très important dans le transport de U et Ra dans l'environnement. Afin de mieux comprendre les mécanismes sous-jacents, les interactions entre les métaux lourds et deux groupes importants de micro-organismes, les bactéries et les diatomées, sont détaillées dans un contexte plus général. Pour ce faire, la partie II présente tout d'abord la structure cellulaire de ces deux groupes de micro-organismes (principalement la structure de la paroi cellulaire), puis explique les mécanismes d'échange de substances des cellules microbiennes avec l'environnement externe et énumère à la fin toutes les interactions possibles avec les métaux lourds. Il est démontré que ces deux groupes microbiens jouent un rôle extrêmement important dans la mobilité et la spéciation des métaux lourds dans la nature. En fait, les micro-organismes sont capables de modifier le comportement des métaux lourds dans l'environnement de plusieurs manières, notamment par des processus biologiques d'oxydoréduction, de bioprécipitation, de biosorption, de bioaccumulation, etc. Leur grande capacité d'élimination des métaux lourds, leur excellent rapport coût-efficacité et leurs faibles coûts d'entretien ont conduit à l'application généralisée des micro-organismes pour la biorestauration. Enfin, ce chapitre se termine par quelques recherches connexes sur U et Ra. Le mécanisme d'interaction U-bactérie a été largement discuté et élucidé dans la littérature. Cependant, la littérature manque d'études sur l'interaction Ra-bactérie, et encore moins d'études sur l'interaction des diatomées avec U ou Ra. Il reste encore un certain nombre de lacunes à combler dans notre compréhension des mécanismes sous-jacents. C'est pourquoi ce travail vise à étudier l'interaction de U et de Ra avec la culture de diatomées sous différents angles afin d'en approfondir la compréhension.

Dans le chapitre 2, la stratégie appliquée pour étudier l'interaction entre U, Ra avec une culture xénique de diatomées *Achnanthidium saprophilum* (*A. saprophilum*) est présentée. D'une part, la culture et la caractérisation des diatomées *A. saprophilum* ont été effectuées dans ce travail, suivies d'une étude sur la diversité de la communauté bactérienne présente dans la culture de diatomées xéniques basée sur des analyses de séquences. En outre, des efforts ont été faits pour

isoler des souches bactériennes de la culture de diatomées *A. saprophilum* et pour cultiver les isolats obtenus en vue d'études de spéciation plus approfondies. D'autre part, des expériences de bio-association U/Ra de type batch ont été menées pour caractériser l'interaction U/Ra-diatomées à l'échelle macroscopique, ce qui a permis d'obtenir un large éventail d'informations, y compris l'adsorption de surface et le comportement d'accumulation intracellulaire, la cinétique d'adsorption, la constante de distribution, etc. Entre-temps, diverses techniques analytiques ont été utilisées dans ce travail pour caractériser l'interaction entre les diatomées U et les bactéries d'un point de vue cellulaire et moléculaire. Par exemple, des analyses MEB, MET et EDX ont été réalisées pour révéler la localisation de U au niveau cellulaire, tandis que FTIR et TRLFS ont été appliqués pour étudier la spéciation de U.

Dans le chapitre 3, la culture de diatomées étudiée dans ce travail est caractérisée sous différents angles. L'étude taxonomique a indiqué que la culture de diatomées est purement constituée de l'espèce *A. saprophilum*, ce qui montre que le processus d'isolement et de purification des diatomées a été très efficace. Les analyses de séquences ciblant les gènes 16S rRNA ont confirmé la propriété xénique de la culture de diatomées et ont révélé la présence d'une communauté bactérienne avec une diversité relativement faible. Les genres bactériens prédominants dans la culture de diatomées étaient *Pseudomonas*, *Acidovorax* et *Brevundimonas*. En outre, des efforts ont été déployés dans le cadre de ce travail afin d'isoler les bactéries de la culture en vue d'études plus approfondies.

L'utilisation de différentes techniques microscopiques a permis d'obtenir davantage d'informations sur les diatomées *A. saprophilum*, notamment sur la taille et les caractéristiques morphologiques des cellules. L'association entre les bactéries et les diatomées a également été illustrée à l'aide du MEB. En fait, les bactéries semblent produire de l'EPS pour s'attacher à la surface des diatomées.

En outre, la courbe de croissance de la diatomée *A. saprophilum* dans les conditions d'incubation appliquées a été étudiée. Toutes les phases de croissance typiques ont été identifiées, y compris la phase d'accélération de la croissance, la phase de croissance exponentielle, la phase de décélération de la croissance et la phase de croissance stationnaire, comme cela est généralement

indiqué dans la littérature. Il est intéressant de noter qu'une accélération de la croissance de la diatomée a été observée dans ce travail en comparant les courbes de croissance mesurées respectivement en 2021 et 2023, ce qui pourrait impliquer la grande capacité d'adaptation de l'espèce *A. saprophilum* face aux environnements changeants (des conditions in natura aux conditions de laboratoire).

En conclusion, ce chapitre fournit des informations fondamentales sur la culture de diatomées qui a été utilisée dans ce travail, ce qui est d'une importance vitale pour l'étude de l'interaction entre les diatomées et U, Ra.

Dans le chapitre 4, l'interaction de U, Ra avec la culture de diatomées xéniques *A. saprophilum* est examinée quantitativement au niveau macroscopique. En réalisant des expériences de bio-association de U et de Ra, ce travail contribue à une meilleure compréhension de l'interaction entre U/Ra et les diatomées et fournit des informations précieuses, notamment sur la cinétique d'adsorption, l'isotherme d'adsorption et les effets potentiels de la phase de croissance des diatomées sur le comportement d'adsorption/incorporation.

Comme le suggèrent les données expérimentales, l'adsorption de U sur les diatomées s'avère être un processus rapide (l'équilibre d'adsorption est atteint dans les 15 premières minutes d'exposition), tandis que l'état d'équilibre d'adsorption pour Ra semble prendre relativement plus de temps à s'établir (environ 45 minutes). D'autre part, les expériences de bio-association dépendantes de la concentration suggèrent que l'isotherme d'adsorption de U sur les diatomées suit probablement les modèles de Langmuir-Freundlich. Cependant, peu d'informations peuvent être déduites dans le cas de Ra en raison de l'accès limité à des concentrations plus élevées applicables pour les expériences. En outre, les expériences de bio-association en fonction du temps montrent que l'adsorption de U et de Ra sur les diatomées diminue généralement avec le temps et se stabilise ensuite avec le vieillissement de la population de diatomées. Cette diminution de l'adsorption pourrait s'expliquer par la compétition entre la complexation de U et de Ra avec différents composants présents dans la culture, par exemple les cellules des diatomées et la matière organique libérée par les diatomées dans la solution.

Quant à l'incorporation, ce processus est significatif dans le cas de U. Les données expérimentales suggèrent également des altérations progressives de la perméabilité de la membrane cellulaire des diatomées à l'égard de U, puisque la quantité de U incorporée par cellule de diatomée augmente avec le temps. Contrairement à U, aucune incorporation significative n'a été observée pour le Ra. Ceci est plutôt surprenant, étant donné que Ra appartient à la famille des éléments alcalino-terreux et que ces derniers jouent généralement un rôle crucial dans le métabolisme cellulaire des organismes vivants (comme Mg et Ca).

Dans le chapitre 5, l'interaction de U avec la culture d'*A. saprophilum* est caractérisée en combinant des approches microscopiques et spectroscopiques. Comme le démontrent les analyses MEB, MET et EDX, U peut être trouvé à la surface et à l'intérieur des cellules des diatomées, ce qui prouve le comportement d'adsorption et d'incorporation de U au niveau des diatomées. Un scénario similaire peut être observé dans les bactéries associées aux diatomées. Il est intéressant de noter que certaines espèces U ressemblant à des précipités sont observées à l'intérieur des cellules des diatomées et dans la vacuole en particulier, comme le montrent les zones denses en électrons observées dans la micrographie MET. En outre, l'analyse EDX révèle la colocalisation de U avec P au niveau de la diatomée et de la bactérie et démontre en même temps une co-précipitation possible de divers métaux à l'intérieur de la vacuole des diatomées.

D'autre part, les mesures FTIR et TRLFS effectuées fournissent des informations précieuses concernant les interactions U(VI)-diatomes d'un point de vue moléculaire. Les données FTIR confirment la contribution significative des groupes carboxyles à la coordination de U(VI) dans l'échantillon de diatomées. En outre, l'expérience in situ "flow-through" démontre la formation de plusieurs espèces de U(VI) dans le système de diatomées étudié et souligne la faible labilité des espèces de U(VI)-diatomées formées. En outre, les données de la TRLFS fournissent des informations complémentaires sur la spéciation de U(VI) dans les diatomées, montrant un changement dans la prédominance de deux espèces de U(VI) identifiées dans les diatomées au cours de leur croissance. Ceci peut être en accord avec l'évolution de l'adsorption/incorporation de U observée dans l'expérience batch de bio-association de U dépendante du temps. En comparant

les données spectroscopiques de luminescence avec les composés de référence de U(VI) cités dans la littérature, on peut conclure que les groupes fonctionnels carboxyle et phosphate portés par diverses biomolécules sont probablement responsables de la liaison de U(VI) sur/dans les diatomées. Les mesures TRLFS effectuées sur quatre isolats bactériens (*A. facilis*, *A. fabrum*, *B. mediterranea* et *P. peli*) démontrent la présence d'une espèce bactérienne particulière de U(VI) qui est probablement commune à ce qui est identifié dans les diatomées. En fin de compte, des motifs de liaison similaires de U(VI) à des biomolécules comparables trouvées à la fois dans les bactéries et les diatomées peuvent conduire à des similitudes dans les spectres. Néanmoins, l'implication des bactéries dans l'interaction avec U(VI) dans la culture de diatomées d'*A. saprophilum* reste incontestée. Dans le cas des bactéries, les espèces de U(VI) de type phosphate sont plus susceptibles de se produire dans le système.

Acknowledgements

First and foremost, I would like to express my sincere appreciation to all the jury members for their precious advice for this thesis work. I want to convey my profound gratitude to my mentors: Gilles MONTAVON, Olivier PERON and Susanne SACHS. I'm profoundly thankful for your contributions to this work and your invaluable guidance. Thank you for listening to my every question during the work. You consistently provided me with the most precious suggestions, helping me surmount every challenge. Each discussion with you has proven to be an enriching experience. I'm aware that there's always room for improvement in my abilities, and I appreciate your patience and kindness during our time working together.

I extend my sincere thanks to SUBATECH and HZDR for providing me all the technical supports, without which I will never be able to transform ideas into the research outcomes presented in this work. I'm deeply grateful to every colleague in SUBATECH, especially Céline B., Nicolas B., Karine D., Valérie B. and Katy P. for your daily assistance. I would like to say to all my doctoral colleagues who have either graduated or are about to, especially Anne-Laure N., Lu L., Haohan Z. and Jule G., that it has been a pleasure working alongside you and thank you for your helps. Besides, I would like to acknowledge LMGE for the cooperation. I really appreciate the technical support and meticulous guidance provided by Clarisse M. and Anne-Hélène L. J. during my three-month visit in LMGE. Without your assistance and guidance on the cultivation of diatoms, this project wouldn't have come to fruition. Furthermore, I'd like to express my heartfelt appreciation to my supervisor Susanne SACHS. Thank you for your welcome and warm support during my stay in HZDR. Thank you so much for your birthday gift that made me feel the warmest welcome in Germany. I acknowledge the support and assistance provided by all the colleagues in HZDR that are involved in this work, especially Sindy K., Henry M., Vladyslav S., Sean Ting-Shyang W., Katrin F., Harald F., Robin S., René H. and Johannes R. At the same time, I would like to thank Ms. LANG for her assistance with visa and all relative administrative matters, which enabled me to smoothly embark on a six-month journey of work in Germany. Thank you, Ms. HERRMANN, for providing me with a cozy and well-kept residence in Dresden, where I have spent unforgettable moments. By the way, your magnificent piano and the cherries from your garden were truly delightful! Lastly, I would like to acknowledge the Alliance mobility funding that provided financial support for my stay in Germany.

Special thanks go to Tomo S-M. and Catherine L. for providing me with precious internship opportunities. It's because of you that pursuing my doctoral study in France became a reality, marking the beginning of this beautiful journey in a foreign country. To all my friends in France,

thank you for your companionship and attentive listening. I deeply miss every moment spent with you, which will forever remain some of the most cherished memories in my life. Thank you for introducing me to various activities I had never experienced before and bringing me endless joy.

Finally, I would like to express my deepest gratitude to my family. Thank you for your unwavering support throughout my stay in France. Due to certain circumstances, I couldn't return home during these three years. Grandparents, I really miss you!

Thank you to everyone who helped me, without your help this work could never be realized.

Contents

List of figures

LIST OF FIGURES

LIST OF FIGURES

List of tables

List of abbreviations

Institutions, organizations, projects

CCAP	Culture Collection of Algae & Protozoa
CNRS	*Centre National de la Recherche Scientifique*
CRTD	Center for Regenerative Therapies Dresden
IAEA	International Atomic Energy Agency
LMGE	*Laboratoire Microorganismes : Génome Environnement*
LTSER	Long-Term Social-Ecological Research observatories
NCBI	National Center for Biotechnology Information
NEA	Nuclear Energy Agency
NORM	Naturally occurring radioactive materials
TIRAMISU	Biodiversity in Radioactive Mineral Springs of the Auvergne Region
UNSCEAR	United Nations Scientific Committee on the Effects of Atomic Radiation
ZA	*Zones Ateliers*
ZATU	*la Zone Atelier Territoires Uranifères*

Chemical symbols

Al	Aluminum	N	Nitrogen
Ba	Barium	Ni	Nickel
C	Carbon	P	Phosphorus
Ca	Calcium	Pb	Lead
Cd	Cadmium	Po	Polonium
Cm	Curium	Pu	Plutonium
Co	Cobalt	Ra	Radium
Cr	Chromium	Rn	Radon
Cu	Copper	S	Sulfur
Eu	Europium	Se	Selenium
Fe	Iron	Si	Silicon
Ga	Gallium	Sr	Strontium
Hg	Mercury	Tc	Technetium
Mg	Magnesium	Th	Thorium
Mn	Manganese	U	Uranium
Mo	Molybdenum	Zn	Zinc

LIST OF ABBREVIATIONS

Chemicals

EDTA	Ethylenediaminetetraacetic acid
H_2O_2	Hydrogen peroxide
HCl	Hydrochloric acid
HEPES	4-(2-hydroxyethyl)-1-piperazineethanesulfonic acid
HNO_3	Nitric acid
MCE	Mixed cellulose esters
NaCl	Sodium chloride
$NaNO_3$	Sodium nitrate
OsO_4	Osmium tetroxide
PFA	Paraformaldehyde
PTFE	Polytetrafluoroethylene
UO_2^{2+}	Uranyl ion

Biological notions, materials, substances

ASV(s)	Amplicon sequence variant(s)
ATP	Adenosine triphosphate
CEC	Cation exchange capacity
DM	Diatom Medium
DNA	Deoxyribonucleic acid
DOC	Dissolved organic carbon
EPS	Extracellular polymeric substances
GlcNAc	N-acetylglucosamine
LB	Lysogeny broth
LPS	Lipopolysaccharide
mRNA	Messenger ribonucleic acid
MT(s)	Metallothionein(s)
MurNAc	Acetylmuramic acid
PCD	Programmed cell death
PCR	Polymerase chain reaction
PC(s)	Phytochelatin(s)
PG	Peptidoglycan
POC	Particulate organic carbon
QS	Quorum sensing
ROS	Reactive oxygen species
rRNA	Ribosomal ribonucleic acid

LIST OF ABBREVIATIONS

Analytical techniques, tools

ATR	Attenuated total reflectance
BLAST	Basic Local Alignment Search Tool
EDX	Energy-dispersive X-ray spectroscopy
FTIR	Fourier-transform infrared spectroscopy
GATE	GEANT4 Application for Tomographic Emission
HAADF-STEM	High-angle annular dark-field scanning transmission electron microscopy
HR-ICP-MS	High resolution inductively coupled plasma mass spectrometry
ICP-MS	Inductively coupled plasma mass spectrometry
IR	Infrared
PARAFAC	Parallel factor
SEM	Scanning-electron microscopy
TEM	Transmission electron microscopy
TRLFS	Time-resolved laser-induced fluorescence spectroscopy

Units

Radioactivity

Bq	Becquerel	Ci	Curie

Concentration

mol/L	Mole per liter	pmol/L	Picomole per liter
mmol/L	Millimole per liter	ppb	Part per billion
µmol/L	Micromole per liter	ppq	Part per quadrillion
nmol/L	Nanomole per liter		

Mass

kg	Kilogram	ng	Nanogram
g	Gram	pg	Picogram
mg	Milligram	fg	Femtogram

Time

h	Hour	sec	Second
min	Minute	ns	Nanosecond

Miscellaneous

°C	Degree Celsius	pH	Acidity
cm^{-1}	Wavenumber	rpm	Revolutions per minute

LIST OF ABBREVIATIONS

Eh	Redox potential	v/v	Volume fraction
g	Gravity of Earth	w/w	Mass fraction
kV	Kilovolt	µL	Microliter
mA	Milliampere	µm	Micrometer
W	Watt	mm^2	Square millimeter
J	Joule	eV	Electronvolt

General introduction

GENERAL INTRODUCTION

Diatoms are a type of unicellular microalgae that belong to the group known as Bacillariophyta. They are among the most abundant and diverse organisms (about 20000 extant species (Guiry, 2012)) on Earth and can be found in various aquatic environments, including oceans, lakes, rivers, and even moist soil. Diatoms are primary producers and contribute to a significant amount of annual oxygen production. These microorganisms also play a vital role in global biogeochemical cycles, such as carbon (C) cycle, silica cycle and urea cycling. Additionally, diatoms are crucial to the Earth's ecosystems and have significant ecological and geological importance. In recent years, diatoms have been the subject of investigation across diverse scientific fields (Lopez et al., 2005). In the ecology for example, they are often referred as bioindicators to assess water quality and environmental health due to their sensitivity to changes in their surroundings, such as nutrient availability, pH, temperature and metal stress (Necchi Jr, 2016).

Bacteria are often neighbors of diatoms in their living environments, some of them can even be found on the surface of diatoms. The relationships between diatoms and bacteria are complex and have received increasing attention in ecological research. The interaction between diatoms (or algae in general) and bacteria involves various mechanisms such as nutrient exchange, signal transduction and gene transfer (Kouzuma and Watanabe, 2015). Amongst the numerous interactions between diatoms and bacteria, the mutually beneficial relationship, also called synergistic interaction, has been investigated by various studies in the literature(Amin et al., 2012; Seymour et al., 2017). It is believed that diatoms release exudates and extracellular polymeric substances (EPS) that can serve as an energy and C source for bacteria living in symbiosis. In turn, bacteria can re-mineralize these organic compounds, breaking them down into inorganic forms that can be readily taken up by diatoms. Bacteria can also produce EPS that facilitates the aggregation of diatom cells and results in the formation of biofilms. Hence, it is important to consider both the diatoms and the associated bacteria living in symbiosis in this work in order to get as close as possible to *in natura* conditions.

The microbial community structure is of vital importance in the ecological studies since it can reflex the ecological health of the aquatic environments. Various studies point out the changes of the microbial community structure caused by the pollution of pesticides, heavy metals or to the acid mine drainage (AMD) (Méndez-Garcí-a et al., 2015; Muturi et al., 2017; Yin et al., 2015). In general, the diversity and abundance of the microbial community is negatively affected by these factors mentioned above. It is also demonstrated that some sensitive diatom or bacterium species will be gradually replaced by the more resistant ones that tolerate the heavy metal or acidity stress for example.

Over the past decades, various researchers have been focusing on the ecological impact due to human mining activities (Salomons, 1995). In fact, the mining activities might bring significant

disturbances to the soil and water environments. One of the most concerning ecological impacts of mining activities is AMD. It happens when sulfide minerals such as pyrite (FeS_2) that are present in the mined rocks or tailings come into contact with air and water due to the mining activities. The oxidation of the sulfides will lead to the eventual formation of sulfuric acid in water, which will lower the pH in the surrounding environments and results in several consequences. One of the most concerning issues is the metal leaching effect, where some heavy metals (such as copper (Cu), zinc (Zn), lead (Pb), cadmium (Cd), etc.) will be leached out from the original ores to the AMD water.

In the case of uranium (U) mining activities, the AMD will enhance the U mobility since U is usually found in the hexavalent (+6) oxidation state (in the form of the uranyl(VI) ion, UO_2^{2+}) under acid and oxidizing conditions and becomes more mobile in the environment. Consequently, the AMD can facilitate the transport and migration of U in soil and water. The acidity and the presence of U or other heavy metals may degrade significantly the terrestrial and aquatic ecosystems and decrease the biodiversity. Due to the radioactivity, some naturally occurring radioactive materials (NORM) including U have further radiological impact on the ecosystem. It raises more ecological concerns especially when the NORM enters into the food chain.

To assess the ecological impact of U mining activities on the living microorganisms, various researchers focus on diatoms or bacteria as bioindicators and analyze their community structure around some U mining impacted regions (Herlory et al., 2013; Sutcliffe et al., 2017). There exist several studies that investigate specifically the interactions of U-bacteria in a more general environmental context, *i.e.*, in U enriched waters or contaminated soils (**Table I-1** in Chapter 1). For that, different microscopic and spectroscopic techniques were employed to elucidate the interaction mechanisms and to investigate the U speciation at the molecular level.

Although the research focusing on the interaction between radionuclides and living organisms (such as plant cells, algae and bacteria in monoculture) has flourished during the past decades, the underlying mechanisms remain relatively unclear, especially in a more complex and realistic system, *e.g.*, a symbiotic diatoms-bacteria system. Gaining insights into the potential effects of radionuclides on the microbial community necessitates a deeper understanding of the potential interactions that may arise. Significant knowledge gaps still persist that impede the comprehensive and precise assessment of the ecological impact of radionuclides on living microorganisms.

Based on this context, various research projects were launched in France within the ZATU (la Zone Atelier Territoires Uranifères) framework, which has become member of the French Zones Ateliers (ZA) network since 2015 and was renewed as one of the Long-Term Social-

Ecological Research (LTSER) observatories by Institute of Ecology and Environment of CNRS (Centre National de la Recherche Scientifique). Among all of the research projects under the ZATU framework, radioactive mineral springs raise particular attention since they represent insular ecosystems wherein ionizing radiation exerts influence on the diversity and composition of microbial communities. Initiated in 2019, the TIRAMISU project (biodiversiTy In RAdioactive MIneral Springs of the Auvergne region) focuses on elucidating the intricate interactions between radionuclides and microorganisms inhabiting these naturally radioactive mineral springs.

The TIRAMISU project unites a collaborative effort encompassing biologists, ecologists, physicists, and radiochemists, with a collective pursuit of four principal objectives:

1. Identification and radiological characterization of naturally occurring radioactive springs.
2. Analyses of microbial communities in terms of their diversity and structure.
3. Investigation of the interaction between radionuclides and microorganisms.
4. Implementation of a multiparametric analysis based on the observed data and modeling of the radiation doses received by organisms inhabiting distinct compartments in the vicinity of the springs (*i.e.*, water, sediment, and interfaces).

With the support of the GATE (GEANT4 Application for Tomographic Emission) Monte Carlo simulation toolkit, the TIRAMISU project aims at integrate biological, chemical and radiological data to evaluate the received doses and to predict the deoxyribonucleic acid (DNA) damage of diatoms and bacteria living in the studied mineral springs due to the presence of radioactivity. To increase the accuracy of simulation, it is thus crucial to investigate the localization of radionuclides such as U, at the cell level, *i.e.*, to study the surface adsorption and intracellular incorporation behavior. It is also necessary to obtain relative chemical parameters such as the distribution coefficient K_d.

Contributing to this structural project, the principal objectives of this work are outlined as follows:

1. Characterization of U, Ra bio-association in a symbiotic diatoms-bacteria system by distinguishing adsorption and incorporation: investigation on the adsorption kinetics, determination of the distribution coefficient and study on the time-dependent retention behavior (growth phases dependent).
2. Localization of U at the cell level using various microscopic techniques.
3. Study of the speciation of U using different spectroscopic techniques.
4. Investigation of bacteria's potential contribution to the overall interactions between diatoms and the studied radionuclides.

In Chapter 1, a general state-of-the-art review is given on a wide array of topics, covering from the generalities of diatoms and bacteria (Part I) to the interactions of heavy metals (including U and Ra) with diatoms and bacteria (Part II). In Chapter 2, the general strategy and methodology applied in this work for studying the interaction of U, Ra with diatoms are presented in detail. The characterization of the studied xenic diatom culture, including information regarding the taxonomy, the bacterial community structure, the growth curve, etc., will be given in Chapter 3. Chapter 4 presents the results of the macroscale study on the U, Ra bio-association behavior in the diatom culture, while information concerning the localization and speciation of U in the diatom-bacteria system is discussed in Chapter 5. At the end, general conclusion and perspectives of this work will be addressed in Chapter 6.

Chapter 1: State of the art

Part I: Diatoms and bacteria: Key components in the microbial world

Contents

1. Diatoms

Diatoms are unicellular photosynthesizing microalgae. They are ubiquitous on Earth, in oceans, freshwaters, soils and even on moist surfaces. Owing to their famous intricate cell walls made of silica, *i.e.*, the frustules, diatoms are often described as "jewels of the sea" or "living opals". Some generalities covering different aspects about these exquisite creatures will be presented in the following sections.

1.1. Taxonomy

Diatoms are protists and belong to the clade of stramenopiles. The classification of diatoms remains unsettled as the progress of phylogeny during last decades, numerous revisions and emendations have been undertaken. Generally speaking, the currently most accepted classification system was developed by Round in 1990 (Round et al., 1990). Recently, a classification was presented by Adl et al., where diatoms are treated as a phylum called Diatomeae or Bacillariophyta and ranked from three classes, namely Mediophyceae, Biddulphiophyceae and Bacillariophyceae (Adl et al., 2019). To date, the classification of diatoms is still a challenging work even with the rapid development of molecular phylogeny. More detailed information on the diatom taxonomy can be found in the literature (Williams, 2020; Williams and Kociolek, 2011). Nowadays, it is estimated that about 12000 diatom species have been described so far, with around 8000 species to be further discovered (Guiry, 2012).

1.2.Morphology

Diatoms have their unique silica cell walls, the frustules, that can have different intricate patterns depending on specific species (**Figure I-1**). As is indicated by its ancient Greek name, *diátomos*, which means “cut in half”, frustules can be divided into two halves, *i.e.*, hypotheca and epitheca, with one slightly smaller than another. In general, each theca consists of a flat plate called valve and a girdle band that helps connecting the two parts. On the valves there are various delicate structures such as small perforations, called punctae, which line up neatly and form striae on the surface of valves. Raphes are slits on the valves through which diatoms are able to generate movements along solid surfaces. Certain diatom species even have spines.

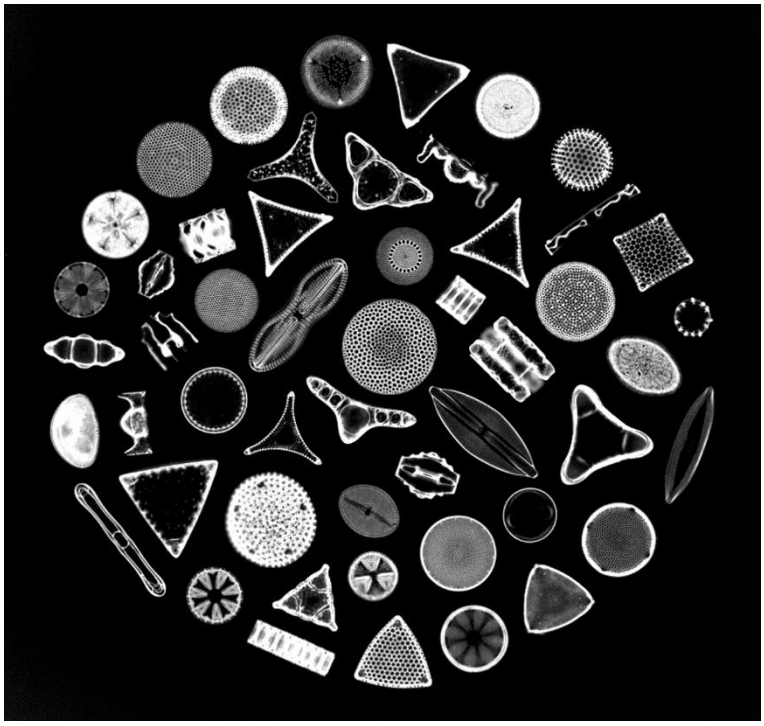

Figure I-1: Photomicrograph depicting the siliceous frustules of fifty species of diatoms (image in public domain, source: https://www.usgs.gov/media/images/diatoms-50-species).

The structure of diatom frustules varies from species to species. Nevertheless, diatoms can be artificially divided into two groups: centric or pennate diatoms, or three groups by further distinguishing between the presence and absence of raphes for pennate diatoms, *i.e.*, raphids or araphids, respectively. The centric diatoms are radially symmetric while the pennate diatoms are bilaterally symmetric and elongated parallel to raphes. The size of diatoms normally varies from 2 to 200 μm (Halse and Syvertsen, 1996).

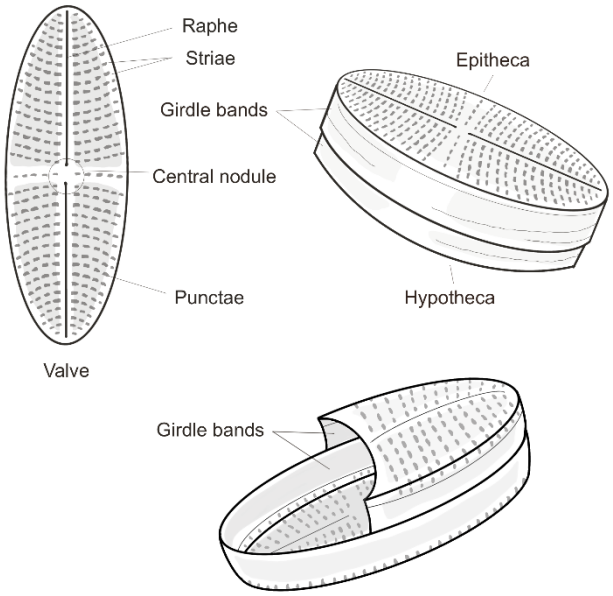

Figure I-2: Frustule structure of a pennate diatom species.

1.3.Life cycle and reproduction

There are two different reproduction mechanisms for diatoms in general: vegetative reproduction and sexual reproduction. Diatom cells undergo vegetative reproduction via a fascinating mechanism, where each of the divided daughter cells will "inherit" one of the precious silica valves from the parent cell as the epitheca (the bigger valve) and build their own hypotheca (the smaller valve). This results in a problem: some of the daughter cells will get smaller and smaller after several generation (note that certain species are able to divide without causing size reduction (Drebes, 1977). When the frustule size reaches a certain threshold, the sexual reproduction and auxospore formation must take place in order to return to its "normal" size.

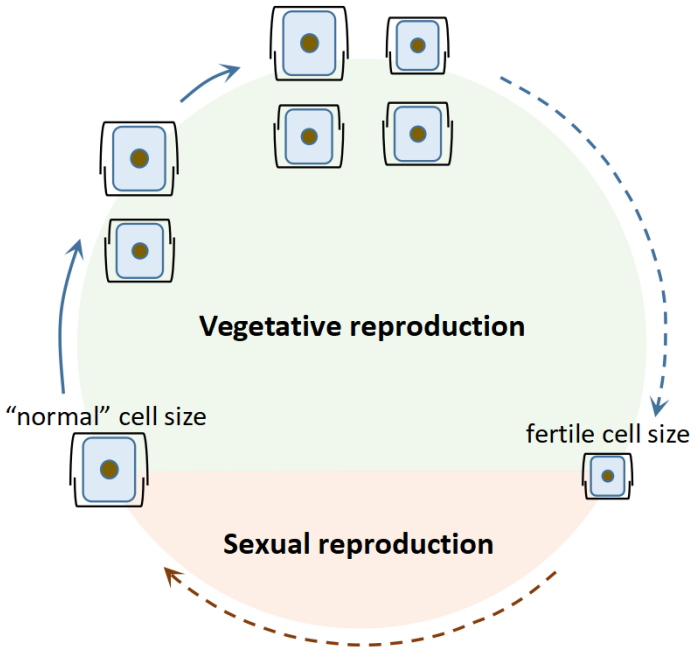

Figure I-3: Simplified illustration of diatom life cycle.

The change on the cell size or even the morphology at different stage of diatom's life cycle might sometimes bring difficulties to diatom identification works, especially for traditional identifications through morphometric measures. For that, mathematics tools such as elliptical Fourier descriptors have been proposed by some researchers to better describe the diatom contour for a more accurate morphological identification purpose (Sánchez et al., 2019).

The vegetative reproduction of diatoms can be more or less frequent depending on the external conditions such as temperature, luminosity and nutrient availability. For example, the depletion of dissolved silica in the diatom growing medium might limit the vegetative reproduction rate of diatoms, since the diatom silicification process will be impacted. In a diatom culture, especially for a closed system, different growth phases of a diatom population can be clearly observed (**Figure I-4**). By plotting the diatom cells number or density in the culture as a function of time, one may observe two growth phases in general: exponential growth phase and stationary growth phase. More detailed growth phases can be artificially defined if needed, such as acceleration growth phase (early exponential growth phase), deceleration growth phase (early stationary phase) and decline phase (late stationary phase), depending on the research purpose. Various studies focus on the change of diatom metabolic activities in different growth phases, such as the release of polyunsaturated aldehydes or other metabolites (Vidoudez and Pohnert, 2012, 2008).

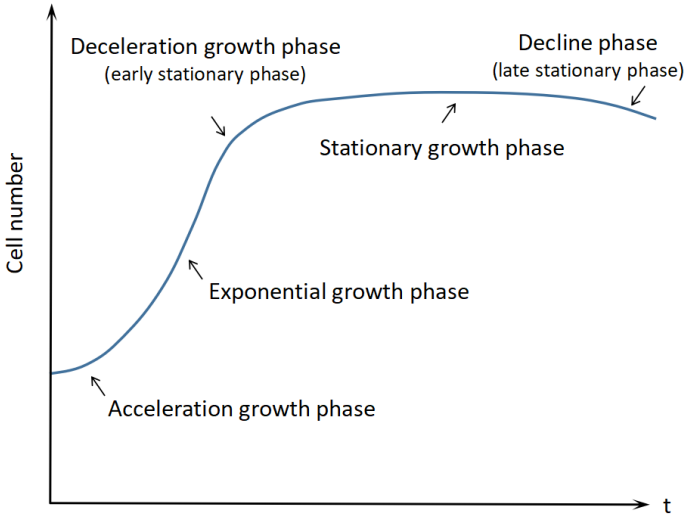

Figure I-4: Example of a typical diatom growth curve with various growth phases.

1.4.Roles in the ecosystem and applications

Diatoms are widespread on Earth and can be found in almost every aquatic environments. It is reported by several studies that diatoms are responsible for 20% of the total global primary production and for about 40% to 45% of the total marine primary production (Mann, 1999; Tréguer et al., 2018). According to the *in situ* measurements, diatoms exhibit greater maximum growth rates (up to 2 to 4 cell divisions per day) in comparison with other similar algae and become predominant species in the algal communities in nutrients enriched area (Kiran Marella et al., 2020; Yool and Tyrrell, 2003). Depending on their life style, diatoms can be generally classified into two different groups, *i.e.*, planktonic ones that live more actively within water columns and benthic ones that prefer solid surfaces such as water-sediment interfaces, biofilms, etc.

Some planktonic diatoms often exhibit a so-called “boom and bust” phenomenon in nutrient-rich oceanic waters. In spring, as the temperature rises and the daylight extends, planktonic diatoms reproduce rapidly in upper mixed water columns where nutrients are abundant, causing a spring blooming. Besides, research suggests that the diatom’s biogenic silica facilitates the conversion of bicarbonate to dissolved carbon dioxide, enhancing the photosynthesis efficiency (Milligan and Morel, 2002). As the nutrients gradually deplete (silicon (Si) shortage especially), these tiny opportunists start to sink to deeper water layers by forming aggregations for example (Sarthou et al., 2005). Under unfavorable conditions, diatoms may also switch to resting mode by producing resting spores and wait for the next booming season. In some particular oceanic areas, diatom booming may also happen in autumn.

The seasonal movements of planktonic diatoms play an important role in the biogeochemical cycles for various elements such as C, nitrogen (N), phosphorus (P), Si and iron (Fe). It is reported that diatoms are one of the major planktons that contribute to a relatively high particulate organic carbon (POC) export flux in oceans, due to their upwelling and sinking movements (Buesseler, 1998). The presence of diatoms is reported even at 4000 m deep in the ocean (Agusti et al., 2015). Due to the intimate interactions between C and Si, the Si biogeochemical cycle generally couples with that of C at different temporal and spatial scales (Ragueneau et al., 2006). The role of diatoms as biological pumps for various elements has been revised during the last decades and there are numerous studies in the literature.

Benthic diatoms are also important contributors of primary production in their living ecosystems (Virta et al., 2019). They may exhibit highly visible migration behavior within biofilms formed in some estuarine ecosystems (Consalvey et al., 2004). Due to the productions of EPS, benthic diatoms play a crucial role in biofilms formation, where photosynthesis activities and nutrient cycles take place, fueling the food chains and even stabilizing the sediments (Osuna-Cruz et al., 2020).

Besides their roles as primary producers and biological pumps in ecosystems, diatoms have several industrial applications due to their unique properties and characteristics. The fossilized remains of dead diatoms, principally their porous siliceous frustules, form various types of naturally occurring sedimentary rocks called diatomaceous earth, or diatomite, which display highly porous and low-density characteristics and is thus widely used in the industry for various applications. Moreover, diatoms have gained increasing attention in the nanotechnology in the past decades for its ability to manufacture micro- or nanoscale structures (Bradbury, 2004).

2. Bacteria

Bacteria are unicellular prokaryotic microorganisms that are believed to be among the first forms of life on Earth (approximately 4 billion years ago). They inhabit almost everywhere in our planet: from the mildest environments (soils, waters) to the most extreme conditions such as high temperature (hot springs, hydrothermal vents), high pressure (oceanic trenches), high salinity (Dead Sea), acidic or alkaline conditions and even high radiation (radioactive waste). Some bacteria are heterotrophic, while others are autotrophic. Some chemotrophic bacteria can even sustain their life through oxidation of organic or inorganic compounds in their living environments. Both of these bacteria are essential to the Earth's ecosystems.

2.1. Taxonomy

Bacteria were first observed by Antonie van Leeuwenhoek in 1676. However, it was until the

late 19th century that the taxonomy of bacteria really started (Schleifer, 2009). Modern classification divides Life into three domains: the Eukaryota, the Archaea and the Bacteria (called three-domain system). Different from the early classifications, which were mainly based on the bacterial morphology, modern classifications focus more on molecular systematics, as lateral gene transfer among some closely related bacteria can sometimes lead to significant variations in both morphological and metabolic characteristics. In spite of the rapid development of molecular phylogenetics during recent decades, the classification of bacteria is still a challenging work.

2.2.Morphology

Bacteria have various morphologies and can be generally classified into five typical groups: bacillus (rod-like), coccus (round or spherical), spirilla (spiral), vibrio (comma-like) and spirochaetes (tightly coiled like a corkscrew). Some other unusual shapes (*e.g.*, star-like) are also reported in the literature. It is possible that the same bacterial strain exhibits different morphological characteristics, depending on the growth conditions and the cell status.

The size of bacteria varies from 0.5 to 5 μm in general. There exist some smaller species, such as *Mycoplasma hominis* which measures only about 250 nm in diameter (Robertson et al., 1975). The largest single-cell bacteria ever reported, *Thiomargarita magnifica*, measure greater than 9000 μm long, can even be observed with naked eye. Bacteria usually live as individual cells, but some species live in groups (in pairs, in chains, in clusters, etc.). When bacteria grow on petri plates, they usually form larger aggregations, called colonies, that display different morphology from the single cell. The bacterial colonies may display a large diversity in terms of sizes, forms, colors, opacities and consistencies, depending on the species and also on the incubation time.

Under natural conditions, bacteria can form biofilms on solid surfaces by producing EPS. The internal structure within biofilms is often complex, comprising a network of channels where nutrients and signaling molecules diffuse more easily. Biofilms are also important structures that protect bacteria from grazers and play more significant roles in the ecosystems.

2.3.Life cycle and reproduction

Bacteria reproduce by binary fission, a form of asexual reproduction (**Figure I-5**). During the fission, DNA divides into two replicates, the bacterial cell elongates and then splits into two clone daughter cells, each carry one set of the DNA replicates. Under favorable conditions, bacteria are able to reproduce extremely rapidly and reach a colossal population until the nutrients run out. As in the case of diatoms, the growth of bacteria in a batch culture follows exactly the same phases: lag phase (acceleration phase), log phase (exponential phase),

stationary phase and death phase (decline phase).

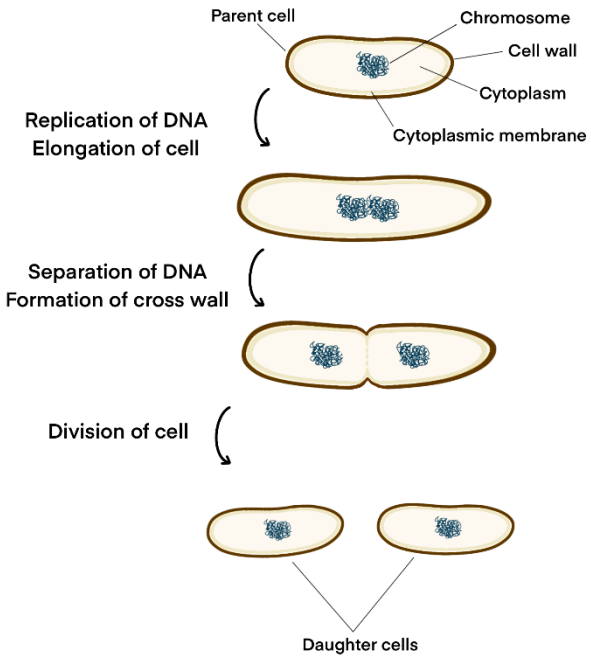

Figure I-5: Binary fission of a bacterial cell.

2.4.Roles in the ecosystem and applications

Bacteria play a vital role in nutrient cycle in the ecosystems. Some species are decomposers that break down dead bodies or decaying organisms, thus help recycling nutrients back to the environments. Certain species, called diazotrophs, can fix gaseous nitrogen from the atmosphere into a more bio-available form such as ammonia. These bacteria are crucial to the N cycle in the terrestrial ecosystems, in soils more specifically. The fixed N, in the form of ammonia, is sometimes an important N source for the primary producers in some cases. It is known that bacteria may have close relationships (symbiosis, parasitism, etc.) with plants or animals. Take the example of diazotrophic bacteria again, certain species (*e.g.*, rhizobia) need to infect the roots of the host plants (*e.g.*, legumes) to express the N fixation genes, resulting in the formations of root nodules. The infection is indeed beneficial to the host plants, as these nodules act as small factories that convert gaseous nitrogen to ammonia and thus fertilize the host plants. In a more general context, certain types of bacteria can make the nutrients more bioavailable to the associated plants through various actions (*i.e.*, siderophores, organic acids, biosurfactants, biomethylations and redox processes)(Rashid et al., 2016; Ullah et al., 2015), or on the contrary, prevent the entrance of toxic substances into the plants (Cetin et al., 2011).

Under some extremely harsh conditions on Earth, certain bacteria still exhibit incredible resilience and take the role as primary producers in the ecosystems. For example, on the seabed

in the vicinity of hydrothermal vents there live some extremophile bacteria that can survive under high pressure, salinity, temperature conditions. Under the high hydrostatic pressure and at high temperatures, water may even exist as a supercritical fluid near the vents. Even under these extreme conditions, some chemoautotrophic bacteria can sustain their life through oxidation of chemical compounds, such as hydrogen sulfide, and form the base of food chain in these special ecosystems. The developed bacterial mat attracts more life forms, such as shrimps, crabs, tube worms and so on.

Bacteria also have high significance in different industries. Certain species of bacteria, such as *Lactobacillus*, are widely used in the food fermentation to produce cheese, vinegar, soy sauce, yogurt, etc. The diazotrophic bacteria, as are mentioned above, are commonly used as biofertilizers in agriculture to increase the productivity of crops. Bacteria are also important tools for the research in the field of genetics and biochemistry. By modifying bacterial DNA and examining the resulting phenotypes, people can better understand the function of genes and enzymes for example. Bacteria are also considered as one of the interesting candidates for the bioremediation to remove pollutants from the environments, which will be discussed more in detail in a later section.

3. Interactions between diatoms and bacteria

It is believed that diatoms and bacteria have shared common oceanic habitats for more than 200 million years (Amin et al., 2012). Over this time the relationships between these two large groups of microorganisms kept evolving. Because of their vital roles in the ecosystems, studies on the potential interactions between diatoms (or algae in general) and bacteria has flourished in the past decades. Generally speaking, interactions between algae and bacteria can be divided in three types: gene transfer, signal transduction and nutrient exchange (Kouzuma and Watanabe, 2015).

3.1. Phycosphere

Phycosphere, a term that signifies the microenvironment immediately surrounding a phytoplankton cell that is full of organic matters (dissolved organic carbon (DOC), polysaccharides, proteins, amino acids, etc.) exuded by the cell into the environment (**Figure I-6**), becomes a focus in the research field (Seymour et al., 2017). In fact, the phycosphere is a planktonic analogue system of the rhizosphere, the region near the plant roots enriched by the plants secreted substances that is widely studied in the terrestrial ecosystems. The phycosphere is the spot where complex interactions between the phytoplankton cell and bacteria take place at the microscale.

Bacteria are indispensable components in a phycosphere. In aquatic systems, the encounter of bacteria with the phytoplankton cells is mainly driven either by random motions, governed by Brownian motion or convections of water currents, or by the motility of bacteria directed by chemotaxis (the movement of organisms in response to certain chemical stimulus) (Seymour et al., 2017). Once bacteria meet up with a phytoplankton cell, some will maintain their spatial proximity to the phycosphere through constant movement, *i.e.*, swimming, while others will simply attach to the surface of the phytoplankton cell (Kogure et al., 1981), or even reside directly inside the phytoplankton cell (Lewis et al., 2001).

Nevertheless, it is reported that the association of bacteria with phytoplankton might be selective, as is suggested in various studies by consistent detection of a restricted number of bacterial taxa, *e.g.*, *Rhodobacteraceae*, *Flavobacteraceae* and *Alteromonadaceae* (Goecke et al., 2013; Seymour et al., 2017).

3.2.Gene transfer

During the protracted evolution in the past, inter-species gene transfer occurred commonly between bacteria and diatoms. This horizontal gene transfer to diatoms is pervasive (account for more than 5% of the diatom gene repertoires (Bowler et al., 2008) and clearly higher than other eukaryotes that have ever been sequenced, with a rate similar to that between bacteria (Keeling and Palmer, 2008). Research also suggests that some of the transferred genes may encode components in diatoms that result in new metabolic capacities, such as organic C and N utilization, urea cycle and cell wall silicification, which contribute to the rapid diversification of diatoms during the evolution and also to their success in the modern ecosystems on Earth (Bowler et al., 2008).

3.3. Signal transduction

Signaling between diatoms and bacteria is believed to play an essential role in the regulation of diatom-bacterium interactions within the phycosphere. In fact, besides the diatom-bacterium interkingdom signaling, intraspecies communications, *i.e.*, diatom-diatom and bacterium-bacterium signaling, are also likely to take place.

The bacterial intraspecies communication is commonly realized by quorum sensing (QS), where bacteria communicate through the synthesis and excretion of small molecules that are called autoinducers. Using QS, bacteria are able to coordinate the expression of some specific genes, affecting the phenotypes expression in response to stress and regulating the behaviors of the entire population. Diatoms use pheromones to realize cell-to-cell communication. Similar to the QS mechanism, pheromones are groups of compounds that are excreted by the cells to coordinate the behaviors of individuals within the same species. In terrestrial systems, it is

reported that both bacteria and diatoms commonly use lipid-based molecules for signaling. These lipid-based molecules usually do not demand energy or active transporters when passing through the cells, which might justify to some extends the possibility of the interkingdom signaling between diatoms and bacteria. In aquatic systems, it is also believed that diatoms may be able to sense the autoinducers released by bacteria for the QS, and in return, that bacteria may also sense the pheromones exuded by diatoms within the phycosphere. These inter-species signaling are believed to be crucial for the coordination of interactions between diatoms and bacteria in phycospheres (Amin et al., 2012).

3.4. Chemicals exchange

Chemicals exchange is another most commonly occurring and studied interactions between diatoms and bacteria. Within the phycosphere, interactions between the phytoplankton and bacteria can be generally categorized into several types, *i.e.*, beneficial relationships (symbiosis, mutualism, commensalism) or exploitative relationships (antagonism, parasitism, competition) (Seymour et al., 2017). In any of these relationships, nutrient resources (macronutrients and micronutrients) and infochemicals (hormones, pheromones, etc.) are exchanged between species. The infochemicals are mainly used for intra- or inter-species signaling and sensing, which has been discussed above. Hence, in this section, information on the exchange of nutrient resources in some of the most typical scenarios, *i.e.*, in a symbiotic system and in a competitive system, will be elucidated in more details.

In a symbiotic system, diatoms and bacteria can mutually or partially benefit from this close relationship by exchanging a wide array of resources, including macronutrients and micronutrients, that are essential for their growth.

From the perspective of diatoms, the bioavailability of N (one of the common macronutrients for phytoplankton) is usually a key limiting factor for their colonization in an ecosystem, as the competition of N between primary producers can sometimes be intense. The N-fixing bacteria, especially the cyanobacteria, is reported to be able to fix excess N and transfer it to their symbiont, which is diatom in the studied case (Foster et al., 2011). In contrast to N, Fe is a micronutrient that plays an indispensable role in almost all life forms on Earth. Diatoms can produce a colossal quantities of mono- or polysaccharides to the phycospheres, which assimilate Fe from the environments (Amin et al., 2012). However, these released compounds show low binding affinity for Fe. On the contrary, the siderophores excreted by bacteria display an extremely strong affinity for Fe. By sensing the excretion of siderophores from bacteria into the phycosphere, diatoms may mobilize the Fe assimilation mechanisms to benefit from this “gift” offered by their symbiotic partners. Nevertheless, since siderophores are hydrophilic molecules, diatoms must response rapidly to the release of these Fe-chelators before they

diffuse away from the phycosphere. Diatoms may also rely on bacteria for vitamins, especially vitamin B. Various studies have investigated the importance of vitamin B_{12}, B_1 and B_7 to the growth of heterokonts (to which diatoms belong) (Croft et al., 2005; Tang et al., 2010). In fact, the vitamin B auxotrophic algae can benefit from the symbiosis with those bacteria that can produce vitamin B to sustain the growth of algae, especially under vitamin B depleting conditions.

In return, bacteria may also take benefits from the symbiotic relationship with diatoms. Besides N and P, C source is largely demanded for the growth of bacteria. It is reported that up to 50% of the C fixed by phytoplankton is ultimately consumed by bacteria (Fuhrman and Azam, 1982). In the phycosphere, heterotrophic bacteria can easily find DOC released by diatoms (such as EPS). Additionally, lysis products or dead body of diatoms may also serve as C sources for bacteria. In fact, bacteria have further impact on algal behaviors such as growth stimulation, morphogenesis, spore germination and colonization (Goecke et al., 2010).

Different scenarios might happen in a competitive system, where diatoms and bacteria compete for the nutrients available in the environment. As like other macronutrients, P is in great demand for the growth of both diatoms and bacteria. In fact, research points out that bacteria have stronger ability to assimilate phosphate in comparison with algae (Thingstad et al., 1993). The competition for limited nutrient resources can be far more intense among different species. For example, algicidal bacteria, which can be used as bio-agent to control harmful agal blooms, are capable to kill algae by releasing chemicals, called algicides, that stop the growth or even destroy the algae cell so that they can have access to more DOC. Some algicides can change the permeability of the algal cell wall, which eventually results in the rupture and lysis of the algal cell (Coyne et al., 2022). In turn, diatoms have self-defense mechanisms against the attack from hostile bacteria. Some diatoms can produce fatty acids and esters as antibacterial compounds to influence the bacterial activity or to prevent unwanted bacteria from attaching on their surface (Lebeau and Robert, 2003).

In general, the interactions between diatoms and bacteria are complex and strongly depend on specific species and conditions. There is still a long way to go before a thorough understanding of all of the underlying mechanisms becomes truly possible.

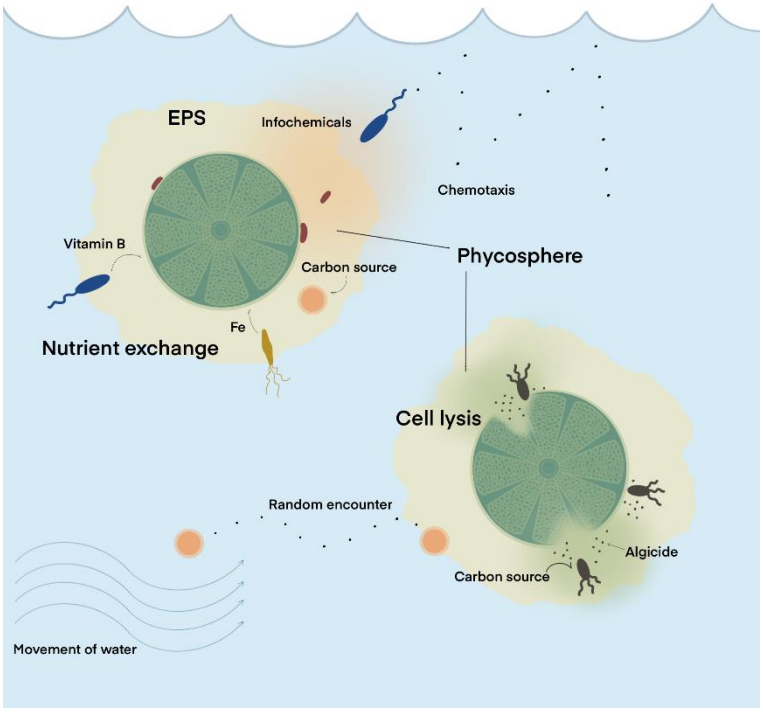

Figure I-6: Interactions between diatoms and bacteria within the phycosphere, example for a symbiotic system (left) and a competitive system (right).

4. The important role of diatoms and bacteria in the field of ecology

4.1. Bioindicator

As industrialization and urbanization persistently progress, a growing awareness was emerging among human societies regarding the impacts of human production activities on natural ecosystems. As a series of issues continue to manifest (air, water and soil pollution, global warming, etc.), people started to pay attention to the health assessment of ecosystems. The concept of biomonitor, or bioindicator, was proposed by ecologists in the last century for the ecological health assessment. Bioindicators can be any species, including animals, plants and microbes that can detect changes in the environment and provide qualitative information on the status of ecosystems.

Diatoms and bacteria are both considered as bioindicators in various ecological studies. Diatoms are believed to be highly sensitive to heavy metal pollutions in aquatic ecosystems. Exposed to heavy metals, diatoms may show both rapid and chronic responses and display shifts on their community structure, *i.e.*, the replacement of sensitive species by more resistant ones (Pandey et al., 2018). In addition, nuclear abnormalities, cell membrane, cytoplasmic content, etc., are also the main parameters that were studied (Saxena et al., 2021). The

teratology of diatoms, particularly the deformity of their silica frustules, is another useful index that has been investigated in various studies to assess the ecological impact of heavy metal pollutions (Falasco et al., 2009; Ferreira Da Silva et al., 2009; Lavoie et al., 2017). Similarly, it is reported that several bacterial species can be referred as good bioindicators to monitor heavy metal contaminations, while some other bacterial species are ideal for acid mine drainage monitoring (Ma et al., 2022). Bacteria may release some specific proteins due to the presence of toxins in waters, which serve as an early warning to the pollution in ecosystems (Zaghloul et al., 2020). With the rapid development of molecular biology, the microbial community structure can be characterized with higher accuracy through different techniques such as polymerase chain reaction (PCR) and DNA sequencing. Shifts on the community structure can thus be easily analyzed and provide more information on the ecological health.

4.2. Bioremediation

Bioremediation has received rising attention during the past decades. The concept of bioremediation is based on the employment of biological systems (such as bacteria, algae, fungi and plants) in contaminated sites to remove pollutants (heavy metals, pesticides, hydrocarbons, etc.) from soil, water and air. Compared to conventional physical or chemical treatments, bioremediation exhibit a wide range of interests: sustainable, environmentally-friendly and cost-effective (Mehrotra et al., 2021).

Due to the high surface-to-volume properties, microorganisms such as diatoms and bacteria have good capacity to adsorb pollutants from the environments. Diatoms and bacteria are common bioagents that are used for the heavy metal removal from industrial effluents or natural contaminated sites. For example, the metalloproteome in diatom is proved to bind significantly with heavy metals including Cd, Hg, Pb, and so on (Chasapis et al., 2022). Using immobilized bacteria to remove contaminants from industrial wastes is reported as a promising bioremediation approach (Mehrotra et al., 2021). It is commonly reported that these microorganisms play an important role in the mobility of heavy metals and have several mechanisms to remove them from effluents, which are described in more detail as follows.

On one hand, microorganisms can mobilize heavy metals through leaching effect, metabolite chelation and methylation, which lead to the dissolution of insoluble compounds or desorption of heavy metal species. One the other hand, microorganisms may also immobilize heavy metals through the process of precipitation, surface adsorption or intracellular sequestration (Gadd, 2004).

Some chemotrophic bacteria (such as iron- and sulfur-oxidizing bacteria) obtain energy from the oxidation of electron donors (*e.g.*, ferrous ions, reduced sulfur (S) compounds), which leads

to the formation of ferric ions or sulfuric acid respectively and, consequently, the increase in acidity in the surroundings. The decrease in pH (and the change in the redox potential (E_h)) will further change the mobility and speciation of several heavy metals in the environment. For example, under oxidizing and acidic conditions, U(IV) will be oxidized to U(VI) and easily dissolved from the host rock. The leaching effect, or acid mine drainage when it comes to mining activities, will highly increase the mobility of certain heavy metals in the environments. The siderophores, produced by certain bacterial species to assimilate Fe, may also bind heavy metals such as magnesium (Mg), manganese (Mn), chromium (Cr), gallium (Ga) and plutonium (Pu) (Birch and Bachofen, 1990). Additionally, the biomethylation is another process that modifies the solubility, volatility and toxicity of metal compounds (Gadd, 2004). The microbial methylation has been proved to be a successful *in situ* bioremediation method in selenium (Se) contaminated land and water (Frankenberger and Arshad, 2001).

Surface adsorption is one of the principal process for microorganisms to immobilize heavy metals. With a high surface-to-volume ratio, microorganisms are good abstracts to adsorb metal ions. It is reported that the carboxyl groups from PG contribute significantly to the binding of metal cations on gram-positive bacterial cell walls, while phosphate groups are main binding site for the gram-negative bacteria (Gadd, 2004). Metal ions may also enter into the cell via passive diffusion or active membrane transport, known as intracellular sequestration. Inside the cell, heavy metal ions may be bound and precipitate within some specific intracellular structure, *e.g.*, in vacuoles (Perales-Vela et al., 2006; Sharma et al., 2016). It is commonly known that microorganisms excrete a large array of compounds to the environments, *i.e.*, EPS, comprising polysaccharides, proteins, exudates and other metabolites. These organic compounds are also potential binding sites that complex with heavy metal cations from the environment. It is also pointed out that EPS may entrap insoluble metal species or particulate matter such as colloids, clay particles, which display strong affinity for the heavy metal ions (Costa et al., 2018). Precipitations of heavy metals, such as Cr, Se, Pb, technetium (Tc), U, etc., are often induced by the change in redox conditions due to the activity of some dissimilatory metal-reducing bacteria or sulfur-reducing bacteria for example (Finneran et al., 2002; Lloyd et al., 1999, 1998; Oremland et al., 1990; Smith and Gadd, 2000).

Chapter 1: State of the art

Part II: Interactions between microorganisms (diatoms and bacteria) and heavy metals

Contents

1. Interactions between diatoms and heavy metals

1.1. Structure of the diatom cell wall

The silica cell wall of diatoms, constituting a distinct and unique structure, serves as the primary interface between diatoms and the external environment. Hence, the knowledge on the fine structure and biochemistry properties of this interface contributes to a better understanding towards the interaction of diatoms with the external matters, such as the heavy metals.

While the knowledge about diatoms having cell walls made of silica and organic matter has been established for many years since the early 20th century, the arrangement of these two components in relation to each other remained a topic of contention during a long period. At that time, some researchers held the belief that the organic matter was thoroughly impregnated with silica by forming a chemical bond between the two substances, while others suggested that the diatom cell walls comprised an inner pectin layer and an outer silica layer (Reimann et al., 1965).

Later, research found out that the diatom's silica frustule is covered by an organic coating layer, which consists of a large variety of organic molecules such as polysaccharides, amino acids, lipids and glycoproteins, tightly associated with silica (Kröger et al., 1994; Reimann et al., 1965; Swift and Wheeler, 1992).

According to the study of Schmid et al., the diatom biosynthetic frustule is made up of highly pure amorphous silica with different degrees of dehydration. It is reported in the same work that the organic casing normally measures about 8 to 10 nm thick on mature frustules, and accounts for more than one third of the total wall material in the studied diatom species. More precisely, authors pointed out the occurrence of all the 18 common amino acids, with relatively high contents for serine, threonine and glycine, in the organic layer. Besides, five sugars were reported in this layer, including rhamnose, fucose, xylose, mannose and glucose. Moreover, a minor fraction of lipids with atypical composition in the organic casing was suggested in the paper, mainly comprising non-phosphatides such as neutral lipids, free fatty acids, sulfolipid, mono- and digalactosyl diglycerides, with a small fraction of phosphatides, primarily phosphatidyl glycerol (Schmid et al., 1981).

The following figure presents the biochemical structure of diatom's frustule, which is based on a widely referred hypothetical arrangement proposed by R. E. Hecky (Hecky et al., 1973).

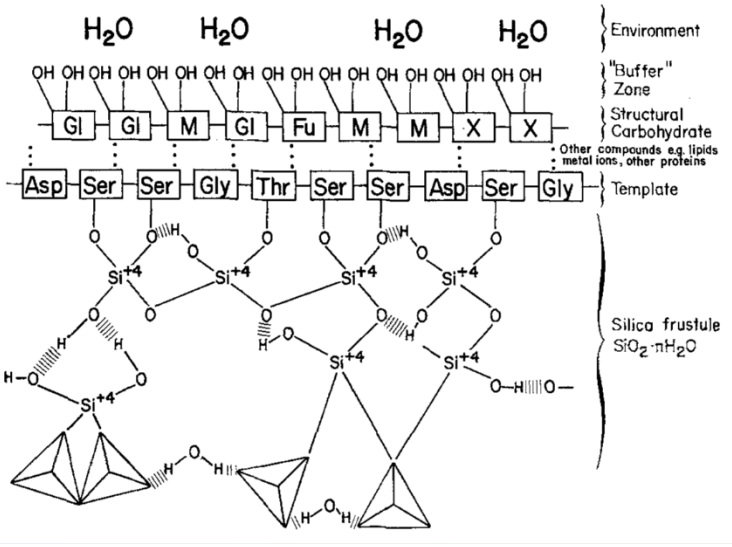

Figure I-7: Hypothetical arrangement of organic layers in the diatom cell wall. Outer layer of polysaccharides consisting of various sugars: *GI* glucose; *M* mannose; *Fu* fucose; *X* xylose. Outward directed hydroxyl groups of sugars depict the hydrophilic buffer zone. Residues in the protein template are: *Ser* serine; *Gly* glycine; *Thr* threonine; *Asp* aspartic acid. Hatched lines represent hydrogen bonds. Tetrahedra emphasize the 3-dimensionality of the silicic acid (and resulting silica) with Si in four-fold coordination with oxygen atoms at the points of the tetrahedra. [reused with permission from Hecky, R.E. and others (1973), Copyright (© 1973, Springer-Verlag), by permission of Marine Biology publication].

Further information on the functional groups located on the frustule can be accessed using spectroscopic techniques. Infrared spectra reveal the occurrence of the following organic groups (Gélabert et al., 2004; Kumar et al., 2018): carboxyl (3400 cm^{-1} for O-H stretching, 1740 cm^{-1} for >C=O stretching of ester/fat acids, and 1400 cm^{-1} for C-O stretching in carboxylates), aliphatic (1455 cm^{-1} for C-H bending in CH_2, 2850 cm^{-1} for CH_3 symmetric stretching, 2930 cm^{-1} for CH_2 asymmetric stretching and 2960 cm^{-1} for CH_3 asymmetric stretching), protein (1640 cm^{-1} for >C=O stretching for primary amides, 1540 cm^{-1} for N-H bending in amides), hydroxyl (3400 cm^{-1} for O-H stretching and 1540 cm^{-1} for O-H bending, with interference of water), silica (1250 –1100 cm^{-1} for Si-O-Si, in particular 1072 cm^{-1}) and polysaccharide (1086 cm^{-1} for C=O stretching of esters).

1.2.Mechanisms of substance exchange

In line with all living cells, diatom cells necessitate an exchange of ions, nutrients, and metabolites with the external environment. The membrane transport mechanisms play a crucial role in the selective or non-selective exchange of diverse substances across the diatom cell membrane. In general, the membrane transport ensures the efficient uptake of essential nutrients, removal of waste, and even cellular communication, thereby providing critical support to algal

survival, growth, and reproduction.

When passing through the tiny perforations (punctae) across the diatom frustule, external substances can have different ways to enter the diatom cell, depending on their chemical nature. The cell membrane transport mechanisms can be mainly classified into passive diffusion and active transport.

Passive diffusion is a transport mechanism that allows the movement of substances across cell membranes without the need for cellular energy. As its name suggests, the passive diffusion follows the Fick's first law, where substances move from areas of high concentration to low concentration, increasing overall system entropy. The rate of passive diffusion is influenced by cell membrane permeability, which is determined by the organization and characteristics of membrane structural lipids and proteins. Passive transport can be further divided into simple diffusion, and facilitated diffusion. Some small molecules such as gasses mainly follow the simple diffusion to move across the cell membrane. The diffusion of water molecules, also known as osmosis, is another example for the simple diffusion mechanism. The facilitated diffusion refers to the passive transport of substances via specific transmembrane integral proteins, which does not require energy as in the case of simple diffusion. However, there exist some differences between these two transports mechanisms. As the facilitated diffusion relies on the transport of some specific protein carriers or membrane-embedded channels, the transport rate of facilitated diffusion can be saturated and substantially influenced by temperature. Some polar molecules or ions cannot diffuse freely across the cell membrane as the later comprises phospholipids in bilayer, which is hydrophobic. As a result, specific protein carriers or ion channels are essential for the transport of these substances such as sodium ions and chloride ions.

Active transport is a fundamental mechanism that involves the transportation of molecules or ions across the cell membrane from regions of lower concentration to higher concentration, against the natural diffusion process. In consequence, active transport relies on cellular energy. There exist two distinct types of active transport mechanisms: primary active transport, which utilizes adenosine triphosphate (ATP) as its energy source, and secondary active transport, which relies on the electrochemical potential difference to drive the movement of substances. Active transport plays a critical role in numerous physiological functions of the cell. One notable example is the sodium-potassium pump, which utilizes ATP to pump sodium ions out of the cell and let potassium ions in, establishing a certain concentration gradient for normal cellular function. This process is regulated and highly selective, with distinct transporters designed for specific molecules or ions. The active transport mechanism allow algal cell to get essential nutrients from the external environment, such as silicic acid (Si source), inorganic carbon species (C source), nitrate (N source), etc., as reported in the literature (Raven, 2010;

Reay et al., 1999; Thamatrakoln and Hildebrand, 2008).

In addition to the transport mechanisms mentioned above, diatoms can assimilate external substances by endocytosis as well. Endocytosis is a process where the substances to be internalized will be surrounded by the cell membrane and then transported into the cell by forming vesicles. It is reported that diatoms assimilate Fe (bound to siderophores) through endocytosis process (Kazamia et al., 2018). Contrary to endocytosis, exocytosis is the inversed process where cell excretes substances by forming vesicles. Exocytosis involves in the formation of frustules for example (De Haan et al., 2023).

1.3.Heavy metals extracellular adsorption

The adsorption of heavy metals on diatom cell surface is normally a physicochemical process which does not require energy produced from the cell. Hence, the main factors that influence this process comprise pH, temperature, contact time, ionic strength, cell wall composition, binding sites concentration on diatom, heavy metals concentration and so on (Kiran Marella et al., 2020). Since the cell metabolic activities generally do not involve in this process, the surface adsorption of heavy metals can occur both on vital cells or nonliving biomaterials (Monteiro et al., 2012). According to Monteiro et al., the extracellular sorption is usually considered as the first stage of interaction between microalgae cells and heavy metals, which is a relatively rapid, passive and reversible process. Authors also revealed a large array of possible interaction mechanisms likely occurring at this stage, comprising physical adsorption, chemisorption, ion exchange, coordination, complexation, chelation, micro-precipitation and entrapment in the polysaccharide structure of the cell wall (Monteiro et al., 2012). In general, interactions between extracellular part of microalgae and heavy metal species that present in cationic form depends strongly on the presence of negatively charged functional groups located on the microalgae cell wall. In fact, the functional groups from lipids, glycoproteins, polysaccharides, amino acids of the organic casing layer over the diatom's frustule are all potential binding sites available for interaction with heavy metal species.

For example, binding of heavy metal cations through counterion interactions with a net overall negatively charged cell surface of microalgae cell wall is reported (Monteiro et al., 2012). Besides, the surface functional groups are commonly associated with metal cations, such as Ca^{2+}, Mg^{2+}, Na^{+}, etc., in natural waters, which might be replaced by heavy metal cations via ion exchange. Research shows that adsorption via ion exchange contributes significantly to the overall metal ion uptake by microalgae cells, which can reach up to 90% as reported in the literature (Suresh Kumar et al., 2015). The combination of cations with ligands containing free electron pairs can be electrostatic or covalent and is called complexation, coordination or chelation. The heavy metal cations are normally the central atom in this case, with interacting

ligands located adjacently or within a critical distance, *i.e.*, inner-sphere complexation or outer-sphere complexation respectively (Suresh Kumar et al., 2015). It is suggested that the amnio and carboxyl groups, the oxygen and N of the peptide bond as well as the imidazole from histidine (an essential amino acid) are responsible for characteristic coordination bonding with metallic ions, *e.g.*, Cu^{2+} (Crist et al., 1981). Precipitation of heavy metal species can also occur on the surface of microalgae. At low pH, the functional groups located on the surface of microalgae are bound with protons and result in a repulsive force for the heavy metal cations (Suresh Kumar et al., 2015). As the pH increases, the functional groups gradually deprotonate and attract heavy metal cations. At the meanwhile, the solubility of heavy metal cations generally decreases, leading to the occurrence of extracellular precipitation, known as biomineralization process (Perpetuo et al., 2011).

1.4.Heavy metals intracellular bioaccumulation

The bound heavy metals can eventually transported inside the diatom cell by passive diffusion or active uptake and potentially involves in some metabolic activities of the cell (Chasapis et al., 2022). Some heavy metals are in fact essential to the metabolic function of the phytoplankton. For example, cobalt (Co), Cd and Zn are involved in carbon dioxide acquisition; Fe and Mn are crucial to C fixation; Zn, Cd and Se relate to silica uptake; Fe and molybdenum (Mo) in N fixation and Fe, Cu and nickel (Ni) in organic N utilization (Baeyens et al., 2018). Besides, Co is a component of vitamin B_{12} which helps to prevent oxidative stress of the cell (Meier et al., 1994). Under Zn-depleted condition, Cd can act as an analogue of Zn and exhibits similar functions for the cell metabolism (Lane and Morel, 2000).

However, other heavy metals, such as Pb and mercury (Hg), are highly toxic to the cell and have diverse impacts on the cell metabolism. The exposure of diatom cell to heavy metal, especially Cr, may induce the production of reactive oxygen species (ROS) in the cell in response to the heavy metal stress (Volland et al., 2014). The accumulation of ROS brings toxic effects to the living cell and will cause DNA damage, lipid peroxidation, membrane disintegration, etc. (Kiran Marella et al., 2020; Suresh Kumar et al., 2015), which will eventually trigger programmed cell death (PCD) process of the cell (Chasapis et al., 2022; Luo et al., 2014).

In consequence, diatoms develop complex defense mechanisms against the negative effects caused by intracellular accumulation of heavy metals, which includes metal exclusion, detoxification, metal ligand production, cell surface ligand modification and antioxidant molecules production (Kiran Marella et al., 2020).

Production of phytochelatins and metallothioneins

To regulate the intracellular heavy metal ion concentration, microalgae including diatoms may produce various metal-binding ligands. These ligands can be classified into two categories: phytochelatins (PCs) and metallothioneins (MTs), which are both cysteine-rich proteins or polypeptides (Cobbett and Goldsbrough, 2002). PCs and MTs both act as heavy metal chelators and have multiple functions in the diatom defense mechanisms under heavy metal stress. Note that the PCs are also referred as Class III MTs in the literature.

The production of PCs requires post-translational activation of PC synthase (the constitutive enzyme) by heavy metals or metalloids (Suresh Kumar et al., 2015). It is reported that *Thalassiosira weissflogii* diatom species possesses a PCs export system to remove Cd-PC complexes from the cytoplasm (Lee et al., 1996). Similar phenomenon is reported for *Phaeodactylum tricornutum* marine diatom species, where the Cd-PC or Pb-PC complexes undergo vacuolarization process and eventually excreted from the cell (Morelli and Scarano, 2001). MTs are gene-encoded polypeptides produced via messenger ribonucleic acid (mRNA) translation (Cobbett and Goldsbrough, 2002). It is stated that long chain MTs can form stable complexes with heavy metals and thus reducing the cytotoxic free-metal ions concentration in the cell (Suresh Kumar et al., 2015). Therefore, PCs and MTs both play a crucial role in the heavy metal detoxification in microalgae.

Storage in vacuoles

The heavy metal-PC or heavy metal-MT complexes usually end up in the vacuole of the cell (Perales-Vela et al., 2006). Indeed, the storage of heavy metals in the vacuole of algae has been widely reported in the literature (Garnham et al., 1992; Monteiro et al., 2012; Perales-Vela et al., 2006; Shanab et al., 2012). The complexation of heavy metals by PCs can facilitate the accumulation in vacuoles or in the cytoplasm as insoluble salts, thus decreasing the toxicity of heavy metals (Perrein-Ettajani et al., 1999). The combinations of metal-polypeptides or metal-proteins that are incorporated into the vacuole can reduce the cytosolic concentrations of metals (Nassiri et al., 1997), facilitating the control of heavy metal ion concentrations in the cytoplasm and preventing or neutralizing the potential toxic effects (Cobbett and Goldsbrough, 2002).

Other mechanisms

It is reported that heavy metals, such as Cd, Cu, may also accumulate inside chloroplast and mitochondria (Avilés et al., 2003; Nagel et al., 1996; Perales-Vela et al., 2006; Soldo et al., 2005). Moreover, the polyphosphate bodies, also named acidocalcisomes or electron-dense vacuoles (Ruiz et al., 2001), are believed to enable storage of nutrients inside the algal cell and also contribute to the heavy metal accumulation in algae (Suresh Kumar et al., 2015; Wang and

Dei, 2006). Heavy metals may also be excreted from the cell via group B transporters, *e.g.*, cation diffusion facilitator. These transporters mediate the exocytosis of excess metal when located in the membrane of the secretory pathway (Suresh Kumar et al., 2015). The efflux of heavy metals back into the extracellular environment help algal cells to resist the toxicity of heavy metals. Another heavy metal detoxification mechanisms include: complexation of metal ions with algae excreted metabolites that may extracellularly bind with heavy metals; change of metal's oxidation state, so a toxic heavy metal species may be transformed into a less toxic one; vaporization and elimination of a toxic metal by forming volatile chemical species; enzymatic methylation that prevents toxic heavy metals from reacting with -SH groups inside the algal cell (Monteiro et al., 2012).

2. Interactions between bacteria and heavy metals

2.1.Structure of the bacterium cell membrane

The cell wall of bacteria plays an important role in maintaining cell shape and structural integrity of bacteria. It is generally a mesh-like structure that possesses complex chemical compositions (Dörr et al., 2019). The majority of the bacterial cell walls can be classified into two groups, depending on the Gram-negative or Gram-positive characteristics of bacteria.

Gram-negative bacteria possess an inner, cytoplasmic membrane enveloped by a thin layer of PG and an outer membrane comprising lipopolysaccharide (LPS), phospholipids, lipoproteins and proteins (Jiang et al., 2004; Rajagopal and Walker, 2015). The outer membrane plays a vital role as a permeability barrier, regulating the movement of ions, nutrients, and environmental toxins in and out of the cell. Additionally, it contributes to osmoprotection, safeguarding the bacterium against changes in osmotic pressure (Rajagopal and Walker, 2015). Depending on the specific applied measurement technique, the PG layer of a typical Gram-negative bacterium measures between 1.5 and 15 nm (Vollmer et al., 2008).

Gram-positive bacteria lack a protective outer membrane comparing with Gram-negative bacteria. In compensation, they possess a much thicker cell wall comprising several layers of PG, which is estimated as thick as 30 to 100 nm (Rajagopal and Walker, 2015), or between 20 and 80 nm thick as suggested by other researchers (Mai-Prochnow et al., 2016). Moreover, the PG mesh of Gram-positive bacteria can be embedded with secondary cell wall polymers, *e.g.*, wall teichoic acids (polymer of glucopyranosyl glycerol phosphate), teichuronic acids (similar to the former one with replacement of phosphate groups by carboxyl groups) and capsule polysaccharides, which are covalently associated to the PG layer (Dörr et al., 2019; Jiang et al., 2004).

PG is the main component of the bacterial cell wall both for Gram-negative or Gram-positive bacteria, which accounts for 40 to 80% of the dry weight of the Gram-positive bacterial cell wall (Jiang et al., 2004). From the chemical composition point of view, PG is a mesh of polysaccharide strands (composed of a poly-[N-acetylglucosamine (GlcNAc)-N-acetylmuramic acid (MurNAc)] backbone) crosslinked via short peptide bridges attached to the MurNAc residues (Vollmer et al., 2008), as is illustrated in **Figure I-8**. Note that even in the same bacterial species, variations in terms of the fine structure can be observed, depending on the growth conditions such as bacterial growth phase, medium composition, intra/extracellular growth or presence of antibiotics (Vollmer et al., 2008).

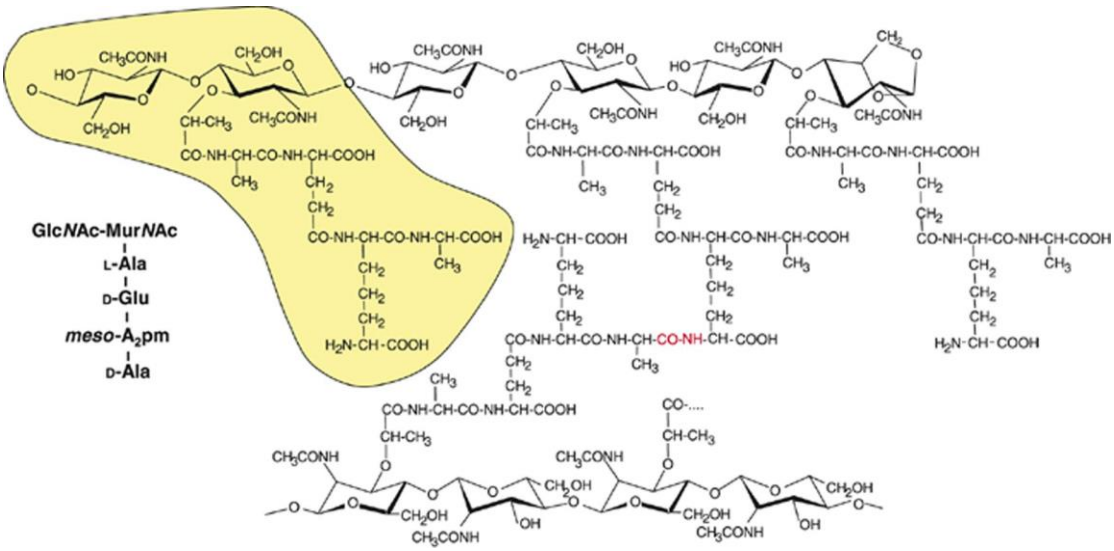

Figure I-8: Structure of the peptidoglycan of Escherichia coli. The glycan strands consist of alternating, β-1→4-linked N-acetylglucosamine (GlcNAc) and N-acetylmuramic acid (MurNAc) residues, and are terminated by a 1,6-anhydroMurNAc residue. The yellowish labelled part represents the basic disaccharide tetrapeptide subunit (monomer), which is also written with the conventional amino acid and hexosamine abbreviations on the left-hand side. The middle part shows a cross-linked peptide, with the amide group connecting both peptide stems drawn in red. [reused with permission from Waldemar Vollmer and others (2008), Copyright (© 2008, Oxford University Press), by permission of FEMS Microbiology Reviews publication].

In addition to PG layer, many bacteria are coated with a proteinaceous layer, called S-layer, that consists of one or more glycoproteins forming through self-assembly process into a two-dimensional crystalline array (Fagan and Fairweather, 2014). It can be found in almost all archaea as well as in many Gram-negative and Gram-positive bacteria. The bacterial S-layers are generally 5 to 10 nm thick and characterized by highly porous protein lattices, exhibiting porosity ranging from 30% to 70%, with uniform pores in the range of 2 to 8 nm (Sleytr et al., 2014, 1997). S-layers are connected to the rigid PG layer in Gram-positive bacteria, whereas in

the more intricate Gram-negative bacterial cell envelope, they adhere to the LPS of the outer membrane (Sleytr et al., 2014). In **Figure I-9**, the arrangement of PG, LPS and S-layer within different prokaryotic cell (archaea and bacteria in particular) envelops is elucidated.

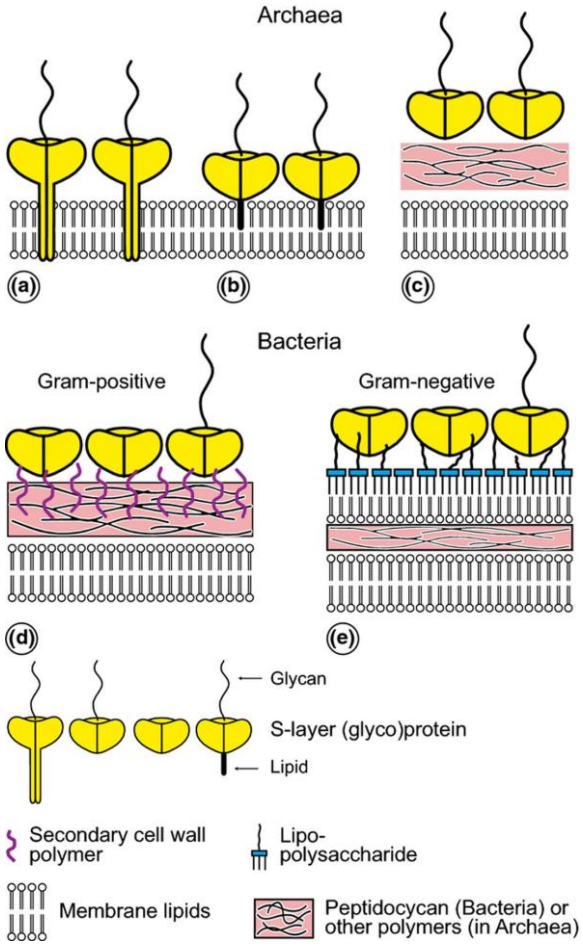

Figure I-9: Schematic illustration of the supramolecular architecture of the major classes of prokaryotic cell envelopes containing surface (S) layers. S-layers in archaea with glycoprotein lattices as exclusive wall component are composed either of mushroom-like subunits with pillar-like, hydrophobic trans-membrane domains (a), or lipid-modified glycoprotein subunits (b). Individual S-layers can be composed of glycoproteins possessing both types of membrane anchoring mechanisms. Few archaea possess a rigid wall layer (*e.g.*, pseudomurein in methanogenic organisms) as intermediate layer between the plasma membrane and the S-layer (c). In Gram-positive bacteria, (d) the S-layer (glyco)proteins are bound to the rigid peptidoglycan-containing layer via secondary cell wall polymers. In Gram-negative bacteria, (e) the S-layer is closely associated with the lipopolysaccharide of the outer membrane. [reused with permission from Uwe B. Sleytr and others (2014), Copyright (© 2014, Oxford University Press), by permission of FEMS Microbiology Reviews publication].

Using infrared (IR) spectroscopy, it is elucidated by various studies that the bacterial cell wall is characterized by a large array of functional groups, dominated by carboxyl, amide, phosphate,

hydroxyl and carbohydrate related moieties. Specifically, it is suggested that phosphate functional groups can present in inorganic form, such as orthophosphate and its oligomers, or in organic forms, such as phosphate mono- and diesters (Jiang et al., 2004). Besides, it is pointed out in the same work that carboxyl and phosphate functional groups are sensitive to pH variations in aqueous solution and their deprotonation result in the net negative surface charge of bacteria within the pH range of 4 to 9.

Despite the fact that Gram-negative and Gram-positive bacteria differ in the structural characteristics regarding their cell walls, the metal adsorption behaviors of these two groups of bacteria are identical at macroscale (Jiang et al., 2004; Yee and Fein, 2003).

2.2.Mechanisms of substance exchange

Similar to the case of diatoms, the biological interfaces (*i.e.*, PG, LPS, S-layer) surrounding the bacterial cells act as selective permeability barriers and protect the cells from harmful substances. Hence, they play an important role in the substances exchange between bacterial cell and external environments and also in the assimilation of some elements or nutrients essential for bacterial metabolic activities. In these outer layers, different types of transport channels are reported to participate in the passive diffusion or active transport of various molecules (Nikaido and Saier, 1992).

Once the nutrient molecules are transported into the periplasm (defined as the space between the outer layers and the cytoplasmic membrane of the bacterial cell), they might enter across the cytoplasmic membrane via various transport mechanisms. Once again, these mechanisms are similar to that have been discussed for diatoms, including facilitated diffusion, secondary transport, group translocation (*e.g.*, phosphotransferase system, a distinct method applied by bacteria for sugar uptake) and primary active transport (energized by ATP hydrolysis) (Nikaido and Saier, 1992).

2.3.Heavy metals extracellular adsorption

Like any living cells, bacteria interact with heavy metals via various mechanisms, which can be categorized into extracellular adsorption and intracellular accumulation, or into metabolism independent or metabolism dependent mechanisms. The heavy metals extracellular adsorption is generally a metabolism independent process. The binding of metal ions to bacterial cell surfaces involves a variety of mechanisms, such as physical interactions (electrostatic or van der Waals interactions) or chemical interactions (displacement of attached metal cations by ion exchange), complexation, diffusion, surface adsorption or precipitation (Priyadarshanee and Das, 2021), as presented in **Figure I-10**.

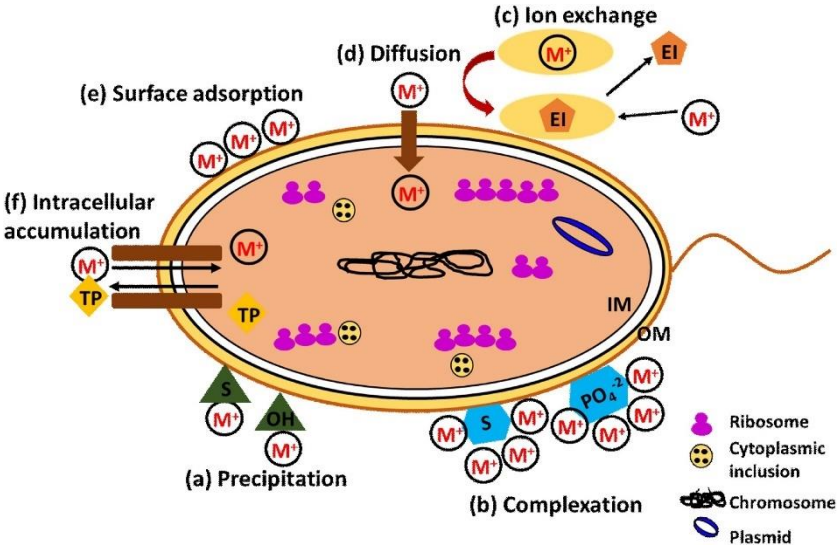

Figure I-10: Mechanisms involved in heavy metal biosorption by bacterial biomass. (a) Precipitation involves chemical interaction between the cell surface and metal species, (b) Complexation of heavy metals occurs by interaction of the metal ions with the surface-active groups of bacterial biomass, (c) Exchange of bivalent metal ions occurs with the counter ions present on the bacterial cell in the ion exchange mechanism, (d) Diffusion is the simple process of biosorption without the involvement of any rate-limiting step, (e) Surface adsorption is a rapid and reversible process in which metal cations bind to the bacterial surface anions via non-specific attraction forces, and (f) Intracellular accumulation of heavy metals takes place by the transport of metal ions across the cell membrane. IM: Inner Membrane, OM: Outer Membrane, EI: Exchangeable Ions, TP: Transport Proteins. [reused with permission from Monika Priyadarshanee and others (2021), Copyright (© 2020, Elsevier Ltd), by permission of Journal of Environmental Chemical Engineering publication].

Generally speaking, the anionic nature and metal-binding affinity of the cell wall mainly arise from the presence of negatively charged functional groups found in the PG, teichoic acids, and teichuronic acids of Gram-positive bacteria, as well as the PG, phospholipids, and LPS of Gram-negative bacteria (Priyadarshanee and Das, 2021). These functional groups can associate metal ions and form monodentate and polydentate complexes (Kanamarlapudi et al., 2018). Metal binding through precipitation takes place when metal ions react with functional groups on the bacterial surface, leading to the formation of insoluble organic metal precipitates that remain attached to the microbial cells. For example, it is reported that *Escherichia coli* C90 bacteria produces alkaline phosphatase to precipitate the metal cations, which are applied for removal of toxic heavy metals (such as Ni(II), Cd(II), Cr(III), Cr(VI) and Co(II)) from various industrial effluent (Priyadarshanee and Das, 2021).

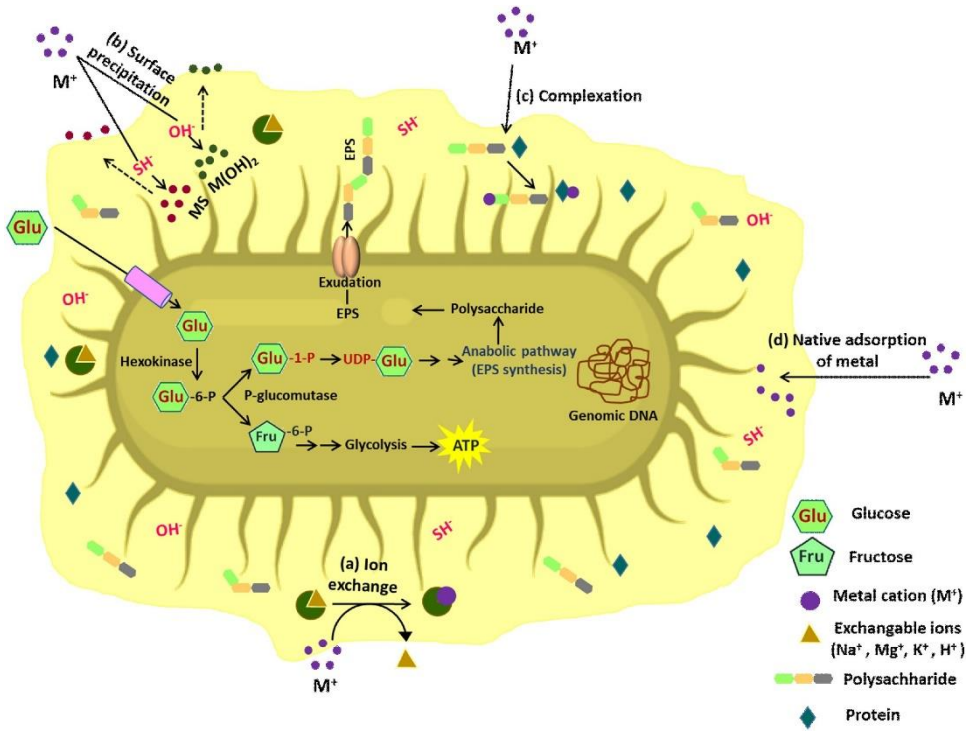

Figure I-11: Mechanisms of interactions between EPS and heavy metal ions. Bacterial EPS is synthesized metabolically using glucose molecules. Glucose is converted to glucose 6-phosphate by hexokinase, which either initiates glycolysis pathway or forms glucose 1-phosphate and further converted to UDP glucose. UDP-glucose then enters into the anabolic pathway for synthesis of EPS. The complex composition of bacterial EPS exhibits several mechanisms for metal binding, (a) Ion exchange between the metal cations and negatively charged functional groups of polysaccharides in EPS, (b) Surface precipitation of metal is induced by pH of the medium as well as the anionic charge of surface active sites, (c) Complexation involves metal binding by the reaction between heavy metals and the proteins and polysaccharides of EPS, and (d) Native adsorption of the metal ions occurs at their native state onto the porous surface of the EPS. [reused with permission from Monika Priyadarshanee and others (2021), Copyright (© 2020, Elsevier Ltd), by permission of Journal of Environmental Chemical Engineering publication].

It is well documented that bacteria produce EPS, a vital component of biofilms, to help them colonize in various environments even under extreme conditions. Comparing to free-living cell, bacteria that live in the biofilm display higher resistance to hostile environmental conditions (Priyadarshanee and Das, 2021). Microbes including bacteria intentionally produce EPS for two primary purposes: (i) as secretions in biofilms, which facilitate secure attachment and improve their local environment; (ii) as waste products resulting from metabolic excess (Decho and Gutierrez, 2017). EPS are primarily found on the outer surface of bacterial cells. These substances consist of diverse organic macromolecules, including high molecular weight compounds like polysaccharides, proteins, nucleic acids, phospholipids, and other low

molecular weight non-polymeric components. Consequently, a wide range of functional groups such as amine, amide, sulfhydryl, carboxyl, hydroxyl and phosphate groups are present in EPS, provide binding sites for heavy metals through various interaction mechanisms such as ion exchange, surface precipitation, complexation, and native adsorption (Priyadarshanee and Das, 2021), as illustrated in **Figure I-11**. Additionally, it is pointed out that bacterial cells covered with EPS provide much more binding sites and thereby show higher affinity for heavy metals adsorption than the EPS-removed cells (Wei et al., 2011).

2.4.Heavy metals intracellular bioaccumulation

As is mentioned in the section for diatoms, intracellular accumulation of heavy metals is generally a metabolism dependent process, which can only be carried out by viable cells (Priyadarshanee and Das, 2021). When entering the bacterial cell, toxic heavy metals may be transformed into non-bioavailable forms through binding with MTs, which are low-molecular-mass cysteine-rich proteins, or with metallochaperones. These intracellular proteins produced by bacteria help reducing the free heavy metal ion concentrations within the bacterial cytoplasm, thus contributing to the detoxification of heavy metals (Etesami, 2018). The excretion of these binding proteins can also result in the bioprecipitation of heavy metals in forms of hydroxides, carbonates, phosphates or sulfides. Nevertheless, it is stated that the overexpression of MTs may lead to enhanced metal sequestration in bacteria (Hansda et al., 2016).

3. Interactions of uranium with diatoms and bacteria: A state-of-the-art review

3.1. Uranium

Generalities

Uranium, with the symbol U and atomic number 92, is a naturally radioactive chemical element. It belongs to the actinide series in the periodic table and is characterized by its silvery-gray metallic appearance. Notably, U possesses the highest atomic weight and atomic number among all naturally occurring elements. In fact, U is one of the primordially occurring elements on Earth, which signifies that U was formed during or after the Big Bang and has existed since before the formation of Earth. U has three naturally occurring isotopes: U-238, U-235, U-234, both of which decay by emitting an alpha particle. U-238 is the most abundant U isotope on Earth (slightly less than 99.28%), followed by U-235 with a natural abundance of about 0.71%. U-234 is a trace isotope which only accounts for about 0.0054%. There also exist another isotopes of U such as U-239, U-237, U-236 and U-233, which are all radiogenic. U-238 has a half-life of about 4.463×10^9 years (to compare, the age of Earth is about 4.54×10^9 years

(Manhes et al., 1980)), signifying that the current amount of U on Earth is roughly half of what it was when the Earth was formed. U-235 has a shorter half-life, about 7.04×10^8 years. The decay chains of U-238 and U-235 are presented in **Figure I-12**.

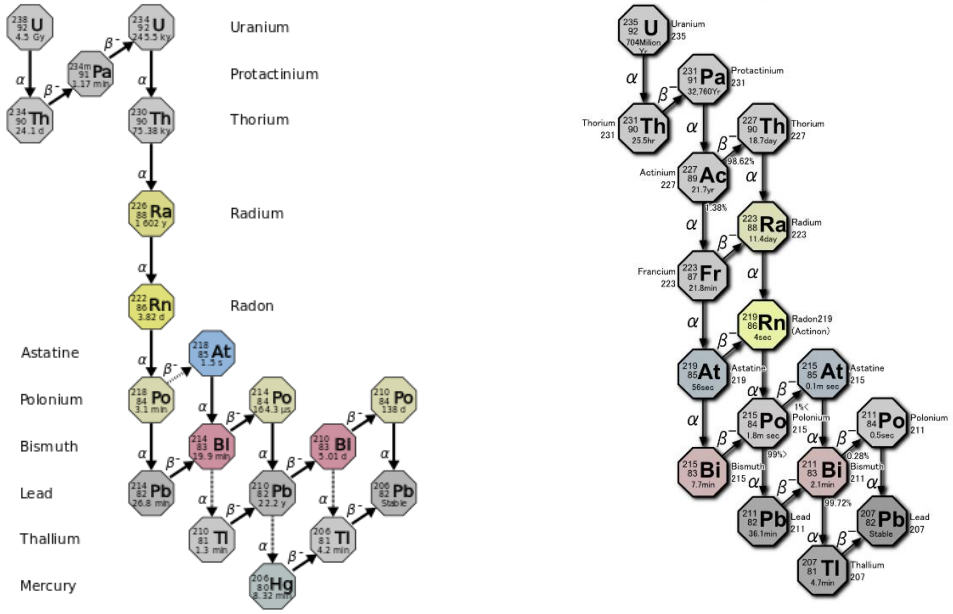

Figure I-12: Decay chains of U-238 (on left) and U-235 (on right), work by Tosaka, CC BY 3.0, source: https://commons.wikimedia.org/w/index.php?curid=33293646, https://commons.wikimedia.org/w/index.php?curid=5531115

According to the 29th edition of "Red Book", *i.e.*, "Uranium 2022: Resources, Production and Demand", a joint report by Nuclear Energy Agency (NEA) and International Atomic Energy Agency (IAEA) (published in 2023, available on NEA website https://www.oecd-nea.org), there exist approximately 7.9 million tonnes of identified recoverable U resource on Earth (<USD 260/kg of U).

Some important U production and mining countries are for example Namibia, Canada, Australia, Uzbekistan, and Russia. Among these countries, Australia has the most abundant U resources around the world, which accounts for one quarter of the total identified recoverable U resources (<USD 260/kg of U) on Earth.

Origins and applications

As is mentioned above, U is a primordial radioelement. It was until 1700s that the German chemist Martin Heinrich Klaproth discovered a yellowish U compound in his laboratory. Few decades later, in 1841, the metallic U was isolated for the first time by Eugène-Melchior Péligot.

U is used in the military sector, with the most known application as fissile material in nuclear weapons. When an atom of U-235 is bombarded by a neutron (a slow neutron, or called thermal neutron), it will fission into two nuclei, releasing more than two neutrons and a huge amount of binding energy (about 200 MeV (megaelectronvolt) of energy) at the same time. When the ejected neutrons from the previous fission reaction is absorbed by another U-235 atoms in the medium, a new fission reaction will take place again. This phenomenon is called nuclear fission chain reaction (**Figure I-13**). Fission reaction can also occur with other fissile isotopes, for example, Pu-239. Compared to the energy released by a typical chemical reaction (on the order of a few electronvolts), the energy released by one fission reaction is colossal, making the nuclear weapons lethal.

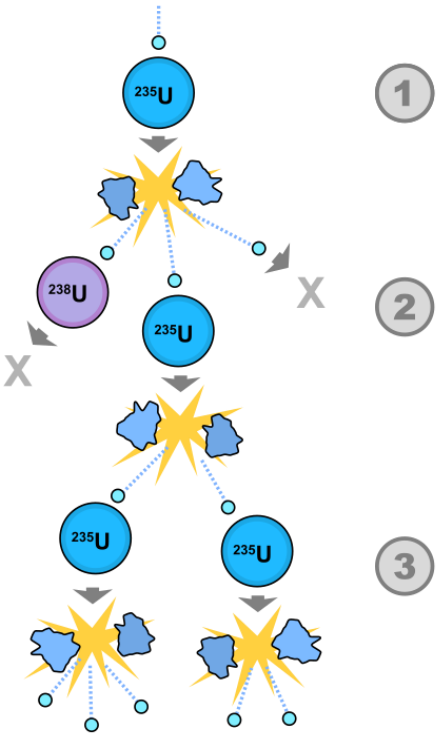

Figure I-13: Nuclear fission chain reaction

Another use of U in the military sector is high-density penetrators. Depleted U is used to fabricate the ammunition, alloyed with other elements in minute percentage. Due to its high density, depleted U can also be used as a shielding material to store or transport radioactive materials.

In the civilian sector, U is used as nuclear fuel in nuclear power plant. Since the discovery of its ability to fission by Otto Hahn and Fritz Strassmann in 1938, U has received great attention by various research teams for the exploitation of nuclear power. The first artificial self-sustained nuclear chain reaction, Chicago Pile-1, was realized in 1942 by Enrico Fermi's team. In order to use the nuclear power in a peaceful way, the idea is to control the nuclear fission chain

reaction by using neutron poison for example.

Nuclear power is indeed a promising energy source. It is reported that 1 kg of U-235 can theoretically produce 2×10^{13} J (joule) of energy, equivalent to the energy produced by 1500 tons of coal (Emsley, 2001). It is generally believed that nuclear power is a safe, sustainable energy source that reduces carbon emissions. As of September 2022, there are 437 civilian fission reactors in the world, with overall capacity of 393 GW (gigawatt) (data from PRIS, IAEA, https://pris.iaea.org/pris/home.aspx).

Chemical properties

U can exist in five oxidation states: +2, +3, +4, +5 and +6. The most common forms of U oxide are uranium dioxide (UO_2) and triuranium octoxide (U_3O_8), which are solid and insoluble in water. On Earth, the primary U ore mineral is uranium dioxide (UO_2), also called as uraninite or pitchblende. Besides, there exist a huge range of other U minerals in nature where U co-precipitates with other metal ions such as calcium (Ca) in autunite, Mg in saleeite, Cu in torbernite, etc. The U ores form in extremely diverse geological settings and differ in ore genesis mechanisms. According to IAEA, U deposits can be classified into 15 main categories, such as unconformity-related deposits (represented by the Athabasca Basin in Canada and the McArthur Basin in Australia for example), sandstone deposits, vein deposits (intragranitic veins in the Central Massif in France), phosphorite deposits and so on. It is well reported in the literature that U usually co-occurs with phosphate rocks as well (Bituh et al., 2009; Menzel, 1968), which might become problematic for the phosphate fertilizer production considering its application in agriculture. In fact, the application of phosphate fertilizers is believed to be the main source for U contamination in agricultural lands. For example, in Germany, it is reported that the application of phosphate fertilizers have led to an average cumulative loading of 1 kg of U per hectare (Schnug and Lottermoser, 2013). Additionally, coal and oil industry may also produce residues that contain U and other radioelements.

In aqueous solution, U may present in different oxidation states (+3, +4, +5, +6) in ionic forms: U^{3+}, U^{4+}, UO_2^{+} and UO_2^{2+}, while the +4 and +6 oxidation states are the most stable and the most commonly occurring in the environment. The UO_2^{2+} ion is stable under oxidizing and acidic conditions, and can strongly complex with various oxygen-containing ligands such as carbonate, sulfate and phosphate. The uranyl ion can also form complexes with organic chelating agents such as acetate and humic acids.

Transport in the environment

U is a rather abundant heavy metal on Earth comparing to some rare metals such as gold and silver. Its average concentration in the Earth's crust reaches approximately 3 mg/kg (Kalin et

al., 2005). In open oceans, it is estimated that U concentration varies from 0.3 to 7 µg/L, with an average of about 3.3 µg/L (Ku et al., 1977). It is reported that U concentration in groundwaters ranges from 0.1 µg/L to 10 mg/L. What's more, In some extreme cases, *e.g.*, in the vicinity of U mining sites, U concentration in mine-discharge water can increases to a level as high as 31.5 mg/L (Brugge et al., 2005).

The transport of U (**Figure I-14**) depends strongly on the environmental biogeochemistry properties. The oxidation states play a determining role in the mobility of U: in reduced form (+ 4 oxidation state), U is insoluble and mostly present in U ores, while in oxidized form (+ 6 oxidation state) U becomes highly mobile in the environment by forming various soluble complexes, colloids and so on. The main processes that determine the U behavior in the environment include complexation, sorption (surface adsorption, bio-accumulation, etc.), microbial redox interactions and so on.

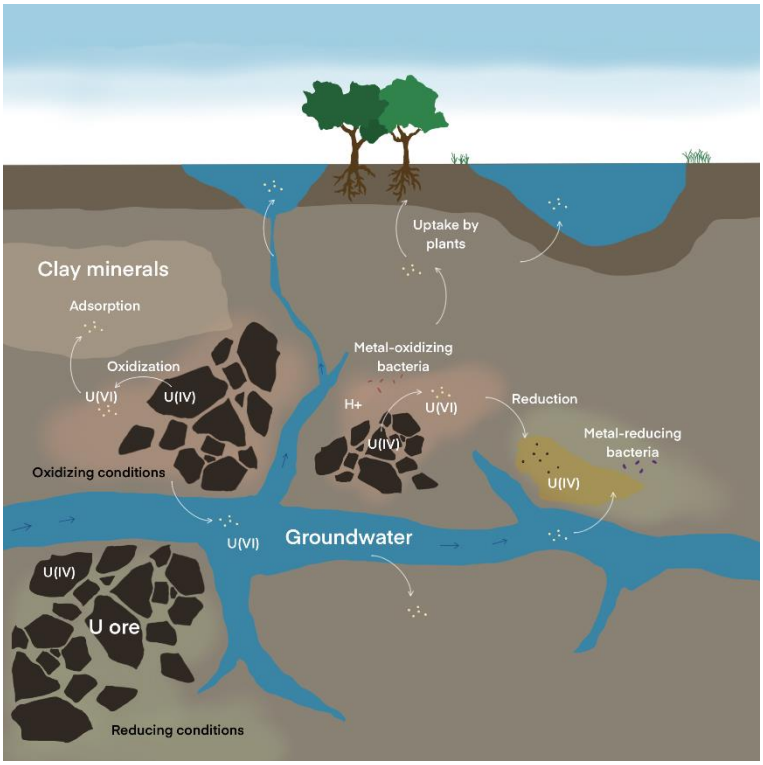

Figure I-14: U transport and migration in the environment.

As is mentioned in previous section, the presence of inorganic or organic ligands (carbonate, citrate or soluble humic acid for example) in waters can enhance the dissolution of U from the host rocks by forming soluble complex (Huang et al., 1998; Sachs and Bernhard, 2011). The dissolution of U is usually induced by microbial activity as well. Certain aerobic microorganisms, such as ferrous- and sulfur-oxidizing bacteria, can catalyze the oxidation of reduced metals or compounds and create an oxidizing acidic condition which results in the

oxidation of U(IV) to U(VI). Consequently, these aerobic bacteria are used for chemical extraction of low-grade U ores through aerobic acid bioleaching process (Bosecker, 1997).

After being mobilized into the environment, U can be retained (and so immobilized once again) by some naturally occurring substances via different interaction mechanisms, such as adsorption on crystalline and amorphous Fe oxides (Duff et al., 2002; Sato et al., 1997), ion exchange in clay minerals (Bachmaf and Merkel, 2011) or binding with organic matter such as humic substances (insoluble fraction). To describe the surface adsorption, various models are developed, including Langmuir and Freundlich isotherms.

In addition, some anaerobic microorganisms, such as metal reducing bacteria, can also contribute to the retard of U migration in the environment through reduction of U(VI) back to U(IV). Hence, anaerobic microbial processes can be applied for the removal of U(VI) from contaminated groundwater, by precipitating soluble U(VI) into insoluble U(IV). Microorganisms or plants can also release biogenic ligands (EPS or DOC) to precipitate heavy metals *in situ* as a detoxification approach. Like other heavy metals, U can also accumulate inside microorganisms or plants, known as bio-accumulation process. Some plants (water lily, mustard, etc. (Chen et al., 2021)) display high tolerance and uptake towards U, making them ideal candidate (hyperaccumulators) for the phytoremediation in U contaminated soils. Due to the uptake by the living organisms, U will eventually enter the food web and potentially cause health issues for humans.

Toxicology of uranium

This section mainly presents the toxicology of U to humans rather than other living organisms. In the normal adult body, U burden is estimated to 90 µg, distributed across various tissues. The majority, constituting 66%, is found in the skeleton, followed by 16% in liver, 8% in kidney, and 10% in other tissues (Carvalho et al., 2023).

Exposure to U can occur through various routes, including inhalation of dust and ingestion. It is suggested that in occupational settings, U systemic absorption from inhaled U-containing dusts ranges from 0.76 to 5%. Gastrointestinal absorption of U can vary from < 0.1 to 6%, depending on the solubility of the U compound. Furthermore, studies on volunteers indicate that approximately 2% of U from drinking water and dietary sources is absorbed in humans. Specifically, U absorption is reported to be 0.2% for insoluble compounds and 2% for soluble hexavalent compounds (Leggett and Harrison, 1995; Smith, 1995; Spencer et al., 1990).

U has been identified as a nephrotoxin, and its toxic effects primarily stem from its chemical properties rather than its radioactivity. Insoluble compounds show low toxicity due to poor

absorption from the gastrointestinal tract. However, when inhaled, U can cause lung disease. Studies on respiratory diseases related to U exposure primarily report noncancerous damage to alveolar epithelium cells. Such changes are characterized by interstitial inflammation of the alveolar epithelium, eventually leading to serious diseases that impair lung function (Ran et al., 2020). Once ingested, U may also cause DNA damage or fragmentation as a result of exposure to low-level ionizing radiation. This implies that ionizing radiation can initiate or promote carcinogenesis while also interfere with reproduction and development (Brugge and Buchner, 2011).

Overall, understanding the distribution of U in the human body, the potential routes of exposure, and the combined effects of its chemical toxicity and radiological impact is crucial in assessing and addressing the health concerns associated with this element.

3.2.Interaction of uranium with diatoms

Diatoms are often considered as bioindicators to study the impact of acid mine drainage (AMD) or mining waste from U mining activities on the ecological health of aquatic ecosystems. A study demonstrated that diatom community structure is clearly affected by mining effluents, where sensitive species (*e.g.*, *Eunotia pectinalis var. undulata*, *Psammothidium rechtensis*, *Gomphonema lagenula* and *Pinnularia major*) are replaced by AMD- or metal-tolerant species (*e.g.*, *Neidium alpinum*, *Gomphonema*) (Herlory et al., 2013). The effects of naturally occurring radioactivity present in mineral springs on the diatom community structure was also investigated. In fact, it was suggested that the radioactivity did not trigger significant differences on the algal communities in a case study on different mineral springs in France, but a correlation was clearly observed between the rate of the diatom's teratological forms and the radon (Rn) activity in these springs (Millan et al., 2020).

However, the mechanism of interaction between U and diatoms is poorly documented in the literature. There is an extreme lack of research and understanding of the U-diatom interaction at the microscopic and molecular level. Most of the existing studies focus on the application of diatomaceous earth (fossil of diatom frustules) in the treatment of mining discharge or effluents to remove U and other heavy metals (Khraisheh et al., 2004; Sprynskyy et al., 2015, 2010).

3.3.Interaction of uranium with bacteria

Different from the case of diatoms, studies focusing on the interactions between U and bacteria are relatively well documented in the literature. Most of these studies are aimed at demonstrating the potential and application of bacteria in bioremediation. The mechanisms of the interaction of U with bacteria are to a large extent the same as that with heavy metals in general. It is commonly believed that bacteria can immobilize U via four basic mechanisms: (i)

microbial mediated reductive precipitation of U(VI) to U(IV); (ii) biosorption and complexation with proteins, polysaccharides or other microbial biomolecules; (iii) U bioaccumulation by cells; (iv) biomineralization or precipitation of U(VI) with phosphates, carbonates (Choudhary and Sar, 2015). Bacterial activities may also mobilize U, *e.g.*, by oxidation of U(IV) to U(VI).

Since U has no essential biological function, it is transported into microbial cells due to increased membrane permeability as a result of U toxicity for example. Furthermore, there is no direct evidence that confirms the presence of U transporters in microorganisms. Therefore, the U uptake in bacteria is considered to be a metabolism-independent process (Merroun and Selenska-Pobell, 2008).

The most documented mechanisms of the interaction between U and bacteria include: (i) surface adsorption (on the cell wall or within the EPS) through complexation with carboxyl and phosphate functional groups; (ii) extracellular or intracellular bio-precipitation via enzymatically mediated bio-reduction or bacterial phosphatase activity, where precipitation or co-precipitation of U-phosphate compounds is commonly observed in form of meta-autunite mineral phase. **Table I-1** summarizes almost the majority of mechanisms described in relevant research existing in the literature.

Table I-1: Overview of possible interactions between uranium and bacteria. EPS: extracellular polymeric substances, G-N: Gram-negative, G-P: Gram-positive.

Bacteria		Remarks	Reference
Reduction			
Desulfosporosinus hippie DSM 8344^T	Sulfate-reducing bacteria	Bio-reduction of uranyl(VI)-lactate complex potentially via a single-electron transfer mechanism, U(V) is detected	(Hilpmann et al., 2023)
Anaeromyxobacter dehalogenans 2CP-C	G-N myxobacteria	Hydrogen as electron donor	(Wu et al., 2006)
Clostridium spp.	G-P, anaerobic bacteria	U(III) is also detected	(Francis et al., 1994; Suzuki et al., 2003)
Desulfovibrio spp. *Desulfosporosinus* spp.	Sulfate-reducing bacteria	Enzymatic reduction (cytochrome c_3)	(Lovley and Phillips, 1992; Payne et al., 2002; Suzuki et al., 2005, 2003)
Geobacter spp. *Shewanella* spp.	Anaerobic Fe(III)-reducing bacteria	Enzymatic reduction	(Coates et al., 2001; Lovley et al., 1991)
Geobacter sulfurreducens		Enzymatic reduction	(Lloyd et al., 2003)
Rhodopseudomonas palustris	G-N	Bio-reduction of U(VI)-carboxylate to U(IV)-phosphate or U(IV)-carboxylate	(Llorens et al., 2012)
Salmonella subterranea sp. nov.	G-N, acidotolerant bacteria		(Shelobolina et al., 2004)
Thermoterrabacterium ferrireducens	G-P, thermophilic bacteria	Reduction of U(VI) to form U(IV) precipitates in form of ningyoite $CaU(PO_4)_2 \cdot H_2O$	(Khijniak et al., 2005)
Thermus	Thermophilic bacteria		(Kieft et al., 1999)
Veillonella alcalescens	G-N	Hydrogen as electron donor	(Woolfolk and Whiteley, 1962)

Oxidation			
Acidithiobacillus ferroxidans	G-N, chemolithoautotrophic acidophilic bacteria	Aerobic oxidation at pH 1.5	(DiSpirito and Tuovinen, 1982)
Geobacter metallireducens	G-N	Anaerobic and nitrate-dependent enzymatic oxidation at neutral pH conditions	(Finneran et al., 2002)
Thiobacillus denitrificans	G-N, chemolithoautotrophic bacteria	Anaerobic and nitrate-dependent oxidation at neutral conditions	(Beller, 2005)
Biosorption and complexation			
Acidithiobacillus ferrooxidans	G-N, chemolithoautotrophic acidophilic bacteria	Biosorption on the cell surface (cell wall and extracellular polysaccharides)	(Merroun et al., 2003)
Acidithiobacillus ferrooxidans	G-N, chemolithoautotrophic acidophilic bacteria	Formation of U/fructose phosphate complexes on EPS	(Merroun and Selenska-Pobell, 2008)
Acidovorax facilis	G-N	Binding of U with phosphate, phosphoryl and carboxyl groups of LPS and PG of the cell wall	(Krawczyk-Bärsch et al., 2018)
Arthrobacter; *Bacillus*; *Citrobacter*; *Corynebacterium*; *Escherichia*; *Micrococcus*; *Nocardia*; *Pseudomonas*; *Thiobacillus*; *Zooglea*		Surface adsorption	(Nakajima and Tsuruta, 2004)
Bacillus sphaericus (*Lysinibacillus sphaericus*)	G-P	Formation of inner sphere complexes with organic phosphate groups on the cell surface	(Panak et al., 2002)
Bacillus sphaericus JG-A12	G-P	Complexation with carboxyl and phosphate groups of the S-layer	(Merroun et al., 2005)

Bacillus subtilis	G-P	Coordination with phosphate and carboxyl groups	(Fowle et al., 2000)
		Formation of uranyl-hydroxide, uranyl-carbonate, and calcium-uranyl-carbonate surface complexes	(Gorman-Lewis et al., 2005)
		Complexation with phosphoryl groups on the cell wall at low pH, with carboxyl groups at higher pH	(Kelly et al., 2002)
Cupriavidus metallidurans CH34	G-N	Biosorption of U(VI)-phosphate and U(VI)-carboxylate	(Llorens et al., 2012)
Magnetospirillum magneticum AMB-1	G-N	PG as main sorbent of U(VI) on the cell wall	(Krawczyk-Bärsch et al., 2022)
Microbacterium		Complexation with organically bound phosphate groups on the cell surface at pH 2	(Nedelkova et al., 2007)
Myxococcus xanthus	G-N	Binding with organic phosphate groups on the cell wall at pH 2	(Jroundi et al., 2007)
Pseudomonas fluorescens	G-N	Accumulation on the cell surface	(Francis et al., 2004)
		Complexation with carboxyl and phosphoryl groups	(Lütke et al., 2012)
Shewanella putrificiens	G-N	Adsorption to hydroxides on the cell surface	(Haas et al., 2001)
Sphingomonas sp. S15–S1 *Bacillus sphaericus* JG-7B	G-N G-P	Binding with carboxyl, phosphate, hydroxyl and amine groups	(Merroun and Selenska-Pobell, 2008)
Stenotrophomonas maltophilia JG-2	G-N	Formation of U/fructose phosphate complexes at pH 2	(Merroun and Selenska-Pobell, 2008)
Biomineralization and precipitation			
Aeromonas hydrophila	G-N	Co-precipitation with nanocrystals of hydroxyapatite (Ca-P-U precipitates)	(Shelobolina et al., 2009)
Bacillus genera *Rahnella* genera	G-P G-N	Precipitation via bacterial phosphatase activity at pH 4-5	(Beazley et al., 2007; Martinez et al., 2007)
Citrobacter sp.	G-N	Enzymatically mediated precipitation of HUO_2PO_4 and $NaUO_2PO_4$ phases at pH 6.9	(Macaskie et al., 2000, 1992)
Microbacterium		Precipitation as a m-autunite-like phase at pH 4.5	(Nedelkova et al., 2007)

Myxococcus xanthus	G-N	Biomineralization as m-autunite mineral phase by EPS at pH 4.5	(Jroundi et al., 2007)
Microbacterium oxydans SW-3	G-P	Precipitation as m-autunite phase at pH 4.5	(Merroun et al., 2006; Merroun and Selenska-Pobell, 2008)
Microbacterium oxydans S15-M2	G-P		
Sphingomonas sp. S15-S1	G-N		
Bacillus sphaericus JG-7B	G-P		
Pseudomonas aeruginosa	G-N	Precipitation of uranyl phosphate at the cell membrane	(Renninger et al., 2004)
Pseudomonas aeruginosa	G-N	Precipitation as needle shaped U-phosphate compounds within the cell envelope	(Choudhary and Sar, 2011)
Pseudomonas stutzeri DSMZ 5190	G-N	Precipitation within EPS as a m-autunite-like mineral phase	(Merroun and Selenska-Pobell, 2008)
Rahnella sp. *Y9602*	G-N	Precipitation as chernikovite (an autunite-type mineral) phase	(Beazley et al., 2009)
Bioaccumulation			
Acidithiobacillus ferrooxidans	G-N, chemolithoautotrophic acidophilic bacteria	Intracellular accumulation with polyphosphate bodies	(Merroun et al., 2003)
Arthrobacter sp.	G-P	Accumulates in form of needle-like fibrils with different sizes	(Merroun et al., 2006; Merroun and Selenska-Pobell, 2008)
Desulfovibrio äspönensis			
Sphingomonas sp. S15–S1	G-N		
Pseudomonas migulae CIP 105470	G-N	Formation of electron-dense granules in the cytoplasm	
Stenotrophomonas maltophilia JG-2	G-N	Intracellular accumulates	
Pseudomonas sp.	G-N	Intracellular sequestration throughout the cell cytoplasm in form of electron dense micro-precipitates	(Kazy et al., 2009)

Rhodanobacter A2-61	G-N	Intracellular precipitation of U-phosphate complexes as a m-autunite-like mineral phase	(Sousa et al., 2013)
		Non-specified accumulation	
Bacillus cereus	G-P	Irreversible accumulation especially by spores	(Selenska-Pobell et al., 1999)
Bacillus megaterium	G-P		
Bacillus spaericus	G-P		

4. Interactions of radium with diatoms and bacteria: A state-of-the-art review

4.1. Radium

Generalities

Ra is 88th chemical element in the periodic table. It belongs to the group of alkaline earth metals. There are four naturally occurring radioactive isotopes (Ra-223, Ra-224, Ra-226, Ra-228) present in the environment, none of them are stable. Ra isotopes can be found in all three primordial radionuclides decay chains and each Ra isotope is the decay product from a thorium (Th) isotope. For example, Ra-226 is part of the U-238 decay chain, Ra-223 is part of the U-235 decay chain, Ra-224 and Ra-228 are part of the Th-232 decay chain (**Figure I-15**).

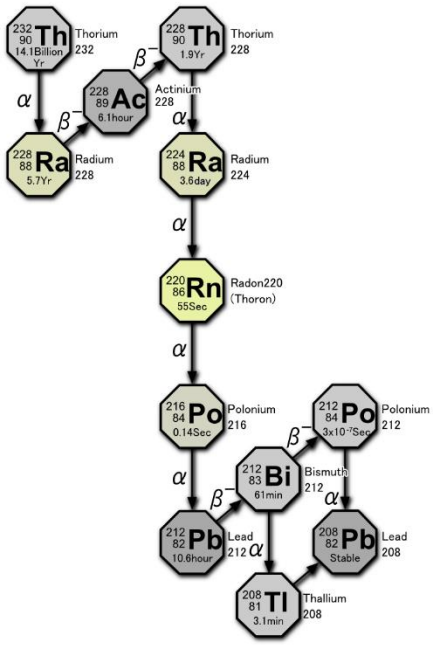

Figure I-15: Decay chain of Th-232, work by Tosaka, CC BY 3.0, source: https://commons.wikimedia.org/w/index.php?curid=5531106.

Compared to other 31 reported Ra isotopes, Ra-226 and Ra-228 have relatively long half-lives (1600 and 5.75 years, respectively). Ra-225 is the only anthropogenic Ra isotope that has a relatively significant half-life of 14.9 days, while the rest of artificial Ra isotopes have a half-life shorter than two hours (Audi et al., 2017).

The commonly used historical unit for measuring radioactivity, *i.e.*, the curie (Ci), is established on the basis of radioactivity of Ra-226. Initially, it was defined as the radioactivity emitted by one gram of Ra-226, but later it was slightly refined as 3.7×10^{10} disintegrations per second. To date, the unit for radioactivity in the International System of Units is becquerel (Bq), which signifies one disintegration per second.

Origins and applications

In 1898, Marie Skłodowska-Curie and Pierre Curie discovered Ra while examining a sample of uraninite. This marked the beginning of its significance in various applications. In the early

1900s, radioluminescent paint containing Ra was invented. Unaware of its toxicity, this paint became widely used in watches, clocks, aircraft instruments, house numbers, doll eyes, etc. The tragic death of “Radium girls” results from the unawareness of Ra’s hazards. These “Radium girls” were in fact dial painters responsible for applying Ra-based luminous paint to watch and clock dials. Unfortunately, they were instructed to lick their brushes to achieve a finer point, resulting in the ingestion of Ra. It is reported that a typical self-luminous watch utilizing Ra paint contains approximately 1 microgram of Ra (Terrill et al., 1954). Tragically, this exposure to Ra led to severe health consequences to these workers, such as sores, anemia, and bone cancer.

During this period, people believed that Ra could cure numerous illnesses, leading to claims of its effectiveness against conditions like migraine, arteriosclerosis, and appendicitis. The potential uses of Ra and U as radiation sources in medical, scientific, and industrial applications were explored, with the first Ra refining companies established in France in 1898. The reputation of Ra's curative powers was so strong that it found its way into products like toothpaste, hair creams, and even food items. Additionally, early biologists used Ra to induce mutations and study genetics in the early 1900s (IAEA, 2014).

In modern era, Ra-223 is used in medicine as an alpha-emitter radiopharmaceutical to treat bone metastasis. Besides, Ra is also applied as radiation source in industrial radiography devices for the inspection of metals or other compounds. Ra can also be used as a neutron source together with beryllium.

Throughout history, Ra's discovery and its historic applications have left a lasting impact, both in beneficial and unintended ways. As scientific understanding progressed, the risks associated with radium's radioactive properties led to more controlled and regulated uses in various fields.

Chemical properties

Ra is a highly reactive silvery-white metal. Ra always exhibits its group oxidation state of +2. The behavior of Ra resembles that of its lighter congener, barium (Ba), due to the similarity of their ionic radii. As a result, Ra often forms the same insoluble salts as Ba, such as barium sulfate ($BaSO_4$) and barium carbonate ($BaCO_3$). In fact, Ba is frequently used as a chemical analogue for predicting the behavior of Ra (Sajih et al., 2014).

In aqueous solution, Ra forms the Ra^{2+} cation. In low salinity solutions over the pH range of 4 to 8, Ra will be present as uncomplexed Ra^{2+} ions (IAEA, 2014). Ra can form ionic compounds and can also complex with sulfate ions (SO_4^{2-}) or organic matters (Rachkova et al., 2010). Interestingly, barite ($BaSO_4$) can incorporate Ra in solid solution as $(Ba,Ra)SO_4$. This precipitation of $(Ba,Ra)SO_4$ has been shown to play a significant role in controlling the solubility of Ra in a variety of natural waters (Bosbach et al., 2010; Martin and Akber, 1999). Under high carbonate concentrations (> 60 mg/L) and at high pH (> 10.25) conditions, a considerable fraction of Ra would be complexed as radium carbonate, *i.e.*, $RaCO_3$ (IAEA, 2014).

Transport in the environment

As is previously mentioned, naturally occurring Ra isotopes are produced through the radioactive decay of primordial radionuclides. As a result, Ra is widely distributed in the Earth's crust as well. IAEA has reviewed and reported the global distribution of Ra on Earth in different compartments: air, rocks, soils, fresh waters and oceans (IAEA, 2014).

According to the IAEA report, when examining different rock types, the highest concentrations of Ra-226 are observed in shale, bitumen slate, volcanic and phosphate rocks, followed by granites, clay rocks, sandstone, sedimentary rocks, lime, and carbonate. In normal areas, the Ra-226 concentrations in soil generally range from 3.7 to 126 Bq/kg, with the average worldwide value reported by United Nations Scientific Committee on the Effects of Atomic Radiation (UNSCEAR) being 32 Bq/kg in 2008. However, there are specific regions in the world where naturally occurring radionuclide concentrations in soils or waters greatly exceed the normal range. Examples include Kerala and Tamil Nadu in South India, where sands containing monazite with high Th content are found, and Ramsar in Iran, where high levels of Ra-226 have been identified in water.

In river water, typical Ra-226 activities range between 0.5 and 20 mBq/L, with occasional reports of enhanced concentrations up to 300 mBq/L. Similarly, in lakes, Ra-226 concentrations fall within a narrow range of 0.5–15 mBq/L, consistent with what is observed in river water. In the open ocean, major processes affecting the distribution of long-lived Ra isotopes involve supply from continents and the seabed, along with removal by radioactive decay and particle scavenging.

Additionally, human activities can also influence the cycling of Ra from groundwater to surface water and sediments. For example, the phosphate industry can contribute significantly to radionuclide discharges in some areas. Residual phosphogypsum produced from the industry contains nearly all the Ra-226, Pb-210, and polonium-210 (Po-210) from the ore, as well as smaller quantities of U and Th isotopes. In this case, Ra activity concentrations in the gypsum stacks can range from background levels to 1700 Bq/kg.

Furthermore, Ra concentrations in air can be estimated to be 1.5 $\mu Bq/m^3$, mainly present in resuspended soil particles. Since Ra is sometimes concentrated in coals, the burning of coal may also contribute to the Ra release in the atmosphere. Carried by fly ash, a typical coal fired power stations can release Ra-226 with concentrations ranging from 44.3 to 2400 Bq/kg.

For various considerations (environmental health assessment, ecological impact, human health risk assessment, etc.), the transport and migration of Ra in the environment has been widely studied. Generally speaking, Ra is known for its high mobility in the environment. The concentrations of Ra in water and its movement through the environment are mainly influenced by interactions with surfaces, particularly through adsorption via ion exchange processes.

Various studies have been conducted to explore Ra's adsorption behavior, and it has been found that Ra readily adsorbs to clays (kaolinite, smectite, illite, etc.) and different mineral oxides (iron oxyhydroxides, manganese oxides, etc.) present in soils, especially under near neutral and alkaline pH conditions (Ames et al., 1983; Beneš et al., 1985, 1984; Koulouris, 1995). However, the Ra adsorption is generally reversible and Ra desorption occurs readily at low pH values. In comparison to other alkaline earth elements, Ra has the highest affinity for ion exchange, with the relative preference order as follows: $Ra^{2+} > Ba^{2+} > Sr^{2+}$ (strontium)$> Ca^{2+} > Mg^{2+}$ (Dorothy, 1959). Additionally, the adsorption of Ra is strongly influenced by the ionic strength of the solution and the concentrations of other competing ions. In general, as the ionic strength increases, the adsorption of Ra decreases. Ra can also be immobilized in soils and sediments through co-precipitations with Ba. Given the low molar concentrations of Ra in the environment,

precipitation of Ra phases is rarely significant. Instead, the removal of Ra from waters typically occurs through co-precipitation of $(Ra,Ba)SO_4$ phases. Recent studies have also suggested that Ra may exhibit strong adsorption affinity for organic matters present in soils. In fact, it is reported that organic matters can adsorbs 10 times as much Ra as clay. (Greeman et al., 1999; Vandenhove and Van Hees, 2007). Research points out that the Ra adsorption affinity of both organic matter and clays is primarily due to their cation exchange capacity (CEC) (Nathwani and Phillips, 1979).

Ra can eventually enter food chain through various pathways. For that, the transport and uptake of Ra in plants and terrestrial animals have been investigated. In plants, Ra isotopes can be taken up through two primary pathways: root uptake from the soil and foliar uptake from the interception of radionuclides on the external surfaces of plants. Certain plants, such as lichens and mosses, mainly obtain water and mineral nutrients through foliar uptake. These plants lack a well-developed root system, making them prone to accumulating contaminants from the atmosphere. They can trap airborne particulates through both passive and active processes, including extracellular ion exchange mechanisms (Zechmeister et al., 2003). Consequently, it is commonly reported that the highest Ra concentrations are observed in mosses, lichens and fungi, followed then by trees, bushes, grasses and finally by cereals and vegetables. Moreover, the concentration of Ra in the bark or stem of a plant is usually higher than in leaves, which is likely due to the continuous Ra accumulation through root uptake (Karunakara et al., 2003). The properties of soil will greatly affect the availability of Ra to plants. In general, the Ra availability decreases with increasing pH as Ra gradually forms insoluble species at higher pH. In addition, in soil with high concentrations of alkaline earth cations (Ca^{2+}, Mg^{2+}, etc.), the uptake of Ra may be suppressed due to adsorption competition. Besides, it is worth noting that there might exist a discrimination mechanism in plant cell membranes for ion uptake from soils (IAEA, 2009).

The transfer of Ra to animals primarily occurs through the ingestion of feed and water, the intake of Ra can vary significantly. Studies on rats and dairy cows have demonstrated that Ra-226 behaves similarly to Ca, a crucial metabolic element (Sansom and Garner, 1966; Taylor et al., 1962). Consequently, Ra-226 is often found in Ca-rich tissues in animals, and its accumulation is influenced by Ca metabolism. Increased Ca concentrations in the diet have been observed to reduce Ra-226 accumulation (IAEA, 2014). More precisely, Ra mainly accumulates in bones as other alkaline earth elements. Consequently, reported data show relatively low transfer of Ra to animal products, which are significant components of the human food chain, such as meat. When comparing Ra transfer coefficients to beef and milk, it is observed that the transfer coefficient for Ra to beef is higher than that for milk.

Toxicology of radium

The radiological impact of Ra arises from exposure to Ra isotopes themselves and their decay progeny such as Rn. Since Ra emits alpha particles and gamma rays during the radioactive decay, the ingestion and inhalation of Ra into human bodies might cause damage to cell chromosomes and potentially lead to occurrence of cancer. As Ra tends to accumulate in bone, it will have hazardous effects on bone marrow cells particularly. The decay products of Ra, Rn for example, also have radiological impact on human health. Specifically, the release of Rn-222 (decay product of Ra-226) and Rn-220 (decay product of Ra-224) from soil, building materials, and naturally occurring radioactive materials poses a significant inhalation hazard. Rn is a

radioactive gas and can be dissolved in water, thus in blood as well when being inhaled. In fact, Rn is a well-known external risk factor for lung cancer.

4.2.Interaction of radium with diatoms

Detailed studies and documentation of Ra-diatom interaction have not been found in the current literature. The mechanisms behind the interaction remain still unknown and need to be explored in the future.

4.3.Interaction of radium with bacteria

In contrast to the case of U, there is much less available information on the interaction between bacteria and Ra in the literature. Underlying mechanisms remain relatively unclear. Zakeri et al. (2012, 2010) studied the impact of high Ra-226 concentrations (up to 10 kBq) on the protein synthesis activity of a radiation-tolerant Gram-negative bacterial species, *Serratia marcescens*, that was isolated from a hot spring with a high natural radiation background in Ramsar (50471 ± 3028 mBq/L of Ra-226). This bacterial strain shows high performance for Ra-226 biosorption, with a cited value of 38 kBq/g. The biosorption of Ra-226 on *Serratia marcescens* dead cells follows pseudo-second-order kinetics and the biosorption equilibrium is better described by Freundlich isotherm model. Moreover, Fourier-transform infrared spectroscopy (FTIR) analysis demonstrated the complexation of Ra-226 with hydroxyl, carboxyl and carbonyl functional groups of proteins, polysaccharides and lipids in the cell biomass. According to their research, a high Ra-226 concentration (10 kBq) has a negative effect on the growth of *S. marcescens*, leading to about 50% of growth inhibition. Transmission electron microscopy revealed the noticeable formation of strongly electron-dense area on the cell wall of Ra-loaded bacteria. The proteomic study suggested the up-regulation of several proteins in the *S. marcescens* cells under Ra-226 stress, which are involved in energy, transport, protein and nucleotide biosynthesis and stress response metabolism (Zakeri et al., 2012, 2010). Another two bacterial strains isolated also from hot springs in Ramsar, *Nostoc punctiforme* and *Chroococcidiopsis thermalis*, were examined and the maximum biosorption capacity for Ra-226 were reported as 37 kBq/g and 55 kBq/g for *N. punctiforme* and *Chroococcidiopsis thermalis*, respectively (Heidari et al., 2018).

Conclusion

In Part I, two ubiquitous microbial groups in nature, *i.e.*, diatoms and bacteria, are presented in detail. They are found in a wide range of different ecosystems on Earth and play an extremely important role. Various aspects of diatoms and bacteria are elucidated, such as taxonomy, morphology, life cycle, reproduction and the different roles they play in ecosystems. To date, their evolution has proven to be extremely successful on Earth. In addition, the mechanisms of interaction between these two groups of microorganisms are discussed. It is shown that the relationships between diatoms and bacteria are complex and diverse, *e.g.*, mutually beneficial or competitive relationship. Their complex interactions map the diversity of natural ecosystems. At the end of Part I, the ecological significance of diatoms and bacteria is mentioned. In fact, they play an important role in assessing the health of ecosystems, and many studies have considered them as bioindicators to investigate the ecological impact of pollutions (*e.g.*, heavy metals, pesticides, industrial effluents, etc.) on ecosystems. In addition to monitoring changes in the state of ecosystems, diatoms and bacteria (and more generally, microorganisms) can also be used for bioremediation. The use of microorganisms in bioremediation has proven to be an efficient, environmentally-friendly and cost-effective approach. The ability of diatoms and bacteria to effectively adsorb heavy metals has led to their widespread use in the post-treatment of industrial wastewater or the decontamination of heavy metal-contaminated sites.

In Part II, various relevant topics are discussed around two radioelements, U and Ra, such as their physico-chemical properties, history of discovery, transport in the environment, biotoxicity and impact on the ecosystem. It is mentioned that microorganisms play a very important role in the transport of U and Ra in the environment. In order to better understand the underlying mechanisms, the interactions between heavy metals and two important groups of microorganisms, bacteria and diatoms, are detailed in a more general context. For that, Part II presents first of all the cellular structure of these two groups of microorganisms (mainly the cell wall structure), followed by explaining the mechanisms of substance exchange of microbial cells with the external environment and listing all possible interactions with heavy metals at the end. It is demonstrated that these two microbial groups play an extremely important role in the mobility and speciation of heavy metals in nature. In fact, microorganisms are capable of changing the behavior of heavy metals in the environment in a number of ways, including biological redox processes, bioprecipitation, biosorption, bioaccumulation and so on. Their high removal capacity towards heavy metals, excellent cost-effectiveness and low maintenance costs have led to the widespread application of microorganisms for bioremediation. At the end, this chapter concludes with some related research focusing on U and Ra. The mechanism of U-bacterium interaction has been quite widely discussed and elucidated in the literature. However, there is a lack of study in the literature regarding the Ra-bacterium interaction, and even fewer study focusing on interaction of diatoms with U or Ra. There are still a number of gaps to be filled in our understanding of the mechanisms behind. Hence, this work aims to study the interaction of U, Ra with the diatom culture from different perspectives in order to provide a deeper understanding.

The next chapter presents the methodology used in this work to study the interaction of diatom culture with U and Ra as well as other related issues.

Chapter 2: Methods

Contents

1. Introduction

In this chapter, detailed information on the methodology used for studying the interactions of U, Ra with the diatom culture is provided. In the first place, the methods for cultivating and characterizing the studied diatom culture are explained in detail, followed by the protocol applied for isolating and characterizing the bacterial strains living with diatoms. In the second place, the general strategy for studying the U, Ra-diatoms interactions at the macroscopic level is presented, including the protocols used for the batch-type U, Ra bio-association experiments. In the last part, various microscopy and spectroscopy techniques will be presented, which are used in this work to characterize the interactions at the molecular level.

2. Diatoms cultivation and characterization

2.1. Choice of diatom species

A freshwater benthic diatom species, called *Achnanthidium saprophilum*, was studied in this work. *A. saprophilum* is a pennate diatom species that is commonly found as single cells or short chains in waters. This species has a relatively low motility (more detailed information related to this diatom taxon is available on https://www.algaebase.org/). The original diatom strains were provided by *Laboratoire Microorganismes : Génome Environnement* (LMGE). The diatoms were collected from a local freshwater lake (*Lac d'Aydat*) in the region of Auvergne in France (45.663996°N 2.984505°E) and were purified and acclimatized in LMGE. Note that the diatom samples provided by LMGE are xenic cultures, signifying that bacteria originating from the lake are also present in the cultures.

2.2. Verification of diatom taxonomy and culture purity

To verify the diatom taxonomy and the purity of the diatom culture (*i.e.*, to verify that only one diatom species is present in the culture), the next-generation sequencing approach was applied on the diatom's 18S ribosomal ribonucleic acid (rRNA) genes amplicon.

For that, it was necessary to extract the total DNA of diatoms from the diatom culture. First of all, 100 mL of the xenic diatom culture was filtrated by an autoclaved bottle top filter (Nalgene) using 0.22 µm of mixed cellulose esters (MCE) membrane (Millipore). The membrane with biomass was then applied to DNeasy PowerWater Kit (QIAGEN) for cleaning the extracted DNA by following the protocol provided with the kit. Secondly, the total cleaned DNA extracted from the diatom culture was subjected to the PCR (Biometra T3000 Thermocycler, Analytikjena) to amplify the V4 region of the 18S rRNA gene of diatoms. Primer set D512f (5'-ATTCCAGCTCCAATAGCG-3') and D978r (5'-GACTACGATGGTATCTAATC-3') (Eurofins Genomics) were used for the PCR (Zimmermann et al., 2011). The setup for the PCR and thermal cycle are listed in **Table A1-1** in Annex 1.

After the PCR, the resulting amplicons were purified using QIAquick PCR Purification Kit (QIAGEN). An aliquot of the resulting amplicons was verified by electrophoresis (detailed information is given in Annex 1) before being subjected to the next-generation sequencing with a MiSeq sequencer (Illumina) at Eurofins Genomics (Germany). Note that the primer sets were removed using Cutadapt 4.2 (Martin, 2011). The amplicon sequences were processed with DADA2 1.26 by firstly trimming both of the forward and reverse reads of low quality (QS <30) and then filtering the reads which exceeded the maximum expected error of 2 or which

contained the ambiguity N symbol. Prior to the generation of amplicon sequence variants (ASVs), the forward and reverse reads were merged and the chimeric sequences were removed. To analyze the diatom taxonomy based on the generated ASVs, the nucleotide Basic Local Alignment Search Tool (BLAST) on the National Center for Biotechnology Information (NCBI) webpage (https://blast.ncbi.nlm.nih.gov/Blast.cgi) was used, which consisted of comparing the generated sequences with the sequence databases (Altschul et al., 1990).

2.3. Cultivation under laboratory conditions

The acclimatized *A. saprophilum* diatoms were cultivated in a specific medium, called Diatom Medium (DM), that is proposed by Culture Collection of Algae & Protozoa (CCAP). The composition of the DM is given in **Table A2** in Annex 2. Diatom cells were cultivated in sterile culture flasks with ventilated cap in an incubator at 20 °C, with a day:night cycle of 12 h:12 h and with a constant horizontal agitation of 50 rpm. It is worth noting that the *A. saprophilum* diatom cultures used in this work are always xenic.

With the gradual depletion of nutrients in the medium, the diatom population in the culture flasks will eventually decline without external intervention. To maintain the diatoms, it is thus necessary to refresh the culture medium regularly. For that, an inoculation of the diatoms was done every fifteen days by transferring old cultures to fresh medium at a dilution ratio of 1:10. The whole process was carried out within a biosafety cabinet under sterile conditions.

The state of diatom cells was regularly verified via observation under a light microscope. There should be no flocculant matter or big cell aggregate visible to the naked eye that remains in the culture even with the agitation. In such cases, it is highly likely that the diatom culture is contaminated. This is the reason why diatom cultures were always replicated during inoculation in this work. Additionally, diatom cells that are in good state should display remarkable brownish-yellow color under the light microscope. Detailed information on the cell observation using light microscope will be presented in the next section.

2.4. Microscopic observations and size measurements

The routine observation of the *A. saprophilum* diatom cells was carried out under the transmitted light microscope in order to examine the state of the cells. Several aspects were of major concern during the routine observation, such as the cellular integrity, the cellular coloration, the percentage of dead cells and the presence of potential contaminants.

The dimensions of the diatoms were measured using light and scanning-electron microscopy (SEM). A conventional slide preparation method was used to observe the cells under the light microscope. However, to prepare diatom specimens for the SEM observation, a more complex preparation procedure was applied, which is described later in detail in section 6.1 of this chapter. To build up a dataset comprising information of the length, width and thickness of the *A. saprophilum* diatoms, a large number of micrographs of different diatom individuals in top view and in front view (see **Figure II-1**) were recorded under the light and scanning electron microscope. Size measurements were realized using the length measuring tool originally included in the microscope operating software. The resulting dataset contained 100 independent measurements of length, width and thickness that were collected from different intact diatom individuals.

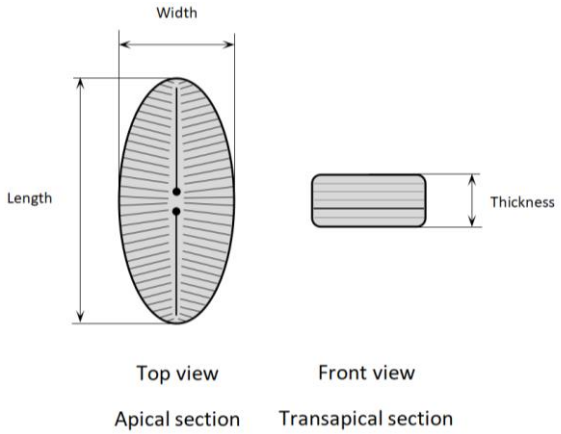

Figure II-1: Apical section and transapical section of a diatom cell.

2.5. Growth curve study

To elaborate the growth curve of *A. saprophilum* diatoms under the applied culture conditions, diatom cells were separated from the culture by centrifugation at 2600 ×g for 10 minutes and transferred into 500 mL of fresh DM. The resulting diatom suspension was equally distributed into 10 culture flasks and incubated under the described culture conditions.

Every two or three days, 30 µL of the diatom suspension (thoroughly agitated before sampling) was sampled for each culture flasks. To determine the diatom cell density in each sample, cells counting was done under the light microscope using a Thoma cell counting chamber. For that, one drop of the diatom suspension sample was added onto the counting chamber for each measurement. Ten independent measurements were carried out for each diatom sample and the corresponding cell density was calculated using the following equation:

$$cell\ density\ = \frac{\bar{n}}{V} \qquad \textbf{Eq. II-1}$$

Where $\bar{n}$ denotes the average value obtained from ten measurements excluding the maximum and minimum of the data, V denotes the volume of the Thoma counting chamber, which is equivalent to 0.1 µL and corresponds to a total counting area of 1 mm^2.

3. Bacteria cultivation

3.1. Bacterial community analyses

To investigate the bacterial diversity present in the xenic diatom culture, the next-generation sequencing targeting the V4 region of the bacterial 16S rRNA genes was applied on the total DNA extracted from the xenic diatom culture (protocol has been described in section 2.2 of this chapter). The applied protocol for the next-generation sequencing only differs in a few points from that was used for diatoms: (i) primer set 515f modified (5'-GTGYCAGCMGCCGCGGTAA-3') and 806r modified (5'-GGACTACNVGGGTWTCTAAT-3') (Eurofins Genomics) were used for bacteria (Walters et al., 2016), (ii) the generated ASVs of the 16S rRNA amplicon were subject to Silva SSU database 138.1 for bacterial taxonomy analyses.

3.2.Strain isolation and cultivation under laboratory conditions

To isolate bacterial strains from the diatom culture for further studies, 10 µL of the diluted (1:100000) diatom culture was spread on different agar plates (sterile) comprising DM or 10%

lysogeny broth (LB) medium (composition is given in **Table A3-1** in Annex 3). After several days of incubation at room temperature, bacterial colonies forming on the agar plates and exhibiting various morphological properties were picked up and inoculated onto new corresponding agar plates using the streak plate technique. The resulting single bacterial colonies were correspondingly transferred into sterile Erlenmeyer flasks filled with liquid DM or 10% LB medium. The cultures of the bacterial isolates were placed on a shaker (KS 501 digital, IKA) at 95 rpm at room temperature.

3.3. Taxonomy identification of the bacterial isolates

To identify the taxonomy of each obtained bacterial isolate, the nearly full bacterial 16S rRNA genes were amplified via PCR. For that, the modified 7f (5'-AAGASTTTGATYNTGGCTCAG-3') and 1513r (5'-TAC GGYTACCTTGTTACGACTT-3') universal primers (Eurofins Genomics) were used. Details of the PCR setup as well as the thermal cycle are given in **Table A3-2** in Annex 3. The resulting amplicons were purified using MSB Spin PCRapace (INVITEK, diagnostics) and verified by the electrophoresis (protocol has been described in section 2.2 of this chapter). The NanoDrop™ 2000c spectrophotometer (Thermo Scientific) was used to quantify the concentration of DNA in the amplicon prior to the Sanger sequencing performed at Eurofins Genomics (Germany). The obtained 16S sequences were applied to Nucleotide BLAST on NCBI webpage for bacterial taxonomy identification.

4. Applied strategy for studying the interaction of diatoms with uranium/radium

In this work, experiments and analyses were conducted at the macroscopic and molecular scale to study the interaction of diatoms with U and Ra, as is presented in **Figure II-2**. Investigations can be generally divided into two subsequent steps: The first step (at the macroscopic level) consists of conducting bio-association experiments of the studied radioelements with biomass (diatoms, bacterial isolates) to study the adsorption kinetics, the adsorption isotherm and the time-dependent adsorption/incorporation behavior. The second step (at the microscopic level) aims to characterize and investigate the U localization and speciation in the biomass, by using various analytical microscopic and spectroscopic techniques.

Note that U-238 and Ra-226 were used in this work and will be simply noted as U and Ra, respectively, in the following chapters for the simplicity of notation.

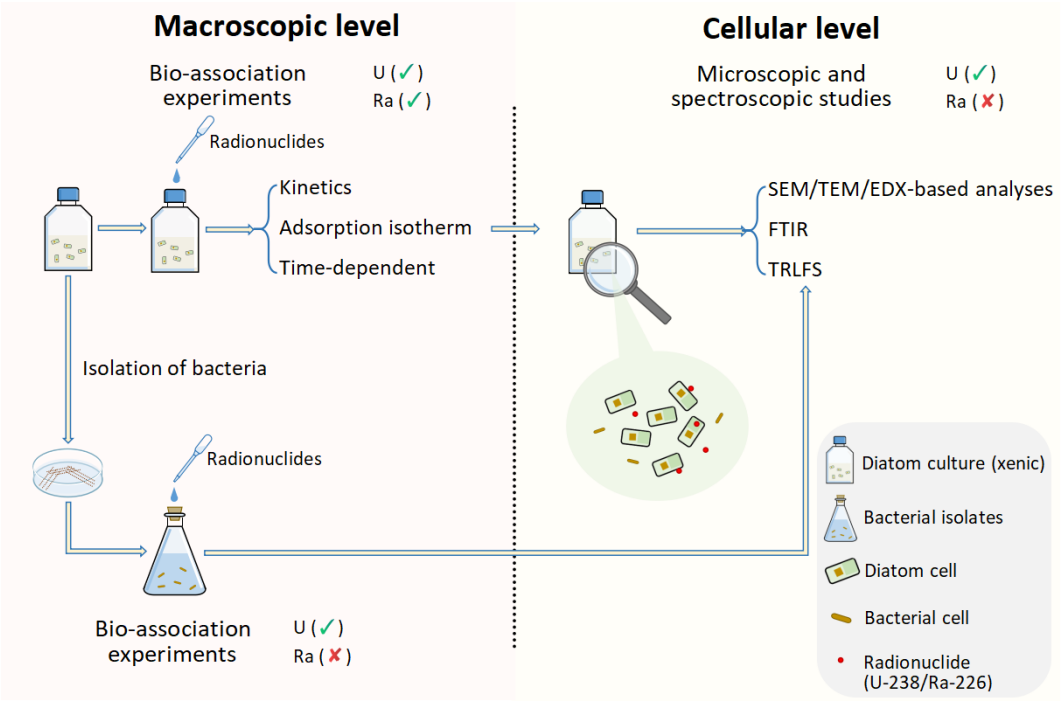

Figure II-2: The applied strategy for studying the interaction of diatoms with U and Ra from the macroscopic level to the cellular level by combining various microscopic and spectroscopic techniques. SEM: scanning electron microscopy, TEM: transmission electron microscopy, EDX: energy dispersive X-ray spectroscopy, FTIR: Fourier-transform infrared spectroscopy, TRLFS: time-resolved laser-induced fluorescence spectroscopy.

5. Investigations at the macroscopic scale

To investigate the interaction of U, Ra with the *A. saprophilum* culture at the macroscopic scale, U, Ra bio-association experiments were conducted under two different experimental conditions: (i) To study the U, Ra adsorption kinetics and the concentration-dependent isotherm, experiments were performed in a simple medium (pH 7.0) consisting of 2 mmol/L of sodium chloride (NaCl) and 3 mmol/L of 4-(2-hydroxyethyl)-1-piperazineethanesulfonic acid (HEPES); (ii) To investigate the impact of the diatom growth phase on the U, Ra bio-association, time-dependent experiments were performed in full DM medium to sustain the growth of diatoms during the experiment.

In the bio-association study, the fractions of U/Ra adsorbed and incorporated by the diatoms were distinguished to have a better understanding on the distribution of U/Ra in the system.

5.1. Cells preparation, elution and digestion

To perform U/Ra bio-association experiments, diatoms in the exponential growth phase were generally used in this work. For that, the *A. saprophilum* culture was centrifuged at 2600 ×*g* for 10 minutes (CL10 Centrifuge Series, Thermo Scientific). The cell pellet was transferred into fresh DM under sterile conditions and incubated for another seven days. Prior to the bio-association experiment, diatom cells were separated from the resulting diatom culture by centrifugation, washed with Milli-Q water and resuspended in different studied media depending on different experiments (which will be detailed later).

As previously mentioned, one of the objectives of the U, Ra bio-association experiments is to distinguish the adsorbed part from the incorporated part of the studied radioelements in the system. To desorb the radionuclides from the diatoms, i.e., the adsorbed part, a 0.01 mol/L ethylenediaminetetraacetic acid (EDTA, ACS reagent, Acros Organics) solution (pH 7.0) was used. The desorption (elution) was carried out at room temperature for 15 minutes. The elution efficiency was determined by preliminary experiments and calculated using the following equation:

$$efficiency = \frac{m_{i,eluted}}{m_{i,adsorbed}} \times 100\% = \frac{V_1 \times C_{i,eluate}}{V_2 \times (C_{i,ini} - C_{i,eq})} \times 100\% \qquad \textbf{Eq. II-2}$$

Where i represents U or Ra; $m_{i,adsorbed}$ is the mass of the radionuclides adsorbed on diatoms; $m_{i,eluted}$ is the mass of the radionuclides desorbed during the elution; V_1 is the volume of the eluate; V_2 is the volume of the solution before the elution; $C_{i,ini}$ is the initial mass concentration of the radionuclides to which diatom cells are exposed; $C_{i,eq}$ is the mass concentration of the radionuclides remaining in the solution when the adsorption equilibrium is reached; $C_{i,eluate}$ is the mass concentration of the radionuclides recovered in the eluate after the elution.

It is worth noting that in the literature, EDTA is reported to increase the porosity of the cell wall observed in the marine green algal species *Tetraselmis suecica* (Wong et al., 2014). However, there is little information available in the literature that points out any similar effect on diatoms. In this work, it is assumed that the presence of EDTA will not affect the permeability of the diatom's cytoplasmic membrane during the relatively short process of elution. Examination of diatom cells in contact with 0.01 mol/L of EDTA solution using light microscope showed no morphological changes or cell lysis of diatoms within the duration applied for the elution. Hence, it is supposed that the part of U or Ra incorporated by the diatom cells is not eluted during the elution process.

In order to destroy the cytoplasmic membrane and lyse the diatom cells, the digestion process in this work was performed using a protocol adapted from the literature (Flower, 1993; Parr et al., 2004). It consists of adding 30% (w/w) of hydrogen peroxide (H_2O_2) solution (Suprapur, Supelco, VWR) to the diatom sample in a 6:1 volumetric ratio and acidifying the resulting mixture with a few drops of distilled solution (distiller Distillacid BSB-939-IR, Berghof) of hydrochloric acid (HCl) or nitric acid (HNO_3). The sample was placed in a water bath at 50 °C for 48 hours with occasional agitation. Unlike the elution process, the digestion process completely destroyed the cytoplasmic membrane of the diatoms, leading to the release of the cellular contents, and eventually the incorporated radionuclides if any, into the solution.

5.2.Uranium, radium batch-type bio-association experiments

Figure II-3 presents the applied workflow for the U/Ra bio-association experiments. At the end of the studied exposure time, diatom cells were recovered from the suspension by centrifugation. The resulting diatom pellet was eluted and digested following the protocol presented in section 5.1 of this chapter. At the end of each centrifugation step, the supernatant was analyzed by the inductively coupled plasma mass spectrometry (ICP-MS) and high resolution inductively coupled plasma mass spectrometry (HR-ICP-MS) to determine the concentration of U and Ra, respectively.

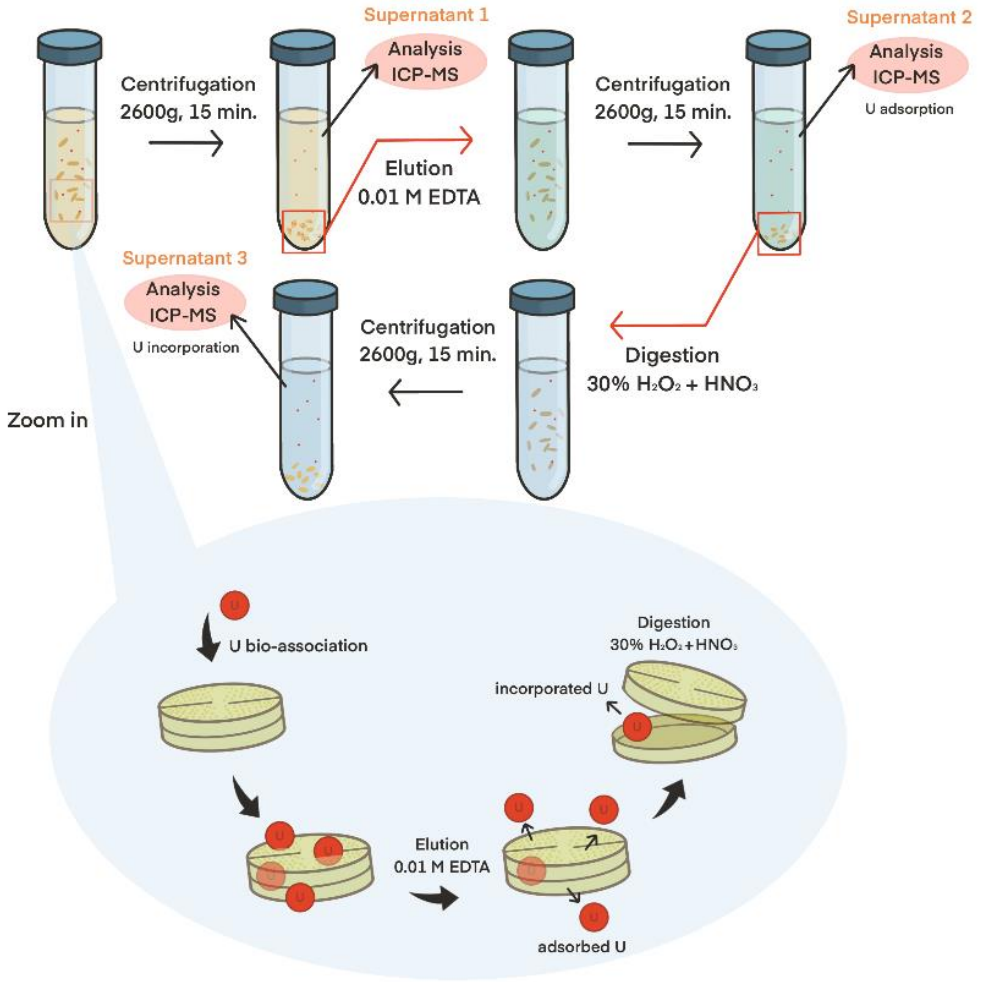

Figure II-3: The detailed workflow applied for U and Ra bio-association experiments, along with an elucidation on the elution and digestion process at the microscopic scale. Example is given for U. Figure adapted from the work of He et al. (2023b).

Study of the U, Ra adsorption kinetics

Studying the adsorption kinetics is the very first step in the study of the U, Ra-diatom interaction before further investigation can be carried out. For that, *A. saprophilum* diatom cells were prepared following the procedure described in the previous section. Prior to the experiment, the cells were re-suspended in the solution of 2 mmol/L of NaCl buffered with 3 mmol/L of HEPES at pH 7.0. Experiments were carried out at room temperature in triplicates, where the prepared diatom suspensions with a cell density of about 3×10^9 cell/L and 8×10^8 cell/L were exposed to about 0.2 µmol/L of U-238 and 6 pmol/L of Ra-226, respectively, for a series of exposure times (10, 45, 60 and 120 minutes). At the end of the experiment, diatoms were post-treated following the work flow presented in **Figure II-3**.

To have a first and global insight into the kinetics of the U, Ra-diatom interaction, the evolution with time of the amount of U or Ra associated to diatoms were deduced using **Eq. II-3**:

$$m_{i,associated} = V_{total} \times \left(C_{i,ini} - C_{i,sup}\right) \qquad \textbf{Eq. II-3}$$

Where i stands for U or Ra; V_{total} is the volume of the diatom suspension; $C_{i,ini}$ and $C_{i,sup}$ represents the initial mass concentration of the radionuclide i present in the suspension and

the mass concentration present in the supernatant 1 (see **Figure II-3**), respectively.

Note that for the moment, the partition between the adsorption and incorporation of U or Ra at the diatom level is not of major concern in the kinetics study. Hence, $m_{i,associated}$ represents the totality of U or Ra that is associated to diatoms, whether adsorbed on the surface of diatoms or incorporated inside the cells.

U, Ra concentration-dependent bio-association isotherm

Prior to the experiments, diatom cells were prepared according to the preparation protocol described in section 5.1 and transferred into the solution of 2 mmol/L NaCl (or sodium nitrate ($NaNO_3$), > 99%, Sigma Aldrich) and 3 mmol/L HEPES (> 99.5%, Sigma Aldrich) at pH 7.0. The resulting diatom suspensions with a cell density of around 5×10^8 cell/L and 4×10^8 cell/L were exposed to U-238 with concentrations ranging from 0.2 to 20 µmol/L and to Ra-226 with concentrations ranging from 0.8 to 4 pmol/L, respectively. The experiments were conducted at room temperature for 45 minutes (the adsorption equilibrium time was preliminarily determined in the U/Ra adsorption kinetics studies) in triplicates for each studied concentration.

To obtain more detailed information on the U, Ra-diatom interaction, the adsorption and incorporation of the radionuclides were distinguished in the concentration-dependent bio-association experiments. Consequently, the mass concentration of U or Ra in the supernatants determined by ICP-MS or HR-ICP-MS was used to deduce the amount of the adsorbed and incorporated part of U or Ra.

Firstly, the amount of U or Ra adsorbed on diatoms can be calculated using the following equation:

$$m_{i,adsorbed} = m_{i,eluted} \times {}^{1}/_{e_i} = V_{eluate} \times C_{i,eluate} \times {}^{1}/_{e_i} \qquad \textbf{Eq. II-4}$$

Where $m_{i,adsorbed}$ is the mass of radionuclide adsorbed on diatoms (i stands for U or Ra); $m_{i,eluted}$ is the mass of radionuclide i eluted during the elution step; e_i denotes the elution efficiency for the radionuclide i; V_{eluate} represents the sample volume of the eluate and $C_{i,eluate}$ is the mass concentration of radionuclide i in the eluate (supernatant 2 in **Figure II-3**) determined either by ICP-MS or HR-ICP-MS.

Secondly, the amount of U or Ra incorporated by diatoms, noted as $m_{i,incorporated}$, was deduced using the **Eq. II-5** as is given below:

$$m_{i,incorporated} = V_{digestion} \times C_{i,digestion} \qquad \textbf{Eq. II-5}$$

Where $V_{digestion}$ is the volume of the diatom sample after the digestion; $C_{i,digestion}$ is the mass concentration of the radionuclides (i stands for U or Ra) in the diatom sample after the digestion (supernatant 3 in **Figure II-3**) determined either by ICP-MS or HR-ICP-MS.

Considering some possible loss (of U/Ra mass) during the sample treatment, it is important to check the totality of U or Ra calculated using **Eq. II-4** and **Eq. II-5** and compare with $m_{i,associated}$, the total mass of U or Ra associated to diatoms (including surface adsorption and intracellular incorporation) calculated with **Eq. II-3**. In other words, the sum of $m_{i,adsorbed}$ and $m_{i,incorporated}$ should be equal to $m_{i,associated}$, which should also match the amount of radionuclide initially introduced into the system.

To better describe the partition of U/Ra in the studied U/Ra-diatom system, the distribution coefficient for the adsorption of the radionuclide i, noted as $K_{d,i}$, was calculated with **Eq. II-6**:

$$K_{d,i} = \frac{m_{i,adsorbed}}{m_{i,eq} \times cell\ density} = \frac{m_{i,adsorbed}}{V_{total} \times C_{i,eq} \times cell\ density} \quad \textbf{Eq. II-6}$$

Where $m_{i,adsorbed}$ is the mass of the radionuclide i adsorbed on diatoms calculated by **Eq. II-3**; $m_{i,eq}$ is the mass of the radionuclide i remaining in the solution (supernatant 1 in **Figure II-3**) at equilibrium state; V_{total} is the volume of the diatom suspension; $C_{i,eq}$ represents the mass concentration of the radionuclide i remaining in the diatom suspension (supernatant 1 in **Figure II-3**) when the equilibrium was reached.

The distribution coefficient for the incorporation of U or Ra in the system can also be calculated by simply replacing the $m_{i,adsorbed}$ by $m_{i,incorporated}$ in **Eq. II-6**. Note that the distribution coefficient $K_{d,i}$ was normalized by the diatom cell density of the sample to allow, if needed, further comparison between different batch experiments that may differ in diatom cell density.

Time-dependent U, Ra bio-association study

In order to study the potential impact of diatom's growth phase on the adsorption and incorporation of U and Ra, time-dependent bio-association experiment was performed in triplicates on the xenic *A. saprophilum* diatom culture at a larger time scale. For that, diatom cells prepared using the protocol described in section 5.1 were transferred into fresh sterile DM and incubated under the cultivation conditions mentioned in section 2.3 of this chapter.

At day 0, the diatom culture was spiked with 0.2 or 1 µmol/L of U-238, or with 5 pmol/L of Ra-226. During different diatom growth phases, *i.e.*, acceleration growth phase, exponential growth phase, deceleration growth phase and stationary growth phase in general, diatom cultures were sampled and processed using the same protocol presented in **Figure II-3** to determine the amount of adsorbed and incorporated U or Ra by diatoms. Note that the pH value as well as the cell density of the diatom culture was also measured during each sampling.

The adsorption and the incorporation part of U or Ra in the interaction with diatoms in each growth phase were distinguished using **Eq. II-4** and **Eq. II-5**. To compare quantitatively the U or Ra adsorption and incorporation behavior in different diatom growth phases, the deduced value of $m_{i,adsorbed}$ and $m_{i,incorporated}$ was normalized by the cell density corresponding to each growth phase.

5.3. Inductively coupled plasma-mass spectrometry and high resolution inductively coupled plasma-mass spectrometry analyses

ICP-MS is a powerful analytical technique that was developed only a few decades ago for the quantification of various metals or non-metals in a liquid sample. In comparison with other techniques, ICP-MS offers a wide range of advantages, such as low detection limit, large element range and high sample throughput. Hence, ICP-MS is commonly used for measuring elements at the trace level. Once entering the instrument via a sample introduction system, the liquid sample containing the elements of interest is first nebulized to form a fine aerosol. The aerosol is then carried into an inductively-coupled high-temperature plasma, where the sample is atomized and ionized. The resulting ions pass by a sequence of electrostatic lenses and are

guided into a quadrupole mass analyzer, where ions of interest are separated based on their mass-to-charge ratio and measured by the detector (Wilschefski and Baxter, 2019). HR-ICP-MS (HR-ICP-MS) works on a similar principle and offers a higher resolution capability. The detection limit is even lower for HR-ICP-MS, which can reach the part per quadrillion (ppq) level depending on the specific element.

In this work, XSERIES 2 Quadrupole ICP-MS (Thermo Scientific) and Element XR HR-ICP-MS (Thermo Scientific) were utilized to measure the mass concentration of U and Ra, respectively, in the liquid samples resulting from bio-association experiments. Prior to the ICP-MS analyses, the U-loaded supernatant samples were diluted with 1% HNO_3 (distilled) solution (prepared with Milli-Q water) to a U concentration ranging from 0.1 to 10 ppb (part per billion). The Ra-loaded supernatant samples, however, were mineralized before analyses. It consists of heating 500 µL of the sample, mixed with 1 mL of the distilled HNO_3 solution and 500 µL of 30% (w/w) H_2O_2 solution (Suprapur, Supelco, VWR) in polytetrafluoroethylene (PTFE) containers (Savillex) at 90 °C for 1 hour. After that, the sample was completely evaporated using an evaporation system (Evapoclean). The resulting salt residues in the PTFE containers were dissolved in 500 µL of 7 mol/L HNO_3 solution and stocked in a refrigerator. Prior to the HR-ICP-MS analyses, the samples were centrifuged (mySPIN 12, Thermo Scientific) at 10000 rpm (revolutions per minute) for 5 minutes. A dilution was carried out on the resulting supernatant to a Ra-226 concentration below 20 ppq.

5.4.Langmuir-Freundlich adsorption modelling

The Langmuir adsorption model was first developed by Irving Langmuir in the early 1900s (Langmuir, 1918) and was commonly used to describe the reversible adsorption/desorption process of an adsorbate, e.g., gases in general, onto a solid adsorbent. Several basic assumptions are required for the validity of the Langmuir adsorption model, such as the assumption of a perfect plane and homogeneous surface (adsorbent), and the formation of a monolayer of the adsorbate on the adsorbent. Although deviations from the Langmuir adsorption model were reported in some specific systems (such as shale systems) (Babatunde et al., 2022), the Langmuir adsorption model remains popular and has been used in thousands of studies up to 2018, especially for the study of the adsorption equilibrium in liquid phase systems (Azizian et al., 2018).

The Langmuir adsorption model can be derived via different approaches. A kinetic derivation approach is given below (Azizian et al., 2018).

Supposing a system comprising the adsorbate A (solute) and the adsorbent B, the reversible adsorption and desorption process can be described by **Eq. II-7**:

$$A + B \rightleftharpoons AB \qquad \textbf{Eq. II-7}$$

With k_a and k_d the rate constants of the adsorption and desorption process, respectively.

By definition, the respective rate for the adsorption, r_a, and desorption, r_d, can be expressed by **Eq. II-8** and **Eq. II-9**, respectively:

$$r_a = k_a \times C \times (1 - \theta) \qquad \textbf{Eq. II-8}$$

$$r_d = k_d \times \theta \qquad \textbf{Eq. II-9}$$

Where C represents the solute concentration in solution and θ denotes the surface coverage, which is defined by the ratio of the adsorbed amount of the solute A per unit mass of adsorbent

(q) and the monolayer adsorption capacity (Q_m).

At equilibrium state, i.e., $r_a = r_d$, **Eq. II-8** and **Eq. II-9** yield:

$$k_a \times C_e \times \left(1 - \frac{q_e}{Q_m}\right) = k_d \times \frac{q_e}{Q_m} \quad \textbf{Eq. II-10}$$

Which can be transformed into the Langmuir adsorption model:

$$q_e = \frac{Q_m \times K_L \times C_e}{1 + K \times C_e} \quad \textbf{Eq. II-11}$$

Where the subscript e represents the equilibrium state and K_L denotes the Langmuir equilibrium constant defined as $\frac{k_a}{k_d}$.

Based on the Langmuir adsorption model, various models were developed. For example, the Langmuir-Freundlich adsorption model takes into account the heterogeneity of the adsorbent surface and can be described as followed (Ayawei et al., 2017):

$$q_e = \frac{Q_m \times (K_{L-F} \times C_e)^n}{1 + (K_{L-F} \times C_e)^n} \quad \textbf{Eq. II-12}$$

Where K_{L-F} is the Langmuir-Freundlich equilibrium constant and n is the heterogeneous parameter that is comprised between 0 and 1.

Note that at low and high adsorbate concentrations, the Langmuir-Freundlich adsorption model approaches to Freundlich adsorption model and Langmuir adsorption model, respectively.

6. Investigations at the microscopic scale

6.1. Scanning electron microscopy, transmission electron microscopy and energy-dispersive X-ray spectroscopy investigations

Scanning electron microscopy (SEM) and transmission electron microscopy (TEM) are both important and versatile techniques that were developed in the 20th century and have been commonly used for the characterization of materials in numerous fields. Compared to the conventional optical microscopy, the imaging radiation that is used in SEM and TEM, *i.e.*, electron beam, has a smaller wavelength (100,000-fold shorter than visible light) and thus increases the resolution and magnification of imaging (Winey et al., 2014). In SEM, the electron beam interacts with the atoms in the specimen and produces electrons (backscattered electrons, Auger electrons, secondary electrons), X-rays and photons. These emerging particles or radiations carry information on the surface topography, crystalline structure, chemical composition and electrical properties of about the first 1 μm layer of the specimen (Vernon-Parry, 2000). In TEM, the electron beam transmitted through a thinner specimen can provide valuable information on the internal structure of the specimens. Nevertheless, the preparation of thin specimens may be impossible in certain circumstances, which is a major limitation of this technique (Williams and Carter, 1996). The electron microscope can be coupled with energy-dispersive X-ray spectroscopy (EDX) to characterize the element composition of the specimen. As is mentioned earlier, X-rays are also emitted when the electron beam interacts with the specimen. These X-rays, also called characteristic X-rays, are generated from the transition of inner-shell electrons of the atoms in the specimen from a higher energy level to a lower energy level after being excited by the incident electron beam. Since the emitted characteristic X-rays have specific energy corresponding to each element, the principle of EDX consists of recording the energy spectrum of the emitted characteristic X-rays, identifying each peak energy and assigning them to the corresponding elements. Elemental mapping is also

possible by scanning the specimen with the electron beam and measuring the emitted X-rays at the same time, which provides information on the distribution of the constituent elements within the specimen (Shindo and Oikawa, 2002).

In this work, U-free and U-loaded diatom samples were analyzed by SEM to visualize the diatom-bacteria association and to study the U distribution at the diatom level, respectively. The U-loaded diatom samples were prepared following the same protocol as used in the concentration-dependent bio-association experiments (see in section 5.2), but with a higher U concentration of 500 µmol/L to improve the quality of the U distribution mapping (no U precipitation was observed in the diatom suspension under this concentration). Detailed information of the experimental conditions applied during the preparation of U-loaded diatoms is given in Annex 4. The resulting U-loaded diatom cells were washed with Milli-Q water. To prepare SEM specimens, one drop of the U-loaded diatom sample was loaded on the SEM pin stub, which was then fixed by adding a solution of 2.5% glutaraldehyde (25%, SERVA Electrophoresis GmbH) prepared in 0.1 mol/L phosphate buffer (10.107 g of $Na_2HPO_4 \cdot 7H_2O$ and 1.697 g of $NaH_2PO_4 \cdot H_2O$ in 500 mL of Milli-Q water). The fixed sample was dehydrated using a series of ethanol solution with increasing concentrations, *i.e.*, 20%, 40%, 60%, 80%, and 98% v/v. After each dehydration step, the sample was naturally dried out under a fume hood. The dehydration process ended with the addition of 1,1,1,3,3,3-hexamethyldisilazane onto the diatom sample. Prior to SEM measurements, the SEM pin stub was gold-coated using a sputter coater (Sputter Coater 108auto, Cressington) at 30 mA for 40 seconds. The morphology observation of the diatom cells was carried out with a scanning electron microscope (EVO 50, Carl Zeiss AG) and EDX-based analyses was done by Bruker AXS QUANTAX 200, with an acceleration voltage of 15.0 kV used during the measurements.

U-loaded diatom samples were also analyzed by TEM. For that, diatom culture originating from the U bio-association experiment (exposed to 10 µmol/L of U) was used to prepare TEM specimens. The U-loaded diatom cells were washed with Milli-Q water and transferred into the fixing solution (pH 6.9) made of 4% paraformaldehyde (PFA, pure; Carl Roth) and 0.1 mol/L of HEPES. Thin sections of the fixed cells were prepared at the Center for Regenerative Therapies Dresden (CRTD) prior to TEM analyses. For that, U-loaded diatom cells were post-fixed with 1% glutaraldehyde prepared from 25% solution (EM grade, Electron Microscopy Sciences) in phosphate-buffered solution. The sample was washed five times before being incubated in 2% osmium tetroxide (OsO_4) aqueous solution (prepared from 4% solution, Electron Microscopy Sciences). After the incubation, the resulting sample was washed several times with water and dehydrated with a series of acetone aqueous solutions with increasing acetone concentration ranging from 30% to 100%. Infiltration was then carried out in a series of EPON:acetone mixtures, after which the sample was polymerized using EMbed 812 Kit (Electron Microscopy Sciences) at 70 °C for 48 hours. The resulting diatom sample was cut into thin sections for TEM-based analyses. Bright-field TEM micrographs of diatom thin sections were recorded using an image-Cs-corrected Titan 80-300 microscope (FEI) operated at an accelerating voltage of 300 kV. Areas of interest were selected and further analyzed by high-angle annular dark-field scanning transmission electron microscopy (HAADF-STEM). Spectrum imaging analyses were conducted using EDX with a Talos F200X microscope equipped with a high-brightness X-FEG electron source and a Super-X EDX detector system (FEI) using an accelerating voltage of 200 kV.

6.2.Fourier-transform infrared spectroscopy investigations

IR spectroscopy is a well-established method for identifying and analyzing the structural properties of chemical compounds. Since the molecular absorption of electromagnetic radiation in the IR region can cause transitions between the rotational and vibrational energy levels of the ground electronic energy state, the IR spectrum of a given sample exhibits various peaks that correspond to different molecular vibrational modes, such as symmetric/asymmetric stretching and bending vibrations. In fact, these characteristic vibrational modes are particular to different functional groups or chemical bonds. Consequently, the IR spectrum of a given chemical compound can be regarded as its unique chemical fingerprint (Ismail et al., 1997). Developed in the late 20th century, Fourier-transform infrared (FTIR) spectroscopy is a specific IR spectroscopic technique that use Fourier transform algorithm to convert the recorded interferograms to IR spectra. Compared to other IR spectroscopic techniques, FTIR spectroscopy can simultaneously record spectral data over a wide range of wavelengths with higher precision (Smith, 2011).

In this work, FTIR spectroscopy analyses were performed on: (i) U-free diatom sample in order to identify the major functional groups present on diatoms; (ii) U-loaded diatom sample to characterize the functional groups in interaction with U; (iii) digested U-loaded diatom samples to study the interaction of U with diatom's silica frustule. More precisely, two different types of experiments were performed. The first one is the standard characterization experiment, which consists of measuring IR spectra respectively of the U-free and U-loaded diatom samples and studying their characteristic vibrational bands. The second one, also referred as the "flow-through" experiment in this work, consists of passing a U solution over a pre-stabilized film of diatom cells/frustules at the first place to study the in-situ interaction (adsorption), followed by passing a U-free solution at the second place to study the desorption process of U from a kinetic point of view.

To prepare diatom cells for the standard FTIR measurement, diatom culture (in the exponential growth phase) was centrifuged at 2600 ×*g* for 10 minutes. The resulting cell pellet was thoroughly washed with Milli-Q water to remove nitrate salts initially present in the culture medium. To prepare U-loaded diatom cells, the washed cells were exposed to 10 µmol/L of uranyl(VI) chloride prepared in the solution of 2 mmol/L NaCl buffered with 3 mmol/L HEPES (pH 7.0) for 45 minutes. Detailed preparation conditions are presented in Annex 4. The entire preparation process was concluded by centrifuging and washing the U-loaded diatom sample with Milli-Q water. 2 µL of the prepared sample was added onto the diamond crystal's surface of an attenuated total reflectance (ATR) device (DURASamplIR, Smiths Inc.) and was completely evaporated prior to the FTIR measurement. The IR spectra in the wavenumber region between 800 to 1800 cm^{-1} were measured respectively with U-free and U-loaded diatom cells.

To perform *in situ* "flow-through" experiments, two different solutions were prepared: one was prepared with 10 µmol/L uranyl(VI) chloride in 0.1 mol/L NaCl solution, another was prepared only with 0.1 mol/L NaCl. Prior to the measurements, one drop of the U-free diatom suspension, prepared in the same way as in the standard FTIR characterization experiment, was pipetted and dried out on the ATR crystal's surface to form a homogeneous solid cell film. The film made of diatom cells was equilibrated with a gentle stream (200 µL/minute) of the prepared U-free NaCl solution using a peristaltic tube system. To verify the stability of the cell film during the flushing, *in situ* IR spectra were measured every 12 minutes for 108 minutes and the "difference spectra" were deduced from the IR spectra recorded at distinct exposure time and

the spectrum measured before the flushing serving as a reference. The cell film was stabilized for 16 hours until no significant changes in the "difference spectra" can be observed. Subsequently, to detect absorbance changes in the IR spectra due to the interaction of U(VI) with the diatom cell film, the stabilized cell film was exposed to a gentle stream (200 µL/minute) of the prepared uranyl(VI) chloride solution for 200 minutes, followed by a desorption process where the film was flushed with the U-free solution at the same flow rate for another 50 minutes. During the experiment, *in situ* IR spectra were constantly measured every 3 minutes and the "difference spectra" were deduced. It is worth noting that the "flow-through" experiments were performed both at pH 5.5 and at pH 7.0 on the diatom cell film in this work.

Moreover, similar "flow-through" experiments were carried out on a diatom frustule sample at pH 5.5. To prepare diatom frustules, diatom cells were digested using the protocol described in section 5.1. After the digestion, the sample was centrifuged at 10000 ×*g* for 15 minutes and the resulting pellet was washed with 96% (v/v) ethanol solution and followed by Milli-Q water for three times before use. **Figure II-4** shows the prepared frustules sample observed using SEM. The same protocol described above was then applied in order to perform the "flow-through" experiments on the solid film made of diatom's frustules.

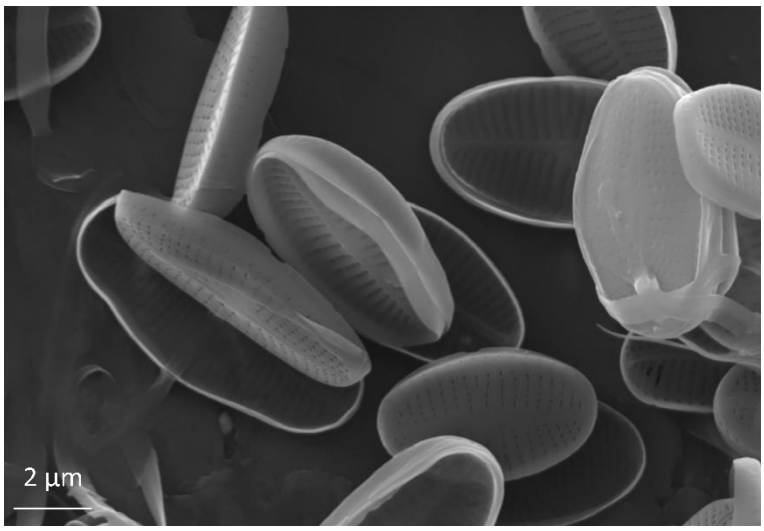

Figure II-4: SEM micrograph of the diatom's frustules. The frustules were prepared from the diatom cells through digestion and a series of washing steps, where the cellular content was removed and only the biosynthesized silica frustules remained in the sample. The diatom's frustule was disintegrated into several parts consisting of valves and girdle bands.

Note that during the experiments, IR (single beam) spectra were recorded using BrukerVertex 80/v or 70/v instruments equipped with Mercury Cadmium Telluride (MCT) detectors. Each obtained IR spectrum had a resolution of 4 cm^{-1} and was averaged over 256 scans.

6.3.Time-resolved laser-induced fluorescence spectroscopy investigations

Time-resolved laser-induced fluorescence spectroscopy (TRLFS) is a powerful analytical technique that is widely used to study the speciation of various fluorescent actinides and lanthanides, such as U, curium (Cm) and europium (Eu) (Collins et al., 2011). Take the U(VI) for example, it is commonly believed that TRLFS displays high sensitivity towards U(VI) and can detect U(VI) compounds at trace level in liquid, solid or powdered samples in a non-destructive way (Sirven et al., 2023). It is stated that the fluorescence of UO_2^{2+} results from the

transitions between electronic excited states and vibronic modes. In fact, the characteristics of U(VI) luminescence spectrum, including positions, spacing and intensities of different emission bands as well as the decay lifetimes, strongly depend on the coordination chemistry of the measured U(VI) compounds. In general, TRLFS analyses provide rich information on the coordination environment of the studied compound by generating inherent multi-dimensional data, which can be solved by multivariate statistical method, *e.g.*, parallel factor (PARAFAC) analysis (Saito et al., 2015). Based on the obtained data (luminescence spectra and luminescence lifetimes), luminescent species can be identified and their distribution in the measured sample can be determined.

In this work, TRLFS measurements were carried out on U-loaded diatom and bacterial isolate samples, respectively. Detailed information regarding the experimental conditions applied during the preparation of U-loaded diatoms and bacterial isolates were summarized in Annex 4.

More specifically, diatoms used for TRLFS analyses were collected from the U(VI) concentration-dependent bio-association experiments described in section 5.2, where a diatom suspension was prepared in the solution comprising 2 mmol/L $NaNO_3$ in the presence or absence of 3 mmol/L HEPES at pH 7.0 and exposed to uranyl(VI) nitrate with a series of concentrations ranging from 0.8 to 20 µmol/L. TRLFS measurements were also performed on the U-loaded diatom cells originating from the time-dependent U(VI) bio-association experiments to study the impact of diatom's growth phase on the U(VI) speciation. For that, a diatom culture was exposed to 1 µmol/L uranyl(VI) nitrate for up to 35 days, and the culture was sampled at the day 4, 11 and 35 for TRLFS analyses. In both cases, diatom cells were separated from the samples by centrifugation (2600 ×*g*, 10 minutes) and washed with Milli-Q water. The resulting supernatant and diatom pellet samples were transferred into disposable plastic cuvettes (half-micro, Rotilabo XK26.1, Carl Roth) and specific sample holders, respectively, and stored at -80 °C prior to the TRLFS measurements.

To study the U(VI) speciation on bacteria present in the *A. saprophilum* culture, isolates of four different bacterial strains, *i.e.*, *Acidovorax facilis* (*A. facilis*), *Agrobacterium fabrum* (*A. fabrum*), *Brevundimonas mediterranea* (*B. mediterranea*) and *Pseudomonas peli* (*P. peli*), were separated from liquid culture by centrifugation at 10000 ×*g* for 5 minutes, washed with Milli-Q water and exposed to 2 µmol/L uranyl(VI) nitrate in 2 mmol/L $NaNO_3$ and 3 mmol/L HEPES solution at pH 7.0 for 45 minutes. At the end of the U(VI) bio-association experiment, samples were centrifuged and washed with Milli-Q water. The resulting pellet was re-suspended with 1 mL of Milli-Q water in disposable plastic cuvettes and subsequently frozen in liquid nitrogen. Similarly, the samples were stored at -80 °C prior to the TRLFS measurements.

To reduce the background noise caused by organic components and quenching effects, the TRLFS measurements were performed under cryogenic conditions (-120 °C) using a Nd:YAG pulsed laser system (Continuum Inlite series; Continuum) with a laser energy of 3 mJ, a frequency quadruplication at 266 nm, and a pulse width of 5–8 ns. More detailed information on the laser system and the applied measuring conditions have been described in the work of F. Rajabi (Rajabi et al., 2021). To evaluate the raw spectral data, Origin 2017 (OriginLab Corporation) was used and the processed data were further subjected to PARAFAC analysis using MATLAB 6.0 software (The Mathworks Corporation). Detailed information is described in the literature(Drobot et al., 2015).

7. Conclusion

In this chapter, the strategy applied for studying the interaction between U, Ra with a xenic *A. saprophilum* diatom culture is presented. On one hand, the cultivation and characterization of *A. saprophilum* diatoms were carried out in this work, followed by a study on the diversity of bacterial community present in the xenic diatom culture based on sequence analyses. Besides, efforts were made in order to isolate bacterial strains from the *A. saprophilum* diatom culture and cultivate the obtained isolates for further speciation investigations. On the other hand, batch-type U/Ra bio-association experiments were conducted to characterize the U/Ra-diatoms interaction at the macroscopic scale, which provided a wide array of information including surface adsorption and intracellular accumulation behavior, the adsorption kinetics, the constant of distribution, etc.

In the meanwhile, various analytical techniques were used in this work to characterize the U-diatoms/bacteria interaction from a cellular and molecular point of view. For example, SEM, TEM and EDX-based analyses were performed to reveal the localization of U at the cell level, while FTIR and TRLFS were applied to study the U speciation.

In the following chapters, relevant results and findings will be presented in detail.

Chapter 3: Characterization of the studied diatom culture

Contents

1. Introduction

Before studying the interaction of U, Ra with the xenic diatom culture obtained from a natural fresh water lake, it is necessary to know, first and foremost, which exact diatom species is/are used in this work? What is the bacterial composition present in the xenic diatom culture? Is there any particular interaction between these different microbial components? What do these diatoms look like and how they grow under the culturing conditions applied in this work?

All of the above questions are addressed in this chapter. The general characteristics of the studied xenic diatom culture are studied and presented in detail: Section 2 presents the results of the diatom taxonomy study based on the sequence analyses. Information on the bacterial diversity present in the diatom culture is provided and the possible interactions between diatoms and bacteria are carefully discussed. In section 3, the co-occurrence of diatoms with associated bacteria is demonstrated using different microscopic techniques. In addition, information on the size of the studied diatom species is given. Section 4 presents results and findings relevant to the diatom's growth as well as their metabolic response to different synthetic media.

Note that parts of the results presented in this chapter are subjected to two planned publications:

(i) He, Y., Sushko, V., Hübner, R., Foerstendorf, H, Steudtner, R., Raff, J., Mallet, C., Beauger, A., Breton, V., Peron, O., Sachs, S., Stumpf, T., Montavon, G. (2023a): Interaction of uranium(VI) with diatoms: a multi-scale study. In preparation.

(ii) He, Y., Wei, S.T., Kluge, S., Flemming, K., Sushko, V., Hübner, R., Steudtner, R., Raff, J., Mallet, C., Beauger, A., Breton, V., Peron, O., Sachs, S., Montavon, G., Stumpf, T. (2023b): Interaction of uranium(VI) with diatoms associated with bacteria living in symbiosis: A microscopic and spectroscopic study. In preparation.

2. Diatom taxonomy verification and bacterial community characterization

2.1. Diatoms

In this work, the 18S rRNA of the diatoms was subject to PCR and the resulting amplicon was sequenced in order to identify the diatom taxon. According to the reported works in the literature (Luddington et al., 2012; Zimmermann et al., 2011), the primer set targeting the V4 region of the 18S rRNA genes and applied for the PCR in this work, exhibits good taxa resolution at the species level and can distinguish the majority (about 96.9%) of the 272 sequences from 272 diatom strains. According to the sequencing results, four ASVs with a sequence length of around 400 base pairs were generated in total from the diatom culture. **Table III-1** summarizes the results of the ASVs analyses, where the most dominant ASV accounts for 87.5% in terms of relative abundance. According to the NCBI Nucleotide BLAST analyses, all the generated ASVs show high identity (> 99.51%) to partial 18S rRNA genes of *A. saprophilum* diatom species (GenBank: MN602031.1), which signifies that the xenic diatom culture used in this work very likely comprises *A. saprophilum* species with high purity.

Table III-1: Analyses of the 18S rRNA amplicon sequence variants generated from diatom culture.

ASVs	Read counts	Relative abundance (%)	Taxonomy	18S sequence identity (%)
ASV_1	32387	87.5	*Achnanthidium saprophilum*	100.00
ASV_2	3594	9.7		99.75
ASV_3	905	2.4		99.75
ASV_4	120	0.3		99.51

2.2.Bacterial community

The sequence analyses on the generated 16S rRNA amplicon reveal the bacterial community structure present in the studied diatom culture, which is summarized in **Table III-2**. According to the Silva SSU database 138.1 (Pruesse et al., 2007), a total of 15 ASVs were identified, revealing the presence of a bacterial community of relatively low diversity in the studied diatom culture. Results suggest that the bacterial community is dominated (with a relative abundance > 10%) by three bacterial genera (ASV_2 to 4): *Pseudomonas*, *Acidovorax* and *Brevundimonas*, which display relative abundance of about 24.5%, 16.2% and 12.9% respectively. The other bacterial genera present only in the minority in the diatom culture, each of them has a relative abundance less than 10%. Note that chloroplast sequences were also detected with a relatively high abundance (> 25%), which may originate from the chloroplast of the *A. saprophilum* diatoms.

Table III-2: Analyses of the 16S rRNA amplicon sequence variants generated from the diatom culture.

ASVs	Kingdom	Phylum	Class	Order	Family	Genus	Read counts	Relative abundance (%)
ASV_1	Bacteria	*Cyanobacteria*	*Cyanobacteriia*	*Chloroplast*	*Chloroplast*	*Chloroplast*	41763	25.87
ASV_2	Bacteria	*Proteobacteria*	*Gammaproteobacteria*	*Pseudomonadales*	*Pseudomonadaceae*	*Pseudomonas*	39616	24.54
ASV_3	Bacteria	*Proteobacteria*	*Gammaproteobacteria*	*Burkholderiales*	*Comamonadaceae*	*Acidovorax*	26117	16.18
ASV_4	Bacteria	*Proteobacteria*	*Alphaproteobacteria*	*Caulobacterales*	*Caulobacteraceae*	*Brevundimonas*	20806	12.89
ASV_5	Bacteria	*Bacteroidota*	*Bacteroidia*	*Flavobacteriales*	*Flavobacteriaceae*	*Flavobacterium*	15021	9.30
ASV_6	Bacteria	*Proteobacteria*	*Gammaproteobacteria*	*Burkholderiales*	*Burkholderiaceae*	*Limnobacter*	10044	6.22
ASV_7	Bacteria	*Proteobacteria*	*Alphaproteobacteria*	*Rhodobacterales*	*Rhodobacteraceae*	*Tabrizicola*	3170	1.96
ASV_8	Bacteria	*Proteobacteria*	*Alphaproteobacteria*	*Rhizobiales*	*Rhizobiaceae*	*Allorhizobium-Neorhizobium-Pararhizobium-Rhizobium*	1538	0.95
ASV_9	Bacteria	*Proteobacteria*	*Alphaproteobacteria*	*Rickettsiales*	*Mitochondria*	*Mitochondria*	1410	0.87
ASV_10	Bacteria	*Proteobacteria*	*Alphaproteobacteria*	*Caulobacterales*	*Caulobacteraceae*	*Phenylobacterium*	1259	0.78
ASV_11	Bacteria	*Actinobacteriota*	*Actinobacteria*	*Propionibacteriales*	*Nocardioidaceae*	*Aeromicrobium*	691	0.43
ASV_12	Bacteria	Uncultured bacteria	Uncultured bacteria	Uncultured bacteria	Uncultured bacteria	Uncultured bacteria	8	0.002
ASV_13	Bacteria	Uncultured bacteria	Uncultured bacteria	Uncultured bacteria	Uncultured bacteria	Uncultured bacteria	5	0.005
ASV_14	Bacteria	Uncultured bacteria	Uncultured bacteria	Uncultured bacteria	Uncultured bacteria	Uncultured bacteria	5	0.003
ASV_15	Bacteria	*Proteobacteria*	*Gammaproteobacteria*	*Pseudomonadales*	*Pseudomonadaceae*	*Pseudomonas*	3	0.003

Additionally, effort has been made to isolate bacteria from the diatom culture. With the protocol described in section 3.2 in Chapter 2, diatom suspension was inoculated onto agar plates comprising DM and 10% LB medium, respectively. After few days of incubation at room temperature, bacterial colonies of various morphologies appeared on both of the plates. However, less colonies were clearly observed on the DM-agar plates. Finally, a total of four bacterial colonies with different appearance were identified on different agar plates and were transferred into liquid DM and 10% LB medium for the following cultivation. Once again, the inoculated bacteria could hardly grow in liquid DM, while a good bacterial development was always observed in 10% LB medium under the applied culturing conditions for all of the four bacterial isolates. Sequence analysis on these bacterial isolates suggested very high identity to *Acidovorax facilis* (*A. facilis*) CCUG 2113 (99.6%), *Agrobacterium fabrum* (*A. fabrum*) C58 (100%), *Brevundimonas mediterranea* (*B. mediterranea*) V4.BO.18 (100%), and *Pseudomonas peli* (*P. peli*) R-20805T (100%), which have already been identified in the bacterial community. Note that the *Agrobacterium* genus is classified as a combined genus named *Allorhizobium-Neorhizobium-Pararhizobium-Rhizobium* in **Table III-2** (Lu and Salzberg, 2020).

Based on these observations, it is reasonable to conclude that the obtained bacterial isolates are very likely to be heterotrophic and might be strongly dependent on the diatoms for normal development in the studied *A. saprophilum* culture (which is in the DM-based culture medium). It is worth mentioning that the applied culture conditions (medium, temperature, etc.) may impose selectivity during the isolation process, which can be justified by the fact that only four out of more than ten bacterial genera were successfully isolated via the streaking technique. Therefore, the discussion relative to bacteria in this work will rather focus on the isolated bacterial strains. To assess the relationship between the diatoms and the associated bacterial community, further investigations are needed. For now, it can only be concluded that the identified bacterial community may benefit from the presence of diatoms. It is clear that the bacterial community does not have a clear inhibitory effect on diatom growth, but a symbiotic relationship between bacteria and diatoms remains uncertain and requires further justification.

3. Microscopic characterization of diatoms and associated bacteria

3.1. Characterization of diatom cells using various microscopic techniques

Figure III-1 shows a micrograph of the *A. saprophilum* diatom culture observed with the light microscope with a magnification of 200x. The figure illustrates how the cells of *A. saprophilum* are uniformly dispersed in the liquid medium. Typically, an *A. saprophilum* diatom cell in good condition exhibits a bright, brownish-yellow color and exists either as a single cell or in short chains consisted of 2 to 4 cells.

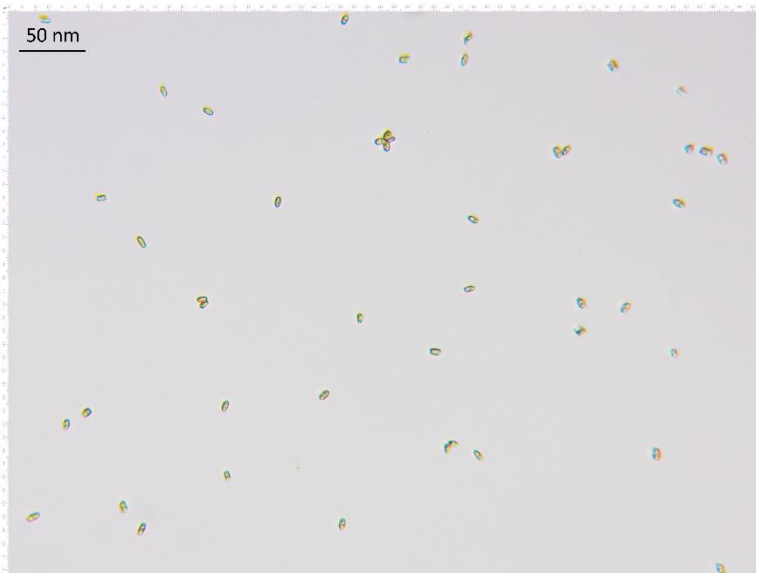

Figure III-1: Micrograph of the *Achnanthidium saprophilum* diatom culture observed with the transmitted light microscope.

Figure III-2 presents a micrograph of an *A. saprophilum* diatom cell observed with the scanning electron microscope, where the intricate structure of the *A. saprophilum* diatom cells are presented in detail, including the raphe, the striae and the punctae for example. The studied diatom species is a pennate species: the cells are bilaterally symmetric and elongate, as can be seen in the figure.

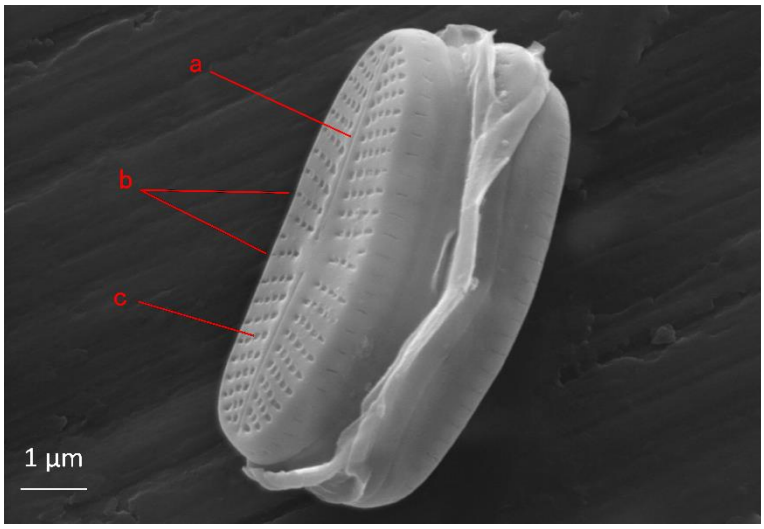

Figure III-2: Micrograph of an *A. saprophilum* diatom cell observed by scanning electron microscopy. The intricate structure of diatom's frustule is illustrated, including: a. raphe; b. striae; c. punctae.

The size of the studied *A. saprophilum* diatoms was measured using light and scanning-electron microscopy with the protocol presented in section 2.4 in Chapter 2. As mentioned in the protocol, the length, width and thickness of one hundred randomly selected cells were measured to represent the typical size of the *A. saprophilum* diatom population used in this work. Note that two independent measurements were made in 2021 and 2022, respectively. **Figure III-3** shows the data collected on the length, width, and thickness of the diatom during these two

independent measurements taken approximately one year apart.

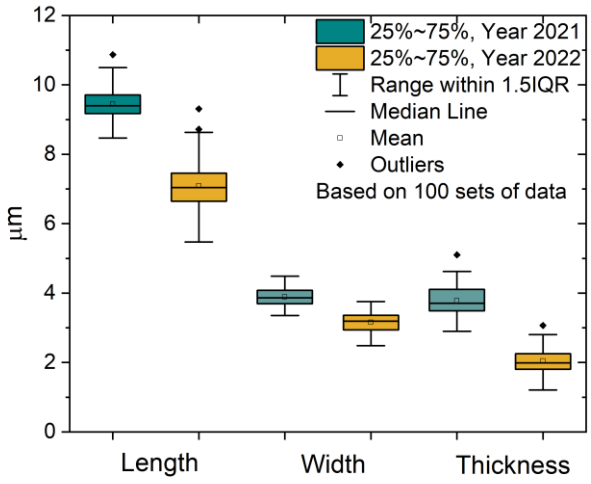

Figure III-3: Size of the *A. saprophilum* diatom cells. Two independent measurements were performed on one hundred randomly selected intact cells in 2021 and 2022, respectively. Measurement was performed with light microscope in 2021 and with scanning electron microscope in 2022.

According to the measurements, the size (length, width and thickness) of the *A. saprophilum* diatom cells decreased to a greater or lesser extent between 2021 and 2022. Assuming that the size of the diatom population can be represented by the group of measured cells, from 2021 to 2022, the average length of the population has approximately decreased from 9.4 to 7.1 µm (-24%), the average width has decreased from 3.9 to 3.2 µm (-18%) and the average thickness has shrunk from 3.8 to 2.0 µm (-47%). The difference between the two independent measurements may be due to the different precision of the two applied microscopy techniques (*e.g.*, measurement error due to the halo effect when using optical microscope), and can be also due to the change of the size in different diatom generations, taking into account the particular cell reproduction mechanism of the diatoms (see section 1.3 in Chapter 1). The variation in the size of diatom cells directly leads to the change in cell surface area, and so the quantity of functional groups available on the diatom surface, which might affect, to some extent, the quantitative study on the U or Ra surface bio-association on diatoms (*e.g.*, the mass of U or Ra adsorbed on the surface of diatoms) for the same diatom cell number or density. In general, the morphological characteristics and the size of the cell presented in this work are in line with the data reported in the literature (Potapova and Hamilton, 2007).

3.2. Association between diatoms and bacteria

The association of diatoms with bacteria is perfectly illustrated by the electron microscopic analysis. For that, the xenic *A. saprophilum* diatom culture (free of U) was observed using SEM (and TEM), the specimen preparation protocol and the applied operating conditions for microscopes are previously described in section 6.1 in Chapter 2. **Figure III-4** presents a SEM micrograph of the *A. saprophilum* diatom specimen. In this micrograph, the presence of some rod-shaped bacteria associated to the surface of diatom cells is clearly illustrated. The observed bacterial cells measure about 1 µm long in general.

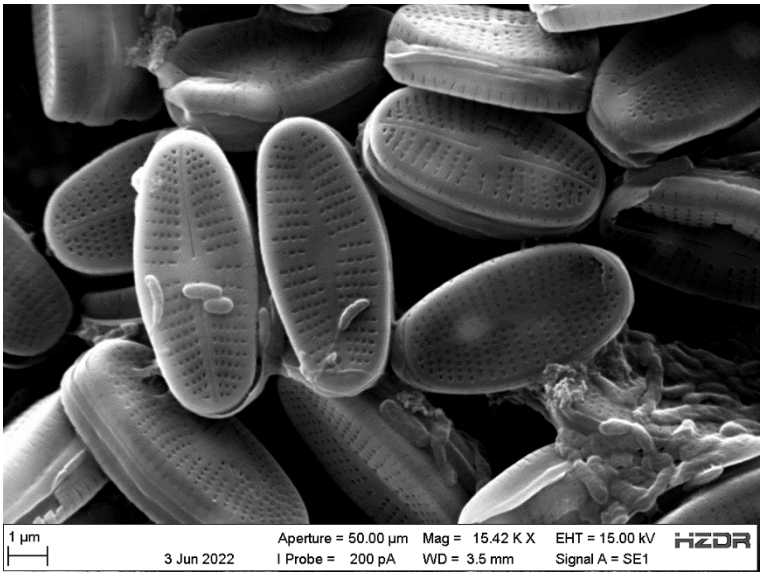

Figure III-4: Micrograph of *A. saprophilum* diatom cells associated with bacteria, observation under scanning electron microscope. The association of rod-shaped bacteria on the surface of diatom cells are observed.

Interestingly, the way how bacteria associate to the surface of diatoms is also revealed by SEM. For example, **Figure III-5** presents a SEM micrograph of some *A. saprophilum* diatom cells that are associated with bacteria, where some rod-shaped bacteria seem to produce EPS (the band-like trace left behind the bacteria highlighted by the marked areas) to help them attaching to the surface of the diatoms. It is reported that the production of EPS by bacteria may facilitate their attachment to the surface of some solid substrates and may contribute to the formation of cell aggregations and eventually to the formation of biofilms (Costa et al., 2018; Decho and Gutierrez, 2017), which has been discussed in section 2 in Chapter 1.

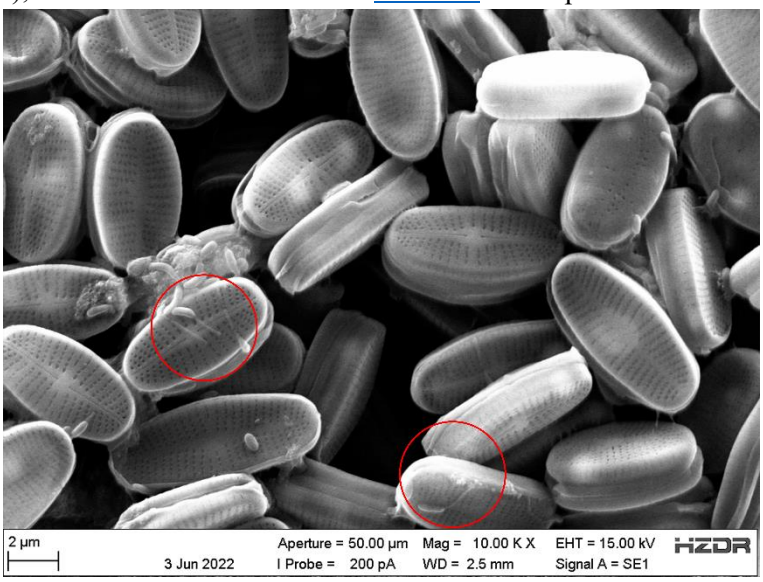

Figure III-5: Micrograph of *A. saprophilum* diatom cells associated with bacteria, observation under scanning electron microscope. Some bacteria likely produce extracellular polymeric substances to attach themselves to the surface of diatoms, as is suggested by the band-like trace behind the bacteria (marked areas).

4. Growth curve of diatoms

The growth curves of the studied *A. saprophilum* diatom cells in DM medium were determined using the protocol described in section 2.5 in Chapter 2. **Figure III-6** shows the growth curves of 10 individual *A. saprophilum* diatom cultures incubated under the applied conditions of this work. According to the results, four major phases can be identified during the growth of *A. saprophilum* diatoms, including (i) acceleration growth phase; (ii) exponential growth phase; (iii) deceleration growth phase and (iv) stationary growth phase.

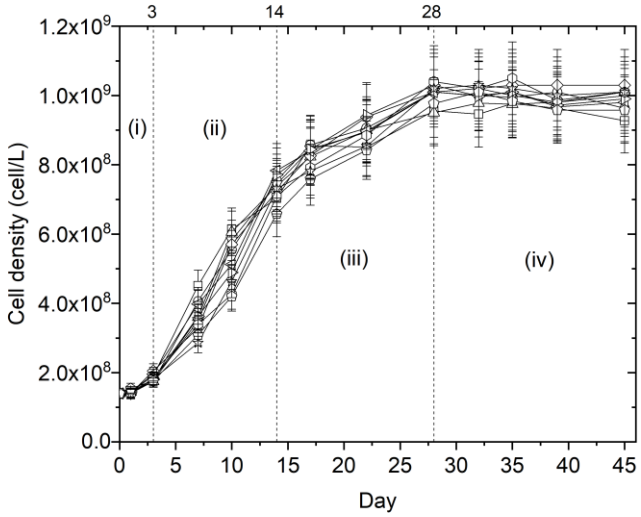

Figure III-6: Growth curve of *A. saprophilum* diatoms. Four different growth phases are observed: (i) acceleration growth phase; (ii) exponential growth phase; (iii) deceleration growth phase; (iv) stationary growth phase.

However, an acceleration of the growth was observed for the studied *A. saprophilum* culture in the frame of this three-year work. In fact, two independent growth-curve studies were conducted at different time points, *i.e.*, in August 2021 and in August 2023, respectively. To compare the corresponding growth curves, data collected from these two experiments are merged into **Figure III-7**. The two independent growth-curve studies were performed under the same experimental conditions and with comparable initial cell density in the diatom cultures. Interestingly, an acceleration of the diatom's growth was clearly demonstrated by **Figure III-7**. It can be observed in the figure that the exponential growth phase seemed to be "compressed" and the stationary growth phase was reached nearly twenty days in advance. In fact, it is reported that the growth of another diatom species that belongs to the same genus, i.e., *A. minutissimum*, can be influenced in the presence of certain bacterial strains (Bruckner et al., 2011, 2008). Considering the long period (from 2021 to 2023) of the cultivation under laboratory conditions, it is likely that the structure of the bacterial community present in the xenic *A. saprophilum* diatom culture also evolved with time, which may lead to the change of the diatom growth reported in this work. Moreover, the regular inoculation of the diatoms may display, to some extent, a potential selectivity towards the diatoms, leading to the eventual acceleration of the diatom growth observed in this work.

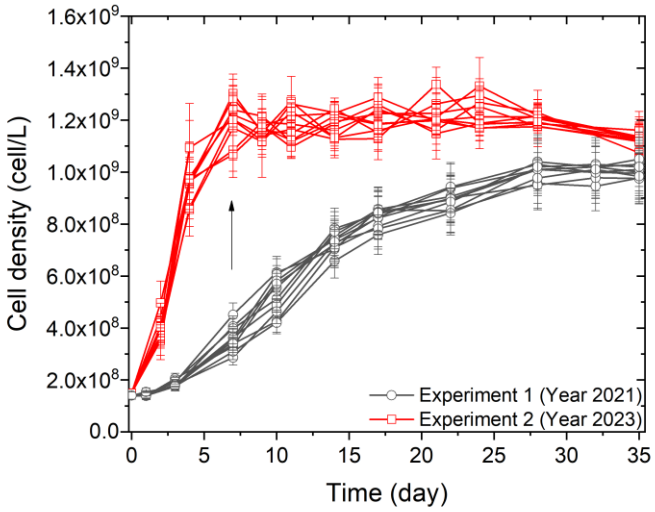

Figure III-7: Growth curve of *A. saprophilum* diatoms. Experiment 1 and 2 were conducted in August 2021 and 2023, respectively.

5. Diatom cell viability and activity test

As mentioned in Chapter 3, a simple medium consisting of 2 mmol/L of NaCl (or $NaNO_3$) and 3 mmol/L of HEPES (pH 7.0) was used in batch-type U/Ra bio-association experiments. In order to verify whether the change of the medium (from the DM medium to the simple NaCl medium) will have an impact on the diatom cell viability and activity, which may further affect the interaction of diatoms with U/Ra, the viability and activity of the diatoms were verified in different media prior to the formal U, Ra bio-association experiments. More specifically, a preliminary cell viability and activity test using flow cytometry (BD FACSAria™ Fusion Flow Cytometer, BD Biosciences) was performed on the *A. saprophilum* diatoms prepared in a series of NaCl solutions with different ionic strength (2 mmol/L, 10 mmol/L) and increasing exposure time (up to 3 hours). Results demonstrated that the cell remained viable and stayed at a constant cellular activity level within three hours of exposure to the medium consisting of 2 mmol/L of NaCl and 3 mmol/L of HEPES. Experimental data are provided in Annex 5.

Hence, it is supposed that the simple medium used in the bio-association experiments will not impact the interaction of U/Ra with diatoms.

6. Conclusion

In this chapter, the diatom culture studied in this work is characterized from different angles. The taxonomy study indicated that the diatom culture purely consists of the *A. saprophilum* species, showing that the diatom isolation and purification process were highly effective. Sequence analyses targeting the 16S rRNA genes confirmed the xenic property of the diatom culture and revealed the presence of a bacterial community with a relatively low diversity. The predominant bacterial genera in the diatom culture were *Pseudomonas*, *Acidovorax* and *Brevundimonas*. Additionally, efforts have been carried out in this work in order to isolate the bacteria from the culture for further investigations.

Using different microscopic techniques, more information on the *A. saprophilum* diatoms were provided, including the size and the morphological features of the cells. The association between bacteria and diatoms was also illustrated using SEM. In fact, the bacteria seemed to produce EPS for the attachment on diatom's surface.

Moreover, the growth curve of the *A. saprophilum* diatom under the applied incubation conditions was investigated. All typical growth phases were identified, including acceleration growth phase, exponential growth phase, deceleration growth phase and stationary growth phase, as commonly stated in the literature. Interestingly, an acceleration of the diatom's growth was observed in this work by comparing the growth curves respectively measured in 2021 and 2023, which might imply the high adaptation ability of the *A. saprophilum* species facing the changing environments (from *in natura* conditions to laboratory conditions).

In conclusion, this chapter provides fundamental information on the diatom culture that was used in this work, which is of vital importance for the study of the interaction between diatoms and U, Ra.

Chapter 4: Uranium, radium batch-type bio-association study on the *Achnanthidium saprophilum* diatoms

Contents

1. Introduction

As is discussed in Chapter 1, the information on the interactions between U, Ra and diatoms are relatively limited in the literature. This chapter quantitatively discusses the U/Ra-diatom interactions at the macroscopic level and presents the experimental data of the U/Ra batch-type bio-association studies, including U/Ra adsorption equilibrium time and U/Ra distribution coefficient. The U/Ra adsorption and incorporation behavior in different diatom growth phases are also discussed in this chapter.

Note that parts of the results presented in this chapter are subjected to two planned publications:

(i) He, Y., Sushko, V., Hübner, R., Foerstendorf, H, Steudtner, R., Raff, J., Mallet, C., Beauger, A., Breton, V., Peron, O., Sachs, S., Stumpf, T., Montavon, G. (2023a): Interaction of uranium(VI) with diatoms: a multi-scale study. In preparation.

(ii) He, Y., Wei, S.T., Kluge, S., Flemming, K., Sushko, V., Hübner, R., Steudtner, R., Raff, J., Mallet, C., Beauger, A., Breton, V., Peron, O., Sachs, S., Montavon, G., Stumpf, T. (2023b): Interaction of uranium(VI) with diatoms associated with bacteria living in symbiosis: A microscopic and spectroscopic study. In preparation.

2. Uranium batch-type bio-association experiments on diatoms

2.1. U adsorption kinetics

To study the U adsorption kinetics, U bio-association experiments were performed with the xenic *A. saprophilum* culture (in the exponential growth phase) using the protocol described in section 5.2 in Chapter 2. The amount of U associated to diatoms at different exposure time was calculated. **Figure IV-1** shows the percentage of U adsorbed on diatoms (ratio of the U mass associated with diatoms to the total U mass introduced into the system) as a function of the exposure time.

As the U fraction associated to the diatoms may comprise a surface adsorbed part (adsorption) as well as an intracellular accumulated part (incorporation) of U, the plotted curve does not uniquely represent, in a strict sense, the kinetics of the U surface adsorption process. Nevertheless, as is stated in the literature, there is no direct proof for the moment that justifies the active uptake of U in diatoms (Kalin et al., 2005), the accumulation of U inside diatom cell, if any, might probably be governed by the passive diffusion mechanism, which is a relatively slow process compared to surface adsorption. As a result, considering the relatively short time scale applied in this kinetics study, it is reasonable to define the equilibrium time for U adsorption based on the evolution of the amount of associated U. Note that the bio-association experiments were limited to three hours of exposure in the model medium according to the cell activity and viability results, which are presented in the previous section (see section 5 in Chapter 3).

Assuming that the cell density of the diatom suspension remains unchanged during the entire experiment, the amount of U associated to diatoms seems to rapidly reach the equilibrium state within the first 10 minutes and stabilizes after. It is worth noting that the adsorption kinetics during the very first minutes remains unclear with the currently applied protocol of this work, since the centrifugation is a relatively time-consuming process (higher rotation speed might damage the diatom cell wall).

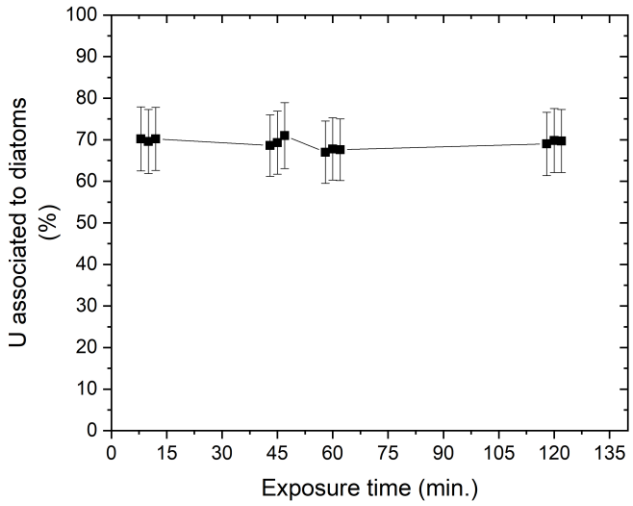

Figure IV-1: Evolution of the amount of U associated to diatoms calculated in percentage. Experiments were performed in triplicates on the *A. saprophilum* diatom suspension (with a cell density of about 3×10^9 cell/L) prepared in the 2 mmol/L NaCl + 3 mmol/L HEPES solution at pH 7. Diatoms were exposed to about 0.2 µmol/L of U(VI) for a series of exposure times (10, 45, 60 and 120 minutes) at room temperature.

2.2.U concentration-dependent bio-association isotherm

The U concentration-dependent bio-association isotherm was studied within the U concentration range from the trace level to the most general concentrations that likely occur in natural conditions (0.2 to 20 µmol/L). To compare, it is reported that the U concentration in groundwaters generally varies from 0.4 nmol/L to 42 µmol/L (Brugge et al., 2005). Experiments were performed with the diatom culture in the exponential growth phase.

The U adsorption isotherm is presented in **Figure IV-2**. The experimental data are fitted using the Langmuir-Freundlich isotherm model (Origin 2018) (Azizian et al., 2018). With the limited data points, it is difficult to conclude the goodness of the fit for the moment. However, a tendency of saturation for U adsorption on diatoms can be observed.

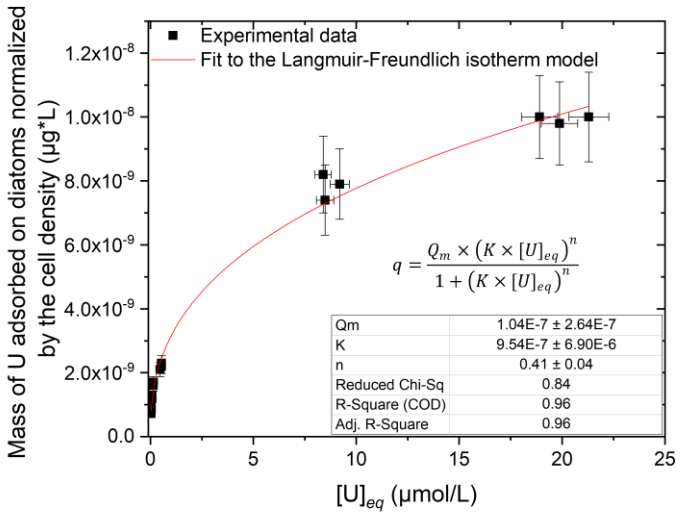

Figure IV-2: U adsorption isotherm, experimental data are fitted with Langmuir-Freundlich isotherm model. Experiments were performed in triplicates on the *A. saprophilum* diatom suspension (with a cell density of about 5×10^8 cell/L) prepared in the 2 mmol/L NaCl + 3 mmol/L HEPES solution at pH 7. Diatoms were exposed to a series of U(VI) concentrations ranging from 0.2 to 20 µmol/L for 45 minutes at room temperature (He et al. 2023b).

On the other hand, with **Eq. II-4** and **Eq. II-5** listed in section 5.2 in Chapter 2, the amount of U adsorbed on diatom' surface and incorporated inside the cells were deduced, and the U distribution coefficient K_d was calculated for the adsorption part and the incorporation part, respectively. **Figure IV-3** presents the log-log plot of the normalized K_d as a function of the U concentration remaining in the solution at the adsorption equilibrium state.

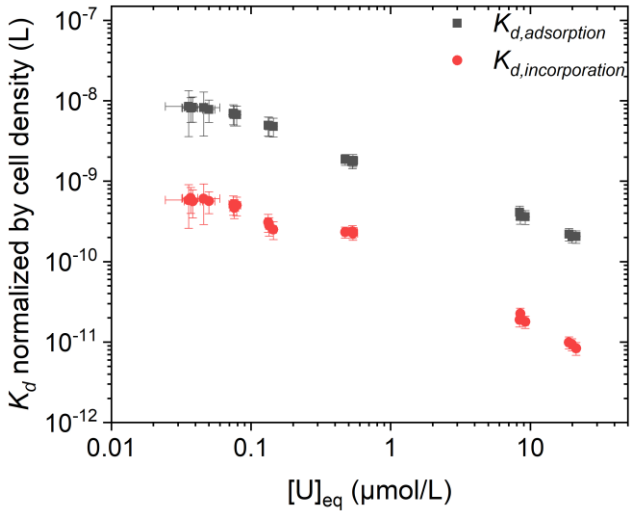

Figure IV-3: Evolution of the U distribution coefficient K_d normalized by the diatom cell density as a function of the U concentration remaining in the solution at the adsorption equilibrium state. Data is presented in log-log scale. Experiments are performed in triplicates on the *A. saprophilum* diatom suspension (with a cell density of about 5×10^8 cell/L) prepared in the 2 mmol/L NaCl + 3 mmol/L HEPES solution at pH 7.0. Diatoms are exposed to a series of U(VI) concentrations ranging from 0.2 to 20 µmol/L for 45 minutes at room temperature.

As shown in **Figure IV-3**, the distribution coefficient for the incorporated U is about one order of magnitude smaller than that of adsorbed part. In fact, the amount (in percentage) of U incorporated by the diatoms decreases with the increasing U exposure concentrations and accounts approximately for up to 7% of the total U present in the entire system. This can be explained by a gradual saturation of U inside the diatom cells, as presented in **Figure IV-4**.

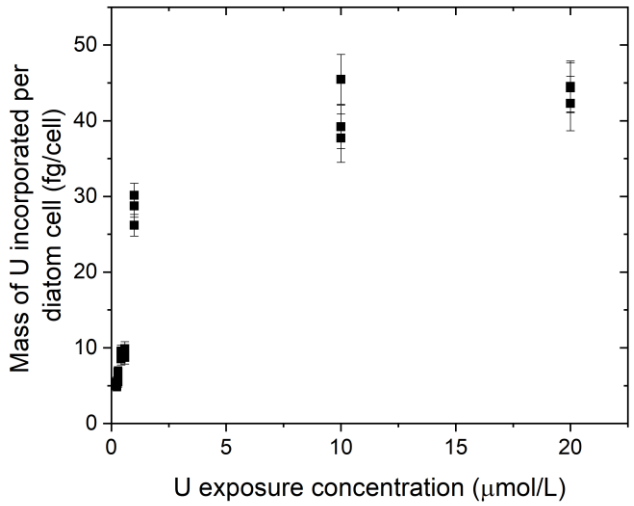

Figure IV-4: The mass of U incorporated per diatom cell as a function of the U exposure concentration. Experiments were performed in the 2 mmol/L NaCl + 3 mmol/L HEPES solution at pH 7.0 at room temperature, with a U exposure time of 45 minutes. The mass is given in femtogram (fg). A clear saturation of the U incorporation by the diatoms was observed, with a maximum U incorporation capacity of about 45 fg/cell.

As shown in **Figure IV-4**, a saturation of the U incorporation was observed for the *A. saprophilum* diatoms as the U(VI) exposure concentration increased. The maximum incorporation capacity of the *A. saprophilum* diatom cell is slightly smaller than 45 fg (femtogram) per cell. Note that the results may be no longer valid with a U exposure time longer than 45 minutes, since the incorporation behavior of U is rather complex as discussed in detail in the next section.

2.3.Time-dependent U bio-association study

Figure IV-5 presents the results of the time-dependent U bio-association study. Different U exposure concentrations and initial cell densities were examined to study the behavior of U (adsorption and incorporation) in different diatom growth phases. The pH varied within the range of 7.1-7.7 during the entire experiment. **Figure IV-5 (a)** shows the evolution of the diatom cell density during the experiment, where all major growth phases can be identified.

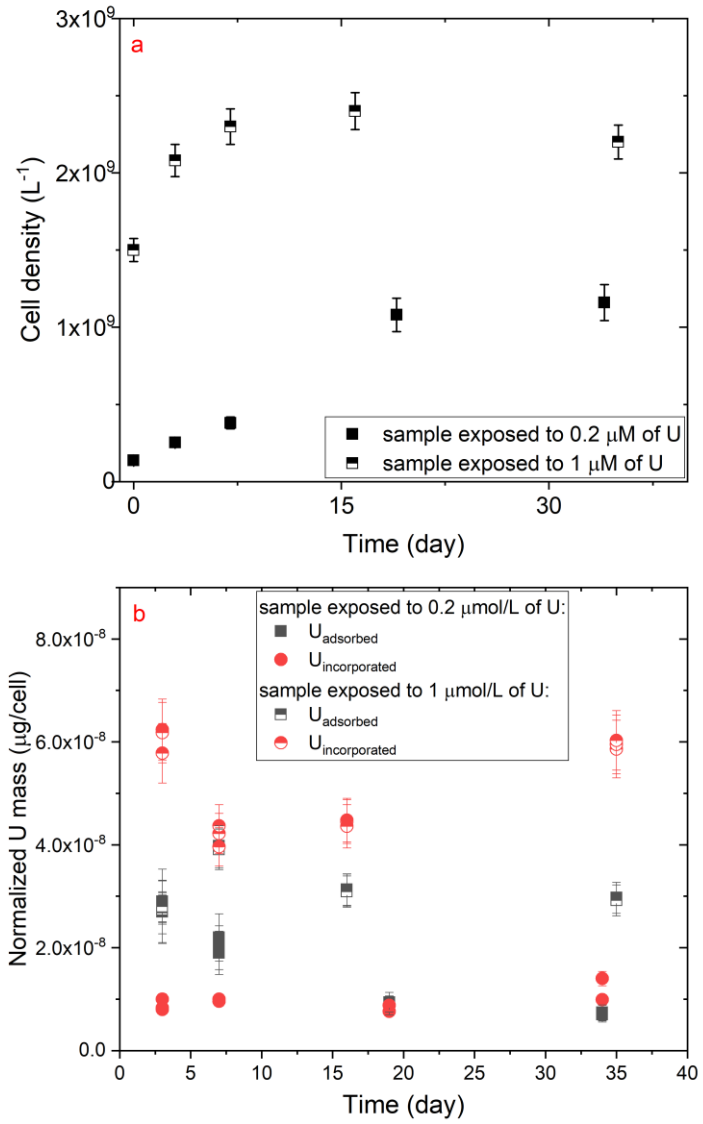

Figure IV-5: Time-dependent U bio-association study. Experiments are performed in triplicates on the *A. saprophilum* diatom suspensions (with an initial cell density of about 1.5×10^8 cell/L and 1.5×10^9 cell/L) prepared in DM at pH around 7.3. Diatoms are respectively exposed to 0.2 and 1 µmol/L of U(VI) at day 0 and incubated for up to 35 days. **(a)** The growth curve of the diatom cultures measured during the experiment and **(b)** The evolution of U mass (normalized by the diatom cell number present in the sample) adsorbed and incorporated by diatoms along with incubation time (He et al. 2023b).

Figure IV-5 (b) shows the mass of U adsorbed and incorporated by diatoms in different growth phases, which is calculated using the mentioned method in section 5.2 of Chapter 2 and normalized by the cell density. In summary, U seems to distribute differently in the studied U-diatom system as the diatom's growth phase evolves, which likely depends on the U exposure concentration as well. The results obtained from the two sets of experiments performed under different conditions, *i.e.*, different initial U exposure concentration and different initial cell density, differ in several aspects, including:

i) Experiment that was performed with a higher initial cell density differentiates better the U adsorption from the U incorporation.

ii) The incorporation part of U surpasses the adsorption part (per unit of diatom cell) in

the diatom culture that is initially exposed to a higher U concentration (1 µmol/L), while these two parts are almost equal in the diatom culture that is initially exposed to a lower U concentration (0.2 µmol/L). This might imply that the *A. saprophilum* diatom cells tend to assimilate more U from the solution either passively (via passive diffusion) or actively (exact mechanisms remain unclear for the moment) as the U concentration increases. Besides, it is worth noting that the ratio between the incorporated U mass and the adsorbed U mass (per diatom cell) accounts for a much higher percentage in this experiment than that in the concentration-dependent U adsorption isotherm study, especially in the diatom culture that is exposed to 1 µmol/L of U. This might be due to the difference in the U exposure time between these two experiments, or can be affected by the diatom growth phase as well. Interestingly, the amount of the incorporated U (per unit diatom cell) decreases from day 3 till day 7 in the culture exposed to 1 µmol/L of U and then gradually increases back to the initial level in the stationary phase (possibly due to cell senescence?), which might indicate a possible U excretion mechanism during the growth of diatoms (a combined microscopic investigation is necessary in this case).

Based on the obtained results, it is now clear that U interacts with diatoms both in the model medium and the DM medium, with the occurrence of the U surface adsorption and the U intracellular accumulation at the diatom level.

Remember that bacteria (associated with diatoms or living freely in the solution) may also contribute to the interaction with U. However, it is impossible to determine the part of U that is associated to bacteria with the applied sample treatment protocol: separation via sonication of the bacteria from the attached diatom's surface will damage the diatom cell and release the incorporated U into the solution; for the bacteria that live freely in the solution, their biomass is too little for U detection. To better assess the contribution of bacteria to the interaction with U in the studied xenic diatom culture, microscopic and spectroscopic techniques were used and further discussion will be given in later sections.

3. Radium batch-type bio-association experiments

3.1. Ra adsorption kinetics

Similar to the case of U, the Ra adsorption kinetics study was conducted on the xenic *A. saprophilum* culture using the protocol described in section 5.2 in Chapter 2. The amount of Ra associated to diatoms at different exposure time was calculated. **Figure IV-6** shows the percentage of Ra adsorbed on diatoms (ratio of the Ra mass associated with diatoms to the total Ra mass introduced into the system) as a function of the exposure time.

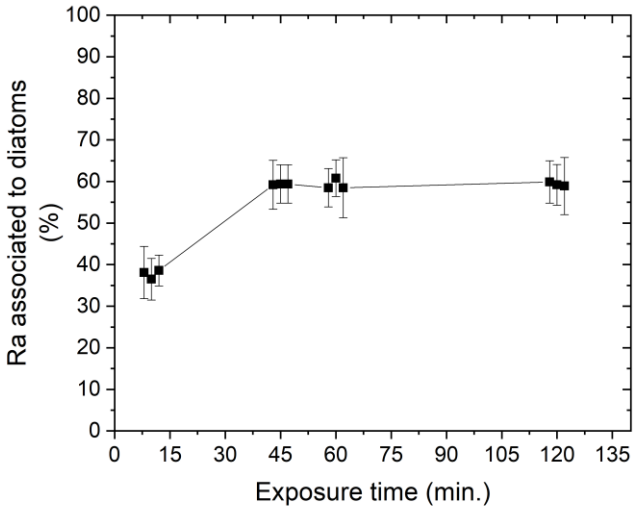

Figure IV-6: Evolution of the amount of Ra associated to diatoms calculated in percentage. Experiments are performed in triplicates on the *A. saprophilum* diatom suspension (with a cell density of about 8×10^8 cell/L) prepared in the 2 mmol/L NaCl + 3 mmol/L HEPES solution at pH 7. Diatoms are exposed to about 6 pmol/L of Ra for a series of exposure times (10, 45, 60 and 120 minutes) at room temperature.

Compared to the case of U, the adsorption of Ra on diatoms is slower. As shown in **Figure IV-6**, the equilibrium state is reached 45 minutes after the exposure of the diatoms to Ra. Consequently, in the batch-type bio-association experiments for studying the Ra adsorption isotherm, the diatom suspension was exposed to Ra for 45 minutes to ensure that the equilibrium state was well established.

3.2. Ra concentration-dependent bio-association isotherm

The isotherm of the Ra bio-association was studied on the *A. saprophilum* diatom suspension with an initial Ra concentration ranging from 0.8 to 4 pmol/L. The applied experimental conditions are provided in detail in section 5.2 in Chapter 2. **Figure IV-7** presents the evolution of the Ra mass adsorbed on diatoms (normalized by the cell density) as a function of Ra concentration remaining in the solution in the adsorption equilibrium state.

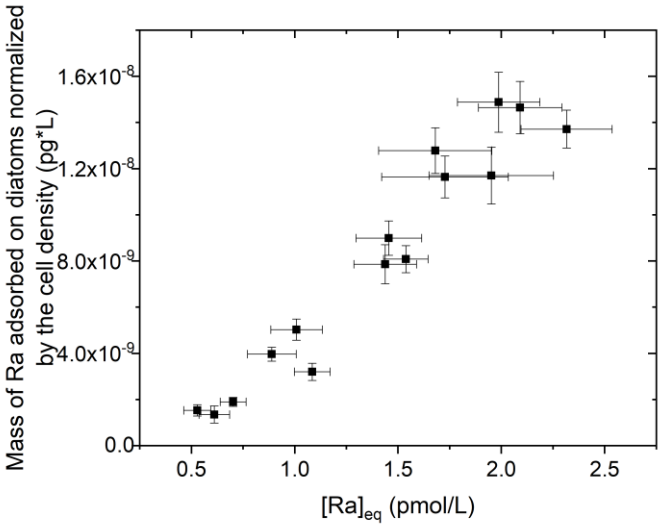

Figure IV-7: Ra adsorption isotherm. Experiments are performed in triplicates on the *A. saprophilum* diatom suspension (with a cell density of about 4×10^8 cell/L) prepared in the 2 mmol/L NaCl + 3 mmol/L HEPES solution at pH 7. Diatoms are exposed to a series of Ra concentrations ranging from 0.8 to 4 pmol/L for 45 minutes at room temperature.

The experimental data were fitted with both Langmuir isotherm and Langmuir-Freundlich isotherm models (Origin 2018) but the fitting failed to converge. Considering the applied initial Ra concentrations at trace level, it is highly likely that the obtained experimental data are found in the "linear" region of the mentioned adsorption isotherm models. Due to the relevant radioprotection regulations, experiments with Ra-226 were not performed at higher concentrations in this work.

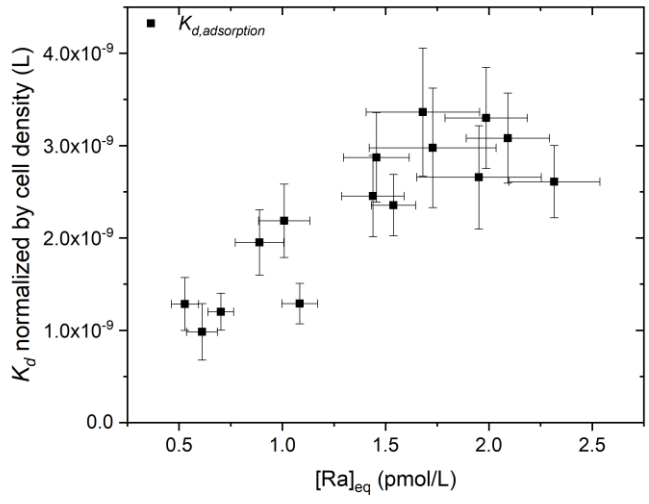

Figure IV-8: Evolution of the Ra distribution coefficient K_d normalized by the diatom cell density as a function of the Ra concentration remaining in the solution at the adsorption equilibrium state. Experiments are performed in triplicates on the *A. saprophilum* diatom suspension (with a cell density of about 4×10^8 cell/L) prepared in the 2 mmol/L NaCl + 3 mmol/L HEPES solution at pH 7. Diatoms are exposed to a series of Ra concentrations ranging from 0.8 to 4 pmol/L for 45 minutes at room temperature.

As shown in **Figure IV-8**, the normalized Ra distribution coefficient increases with the Ra concentration remaining in the solution in the equilibrium state, which is contradictory to the earlier hypothesis that the experimental data are located in the "linear region" of the adsorption isotherm model. This would suggest that the interaction of Ra with diatoms may not be a simple surface adsorption. However, no Ra incorporation was detected in this experiment using the applied sample analyzing protocol (no obvious difference was observed between the total mass of Ra associated to diatoms and the mass of Ra adsorbed on diatoms, which yielded zero Ra incorporation considering the data error).

In general, the obtained experimental data are different to what were observed in the case of U. In fact, experiments were conducted under substantially different conditions in terms of U and Ra exposure concentrations (from ppb level down to ppq level). In addition, it is possible that U and Ra exhibit different bio-association behaviors with the diatoms. Hence, it is hard to compare the bio-association data between U and Ra.

3.3. Time-dependent Ra bio-association study

To better understand the potential impact of diatom's growth phases on the Ra bio-association, time-dependent experiments were conducted on the *A. saprophilum* diatom culture that was initially exposed to 5 pmol/L of Ra and incubated up to 25 days. During the incubation, aliquots of the diatom culture were regularly sampled to determine the Ra distribution in the system using the protocol previously described. Throughout the entire experiment, the pH varied approximately within the range of 7.2-7.8. **Figure IV-9** presents the evolution of the cell density as well as the amount of Ra adsorbed or incorporated by the diatoms along with time.

As presented in **Figure IV-9 (a)**, different diatom growth phases were identified, including acceleration growth phase, exponential growth phase and stationary growth phase. The distribution of Ra in the studied system is illustrated by **Figure IV-9 (b)**, where the mass of the adsorbed and incorporated Ra is presented in normalized form. As indicated by the data, the adsorption predominates the interaction of Ra with diatoms throughout the growth of the diatoms. The mass of the adsorbed Ra (per diatom cell) decreases rapidly during the diatom's acceleration and exponential growth phase, which might be due to: (i) Firstly the increasing diatom cell population, *i.e.*, the increasing surface binding sites available for Ra forming in the system, (ii) Secondly, the constant release of some organic matters (*e.g.*, DOC) or cell exudates by the diatom cells into the solution, resulting in a competition of Ra between the part associated to diatoms and the part present in the solution. With increasing exposure time, the amount of Ra adsorbed per diatom cell gradually stabilized at a relatively low level. A similar pattern was observed in the time-dependent bio-association experiment for U, where the diatom cells were initially exposed to a lower concentration (0.2 μmol/L). However, the incorporation of Ra by diatoms was nearly imperceptible: a very low amount of Ra was clearly detected inside diatom cells during the stationary growth phase. This could potentially be explained by the alterations in the diatom cell membrane permeability towards Ra as the diatom population aged.

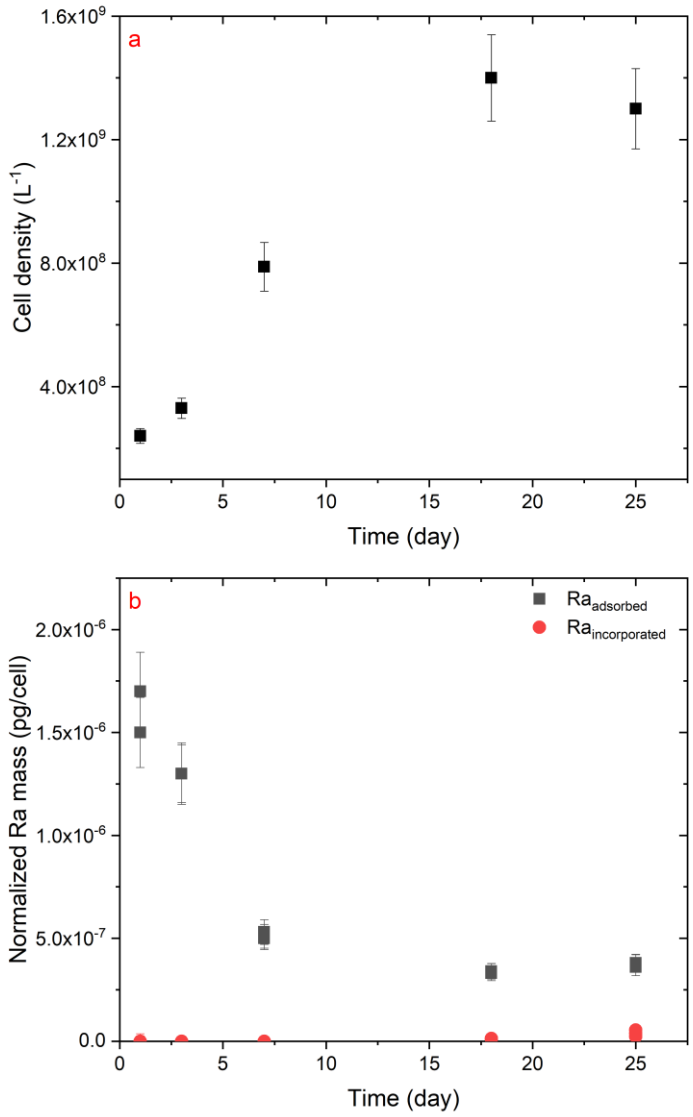

Figure IV-9: Time-dependent Ra bio-association study. Experiments are performed in triplicates on the *A. saprophilum* diatom suspensions (with an initial cell density of about 2×10^8 cell/L) prepared in DM at pH around 7.3. Diatoms are exposed to 5 pmol/L of Ra at day 0 and incubated for up to 25 days. **(a)** The growth curve of the diatom culture measured during the experiment and **(b)** The evolution of the Ra mass (normalized by the diatom cell number present in the sample) adsorbed and incorporated by diatoms along with incubation time.

4. Conclusion

In this chapter, the interaction of U, Ra with the xenic *A. saprophilum* diatom culture is quantitatively discussed at the macroscopic level. By carrying out the U and Ra bio-association experiments, this work contributes to a better understanding of the U and Ra-diatom interaction and provides valuable information including the adsorption kinetics, the adsorption isotherm and the potential effects of diatom's growth phase on the adsorption/incorporation behavior.

As suggested by the experimental data, the U adsorption on diatoms is proved to be a rapid process (adsorption equilibrium reached within the first 15 minutes of exposure), while the adsorption equilibrium state for Ra seems to take a relatively longer time to establish (about 45 minutes). On the other hand, the concentration-dependent bio-association experiments would suggest that the U adsorption isotherm on diatoms likely follows the Langmuir-Freundlich models. However, few information can be deduced in the case of Ra due to the limited access to higher concentrations applicable for experiments. Besides, the time-dependent bio-association experiments show that the adsorption of U and Ra on diatoms generally decreases with time and is then stabilized as the diatom population ages. This decrease in adsorption might be explained by the competition between the complexation of U and Ra with different components present in the culture, *e.g.*, diatom cells and organic matter released by diatoms into the solution.

As for the incorporation, this process is significant for the case of U. Experimental data would also suggest the gradual alterations in the diatom cell membrane permeability towards U, since the incorporated amount of U per diatom cell increases with time. Unlike U, no significant incorporation was observed for Ra. This is rather surprising, given that Ra belongs to the family of alkaline-earth elements and that the latter generally play a crucial role in the cellular metabolism for the living organisms (such as Mg and Ca).

To further understand the interaction of diatoms with radioelements at the cellular and molecular level, various microscopic and spectroscopic techniques were applied. In the next chapter, microscopic and spectroscopic data will be presented for U in particular, since certain techniques were not applicable to Ra due to the radioprotection regulations.

CHAPTER 4: URANIUM, RADIUM BATCH-TYPE BIO-ASSOCIATION STUDY ON THE *ACHNANTHIDIUM SAPROPHILUM* DIATOMS

Chapter 5: Microscopic and spectroscopic characterization of the uranium-diatom interaction

Contents

1. Introduction

This chapter presents the experimental data of the microscopic and spectroscopic investigations on the U-diatom interaction performed in this work. By combining different microscopic and spectroscopic techniques, the U-diatom interaction is elucidated from a microscopic and molecular point of view.

To be concise, section 2 reveals the localization of U characterized by different electron microscopic techniques at the diatom level. Section 3 and 4 present the speciation studies of U in the interaction with diatoms using different spectroscopic techniques (FTIR, TRLFS), where the speciation of U and the functional groups involved in the U-diatom interaction are qualitatively discussed. It is worth noting that the contribution of the bacteria that are present in the xenic *A. saprophilum* culture is discussed in detail in this chapter as well.

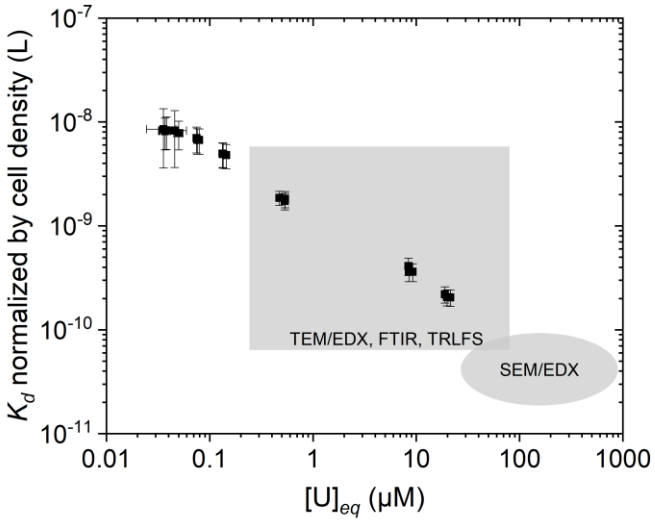

Figure V-1: The microscopic and spectroscopic investigations were performed within the range of the U concentration (at the equilibrium state) highlighted in the evolution curve of the U distribution coefficient as previously presented in **Figure IV-3** (He et al. 2023b).

To better link the macroscopic data to the study at the microscopic level, **Figure V-1** shows the range of the U concentrations (at the equilibrium state) applied for various microscopic (SEM/EDX, TEM/EDX) and spectroscopic (FTIR, TRLFS) investigations. Note that for the TEM/EDX, FTIR and TRLFS measurements, no U precipitation was observed in the studied model medium at the applied U concentration level both in the presence and absence of the diatoms. However, in the absence of the diatoms, a precipitation of U was observed in the model medium under the U concentration applied for the SEM/EDX measurements. However, no obvious U precipitation was observed in the presence of the diatoms during the sample preparation.

Note that parts of the results presented in this chapter are subjected to two planned publications:

(i) He, Y., Sushko, V., Hübner, R., Foerstendorf, H, Steudtner, R., Raff, J., Mallet, C., Beauger, A., Breton, V., Peron, O., Sachs, S., Stumpf, T., Montavon, G. (2023a): Interaction of uranium(VI) with diatoms: a multi-scale study. In preparation.

(ii) He, Y., Wei, S.T., Kluge, S., Flemming, K., Sushko, V., Hübner, R., Steudtner, R.,

Raff, J., Mallet, C., Beauger, A., Breton, V., Peron, O., Sachs, S., Montavon, G., Stumpf, T. (2023b): Interaction of uranium(VI) with diatoms associated with bacteria living in symbiosis: A microscopic and spectroscopic study. In preparation.

2. Scanning electron microscopy, transmission electron microscopy and energy-dispersive X-ray spectroscopy data

SEM specimens of the U-loaded diatom cells were prepared by following the preparation protocol presented in section 6.1 in Chapter 2. **Figure V-2 (a-d)** shows the secondary-electron micrograph of a diatom specimen with corresponding EDX-based element distribution maps for Si, P and U. The Si signal originating from the biosynthesized silica clearly depicts the diatom's frustule. By comparing the obtained element distribution maps, indications for a co-localization of P and U were observed at the diatom level. Nevertheless, it is not possible to distinguish on the map the U adsorbed on diatom's surface from the U incorporated inside the cells. In order to better study the U distribution on/in the diatom cells, TEM was applied on the specimens of diatom's thin section prepared with the protocol described before.

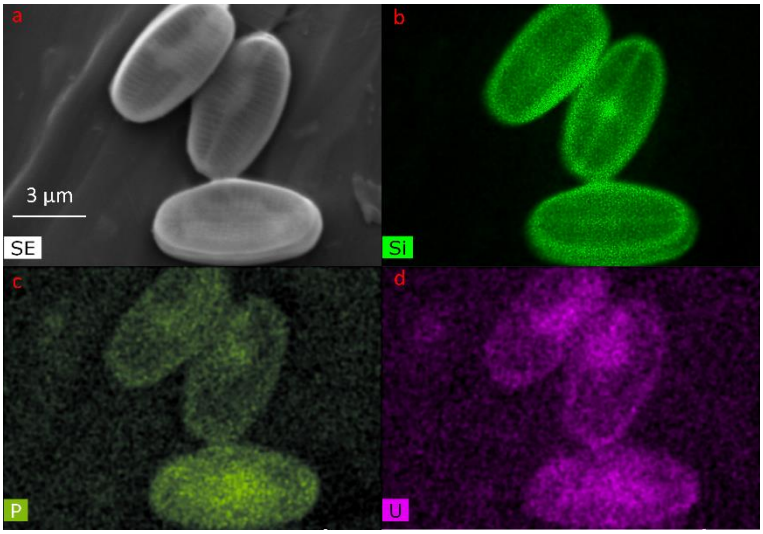

Figure V-2: **(a)** Secondary-electron SEM image of the U-loaded diatom cells, and **(b-d)** corresponding EDX-based element distribution maps for Si, P, and U (He et al. 2023b).

Figure V-3 (a) presents the bright-field TEM micrograph of U-loaded diatom cells. The micrograph clearly illustrates the unique structure of the diatom's silica frustule, which is depicted by the thin electron dense layer in the bright-field micrograph surrounding the cells. The fine structure of punctae, *i.e.*, the tiny perforations across the diatom's frustule, is perfectly shown in the HAADF-STEM image (**Figure V-3 (b)**) which shows a magnification of the area marked in red in the bright-field image. Interestingly, a rod-shaped bacterium cell associated to the diatom's surface can also be observed in this particular area. The interface between the bacterium and the diatom is clearly defined by the silica frustule of the diatom cell, as demonstrated in the EDX-based element distribution map for Si (**Figure V-3 (c)**).

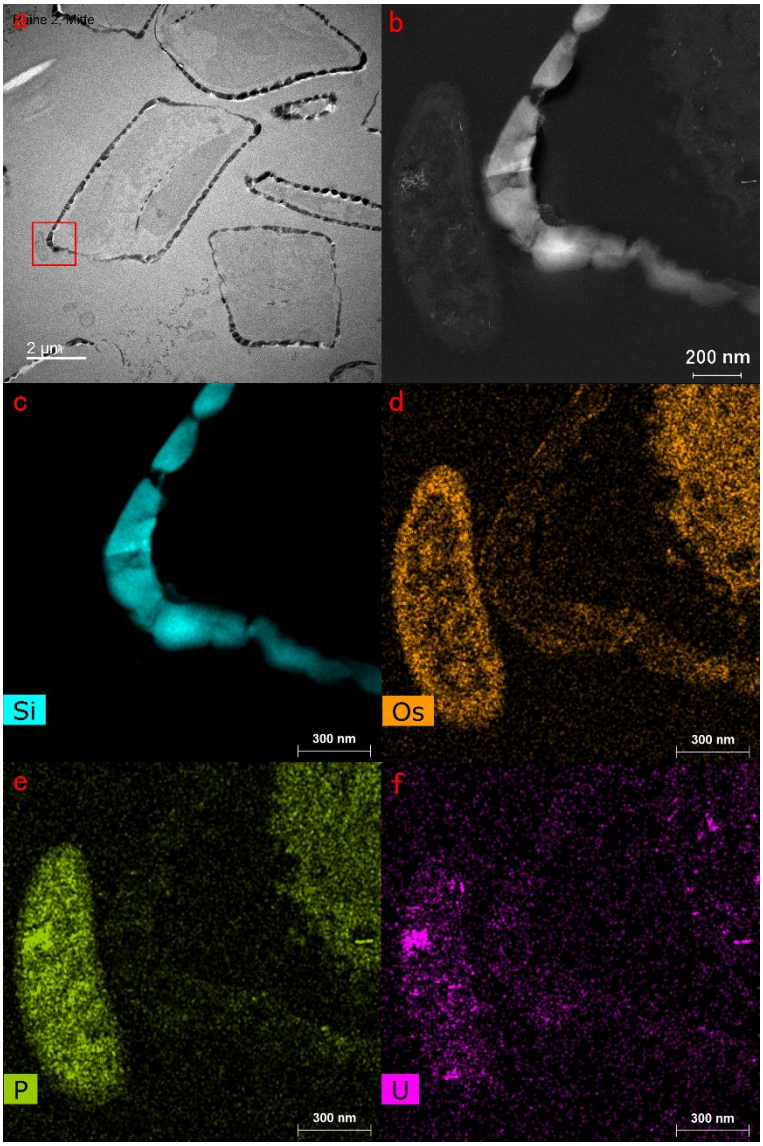

Figure V-3: **(a)** Bright-field TEM micrograph of a thin section of U-loaded diatom cells, **(b)** HAADF-STEM image of the area of interest (marked in red in **(a)**) and **(c-f)** the corresponding EDX-based element distribution maps for Si, Os, P and U. Detailed structure of the diatom's silica frustule and the cell membrane were illustrated by the element distribution maps for Si and Os, respectively. In addition to the diatom, the bacterium associated to the diatom's surface also contributes to the binding of U. A co-localization of U and P was observed in both the diatom and bacterium. Figure adapted from the work of He et al. 2023a.

To understand the distribution of U at the cellular level in this specific area, EDX-based analyses were performed. **Figure V-3 (d-f)** shows the element distribution maps corresponding to various elements of interest (Os, P and U) that were selected for further discussion. **Figure V-3 (d)** presents the distribution map of Os, which originates from osmium tetroxide used during the specimen preparation for its well-known ability to post-fix and stain tissues or cells by interacting with lipids. As a result, the biological membranes, including the cell wall and the cell membrane of the bacterium and diatom cell, are clearly visible. Besides, the distribution of P in the selected area is presented in **Figure V-3 (e)**, where a uniform distribution of P was observed in both the bacterial cell and the biomass of the diatom cell. P is commonly found in cells and can originate from a variety of inorganic and organic substances, e.g., lipids,

lipopolysaccharides, etc. Some of these molecules are important components of the biological membranes of bacteria/diatoms. **Figure V-3 (f)** highlights the distribution of U in the studied area. In fact, it can be observed from the map that U localizes both on the surface and inside the bacterium and the diatom cell. Additionally, U likely occurs inside the cells in form of precipitates as represented by some dense areas on the map. By comparing the element distribution maps, it appears that U co-localizes with P.

Another spot on the same U-loaded diatom cell was subjected to EDX-based analysis, as highlighted by the marked area in **Figure V-4 (a)**. In this selected area, some electron dense precipitate-like matters are likely observed, as shown by the white needle-shaped spots that appeared in the dark-field STEM micrograph (**Figure V-4 (b)**). These electron dense areas were randomly located inside the diatom cell, and probably within an organelle as demonstrated by the EDX-based element distribution maps for Si and Os (**Figure V-4 (c-d)**). In fact, the distribution map for U within the studied area (**Figure V-4 (f)**) suggested that these electron dense matters may highly likely be the precipitates of U, since their locations overlapped well in the two figures. Once again, by comparing the corresponding element distribution maps, a co-localization was always observed between U and P (**Figure V-4 (e)**). Hence, it may be concluded, based on the data obtained so far, that the U can be incorporated by the diatom cells and associated to the cellular organelles through complexation with some P-bearing biomolecules with a possible formation of U precipitates as well.

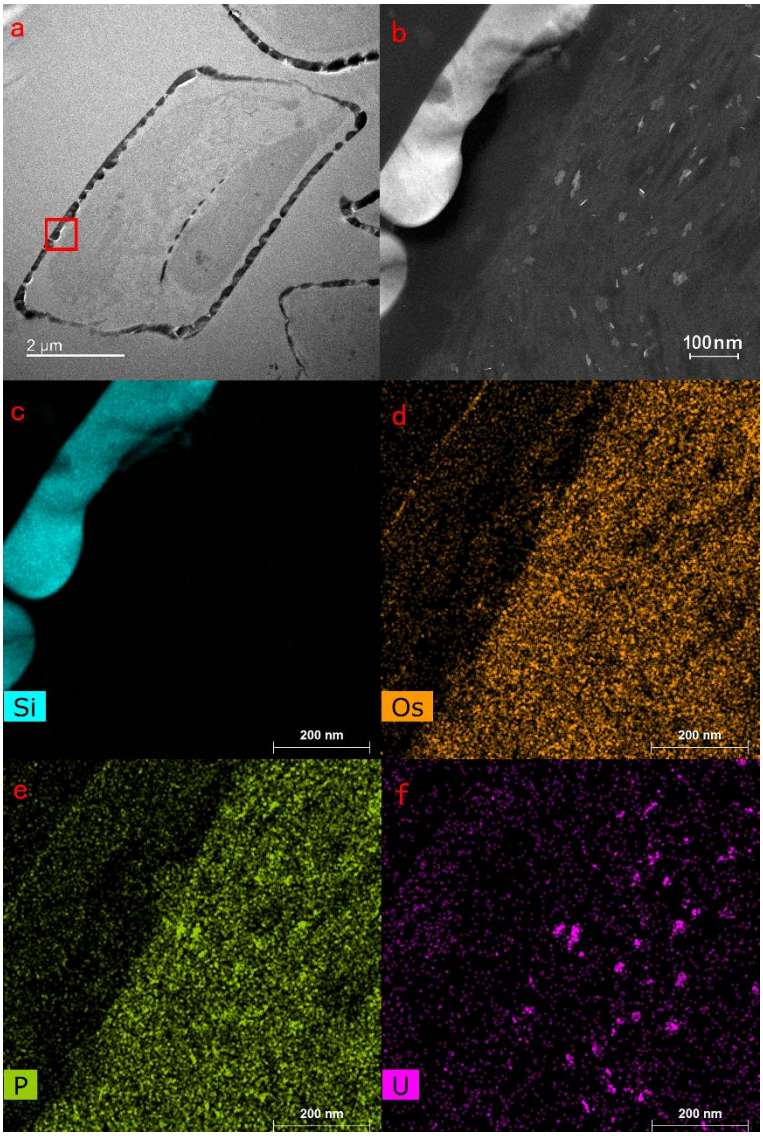

Figure V-4: **(a)** Bright-field TEM micrograph of a thin section of U-loaded diatom cells, (b) HAADF-STEM image of the area of interest (marked in red in **(a)**) and **(c-f)** the corresponding EDX-based element distribution maps for Si, Os, P and U. Some precipitate-like electron dense matters were observed within the area of interest, as illustrated by the U distribution map (**f**).

Moreover, attention was drawn by another diatom cell in the TEM specimen that displays clearly a defined structure characteristic to the vacuole, which was represented by the big and nearly void "pools" within the diatom cell as shown in the TEM bright-field micrograph (**Figure V-5 (a)**). In the square area that is marked in bold line within the vacuole, some precipitate-like U species were found, as depicted by the light regions in **Figure V-5 (b)**, which are also co-localized with P as stated in earlier cases (**Figure V-5 (d-e)**). Interestingly, by looking at the EDX-based element distribution maps for other elements (**Figure V-5 (f-m)** in an electron dense area highlighted by the red square in dotted line in **Figure V-5 (a)**, a co-precipitation of various metal ions including U was observed. Intense signals for N and P were also detected in the same area, suggesting the possible co-precipitations or complexation of metals with biomolecules of the diatom.

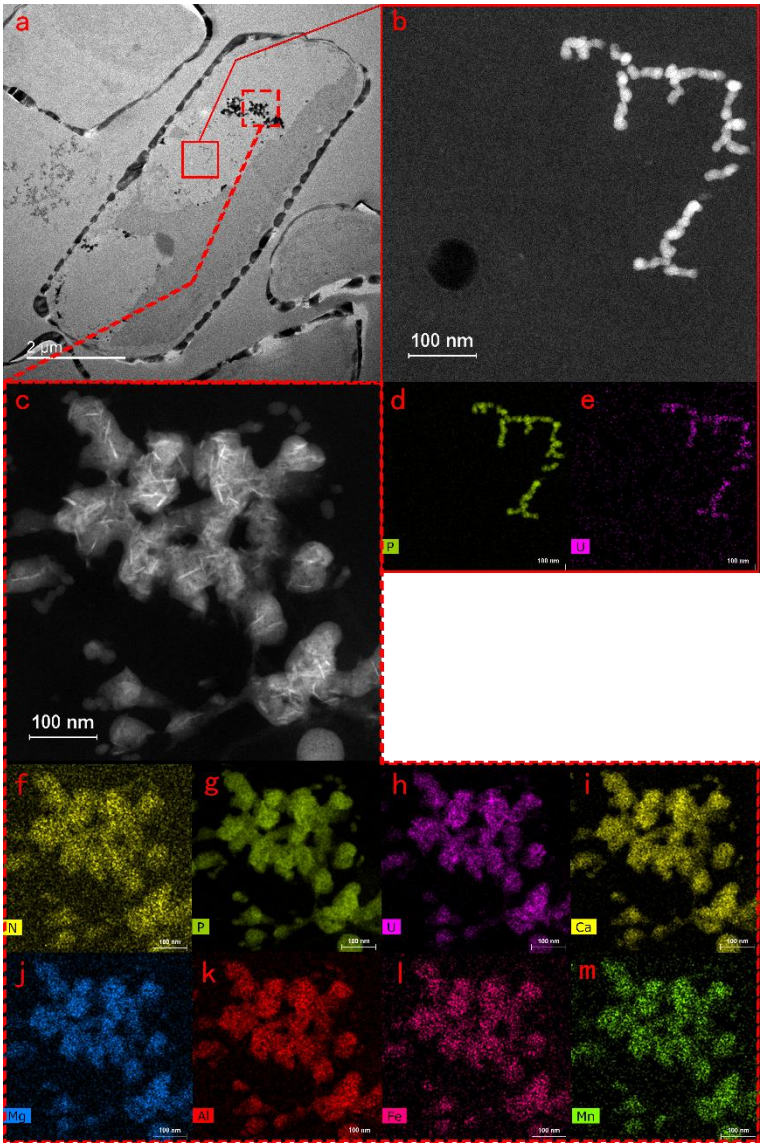

Figure V-5: **(a)** Bright-field TEM micrograph of a thin section of U-loaded diatom cells, **(b)** HAADF-STEM image of the area of interest (marked in red with bold line in **(a)**) and **(d, e)** the corresponding EDX-based element distribution maps for P and U, **(c)** HAADF-STEM image of the area of interest (marked in red with dotted line in **(a)**) and **(f-m)** the corresponding EDX-based element distribution maps for N, P, U, Ca, Mg, Al, Fe and Mn. Co-precipitations of various metals were found inside the diatom and notably within the vacuole, as illustrated by the electron dense matters in the area of interest of the micrograph. Figure adapted from the work of He et al. 2023b.

3. Fourier-transform infrared spectroscopy data

Figure V-6 shows the IR spectra of dry samples made of U-free diatom cells (lower trace) and U-loaded diatom cells (upper trace), respectively. Due to abundant biomolecules present in the sample, the IR spectra displayed characteristic bands around 1650 and 1550 cm^{-1} that respectively correspond to amide-I and amide-II modes of proteins (Jiang et al., 2004). Besides, a band representing C=O stretching modes of ester and carboxyl groups was observed at higher frequencies around 1740 cm^{-1} in the spectra (Regvar et al., 2013). Moreover, a noticeable intense band was observed at 1072 cm^{-1}, which most likely corresponds to silanol groups of the

diatom's frustules. Nevertheless, functional groups of further organic compounds may also contribute in this spectral region. For example, modes of phosphorylated biomolecules, along with the ν(C–O) and ν(C–C) modes of sugar moieties of (lipo)polysaccharides and glycoproteins that are present in the diatom samples were expected to also display intense vibrational bands in this frequency range (Jiang et al., 2004; Oliveira et al., 2014; Regvar et al., 2013), which was not the case as observed in **Figure V-6**.

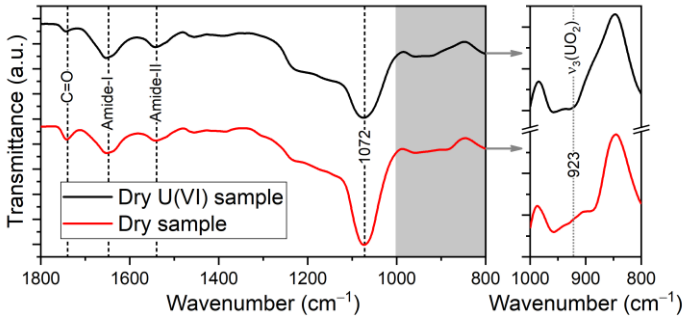

Figure V-6: IR spectra of diatom batch samples in the absence (red trace) and presence of U(VI) (black trace). The samples were prepared as dry films on the ATR crystal's surface. Figure adapted from the work of He et al. 2023b.

By comparing the spectral ranges of the $\nu_3(UO_2)$ mode, *i.e.*, between 960 and 900 cm^{-1} (Bader et al., 2018, 2017; Barkleit et al., 2008; Müller et al., 2019), small but distinct spectral changes were observed between the U-free and U-loaded diatom samples. Considering the relatively low amount of U(VI) introduced into the system during the batch-type bio-association experiment, these observed spectral changes reveal a given affinity of the diatom cells to U(VI). To better identify the functional groups that interact with U(VI), *in situ* "flow-through" experiments were conducted.

Figure V-7 shows the "difference spectra" measured during the *in situ* "flow-through" experiment, where the diatoms were exposed to U(VI) at pH 5.5 (adsorption process) and subsequently flushed with U(VI)-free solution (desorption process). Note that the "difference spectra" were calculated by subtracting the single beam spectra recorded at different time of U(VI) exposure (or flushing) from the spectra recorded prior to the U(VI) exposure (or flushing) serving as references. Hence, the "difference spectra" can clearly reveal the IR absorbance changes of the diatom sample during the U(VI) adsorption or desorption process. It is worth noting that positive and negative bands in the "difference spectra" represent the sample after and before the induced change, respectively.

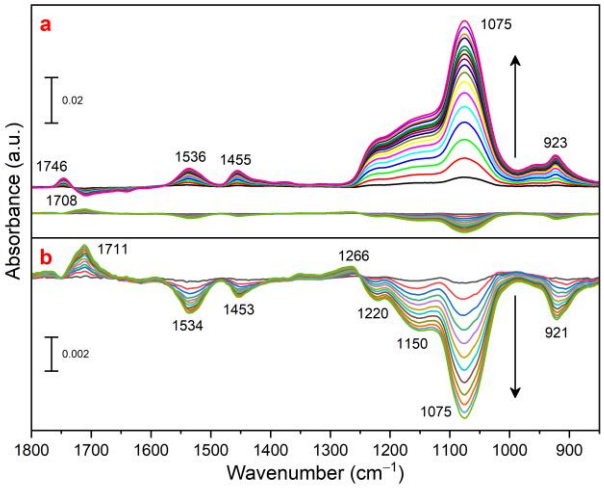

Figure V-7: *In situ* IR spectra of the diatom films after distinct times of exposure to aqueous U(VI) at pH 5.5 (**a**, upper traces) and of the subsequent flushing with background electrolyte (**a**, lower traces). For clarity, the latter spectra are shown at an expanded scale (**b**). Exposure times were 7, 14, 21, …, 90, 111, 125, 160 and 215 minutes (**a**, as indicated by arrow), flushing times were 7, 14, 21, …, 84 minutes (**b**, as indicated by arrow). Figure adapted from the work of He et al. 2023b.

In these "difference spectra", some intense overlapping bands were observed in the frequency range of 1300 to 1000 cm^{-1} during the U(VI) adsorption process, while smaller bands appeared in other spectral regions (**Figure V-7 (a)**, upper traces). The negative and positive bands observed at 1708 and 1536 and 1455 cm^{-1} can be assigned to the modes of carboxyl and carboxylate groups, respectively (Bader et al., 2018, 2017; Regvar et al., 2013). In fact, the C=O stretching modes of carboxyl groups are generally observed around 1700 cm^{-1}, which is split into an antisymmetric $\nu_{as}(COO)$ and a symmetric $\nu_{s}(COO)$ mode due to the deprotonation resulting in the formation of carboxylate groups, *i.e.*, $R–COO^-$. Consequently, these bands nicely demonstrate the coordination of the uranyl(VI) ion with carboxyl groups, which induces the deprotonation of these functional groups. The positive band observed in the frequency region around 1746 cm^{-1} strongly implied the C=O stretching vibration of ester groups. As clearly shown in the spectra, the intensity of these various modes increased when exposing the diatom sample to U(VI), as indicated by the arrow in the figure, which suggests the interactions of the uranyl(VI) species with these functional groups. Additionally, the band at 923 cm^{-1} displayed an increasing intensity with increasing exposure time, which corresponds to the antisymmetric stretching mode of the uranyl(VI) moiety ($\nu_3(UO_2)$) (Müller et al., 2019). In fact, the band observed in this frequency region generally suggests the coordination of carboxyl groups that can be observed not only in complex bio-systems but also in some model systems of low molecular weight, such as carboxylic acids (Bader et al., 2017; Müller et al., 2019).

Noticeably, the most striking spectral features were observed in the frequency region between 1300 and 1000 cm^{-1} in the IR spectra. In general, vibrational modes of organic phosphate groups and of sugar molecules are expected to have contribution in this spectral region (Jiang et al., 2004). Moreover, the biosynthesized silica of the diatoms' frustules generated a very strong absorption band around 1075 cm^{-1}, as already presented in **Figure V-6**. Hence, it can be assumed that the intense bands observed in this frequency region in **Figure V-7** might suggest

characteristic interactions of the aqueous uranyl(VI) species with the diatom's frustules or with organic phosphate groups.

For clarity, the IR spectra of the flushing process are shown at an expanded scale in **Figure V-7 (b)**. Based on these series of spectra, it is clear that the U(VI)-diatom interaction is reversible, since the overall spectra measured during the flushing process displayed an inverse shape to those measured during the sorption step, however, to a much lesser extent. In fact, the IR spectra measured during the flushing process exhibited significantly lower intensity, showing the weak lability of the formed U(VI)-diatom species.

The evolution of the band representing the $\nu_3(UO_2)$ mode potentially suggests the formation of multiple U(VI) species with time. **Figure V-8** presents the spectral region of the $\nu_3(UO_2)$ mode in detail during the exposure (**Figure V-8 (a)**) and the subsequent flushing (**Figure V-8 (b)**) steps. It can be observed that, at an early time of exposure (**Figure V-8 (a)**, lower traces), the band around 923 cm^{-1} displayed a relatively broad shape, suggesting the occurrence of more than one U(VI) species in the system, whereas at later exposure times (**Figure V-8 (a)**, upper traces), the shape of the band appeared more symmetric, assuming the dominance of one type of U(VI) species.

The occurrence of several types of coordinated U(VI) species became more obvious in the IR spectra of the flushing process (**Figure V-8 (b)**). The shape of the band continuously evolves with the flushing time (**Figure V-8 (b)**, from upper to lower traces), exhibiting maxima at 906 cm^{-1} and at 921 cm^{-1} at an early and late stage of the flushing, respectively. It is worth noting that the assignment of these bands to distinct coordinating functional groups on the diatoms is arbitrary, as the diatoms provide all types of biomolecules that can potentially coordinate to U(VI) cationic species. Nevertheless, the functional groups dominating the U(VI) coordination are most likely carboxylate groups, since the frequency of the $\nu_3(UO_2)$ modes was eventually found around 923 cm^{-1} in both reaction (sorption/flushing) steps.

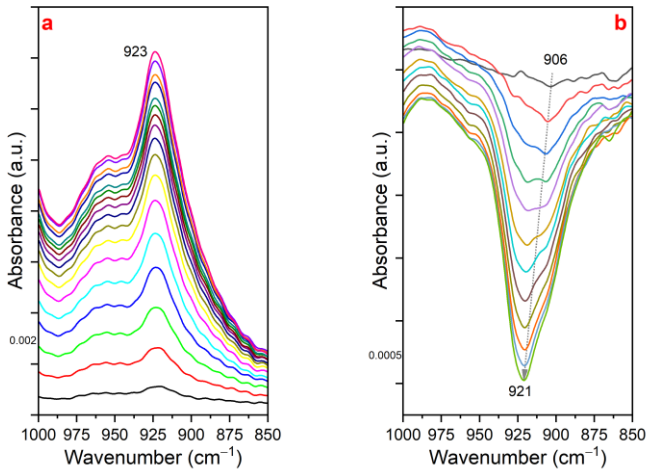

Figure V-8: Spectral region of the $\nu_3(UO_2)$ mode of the spectra recorded during the exposure to U(VI) (**a**) and the subsequent flushing step (**b**). Times of U(VI) exposure and flushing are given in caption of **Figure V-7**. Figure adapted from the work of He et al. 2023b.

To evaluate the contribution of the silica functional groups of the diatom's frustules to the coordination of U(VI), *in situ* "flow-through" experiment was performed on a frustule sample prepared from diatom cells via digestion. The *in situ* IR spectra measured during the experiment, where the frustules served as a stationary phase this time, are shown in **Figure V-9**. The IR spectra showed a considerable decrease in intensity compared to those of the diatom samples previously presented in **Figure V-7 (a)**, which indicates a reduced affinity of U(VI) to the frustules film. Once again, the negative bands at 1708 cm^{-1} and positive bands at 1533, 1459, and 923 cm^{-1} are respectively assigned to carboxyl, carboxylate and uranyl(VI) functional groups, as already observed in the corresponding spectra of the diatoms (**Figure V-7**). These relatively weak bands would possibly suggest the presence of some residual biomass that has not been completely eliminated during the digestion process. Note that the intense band around 1630 cm^{-1} might be resulted from the contributions of the bulk water that might not be subtracted accurately during the data processing.

It can be observed from the figure that the spectral region between 1300 and 1000 cm^{-1} displayed only a weak, broad band around 1037 cm^{-1}, which strongly differs from the spectra measured on the diatom film, where an intense band around 1075 cm^{-1} was evolving with time. In consequence, the assignment of this strong band to the coordination of U(VI) to the silanol groups of the frustules can be ruled out. Instead, the high affinity of U(VI) to the diatoms must be due to the presence and characteristics of the biomass in the diatoms that contributes to the coordination of aqueous U(VI). As suggested by the spectra, the functional groups of the frustule's surface may have minor relevance for the U(VI)-diatom interaction. As a result, the spectra of the *in situ* "flow-through" experiment performed on the frustules indicate the association of U(VI) to residual biomass in the samples eventually.

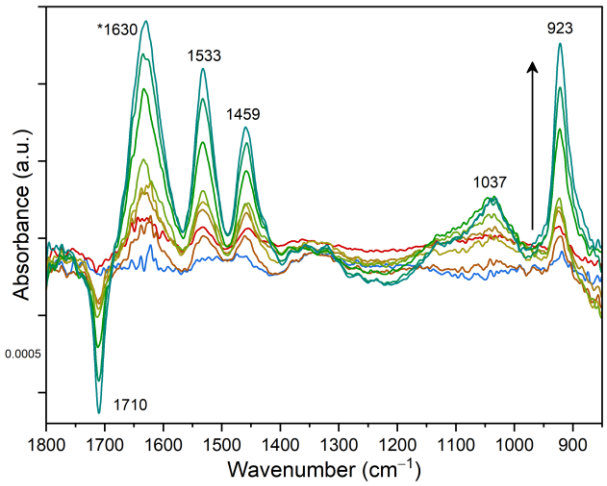

Figure V-9: *In situ* IR spectra of the frustules films after distinct times of exposure to aqueous U(VI) at pH 5.5. Exposure times were 5, 10, 15, 20, 25, 30, 60, 90, 120 minutes (as indicated by arrow). *Contributions from bulk water that may be inaccurately subtracted. Figure adapted from the work of He et al. 2023b.

To sum up the FTIR data, interaction of U(VI) with various functional groups, including carboxyl and phosphate groups that are originated from the diatom's biomass or the organic coating layer of the frustule, was clearly observed by performing the *in situ* "flow-through"

experiments. Moreover, the coordination of U(VI) with the silanol functional groups of the diatom's silica frustule was ruled out. In fact, various U(VI) species with different labilities were formed during the U(VI)-diatom interaction.

4. Time-resolved laser-induced fluorescence spectroscopy data

4.1. Uranium(VI) speciation study in the diatom sample

To further investigate the speciation of U(VI) after interaction with the *A. saprophilum* diatoms, TRLFS analyses were performed under the conditions described in section 6.3 of Chapter 2.

Figure V-10 (a-b) shows the luminescence spectra of the supernatant samples and the diatom cell pellet samples originating from the U(VI) bio-association experiments, where the diatoms were exposed to different U(VI) concentrations (0.8 to 20 µmol/L) for 45 minutes in 2 mmol/L $NaNO_3$ solution buffered with 3 mmol/L HEPES (pH 7.0). The intensity of the spectra is U(VI)-concentration-dependent. **Figure V-10 (a)** shows that all the measured spectra of the supernatant samples exhibit the same emission maxima (482, 503, 524, 548 and 574 nm). Noticeably, the spectrum of a reference sample, measured for a similar U(VI)-diatom system in the absence of HEPES and represented by the dotted line in the figure, displays different emission maxima (479, 499, 520, 543 and 567 nm). Consequently, it can be assumed that a U(VI)-HEPES species was formed in the solution that may also interact with the diatoms. **Figure V-10 (b)** presents the luminescence spectra of the diatom samples, both of which show different emission maxima (495, 516, 539 and 564 nm) compared to that measured in the supernatant. By comparing the spectra of the supernatant and the diatom samples, it can be assumed that different U(VI) species were formed on the diatoms and in the aqueous solution. To further characterize the U(VI) species, the measured spectral data were subjected to PARAFAC analysis.

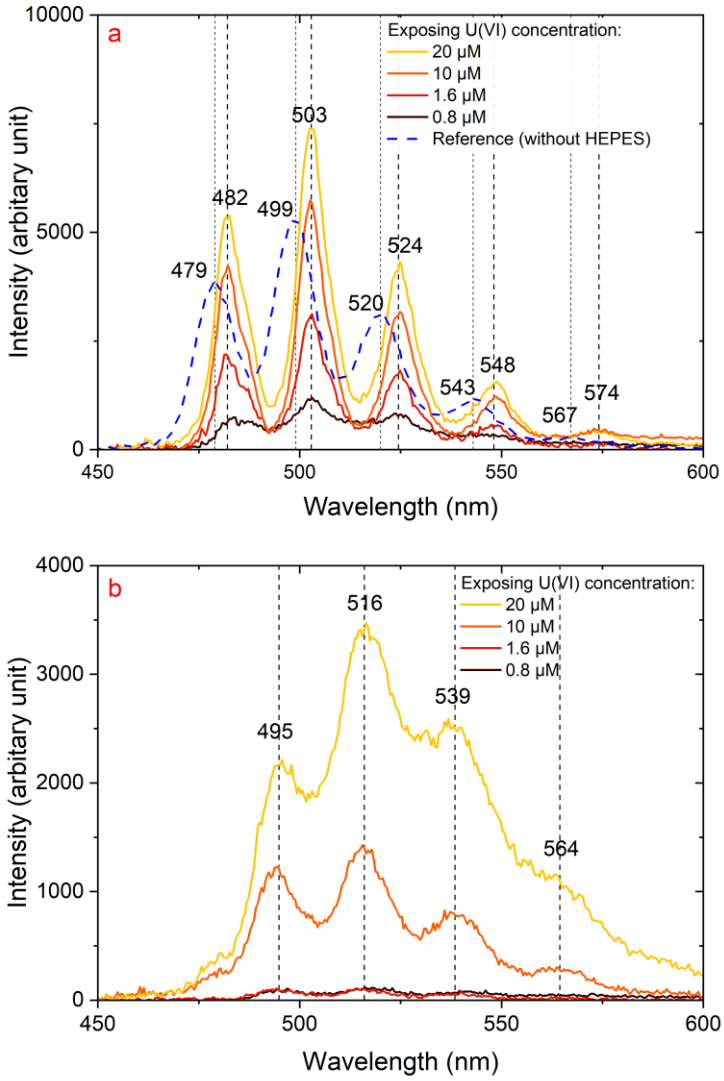

Figure V-10: Luminescence spectra of *A. saprophilum* diatom samples exposed to different U(VI) concentrations (0.8 to 20 µmol/L) in the 2 mmol/L $NaNO_3$ + 3 mmol/L HEPES solution at pH 7.0. **(a)**: luminescence spectra of the supernatant samples and **(b)**: luminescence spectra of the diatom samples. Figure adapted from the work of He et al. 2023b.

Figure V-11 shows the results of the PARAFAC analysis. **Figure V-11 (a)** and **(c)** presents the extracted single-component spectra of the U(VI) species present in supernatant samples and the diatom samples, respectively. As suggested by the PARAFAC analysis, three different U(VI) species, namely U(VI)-supernatant species 1 to 3, were likely present in the supernatant samples, while only one U(VI) species, namely U(VI)-diatom species 1, was identified in the diatom samples. In particular, the three U(VI) species identified in the supernatant seemed to display the same emission maxima (481, 502, 524, 548 and 573 nm), which are quite similar to that cited in the previous paragraph. However, these U(VI)-supernatant species have different lifetimes ($\tau_{s,1}$ = 277 ± 4 µs, $\tau_{s,2}$ = 952 ± 8 µs, $\tau_{s,3}$ = 5782 ± 1 µs) as shown in **Figure V-11 (b)**. As previously argued, the U(VI) species identified in the diatom samples differs from those in the supernatant in terms of both emission maxima (481, 497, 516, 539 and 564 nm) and lifetime ($\tau_{d,1}$ = 119 ± 6 µs) as presented in **Figure V-11 (c-d)**). Based on this information, a complex U(VI) speciation scheme can be imagined in the studied U(VI)-diatom system, where U(VI)

may be present in an "immobilized" form via the association with diatoms, and in a more mobile form in the aqueous solution. Note that, however, only fluorescent species can be detected by TRLFS, signifying that more U(VI) species might exist in the system.

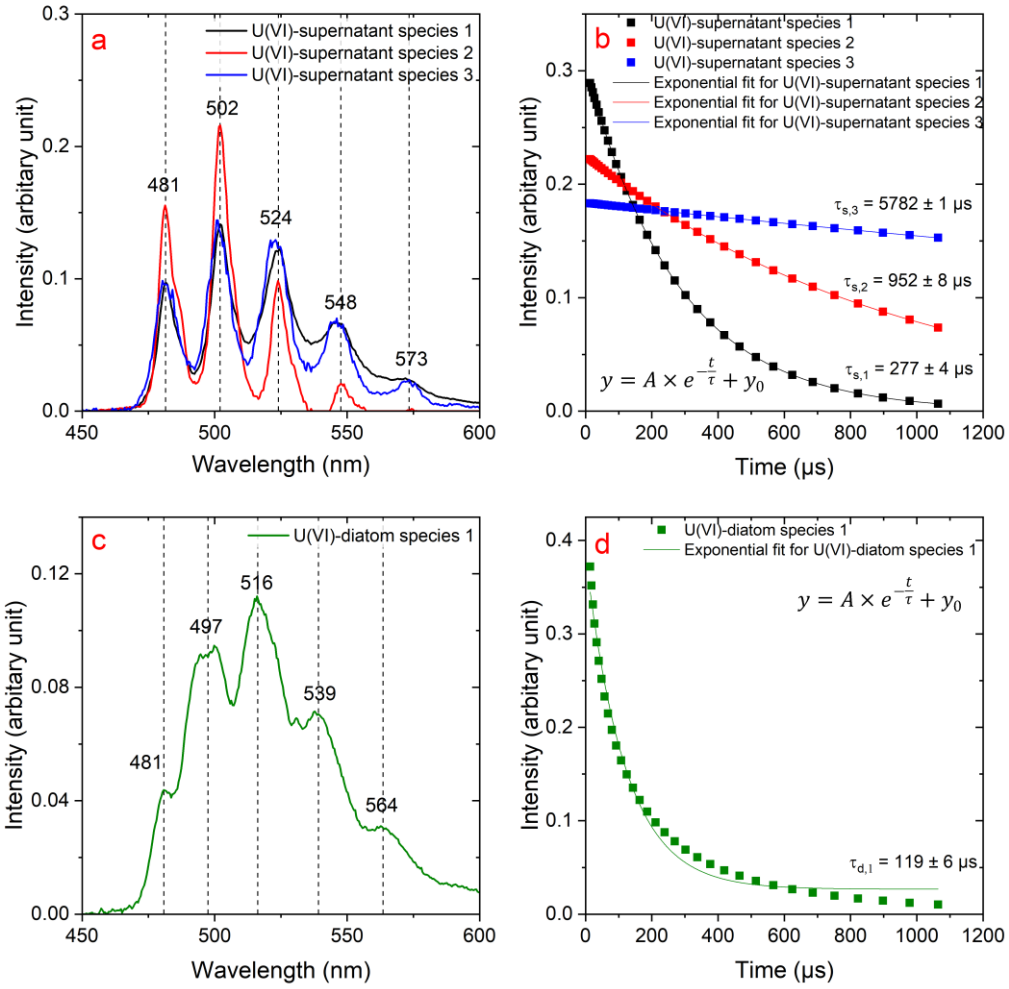

Figure V-11: PARAFAC analysis of the luminescence spectra (**Figure V-10**) measured on the supernatant and the diatom samples. **(a)**: Single-component spectra of the U(VI) species present in the supernatant samples extracted by PARAFAC analysis. **(b)**: Lifetime of the U(VI) species identified in the supernatant. **(c)**: Luminescence spectrum of the U(VI)-diatom species calculated with PARAFAC analysis. **(d)**: Lifetime of the U(VI) species identified in the diatom samples.

To investigate the evolution of the U(VI) speciation in the system at a longer time scale, TRLFS measurements were conducted on samples that were collected at different diatom's growth phases, *i.e.*, at different U(VI) exposure times. **Figure V-12** shows the normalized luminescence spectra of **(a)** the supernatant samples and **(b)** the diatom samples measured after 4, 11 and 35 days of U(VI) exposure. The experiment was performed in the DM medium to sustain the growth of the diatom cells. The diatom culture was exposed to 1 µmol/L of U(VI) at day 0. **Figure V-12 (c)** presents the growth curve of the diatom culture measured during the experiment, where day 3, 11 and 35 corresponded to the exponential growth phase, late-exponential growth phase and stationary growth phase, respectively. Besides, the pH of the

diatom culture varied within the range of 7.4–7.8 during the study.

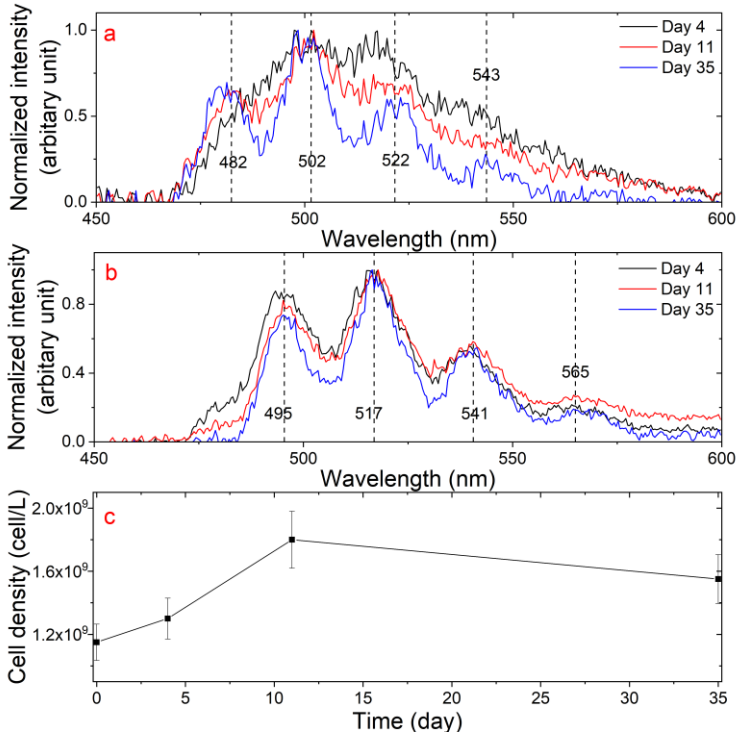

Figure V-12: Normalized luminescence spectra of *A. saprophilum* diatom culture exposed to 1 µmol/L of U(VI) for up to 35 days in DM medium. Luminescence spectra of **(a)**: the supernatant samples, and **(b):** the diatom samples measured after 4, 11 and 35 days of U(VI) exposure. **(c)**: The growth curve of the diatom culture measured during the experiment.

As shown in **Figure V-12**, different U(VI) species were formed in the supernatant and diatom samples. Note that the obtained luminescence spectra appeared noisier compared to that measured in the previous experiment performed in the simple $NaNO_3$ medium, since the U(VI) concentrations was lower in this case. Moreover, the chloride ions present in the DM medium may cause quenching effects on the luminescence spectra, as reported in the literature (Demnitz et al., 2020). To further identify the U(VI) species formed in the studied system, PARAFAC analysis was performed.

Different from what was observed in the previous case, *i.e.*, the experiment performed in the medium containing $NaNO_3$ and HEPES, PARAFAC analysis identified the presence of only one detectable U(VI) species, namely U(VI)-supernatant species 4, in the supernatant sample during the entire time-dependent experiment. As shown in **Figure V-13 (a-b)**, U(VI)-supernatant species 4 displays different emission maxima (481, 501, 521 and 543 nm) and lifetime ($\tau_{s,4}$ = 241 ± 13 µs) compared to U(VI)-supernatant species 1-3, which might be due to the different medium composition. Surprisingly, considering the complex composition of the DM medium, which consists of various inorganic salts and organic compounds (*e.g.*, EDTA, vitamins, etc.), more U(VI) species were expected to be found in the supernatant. Once again, this could be explained by the fact that only fluorescent species can be detected by TRLFS.

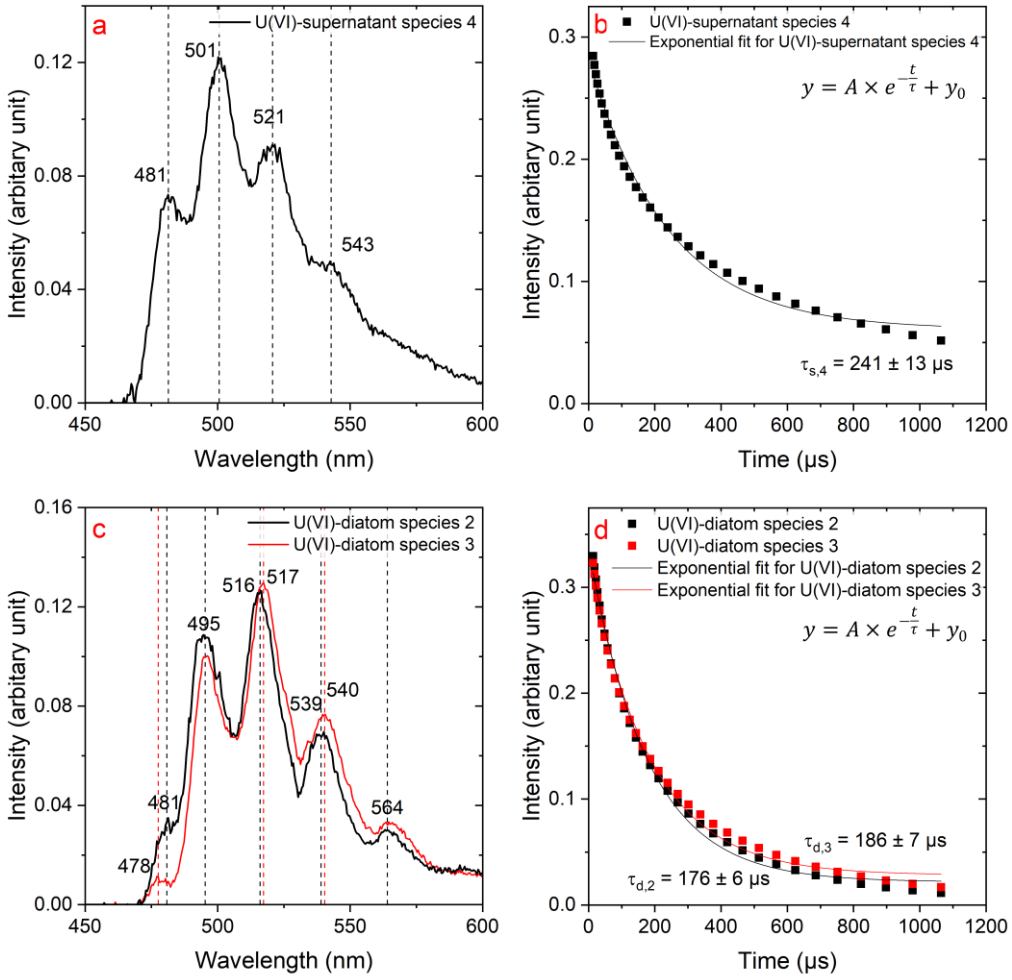

Figure V-13: PARAFAC analysis of the luminescence spectra (**Figure V-12**) measured on the supernatant and the diatom samples. **(a)**: Luminescence spectrum of the supernatant samples calculated with PARAFAC analysis. **(b)**: Lifetime of the U(VI) species identified in the supernatant. **(c)**: Single-component spectra of the U(VI)-diatom species in the diatom samples extracted by PARAFAC analysis. **(d)**: Lifetime of the U(VI) species identified in the diatom samples. Figure adapted from the work of He et al. 2023b.

In the diatom samples that were sampled and analyzed after 4, 11 and 35 days of exposure to U(VI), two U(VI) species were identified through PARAFAC analysis which exhibit similar spectral characteristics and close decay lifetimes, as demonstrated in **Figure V-13 (c-d)**. Although these two identified U(VI)-diatom species display rather close emission maxima compared to the U(VI)-diatom species 1, they can be distinguished by their lifetime. Based on the spectroscopic data, the species distribution was calculated by PARAFAC analysis. **Figure V-14** shows the evolution of the distribution of U(VI)-diatom species 2 and 3 in the diatom samples as a function of time. Interestingly, a shift in the speciation predominance between the U(VI)-diatom species 2 and 3 were clearly observed in the diatom samples after 11 days of U(VI) exposure, which corresponds to the late exponential growth phase. In fact, the U(VI)-diatom species 2, which was initially predominant in the diatom samples, became gradually a minor species. The variation of the speciation predominance may possibly provide an indication for the distribution change between the U(VI) adsorption and incorporation in the system, as is

previously mentioned in the batch-type time-dependent U(VI) bio-association experiment (see section 2.3 in Chapter 4).

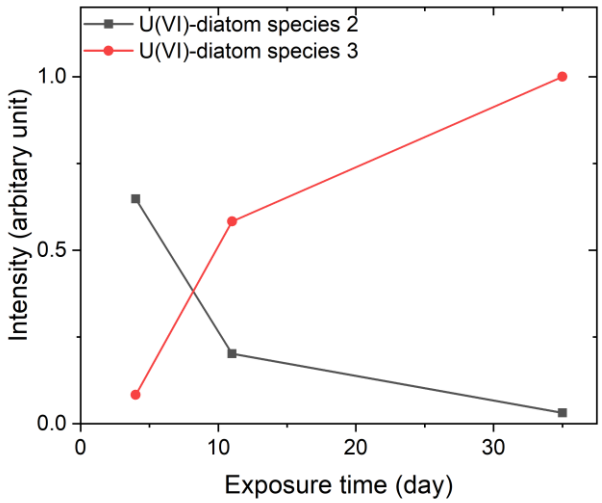

Figure V-14: Evolution of the distribution of the identified U(VI)-diatom species in the diatom samples as a function of the exposure time. Figure adapted from the work of He et al. 2023b.

4.2. Uranium(VI) speciation study in the bacterial isolates

The *A. saprophilum* culture used in this work contains a variety of bacterial genera that may also interact with U(VI) as previously demonstrated by the microscopic data. To understand their impact on the U(VI) speciation, TRLFS measurements were performed on four bacterial isolates, *i.e.*, *A. facilis*, *A. fabrum*, *B. mediterranea* and *P. peli*, which were exposed to 2 µmol/L of U(VI) in the solution consisting of 2 mM $NaNO_3$ and 3mM HEPES (pH 7.0) for 45 minutes. To prepare U(VI)-loaded bacterial isolates samples, protocol was applied as described in section 6.3 of Chapter 2.

Figure V-15 (a) compares the luminescence spectra of the diatom samples (upper spectrum, as previously shown in **Figure V-10 (b)**) with the spectra measured on the four bacterial isolates (lower spectra). The luminescence spectra measured on the isolates of *A. facilis*, *A. fabrum* and *B. mediterranea* shared common characteristics regarding the emission maxima, which clearly differed from that measured on the diatom samples. Interestingly, the luminescence spectra measured on the *P. peli* sample seemed to combine the characteristic emission maxima of both the diatom and bacterial samples: two sets of emission maxima were observed in the spectrum. This might provide a first indication that some similar U(VI) species were formed in the diatom samples and in the *P. peli* sample.

To further confirm this, PARAFAC analysis was performed on these measured luminescence spectra and the deconvoluted spectra were shown in **Figure V-15 (b)**, where two distinct U(VI) species were eventually identified in the four bacterial isolates, namely U(VI)-bacteria species 1 and 2. These two identified U(VI) species exhibit clearly different emission maxima, *i.e.*, 494, 516, 540 and 565 nm for the U(VI)-bacteria species 1 and 481, 502, 524 and 548 nm (possibly with a fifth emission maximum) for the U(VI)-bacteria species 2. Moreover, between these two U(VI)-bacteria species, the U(VI)-bacteria species 1 shows closer emission maxima to the

U(VI)-diatom species 1.

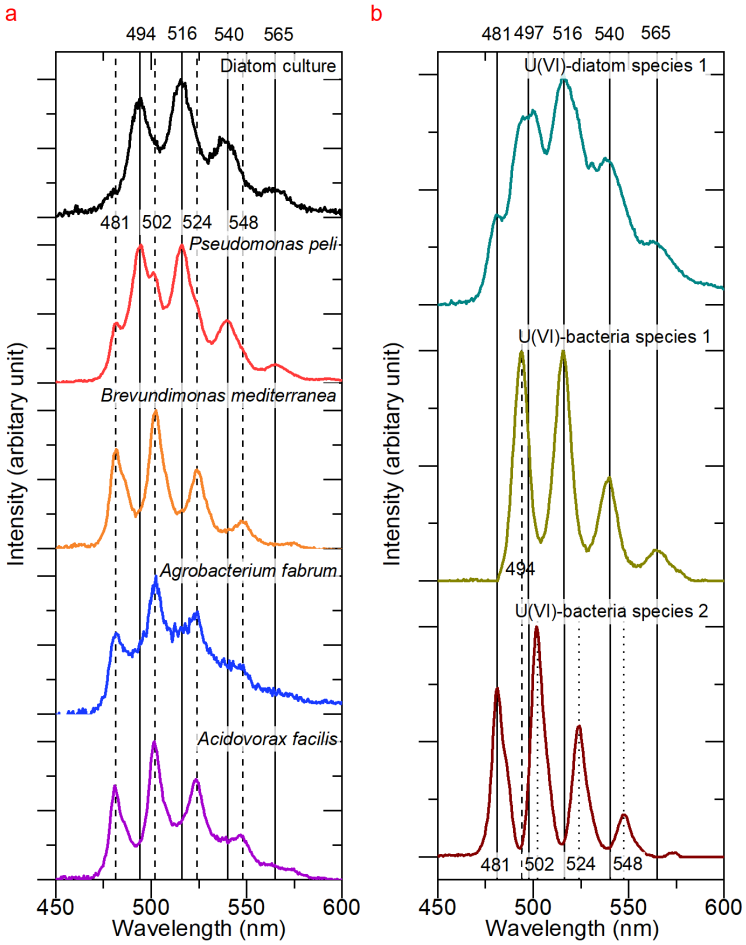

Figure V-15: **(a)**: Luminescence spectra of the diatom and four bacterial isolate samples (*P. peli*, *B. mediterranea*, *A. fabrum* and *A. facilis*) exposed to U(VI); **(b)**: Luminescence spectra of the diatom and bacterial isolate samples deconvoluted through PARAFAC analysis. Figure adapted from the work of He et al. 2023a.

Figure V-16 (a) presents the lifetime of the two identified U(VI)-bacteria species, with their corresponding distribution in the bacterial isolates shown in **Figure V-16 (b)**. It can be observed in the figure that both of these two U(VI)-bacteria species were present in the four bacterial isolate samples. In particular, a ratio close to 1:1 between these two species was found in the *P. peli* sample, which may explain the special spectral form observed in the *P. peli*'s luminescence spectrum. The difference of the distribution of the two U(VI)-bacteria species in the four bacterial isolates may reflect the different compositions of the bacterial cell wall, displaying distinct affinity for U(VI).

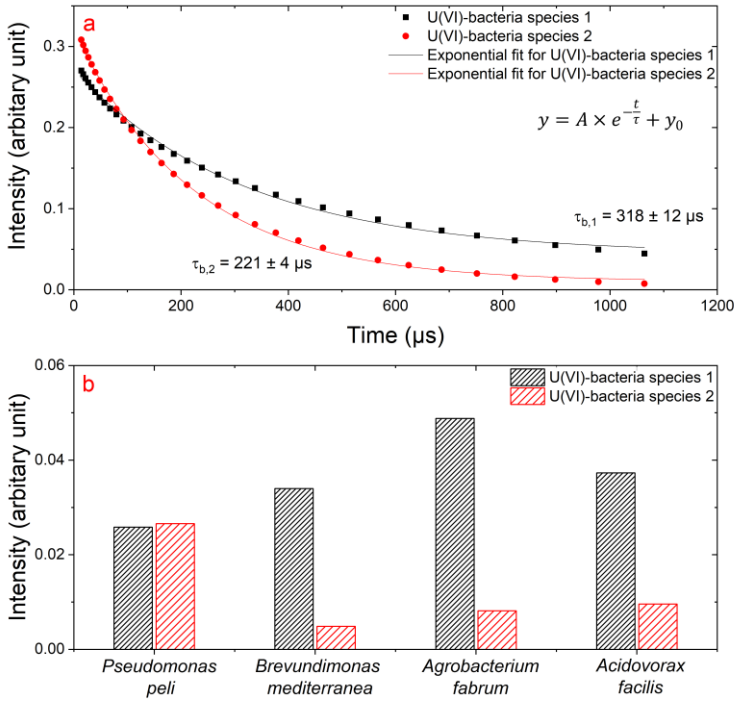

Figure V-16: **(a)**: Lifetimes of the U(VI) species identified in the bacterial isolates; **(b)**: Distribution of the identified U(VI)-bacteria species in four different U(VI)-exposed bacterial isolates calculated by PARAFAC analysis.

4.3. Assignment of the identified U(VI) species

With the deconvoluted spectral data obtained through PARAFAC analysis, comparison with the data reported in the literature was done to assign the type of the U(VI) species identified in the diatoms and bacteria.

There exists a wide array of spectral data (emission maxima) for various inorganic and organic U(VI) compounds/species documented in the literature. Here, the U(VI) species identified in this work are compared to some reference U(VI) species that show closely similar emission maxima, as summarized in **Table V-1**. In fact, the U(VI) species found in the diatom samples exhibit similar emission maxima to the uranyl(VI) species formed with low molecular organic acids and biomolecules, such as $UO_2(malonate)_2^{2-}$, $UO_2(glycine)_2^{2+}$ and U(VI) phosphoserine, which carries carboxyl, amino or phosphate functional groups. This might provide hints for the interaction of U(VI) with some carboxyl-, phosphate-carrying biomolecules, *e.g.*, proteins, amino acids and lipids, that can be easily found on the diatom cell wall (the organic coating layer) or inside the diatom cell.

As previously discussed, one of the two U(VI) species found in the *P. peli*, *B. mediterranea*, *A. fabrum* and *A. facilis* bacterial isolates, *i.e.*, the U(VI)-bacteria species 1, is more closely related to the species found in the diatoms, while another species, *i.e.*, the U(VI)-bacteria species 2, shows emission maxima closer to some inorganic uranyl(VI) phosphate species or the phosphate groups-carrying organic compound (UO_2(O-phospho-L-threonine)) stated in the literature (Günther et al., 2008). This would highlight the important role of the phosphate functional groups in the U(VI)-bacteria interaction.

However, the assignment for the U(VI) species found in the supernatant samples is limited by the few available data existing in the literature. Further investigations are needed to confirm the potential chemical forms of these U(VI) species present in the supernatant.

Generally speaking, the TRLFS data obtained in this work point out the crucial role of the carboxyl and phosphate functional groups in the interaction of U(VI) with the *A. saprophilum* diatoms, highlighting at the same time the presence of some similar U binding motifs in the bacteria associated to the diatoms. These findings are in good agreement with the microscopic data (SEM, TEM) and FTIR spectroscopic data that have been previously discussed in the earlier sections.

Table V-1: Luminescence emission maxima of the U(VI) species identified in this work compared to other reference species cited in the literature.

U(VI) species	Emission maxima (nm)						Reference
U(VI)-supernatant species 1	481	502	524	548	573		
U(VI)-supernatant species 2	481	502	524	548	573		
U(VI)-supernatant species 3	481	502	524	548	573		
U(VI)-supernatant species 4	481	501	521	543			
U(VI)-diatom species 1	481	497	516	539	564		This work
U(VI)-diatom species 2	481	495	516	539	564		(He et al. 2023a, 2023b)
U(VI)-diatom species 3	478	495	517	540	564		
U(VI)-bacteria species 1		494	516	540	565		
U(VI)-bacteria species 2	481	502	524	548			
U(VI)-HEPES species?	479	499	520	543	567		
$UO_2(H_2PO_4)^+/UO_2(HPO_4)$ (pH 3)		494	517	541	565		(Panak et al., 2000)
$UO_2H_xPO_4$		494	517	541	565		(Bernhard et al., 1996)
$UO_2(malonate)_2^{2-}$	479	496	517	542	566		(Brachmann et al., 2002)
$UO_2(glycine)_2^{2+}$	478.7	495.3	516.7	540.6	565.0	594.4	(Günther et al., 2007)
UO_2(O-phospho-L-threonine)	483.7	501.8	523.4	546.8	572.6	601.0	(Günther et al., 2006)
U(VI) phosphoserine	480.9	496.9	517.6	540.5	565.0	591	(Koban and Bernhard, 2007)
$UO_2[CH_3(CO_2)_2]$		494	515	540	564		(Lütke et al., 2012)

5. Conclusion

In this chapter, the interaction of U with the *A. saprophilum* culture is characterized by combining microscopic and spectroscopic approaches. As demonstrated by the SEM-, TEM- and EDX-based analyses, U can be found on the surface and inside the diatom cells, proving the adsorption and incorporation behavior of U at the diatom level. A similar scenario can be observed in the bacteria that are associated to the diatoms. Interestingly, some precipitate-like U species are observed inside the diatom cells and within the vacuole in particular, as represented by the electron dense areas observed in the TEM micrograph. Additionally, EDX-based analysis reveals the co-localization of U with P both at the diatom and bacterium level and demonstrates at the same time a possible co-precipitation of various metals within the vacuole of the diatoms.

On the other hand, the performed FTIR and TRLFS measurements provide valuable information regarding the U(VI)-diatom interactions from a molecular point of view. The FTIR data argue the significant contribution of the carboxyl groups to the coordination for U(VI) in the diatom sample. Moreover, the *in situ* "flow-through" experiment demonstrates the formation of several U(VI) species in the studied diatom system and points out the weak lability of the formed U(VI)-diatom species. Besides, TRLFS data provide complementary information on the U(VI) speciation in the diatoms, showing a shift in the predominance of two identified U(VI)-diatom species during the diatom's growth. This may be in agreement with the evolution of the U adsorption/incorporation observed in the batch-type time-dependent U bio-association experiment. By comparing the luminescence spectroscopic data with reference U(VI) compounds cited in the literature, it can be concluded that the carboxyl and phosphate functional groups carried by diverse biomolecules are likely responsible for the U(VI) binding on/in the diatoms. The TRLFS measurements performed on four bacterial isolates (*A. facilis*, *A. fabrum*, *B. mediterranea* and *P. peli*) demonstrate the presence of one particular U(VI)-bacteria species that is likely common to what is identified in the diatoms. Ultimately, similar binding motifs of U(VI) to comparable biomolecules found in both bacteria and diatoms may lead to similarities in the spectra. Nevertheless, the involvement of bacteria in the interaction with U(VI) in the *A. saprophilum* diatom culture remains undisputed. In the case of bacteria, phosphate-like U(VI) species are more likely occurring in the system.

CHAPTER 5: MICROSCOPIC AND SPECTROSCOPIC CHARACTERIZATION OF THE URANIUM-DIATOM INTERACTION

Chapter 6: Conclusion and perspectives

CHAPTER 6: CONCLUSION AND PERSPECTIVES

Diatoms are unicellular eukaryotic microalgae that belong to the Bacillariophyta phylum. They display a vast range of shapes, sizes, and species diversity, gaining increasing attention in the research field during the past decades. Diatoms are easily recognized by their unique and intricate cell walls, called frustules that mainly consists of biosynthesized amorphous silica. These frustules exhibit exquisite patterns and structures at the microscopic level, which provide protection to diatoms and make them flourishing in diverse environments on Earth. Being benthic or planktonic, diatoms are well-known for their vital role as primary producers in various ecosystems (Mann, 1999; Tréguer et al., 2018). They contribute to the global oxygen production and are involved in numerous biogeochemical cycles for various elements including C, Si and so on (Ragueneau et al., 2006; Tréguer et al., 2018). Moreover, diatoms play a crucial role in the phycosphere in aquatic ecosystems. In fact, various studies focused on the interaction between diatom and bacteria within the phycosphere, a complex system where numerous mechanisms, such as gene transfer, chemicals exchange, etc., are taking place (Amin et al., 2012; Kouzuma and Watanabe, 2015). Furthermore, diatoms are commonly considered as important bio-indicators in natural environments, with their community structure and diversity reflecting water quality and ecological health. Various studies pointed out the impact of the heavy metal contamination on the diatom community structure, where a decrease in the species diversity and a replacement of the heavy metal-sensitive species by the more tolerant ones are generally observed in the heavy metal contaminated sites (Pandey et al., 2018). Additionally, the morphological abnormalities on the diatom's frustules are more frequently observed in the presence of heavy metals stress (Falasco et al., 2009; Ferreira Da Silva et al., 2009; Lavoie et al., 2017). Diatoms have wide applications in the industrial sector as well. In fact, due to the high surface-to-volume ratio, diatoms are good biosorbents that can be used for the removal of heavy metals from industrial effluents or for bioremediation purpose in heavy metals contaminated sites (Chasapis et al., 2022). Currently, the strategy using microorganisms such as diatoms and bacteria for the bioremediation is believed to be a cost-effective, eco-friendly and sustainable (Mehrotra et al., 2021). Hence, the capability for diatoms to accumulate the heavy metals as well as the mechanisms underlying have become one of the major subjects for numerous studies.

Due to the chemical toxicity and the radiological properties, radioelements such as U have received particular attention in the ecology field. U is one of the primordial elements that is rather ubiquitous on Earth and is well-known for its applications both in the military sector (nuclear weapons) as well as in the civilian sector (nuclear power plants). For that, U mining activities has thrived in the last century. However, research have demonstrated the negative impact of the acid mine drainage (AMD) and the U contamination on the ecosystems induced by the U mining activities (Herlory et al., 2013). Consequently, various studies have focused on the U migration behavior in the environment and tried to understand the transfer of U into the food chain via the interactions with living organisms. So far, there exist numerous studies that investigate the interactions of U with plant cells or bacteria using various analytical techniques. Nevertheless, data remain extremely limited in the current literature regarding the interaction between diatoms and U at the mechanism level. To the best of knowledge, there is no information neither on the interaction of diatoms with Ra, another radioelement that is widely studied for its hazardous radiological effects on humans.

In consequence, several critical questions arise, how does U/Ra interact with diatom? Is U/Ra only adsorbed on the surface of diatoms or can it be also accumulated inside the cells? If yes, how does it actually distribute at the cell level and which species are formed during the

interaction? Moreover, do the bacteria living with the diatoms also contribute to the retention of U? And how?

To answer the above questions, a xenic culture of *A. saprophilum*, a freshwater diatom species, was used in this work to study the interaction between U/Ra with diatoms at the macroscopic scale and at the molecular level, by combining batch-type bio-association studies with various microscopic and spectroscopic techniques. The *A. saprophilum* diatoms were initially collected from a lake located in the Auvergne region of France, and were subjected to a series of isolation, purification and acclimatization steps to obtain a mono-culture of the *A. saprophilum* diatoms. Different from the majority of the existing studies in the literature, a xenic diatom culture was used in this work, *i.e.*, the bacteria initially present in the natural sample were not eliminated during the cultivation. As a result, the interaction between U/Ra with the *A. saprophilum* diatom culture can be investigated in a way closer to *in natura* conditions, thus potentially providing more realistic and interesting information.

Prior to the investigation of the U/Ra-diatom interaction, the cultivation of the diatoms was mastered under laboratory conditions and a characterization of the xenic *A. saprophilum* culture was carried out, providing intrinsic information including the diatom size, the growth curve, the taxonomy and the bacterial community diversity, etc. Using a sequencing approach, it was demonstrated that the diatom culture used in this work comprised only one diatom species, *i.e.*, *A. saprophilum*, along with a bacterial community of relatively low diversity. Among all of the bacteria genera present in the culture, four bacterial strains, *i.e.*, *A. facilis*, *A. fabrum*, *B. mediterranea* and *P. peli*, were successfully isolated and cultured under the applied conditions. Moreover, it was assumed that a symbiotic mechanism between the *A. saprophilum* diatoms and the co-occurring bacterial consortium were likely taking place based on experimental observations.

Batch-type U/Ra bio-association experiments were performed to obtain macroscopic information on the U/Ra-diatom interaction, including adsorption kinetics, adsorption isotherm, etc. According to the experimental results, the adsorption of U on diatoms occurs rapidly (< 10 minutes), while in the case of Ra it takes a longer time (about 45 minutes) to reach the adsorption equilibrium. Besides, it seems that the adsorption of U on diatoms follows the Langmuir-Freundlich isotherm model. In the case of Ra, however, few information regarding the adsorption isotherm can be retrieved from the experimental data, since an ultra-trace level of Ra was used for the study. In addition, time-dependent bio-association studies clearly revealed the presence of both an adsorbed and incorporated part of U at the diatom level and demonstrated their evolution as a function of the diatom's growth phase, where the incorporated part generally increased with the exposure time. Unlike U, no significant Ra incorporation was observed in the diatoms and Ra was mainly adsorbed on the diatom's surface.

To better understand the interaction between U and diatoms, various microscopic (SEM, TEM coupled with EDX) and spectroscopic (FTIR, TRLFS) techniques were applied to provide information on the localization as well as the speciation of U at the diatom level. SEM and TEM coupled with EDX analysis demonstrated the U distribution not only within the diatoms but also in the bacteria that are associated to the surface of diatoms, clearly confirming the incorporation of U by the diatoms and bacterial cells. It is worth noting that some electron dense areas were found inside the diatoms, and particularly within the vacuole of the diatom cell. EDX-based analysis performed on these particular areas of interest indicated the presence of U,

with a co-localization of U and P. Moreover, element distribution maps would suggest, in addition to U, a potential co-precipitation of various metals inside the diatoms, as represented by the electron dense areas in the TEM micrograph.

At the molecular level, IR spectra measured during the *in situ* "flow-through" experiments performed on a pre-stabilized diatom cell film demonstrated the weak lability nature of several U(VI) species formed on/in the diatoms. The observed vibrational modes in the IR spectra suggested the significant contribution of the carboxyl and phosphate functional groups to the coordination with U(VI). On the other hand, similar experiments performed on diatom's frustules demonstrated the minor contribution of the diatom's silica frustule to the binding of U(VI). Hence, it can be assumed that the U(VI) is principally associated with the biomolecules of the diatom biomass that carry carboxyl and phosphate functional groups, which is coherent with the SEM/TEM/EDX data.

By using the TRLFS technique, the contribution of carboxyl and phosphate functional groups to the interaction of U(VI) with diatoms was confirmed to some extent. In fact, PARAFAC analysis performed on the measured luminescence spectra indicated the presence of several U(VI) species in the diatom samples that display similar spectroscopic characteristics to some carboxylate- and phosphate-like U(VI) compounds reported in the literature. Interestingly, TRLFS data provides proof for the evolution of the U(VI) speciation in the diatoms in different stages of growth: a shift in the predominance of two identified U(VI) species was clearly observed. This finding may be in line with the change of the U adsorption and incorporation behavior observed in different diatom growth phases, as demonstrated in the time-dependent U bio-association experiment. More importantly, the TRLFS measurements conducted on four bacterial isolates highlighted the contribution of bacteria in the overall interaction between U(VI) and the xenic diatom culture. In fact, U(VI) species of similar spectroscopic properties were found both in the diatom sample and in the bacterial isolate samples, suggesting the presence of some possibly similar U(VI) binding motifs in the diatoms and bacteria. Besides, a phosphate-like U(VI) species was identified in the bacterial isolates, showing once again the crucial role of the phosphate functional groups in the interaction between U(VI) and bacteria. With the data obtained from the four bacterial isolates, it is difficult to quantitatively evaluate, for the moment, the impact of the entire bacterial community on the speciation of U(VI) in a relatively complex bio-system. However, it is clear that both bacteria and diatoms are involved in the interaction of U(VI) in the studied *A. saprophilum* diatom culture.

In conclusion, the microscopic and spectroscopic data obtained in this work are generally in good agreement and provide detailed information complementary to the macroscopic data. It is clearer now how U distributes in the studied xenic *A. minutissium* culture at the cellular level. Conclusions are drawn regarding the major functional groups found in diatoms and bacteria that interact with U. However, there is still a lack of direct proof that justifies the exact chemical forms of the U(VI) species identified on/in the diatoms and bacteria. In general, the objectives of this work are achieved and the obtained results contribute to the TIRAMISU project by providing chemical data for the interaction of U and Ra in a xenic diatom culture. The obtained results also highlight the importance of the diatoms and bacteria in the transport of radioelements in the environment.

For the perspectives, the biological, chemical and physical data obtained in the TIRAMISU project should be integrated to produce a simulation model that can predict the dose effect of

the radioelements on the microorganisms living in the aquatic ecosystems. Information such as the localization and speciation of the radioelements, e.g., U, provided by this work may help to build a more accurate diatom-U interaction model, improving the accuracy of the dose calculation. However, information such as the density of the functional groups on the diatom and bacterial cell that are involved in the interaction with U is still missing. Moreover, further investigations are necessary to identify the exact speciation of U both at the diatoms and bacteria level. It will also be interesting to quantify the contribution of the bacteria to the global interaction with U in a complex diatoms-bacteria system.

References

Adl, S.M., Bass, D., Lane, C.E., Lukeš, J., Schoch, C.L., Smirnov, A., Agatha, S., Berney, C., Brown, M.W., Burki, F., Cárdenas, P., Čepička, I., Chistyakova, L., Del Campo, J., Dunthorn, M., Edvardsen, B., Eglit, Y., Guillou, L., Hampl, V., Heiss, A.A., Hoppenrath, M., James, T.Y., Karnkowska, A., Karpov, S., Kim, E., Kolisko, M., Kudryavtsev, A., Lahr, D.J.G., Lara, E., Le Gall, L., Lynn, D.H., Mann, D.G., Massana, R., Mitchell, E.A.D., Morrow, C., Park, J.S., Pawlowski, J.W., Powell, M.J., Richter, D.J., Rueckert, S., Shadwick, L., Shimano, S., Spiegel, F.W., Torruella, G., Youssef, N., Zlatogursky, V., Zhang, Q., 2019. Revisions to the Classification, Nomenclature, and Diversity of Eukaryotes. J Eukaryotic Microbiology 66, 4–119. https://doi.org/10.1111/jeu.12691

Agusti, S., González-Gordillo, J.I., Vaqué, D., Estrada, M., Cerezo, M.I., Salazar, G., Gasol, J.M., Duarte, C.M., 2015. Ubiquitous healthy diatoms in the deep sea confirm deep carbon injection by the biological pump. Nat Commun 6, 7608. https://doi.org/10.1038/ncomms8608

Altschul, S.F., Gish, W., Miller, W., Myers, E.W., Lipman, D.J., 1990. Basic Local Alignment Search Tool. J. Mol. Biol 215, 403–410. https://doi.org/10.1016/S0022-2836(05)80360-2

Ames, L.L., McGarrah, J.E., Walker, B.A., 1983. Sorption of trace constituents from aqueous solutions onto secondary minerals. II. Radium. Clays Clay Miner 31, 335–342. https://doi.org/10.1346/CCMN.1983.0310502

Amin, S.A., Parker, M.S., Armbrust, E.V., 2012. Interactions between Diatoms and Bacteria. Microbiol Mol Biol Rev 76, 667–684. https://doi.org/10.1128/MMBR.00007-12

Audi, G., Kondev, F.G., Wang, M., Huang, W.J., Naimi, S., 2017. The NUBASE2016 evaluation of nuclear properties. Chinese Phys. C 41, 030001. https://doi.org/10.1088/1674-1137/41/3/030001

Avilés, C., Loza-Tavera, H., Terry, N., Moreno-Sánchez, R., 2003. Mercury pretreatment selects an enhanced cadmium-accumulating phenotype in *Euglena gracilis*. Archives of Microbiology 180, 1–10. https://doi.org/10.1007/s00203-003-0547-2

Ayawei, N., Ebelegi, A.N., Wankasi, D., 2017. Modelling and Interpretation of Adsorption Isotherms. Journal of Chemistry 2017, 1–11. https://doi.org/10.1155/2017/3039817

Azizian, S., Eris, S., Wilson, L.D., 2018. Re-evaluation of the century-old Langmuir isotherm for modeling adsorption phenomena in solution. Chemical Physics 513, 99–104. https://doi.org/10.1016/j.chemphys.2018.06.022

Babatunde, K.A., Negash, B.M., Jufar, S.R., Ahmed, T.Y., Mojid, M.R., 2022. Adsorption of gases on heterogeneous shale surfaces: A review. Journal of Petroleum Science and Engineering 208, 109466. https://doi.org/10.1016/j.petrol.2021.109466

Bachmaf, S., Merkel, B.J., 2011. Sorption of uranium(VI) at the clay mineral–water interface. Environ Earth Sci 63, 925–934. https://doi.org/10.1007/s12665-010-0761-6

Bader, M., Müller, K., Foerstendorf, H., Drobot, B., Schmidt, M., Musat, N., Swanson, J.S., Reed, D.T., Stumpf, T., Cherkouk, A., 2017. Multistage bioassociation of uranium onto an extremely halophilic archaeon revealed by a unique combination of spectroscopic and microscopic techniques. Journal of Hazardous Materials 327, 225–232. https://doi.org/10.1016/j.jhazmat.2016.12.053

Bader, M., Müller, K., Foerstendorf, H., Schmidt, M., Simmons, K., Swanson, J.S., Reed, D.T., Stumpf, T., Cherkouk, A., 2018. Comparative analysis of uranium bioassociation with halophilic bacteria and archaea. PLoS ONE 13, e0190953. https://doi.org/10.1371/journal.pone.0190953

Baeyens, W., Gao, Y., Davison, W., Galceran, J., Leermakers, M., Puy, J., Superville, P.-J., Beguery, L., 2018. In situ measurements of micronutrient dynamics in open seawater show that complex dissociation rates may limit diatom growth. Sci Rep 8, 16125. https://doi.org/10.1038/s41598-018-34465-w

REFERENCES

Barkleit, A., Foerstendorf, H., Heim, K., Sachs, S., Bernhard, G., 2008. Complex Formation of Uranium(VI) with L-Phenylalanine and 3-Phenylpropionic Acid Studied by Attenuated Total Reflection Fourier Transform Infrared Spectroscopy. Appl Spectrosc 62, 798–802. https://doi.org/10.1366/000370208784909607

Beazley, M.J., Martinez, R.J., Sobecky, P.A., Webb, S.M., Taillefert, M., 2009. Nonreductive Biomineralization of Uranium(VI) Phosphate Via Microbial Phosphatase Activity in Anaerobic Conditions. Geomicrobiology Journal 26, 431–441. https://doi.org/10.1080/01490450903060780

Beazley, M.J., Martinez, R.J., Sobecky, P.A., Webb, S.M., Taillefert, M., 2007. Uranium Biomineralization as a Result of Bacterial Phosphatase Activity: Insights from Bacterial Isolates from a Contaminated Subsurface. Environ. Sci. Technol. 41, 5701–5707. https://doi.org/10.1021/es070567g

Beller, H.R., 2005. Anaerobic, Nitrate-Dependent Oxidation of U(IV) Oxide Minerals by the Chemolithoautotrophic Bacterium *Thiobacillus denitrificans*. Appl Environ Microbiol 71, 2170–2174. https://doi.org/10.1128/AEM.71.4.2170-2174.2005

Beneš, P., Borovec, Z., Strejc, P., 1985. Interaction of radium with freshwater sediments and their mineral components. II. Kaolinite and montmorillonite. Journal of Radioanalytical and Nuclear Chemistry 89, 339–351. https://doi.org/10.1007/BF02040598

Beneš, P., Strejc, P., Lukavec, Z., 1984. Interaction of radium with freshwater sediments and their mineral components. I.: Ferric hydroxide and quartz. Journal of Radioanalytical and Nuclear Chemistry, Articles 82, 275–285. https://doi.org/10.1007/BF02037050

Bernhard, G., Geipel, G., Brendler, V., Nitsche, H., 1996. Speciation of Uranium in Seepage Waters of a Mine Tailing Pile Studied by Time-Resolved Laser-Induced Fluorescence Spectroscopy (TRLFS). Radiochimica Acta 74, 87–92. https://doi.org/10.1524/ract.1996.74.special-issue.87

Birch, L., Bachofen, R., 1990. Complexing agents from microorganisms. Experientia 46, 827–834. https://doi.org/10.1007/BF01935533

Bituh, T., Marovic, G., Franic, Z., Sencar, J., Bronzovic, M., 2009. Radioactive contamination in Croatia by phosphate fertilizer production. Journal of Hazardous Materials 162, 1199–1203. https://doi.org/10.1016/j.jhazmat.2008.06.005

Bosbach, D., Böttle, M., Metz, V., 2010. Experimental study on Ra^{2+} uptake by barite ($BaSO_4$) - Kinetics of solid solution formation via $BaSO_4$ dissolution and $Ra_xBa_{1-x}SO_4$ (re)precipitation (Technical Report No. TR-10-43). Swedish Nuclear Fuel and Waste Management Co.

Bosecker, K., 1997. Bioleaching: metal solubilization by microorganisms. FEMS Microbiol Rev 20, 591–604. https://doi.org/10.1111/j.1574-6976.1997.tb00340.x

Bowler, C., Allen, A.E., Badger, J.H., Grimwood, J., Jabbari, K., Kuo, A., Maheswari, U., Martens, C., Maumus, F., Otillar, R.P., Rayko, E., Salamov, A., Vandepoele, K., Beszteri, B., Gruber, A., Heijde, M., Katinka, M., Mock, T., Valentin, K., Verret, F., Berges, J.A., Brownlee, C., Cadoret, J.-P., Chiovitti, A., Choi, C.J., Coesel, S., De Martino, A., Detter, J.C., Durkin, C., Falciatore, A., Fournet, J., Haruta, M., Huysman, M.J.J., Jenkins, B.D., Jiroutova, K., Jorgensen, R.E., Joubert, Y., Kaplan, A., Kröger, N., Kroth, P.G., La Roche, J., Lindquist, E., Lommer, M., Martin–Jézéquel, V., Lopez, P.J., Lucas, S., Mangogna, M., McGinnis, K., Medlin, L.K., Montsant, A., Secq, M.-P.O., Napoli, C., Obornik, M., Parker, M.S., Petit, J.-L., Porcel, B.M., Poulsen, N., Robison, M., Rychlewski, L., Rynearson, T.A., Schmutz, J., Shapiro, H., Siaut, M., Stanley, M., Sussman, M.R., Taylor, A.R., Vardi, A., Von Dassow, P., Vyverman, W., Willis, A., Wyrwicz, L.S., Rokhsar, D.S., Weissenbach, J., Armbrust, E.V., Green, B.R., Van De Peer, Y., Grigoriev, I.V., 2008. The *Phaeodactylum* genome reveals the evolutionary history of diatom genomes. Nature 456, 239–244. https://doi.org/10.1038/nature07410

Brachmann, A., Geipel, G., Bernhard, G., Nitsche, H., 2002. Study of uranyl(VI) malonate complexation by time resolved laser-induced fluorescence spectroscopy (TRLFS). Radiochimica Acta 90, 147–153. https://doi.org/doi:10.1524/ract.2002.90.3_2002.147

Bradbury, J., 2004. Nature's Nanotechnologists: Unveiling the Secrets of Diatoms. PLoS Biol 2, e306. https://doi.org/10.1371/journal.pbio.0020306

Bruckner, C.G., Bahulikar, R., Rahalkar, M., Schink, B., Kroth, P.G., 2008. Bacteria Associated with Benthic Diatoms from Lake Constance: Phylogeny and Influences on Diatom Growth and Secretion of Extracellular Polymeric Substances. Appl Environ Microbiol 74, 7740–7749. https://doi.org/10.1128/AEM.01399-08

Bruckner, C.G., Rehm, C., Grossart, H., Kroth, P.G., 2011. Growth and release of extracellular organic compounds by benthic diatoms depend on interactions with bacteria. Environmental Microbiology 13, 1052–1063. https://doi.org/10.1111/j.1462-2920.2010.02411.x

Brugge, D., Buchner, V., 2011. Health effects of uranium: new research findings. Reviews on Environmental Health 26. https://doi.org/10.1515/REVEH.2011.032

Brugge, D., deLemos, J.L., Oldmixon, B., 2005. Exposure Pathways and Health Effects Associated with Chemical and Radiological Toxicity of Natural Uranium: A Review. Reviews on Environmental Health 20. https://doi.org/10.1515/REVEH.2005.20.3.177

Buesseler, K.O., 1998. The decoupling of production and particulate export in the surface ocean. Global Biogeochem. Cycles 12, 297–310. https://doi.org/10.1029/97GB03366

Cantonati, M., Angeli, N., Virtanen, L., Wojtal, A.Z., Gabrieli, J., Falasco, E., Lavoie, I., Morin, S., Marchetto, A., Fortin, C., Smirnova, S., 2014. *Achnanthidium minutissimum* (Bacillariophyta) valve deformities as indicators of metal enrichment in diverse widely-distributed freshwater habitats. Science of The Total Environment 475, 201–215. https://doi.org/10.1016/j.scitotenv.2013.10.018

Carvalho, F.P., Fesenko, S., Harbottle, A.R., Lavrova, T., Mitchell, N.G., Payne, T.E., Rigol, A., Thorne, M.C., Ulanowski, A., Vidal, M., Voitsekhovych, O., West, J.M., Yankovich, T., 2023. The environmental behaviour of uranium (No. 488), Technical reports series. International Atomic Energy Agency, Vienna.

Cetin, S.C., Karaca, A., Kizilkaya, R., Turgay, O.C., 2011. Role of Plant Growth Promoting Bacteria and Fungi in Heavy Metal Detoxification, in: Sherameti, I., Varma, A. (Eds.), Detoxification of Heavy Metals, Soil Biology. Springer Berlin Heidelberg, Berlin, Heidelberg, pp. 369–388. https://doi.org/10.1007/978-3-642-21408-0_19

Chasapis, C.T., Peana, M., Bekiari, V., 2022. Structural Identification of Metalloproteomes in Marine Diatoms, an Efficient Algae Model in Toxic Metals Bioremediation. Molecules 27, 378. https://doi.org/10.3390/molecules27020378

Chen, L., Liu, J., Zhang, W., Zhou, J., Luo, D., Li, Z., 2021. Uranium (U) source, speciation, uptake, toxicity and bioremediation strategies in soil-plant system: A review. Journal of Hazardous Materials 413, 125319. https://doi.org/10.1016/j.jhazmat.2021.125319

Choudhary, S., Sar, P., 2015. Interaction of uranium (VI) with bacteria: potential applications in bioremediation of U contaminated oxic environments. Rev Environ Sci Biotechnol 14, 347–355. https://doi.org/10.1007/s11157-015-9366-6

Choudhary, S., Sar, P., 2011. Uranium biomineralization by a metal resistant *Pseudomonas aeruginosa* strain isolated from contaminated mine waste. Journal of Hazardous Materials 186, 336–343. https://doi.org/10.1016/j.jhazmat.2010.11.004

Coates, J.D., Bhupathiraju, V.K., Achenbach, L.A., Mclnerney, M.J., Lovley, D.R., 2001. *Geobacter hydrogenophilus*, *Geobacter chapellei* and *Geobacter grbiciae*, three new, strictly anaerobic, dissimilatory Fe(III)-reducers. International Journal of Systematic and Evolutionary Microbiology 51, 581–588. https://doi.org/10.1099/00207713-51-2-581

Cobbett, C., Goldsbrough, P., 2002. PHYTOCHELATINS AND METALLOTHIONEINS : Roles in Heavy Metal Detoxification and Homeostasis. Annu. Rev. Plant Biol. 53, 159–182. https://doi.org/10.1146/annurev.arplant.53.100301.135154

Collins, R.N., Saito, T., Aoyagi, N., Payne, T.E., Kimura, T., Waite, T.D., 2011. Applications of Time-Resolved Laser Fluorescence Spectroscopy to the Environmental Biogeochemistry of Actinides. J. Environ. Qual. 40, 731–741. https://doi.org/10.2134/jeq2010.0166

Consalvey, M., Paterson, D.M., Underwood, G.J.C., 2004. The Ups and Downs of Life in a

Benthic Biofilm: Migration of Benthic Diatoms. Diatom Research 19, 181–202. https://doi.org/10.1080/0269249X.2004.9705870

Costa, O.Y.A., Raaijmakers, J.M., Kuramae, E.E., 2018. Microbial Extracellular Polymeric Substances: Ecological Function and Impact on Soil Aggregation. Front. Microbiol. 9, 1636. https://doi.org/10.3389/fmicb.2018.01636

Coyne, K.J., Wang, Y., Johnson, G., 2022. Algicidal Bacteria: A Review of Current Knowledge and Applications to Control Harmful Algal Blooms. Front. Microbiol. 13, 871177. https://doi.org/10.3389/fmicb.2022.871177

Crist, R.H., Oberholser, K., Shank, N., Nguyen, M., 1981. Nature of bonding between metallic ions and algal cell walls. Environ. Sci. Technol. 15, 1212–1217. https://doi.org/10.1021/es00092a010

Croft, M.T., Lawrence, A.D., Raux-Deery, E., Warren, M.J., Smith, A.G., 2005. Algae acquire vitamin B_{12} through a symbiotic relationship with bacteria. Nature 438, 90–93. https://doi.org/10.1038/nature04056

De Haan, D., Aram, L., Peled-Zehavi, H., Addadi, Y., Ben-Joseph, O., Rotkopf, R., Elad, N., Rechav, K., Gal, A., 2023. Exocytosis of the silicified cell wall of diatoms involves extensive membrane disintegration. Nat Commun 14, 480. https://doi.org/10.1038/s41467-023-36112-z

Decho, A.W., Gutierrez, T., 2017. Microbial Extracellular Polymeric Substances (EPSs) in Ocean Systems. Front. Microbiol. 8, 922. https://doi.org/10.3389/fmicb.2017.00922

Demnitz, M., Hilpmann, S., Lösch, H., Bok, F., Steudtner, R., Patzschke, M., Stumpf, T., Huittinen, N., 2020. Temperature-dependent luminescence spectroscopic investigations of uranyl(VI) complexation with the halides F^- and Cl^-. Dalton Trans. 49, 7109–7122. https://doi.org/10.1039/D0DT00646G

DiSpirito, A.A., Tuovinen, O.H., 1982. Uranous Ion Oxidation and Carbon Dioxide Fixation by *Thiobacillus ferrooxidans*. Archives of Microbiology 133, 28–32.

Dorothy, C., 1959. Ion exchange in clays and other minerals. Geological Society of America Bulletin 70, 749–779. https://doi.org/10.1130/0016-7606(1959)70[749:IEICAO]2.0.CO;2

Dörr, T., Moynihan, P.J., Mayer, C., 2019. Editorial: Bacterial Cell Wall Structure and Dynamics. Front. Microbiol. 10, 2051. https://doi.org/10.3389/fmicb.2019.02051

Drebes, G., 1977. Chapter 9: Sexuality, in: Dietrich Werner (Ed.), The Biology of Diatoms, Botanical Monographs. University of California Press, pp. 250–283.

Drobot, B., Steudtner, R., Raff, J., Geipel, G., Brendler, V., Tsushima, S., 2015. Combining luminescence spectroscopy, parallel factor analysis and quantum chemistry to reveal metal speciation – a case study of uranyl(VI) hydrolysis. Chem. Sci. 6, 964–972. https://doi.org/10.1039/C4SC02022G

Duff, M.C., Coughlin, J.U., Hunter, D.B., 2002. Uranium co-precipitation with iron oxide minerals. Geochimica et Cosmochimica Acta 66, 3533–3547. https://doi.org/10.1016/S0016-7037(02)00953-5

Emsley, J., 2001. Uranium, in: Nature's Building Blocks: An A to Z Guide to the Elements. Oxford University Press, p. 479.

Esteves, S.M., Keck, F., Almeida, S.F.P., Figueira, E., Bouchez, A., Rimet, F., 2017. Can we predict diatoms herbicide sensitivities with phylogeny? Influence of intraspecific and interspecific variability. Ecotoxicology 26, 1065–1077. https://doi.org/10.1007/s10646-017-1834-z

Etesami, H., 2018. Bacterial mediated alleviation of heavy metal stress and decreased accumulation of metals in plant tissues: Mechanisms and future prospects. Ecotoxicology and Environmental Safety 147, 175–191. https://doi.org/10.1016/j.ecoenv.2017.08.032

Fagan, R.P., Fairweather, N.F., 2014. Biogenesis and functions of bacterial S-layers. Nat Rev Microbiol 12, 211–222. https://doi.org/10.1038/nrmicro3213

Falasco, E., Bona, F., Badino, G., Hoffmann, L., Ector, L., 2009. Diatom teratological forms and environmental alterations: a review. Hydrobiologia 623, 1–35. https://doi.org/10.1007/s10750-008-9687-3

Ferreira Da Silva, E., Almeida, S.F.P., Nunes, M.L., Luís, A.T., Borg, F., Hedlund, M., De Sá, C.M., Patinha, C., Teixeira, P., 2009. Heavy metal pollution downstream the abandoned Coval da Mó mine (Portugal) and associated effects on epilithic diatom communities. Science of The Total Environment 407, 5620–5636. https://doi.org/10.1016/j.scitotenv.2009.06.047

Finneran, K.T., Housewright, M.E., Lovley, D.R., 2002. Multiple influences of nitrate on uranium solubility during bioremediation of uranium-contaminated subsurface sediments. Environ Microbiol 4, 510–516. https://doi.org/10.1046/j.1462-2920.2002.00317.x

Flower, R.J., 1993. Diatom preservation: experiments and observations on dissolution and breakage in modern and fossil material, in: van Dam, H. (Ed.), Twelfth International Diatom Symposium. Springer Netherlands, Dordrecht, pp. 473–484.

Foster, R.A., Kuypers, M.M.M., Vagner, T., Paerl, R.W., Musat, N., Zehr, J.P., 2011. Nitrogen fixation and transfer in open ocean diatom–cyanobacterial symbioses. ISME J 5, 1484–1493. https://doi.org/10.1038/ismej.2011.26

Fowle, D.A., Fein, J.B., Martin, A.M., 2000. Experimental Study of Uranyl Adsorption onto *Bacillus subtilis*. Environ. Sci. Technol. 34, 3737–3741. https://doi.org/10.1021/es991356h

Francis, A.J., Dodge, C.J., Lu, Fulong., Halada, G.P., Clayton, C.R., 1994. XPS and XANES Studies of Uranium Reduction by *Clostridium* sp. Environ. Sci. Technol. 28, 636–639. https://doi.org/10.1021/es00053a016

Francis, A.J., Gillow, J.B., Dodge, C.J., Harris, R., Beveridge, T.J., Papenguth, H.W., 2004. Uranium association with halophilic and non-halophilic bacteria and archaea. Radiochimica Acta 92, 481–488. https://doi.org/10.1524/ract.92.8.481.39281

Frankenberger, W.T., Arshad, M., 2001. Bioremediation of selenium-contaminated sediments and water. BioFactors 14, 241–254. https://doi.org/10.1002/biof.5520140130

Fuhrman, J.A., Azam, F., 1982. Thymidine incorporation as a measure of heterotrophic bacterioplankton production in marine surface waters: Evaluation and field results. Mar. Biol. 66, 109–120. https://doi.org/10.1007/BF00397184

Gadd, G.M., 2004. Microbial influence on metal mobility and application for bioremediation. Geoderma 122, 109–119. https://doi.org/10.1016/j.geoderma.2004.01.002

Garnham, G.W., Codd, G.A., Gadd, G.M., 1992. Kinetics of uptake and intracellular location of cobalt, manganese and zinc in the estuarine green alga *Chlorella salina*. Applied Microbiology and Biotechnology 270–276.

Gélabert, A., Pokrovsky, O.S., Schott, J., Boudou, A., Feurtet-Mazel, A., Mielczarski, J., Mielczarski, E., Mesmer-Dudons, N., Spalla, O., 2004. Study of diatoms/aqueous solution interface. I. Acid-base equilibria and spectroscopic observation of freshwater and marine species. Geochimica et Cosmochimica Acta 68, 4039–4058. https://doi.org/10.1016/j.gca.2004.01.011

Goecke, F., Labes, A., Wiese, J., Imhoff, J., 2010. Chemical interactions between marine macroalgae and bacteria. Mar. Ecol. Prog. Ser. 409, 267–299. https://doi.org/10.3354/meps08607

Goecke, F., Thiel, V., Wiese, J., Labes, A., Imhoff, J.F., 2013. Algae as an important environment for bacteria – phylogenetic relationships among new bacterial species isolated from algae. Phycologia 52, 14–24. https://doi.org/10.2216/12-24.1

Gorman-Lewis, D., Elias, P.E., Fein, J.B., 2005. Adsorption of Aqueous Uranyl Complexes onto *Bacillus subtilis* Cells. Environ. Sci. Technol. 39, 4906–4912. https://doi.org/10.1021/es047957c

Greeman, D.J., Rose, A.W., Washington, J.W., Dobos, R.R., Ciolkosz, E.J., 1999. Geochemistry of radium in soils of the Eastern United States. Applied Geochemistry 14, 365–385. https://doi.org/10.1016/S0883-2927(98)00059-6

Guiry, M.D., 2012. How Many Soecies of Algae Are There? Journal of Phycology 48, 1057–1063. https://doi.org/10.1111/j.1529-8817.2012.01222.x

Günther, A., Geipel, G., Bernhard, G., 2007. Complex formation of uranium(VI) with the amino acids l-glycine and l-cysteine: A fluorescence emission and UV–Vis absorption study.

Polyhedron 26, 59–65. https://doi.org/10.1016/j.poly.2006.07.030

Günther, A., Geipel, G., Bernhard, G., 2006. Complex formation of U(VI) with the amino acid *L* -threonine and the corresponding phosphate ester O-phospho- *L* -threonine. Radiochimica Acta 94, 845–851. https://doi.org/10.1524/ract.2006.94.12.845

Günther, A., Raff, J., Geipel, G., Bernhard, G., 2008. Spectroscopic investigations of U(VI) species sorbed by the green algae *Chlorella vulgaris*. Biometals 21, 333–341. https://doi.org/10.1007/s10534-007-9122-7

Haas, J.R., Dichristina, T.J., Jr, R.W., 2001. Thermodynamics of U(VI) sorption onto *Shewanella putrefaciens*.

Halse, G.R., Syvertsen, E.E., 1996. Chapter 2 - Marine Diatoms, in: Identifying Marine Diatoms and Dinoflagellates. Academic Press, pp. 5–385. https://doi.org/10.1016/B978-012693015-3/50005-X

Hansda, A., Kumar, V., Anshumali, 2016. A comparative review towards potential of microbial cells for heavy metal removal with emphasis on biosorption and bioaccumulation. World J Microbiol Biotechnol 32, 170. https://doi.org/10.1007/s11274-016-2117-1

Hecky, R.E., Mopper, K., Kilham, P., Degens, E.T., 1973. The amino acid and sugar composition of diatom cell-walls. Marine Biology 19, 323–331. https://doi.org/10.1007/BF00348902

Heidari, F., Riahi, H., Aghamiri, M.R., Zakeri, F., Shariatmadari, Z., Hauer, T., 2018. ^{226}Ra, ^{238}U and Cd adsorption kinetics and binding capacity of two cyanobacterial strains isolated from highly radioactive springs and optimal conditions for maximal removal effects in contaminated water. International Journal of Phytoremediation 20, 369–377. https://doi.org/10.1080/15226514.2017.1393392

Herlory, O., Bonzom, J.-M., Gilbin, R., Frelon, S., Fayolle, S., Delmas, F., Coste, M., 2013. Use of diatom assemblages as biomonitor of the impact of treated uranium mining effluent discharge on a stream: case study of the Ritord watershed (Center-West France). Ecotoxicology 22, 1186–1199. https://doi.org/10.1007/s10646-013-1106-5

Hilpmann, S., Rossberg, A., Steudtner, R., Drobot, B., Hübner, R., Bok, F., Prieur, D., Bauters, S., Kvashnina, K.O., Stumpf, T., Cherkouk, A., 2023. Presence of uranium(V) during uranium(VI) reduction by *Desulfosporosinus hippei* DSM 8344T. Science of The Total Environment 875, 162593. https://doi.org/10.1016/j.scitotenv.2023.162593

Huang, F.Y.C., Brady, P.V., Lindgren, E.R., Guerra, P., 1998. Biodegradation of Uranium−Citrate Complexes: Implications for Extraction of Uranium from Soils. Environ. Sci. Technol. 32, 379–382. https://doi.org/10.1021/es970181d

IAEA, 2014. The environmental behaviour of radium, Revised. ed, Technical reports series / International Atomic Energy Agency. International Atomic Energy Agency, Vienna.

IAEA, 2009. Quantification of radionuclide transfer in terrestrial and freshwater environments for radiological assessments, TECDOC series. INTERNATIONAL ATOMIC ENERGY AGENCY, Vienna.

Ismail, A.A., Van De Voort, F.R., Sedman, J., 1997. Chapter 4 Fourier transform infrared spectroscopy: Principles and applications, in: Techniques and Instrumentation in Analytical Chemistry. Elsevier, pp. 93–139. https://doi.org/10.1016/S0167-9244(97)80013-3

Jiang, W., Saxena, A., Song, B., Ward, B.B., Beveridge, T.J., Myneni, S.C.B., 2004. Elucidation of Functional Groups on Gram-Positive and Gram-Negative Bacterial Surfaces Using Infrared Spectroscopy. Langmuir 20, 11433–11442. https://doi.org/10.1021/la049043+

Jroundi, F., Merroun, M.L., Arias, J.M., Rossberg, A., Selenska-Pobell, S., González-Muñoz, M.T., 2007. Spectroscopic and Microscopic Characterization of Uranium Biomineralization in *Myxococcus xanthus*. Geomicrobiology Journal 24, 441–449. https://doi.org/10.1080/01490450701437651

Kalin, M., Wheeler, W.N., Meinrath, G., 2005. The removal of uranium from mining waste water using algal/microbial biomass. Journal of Environmental Radioactivity 78, 151–177. https://doi.org/10.1016/j.jenvrad.2004.05.002

Kanamarlapudi, S.L.R.K., Chintalpudi, V.K., Muddada, S., 2018. Application of Biosorption for Removal of Heavy Metals from Wastewater, in: Derco, J., Vrana, B. (Eds.),

Biosorption. InTech, p. 69. https://doi.org/10.5772/intechopen.77315

Karunakara, N., Somashekarappa, H.M., Narayana, Y., Avadhani, D.N., Mahesh, H.M., Siddappa, K., 2003. ^{226}Ra, ^{40}K and ^{7}Be activity concentrations in plants in the environment of Kaiga, India. J Environ Radioact. 65, 255–266. https://doi.org/10.1016/S0265-931X(02)00101-7

Kazamia, E., Sutak, R., Paz-Yepes, J., Dorrell, R.G., Vieira, F.R.J., Mach, J., Morrissey, J., Leon, S., Lam, F., Pelletier, E., Camadro, J.-M., Bowler, C., Lesuisse, E., 2018. Endocytosis-mediated siderophore uptake as a strategy for Fe acquisition in diatoms. Sci. Adv. 4, eaar4536. https://doi.org/10.1126/sciadv.aar4536

Kazy, S.K., D'Souza, S.F., Sar, P., 2009. Uranium and thorium sequestration by a *Pseudomonas* sp.: Mechanism and chemical characterization. Journal of Hazardous Materials 163, 65–72. https://doi.org/10.1016/j.jhazmat.2008.06.076

Keeling, P.J., Palmer, J.D., 2008. Horizontal gene transfer in eukaryotic evolution. Nat Rev Genet 9, 605–618. https://doi.org/10.1038/nrg2386

Kelly, S.D., Kemner, K.M., Fein, J.B., Fowle, D.A., Boyanov, M.I., Bunker, B.A., Yee, N., 2002. X-ray absorption fine structure determination of pH-dependent U-bacterial cell wall interactions. Geochimica et Cosmochimica Acta 66, 3855–3871. https://doi.org/10.1016/S0016-7037(02)00947-X

Khijniak, T.V., Slobodkin, A.I., Coker, V., Renshaw, J.C., Livens, F.R., Bonch-Osmolovskaya, E.A., Birkeland, N.-K., Medvedeva-Lyalikova, N.N., Lloyd, J.R., 2005. Reduction of Uranium(VI) Phosphate during Growth of the Thermophilic Bacterium *Thermoterrabacterium ferrireducens*. Appl Environ Microbiol 71, 6423–6426. https://doi.org/10.1128/AEM.71.10.6423-6426.2005

Khraisheh, M., Aldegs, Y., Mcminn, W., 2004. Remediation of wastewater containing heavy metals using raw and modified diatomite. Chemical Engineering Journal 99, 177–184. https://doi.org/10.1016/j.cej.2003.11.029

Kieft, T.L., Fredrickson, J.K., Onstott, T.C., Gorby, Y.A., Kostandarithes, H.M., Bailey, T.J., Kennedy, D.W., Li, S.W., Plymale, A.E., Spadoni, C.M., Gray, M.S., 1999. Dissimilatory Reduction of Fe(III) and Other Electron Acceptors by a *Thermus* Isolate. Appl Environ Microbiol 65, 1214–1221. https://doi.org/10.1128/AEM.65.3.1214-1221.1999

Kiran Marella, T., Saxena, A., Tiwari, A., 2020. Diatom mediated heavy metal remediation: A review. Bioresource Technology 305, 123068. https://doi.org/10.1016/j.biortech.2020.123068

Koban, A., Bernhard, G., 2007. Uranium(VI) complexes with phospholipid model compounds – A laser spectroscopic study. Journal of Inorganic Biochemistry 101, 750–757. https://doi.org/10.1016/j.jinorgbio.2007.01.001

Kogure, K., Simidu, U., Taga, N., 1981. Bacterial attachment to phytoplankton in sea water. Journal of Experimental Marine Biology and Ecology 56, 197–204. https://doi.org/10.1016/0022-0981(81)90189-1

Koulouris, G., 1995. Dynamic studies on sorption characteristics of ^{226}Ra on manganese dioxide. Journal of Radioanalytical and Nuclear Chemistry, Articles 193, 269–279. https://doi.org/10.1007/BF02039884

Kouzuma, A., Watanabe, K., 2015. Exploring the potential of algae/bacteria interactions. Current Opinion in Biotechnology 33, 125–129. https://doi.org/10.1016/j.copbio.2015.02.007

Krawczyk-Bärsch, E., Gerber, U., Müller, K., Moll, H., Rossberg, A., Steudtner, R., Merroun, M.L., 2018. Multidisciplinary characterization of U(VI) sequestration by *Acidovorax facilis* for bioremediation purposes. Journal of Hazardous Materials 347, 233–241. https://doi.org/10.1016/j.jhazmat.2017.12.030

Krawczyk-Bärsch, E., Ramtke, J., Drobot, B., Müller, K., Steudtner, R., Kluge, S., Hübner, R., Raff, J., 2022. Peptidoglycan as major binding motif for Uranium bioassociation on *Magnetospirillum magneticum* AMB-1 in contaminated waters. Journal of Hazardous Materials 437, 129376. https://doi.org/10.1016/j.jhazmat.2022.129376

Kröger, N., Bergsdorf, C., Sumper, M., 1994. A new calcium binding glycoprotein family

constitutes a major diatom cell wall component. The EMBO Journal 13, 4676–4683. https://doi.org/10.1002/j.1460-2075.1994.tb06791.x

Ku, T.-L., Mathieu, G.G., Knauss, K.G., 1977. Uranium in open ocean: concentration and isotopic composition. Deep Sea Research 24, 1005–1017. https://doi.org/10.1016/0146-6291(77)90571-9

Kumar, V., Kashyap, M., Gautam, S., Shukla, P., Joshi, K.B., Vinayak, V., 2018. Fast Fourier infrared spectroscopy to characterize the biochemical composition in diatoms. J Biosci 43, 717–729. https://doi.org/10.1007/s12038-018-9792-z

Lane, T.W., Morel, F.M.M., 2000. A biological function for cadmium in marine diatoms. Proc. Natl. Acad. Sci. U.S.A. 97, 4627–4631. https://doi.org/10.1073/pnas.090091397

Langmuir, I., 1918. The adsorption of gases on plane surfaces of glass, mica and platinum. J. Am. Chem. Soc. 40, 1361–1403. https://doi.org/10.1021/ja02242a004

Lavoie, I., Hamilton, P.B., Morin, S., Kim Tiam, S., Kahlert, M., Gonçalves, S., Falasco, E., Fortin, C., Gontero, B., Heudre, D., Kojadinovic-Sirinelli, M., Manoylov, K., Pandey, L.K., Taylor, J.C., 2017. Diatom teratologies as biomarkers of contamination: Are all deformities ecologically meaningful? Ecological Indicators 82, 539–550. https://doi.org/10.1016/j.ecolind.2017.06.048

Lebeau, T., Robert, J.-M., 2003. Diatom cultivation and biotechnologically relevant products. Part II: Current and putative products. Appl Microbiol Biotechnol 60, 624–632. https://doi.org/10.1007/s00253-002-1177-3

Lee, J.G., Ahner, B.A., Morel, F.M.M., 1996. Export of Cadmium and Phytochelatin by the Marine Diatom *Thalassiosira weissflogii*. Environ. Sci. Technol. 30, 1814–1821. https://doi.org/10.1021/es950331p

Leggett, R.W., Harrison, J.D., 1995. Fractional absorption of ingested uranium in humans. Health Phys. 68(4), 484–498. https://doi.org/10.1097/00004032-199504000-00005

Lewis, J., Kennaway, G., Franca, S., Alverca, E., 2001. Bacteria–dinoflagellate interactions: investigative microscopy of *Alexandrium* spp (Gonyaulacales, Dinophyceae). Phycologia 40, 280–285. https://doi.org/10.2216/i0031-8884-40-3-280.1

Llorens, I., Untereiner, G., Jaillard, D., Gouget, B., Chapon, V., Carriere, M., 2012. Uranium Interaction with Two Multi-Resistant Environmental Bacteria: *Cupriavidus metallidurans* CH34 and *Rhodopseudomonas palustris*. PLoS ONE 7, e51783. https://doi.org/10.1371/journal.pone.0051783

Lloyd, J.R., Leang, C., Myerson, A.L.H., Coppi, M.V., Cuifo, S., Methe, B., Sandler, S.J., Lovley, D.R., 2003. Biochemical and genetic characterization of PpcA, a periplasmic *c*-type cytochrome in *Geobacter sulfurreducens*. Biochemical Journal 369, 153–161. https://doi.org/10.1042/bj20020597

Lloyd, J.R., Ridley, J., Khizniak, T., Lyalikova, N.N., Macaskie, L.E., 1999. Reduction of Technetium by *Desulfovibrio desulfuricans*: Biocatalyst Characterization and Use in a Flowthrough Bioreactor. Appl Environ Microbiol 65, 2691–2696. https://doi.org/10.1128/AEM.65.6.2691-2696.1999

Lloyd, J.R., Yong, P., Macaskie, L.E., 1998. Enzymatic Recovery of Elemental Palladium by Using Sulfate-Reducing Bacteria. Appl Environ Microbiol 64, 4607–4609. https://doi.org/10.1128/AEM.64.11.4607-4609.1998

Lopez, P.J., Desclés, J., Allen, A.E., Bowler, C., 2005. Prospects in diatom research. Current Opinion in Biotechnology 16, 180–186. https://doi.org/10.1016/j.copbio.2005.02.002

Lovley, D.R., Phillips, E.J., 1992. Reduction of uranium by *Desulfovibrio desulfuricans*. Appl Environ Microbiol 58, 850–856. https://doi.org/10.1128/aem.58.3.850-856.1992

Lovley, D.R., Phillips, E.J.P., Gorby, Y.A., Landa, E.R., 1991. Microbial reduction of uranium. Nature 350, 413–416. https://doi.org/10.1038/350413a0

Lu, J., Salzberg, S.L., 2020. Ultrafast and accurate 16S rRNA microbial community analysis using Kraken 2. Microbiome 8, 124. https://doi.org/10.1186/s40168-020-00900-2

Luddington, I.A., Kaczmarska, I., Lovejoy, C., 2012. Distance and Character-Based Evaluation of the V4 Region of the 18S rRNA Gene for the Identification of Diatoms (Bacillariophyceae). PLoS ONE 7, e45664. https://doi.org/10.1371/journal.pone.0045664

Luo, C.-S., Liang, J.-R., Lin, Q., Li, C., Bowler, C., Anderson, D.M., Wang, P., Wang, X.-W., Gao, Y.-H., 2014. Cellular Responses Associated with ROS Production and Cell Fate Decision in Early Stress Response to Iron Limitation in the Diatom *Thalassiosira pseudonana*. J. Proteome Res. 13, 5510–5523. https://doi.org/10.1021/pr5004664

Lütke, L., Moll, H., Bernhard, G., 2012. Insights into the uranium(VI) speciation with *Pseudomonas fluorescens* on a molecular level. Dalton Trans. 41, 13370. https://doi.org/10.1039/c2dt31080e

Ma, F., Wang, C., Zhang, Y., Chen, J., Xie, R., Sun, Z., 2022. Development of Microbial Indicators in Ecological Systems. IJERPH 19, 13888. https://doi.org/10.3390/ijerph192113888

Macaskie, L.E., Bonthrone, K.M., Yong, P., Goddard, D.T., 2000. Enzymically mediated bioprecipitation of uranium by a *Citrobacter* sp.: a concerted role for exocellular lipopolysaccharide and associated phosphatase in biomineral formation. Microbiology 146, 1855–1867. https://doi.org/10.1099/00221287-146-8-1855

Macaskie, L.E., Empson, R.M., Cheetham, A.K., Grey, C.P., Skarnulis, A.J., 1992. Uranium Bioaccumulation by a *Citrobacter* sp. as a Result of Enzymically Mediated Growth of Polycrystalline HUO_2PO_4. Science 257, 782–784. https://doi.org/10.1126/science.1496397

Mai-Prochnow, A., Clauson, M., Hong, J., Murphy, A.B., 2016. Gram positive and Gram negative bacteria differ in their sensitivity to cold plasma. Sci Rep 6, 38610. https://doi.org/10.1038/srep38610

Manhes, G., Allègre, C.J., Dupré, B., Hamelin, B., 1980. Lead isotope study of basic-ultrabasic layered complexes: Speculations about the age of the earth and primitive mantle characteristics. Earth and Planetary Science Letters 47, 370–382. https://doi.org/10.1016/0012-821X(80)90024-2

Mann, D.G., 1999. The species concept in diatoms. Phycologia 38, 437–495. https://doi.org/10.2216/i0031-8884-38-6-437.1

Martin, M., 2011. Cutadapt removes adapter sequences from high-throughput sequencing reads. EMBnet.journal 17, 10–12. https://doi.org/10.14806/ej.17.1.200

Martin, P., Akber, R.A., 1999. Radium isotopes as indicators of adsorption–desorption interactions and barite formation in groundwater. Journal of Environmental Radioactivity 46, 271–286. https://doi.org/10.1016/S0265-931X(98)00147-7

Martinez, R.J., Beazley, M.J., Taillefert, M., Arakaki, A.K., Skolnick, J., Sobecky, P.A., 2007. Aerobic uranium (VI) bioprecipitation by metal-resistant bacteria isolated from radionuclide- and metal-contaminated subsurface soils. Environ Microbiol 9, 3122–3133. https://doi.org/10.1111/j.1462-2920.2007.01422.x

Mehrotra, T., Dev, S., Banerjee, A., Chatterjee, A., Singh, R., Aggarwal, S., 2021. Use of immobilized bacteria for environmental bioremediation: A review. Journal of Environmental Chemical Engineering 9, 105920. https://doi.org/10.1016/j.jece.2021.105920

Meier, B., Sehn, A.P., Sette, M., Paci, M., Desideri, A., Rotilio, G., 1994. In vivo incorporation of cobalt into *Propionibacterium shermanii* superoxide dismutase. FEBS Letters 348, 283–286. https://doi.org/10.1016/0014-5793(94)00624-5

Méndez-Garcí-a, C., Peláez, A.I., Mesa, V., Sánchez, J., Golyshina, O.V., Ferrer, M., 2015. Microbial diversity and metabolic networks in acid mine drainage habitats. Front. Microbiol. 6. https://doi.org/10.3389/fmicb.2015.00475

Menzel, R.G., 1968. Uranium, radium, and thorium content in phosphate rocks and their possible radiation hazard. J. Agric. Food Chem. 16, 231–234. https://doi.org/10.1021/jf60156a002

Merroun, M., Nedelkova, M., Rossberg, A., Hennig, C., Selenska-Pobell, S., 2006. Interaction mechanisms of bacterial strains isolated from extreme habitats with uranium. Radiochimica Acta 94, 723–729. https://doi.org/doi:10.1524/ract.2006.94.9-11.723

Merroun, M.L., Geipel, G., Nicolai, R., Heise, K.-H., 2003. Complexation of uranium (VI) by three eco-types of *Acidithiobacillus ferrooxidans* studied using time-resolved laser-induced fuorescence spectroscopy and infrared spectroscopy. BioMetals 16, 331–339.

Merroun, M.L., Raff, J., Rossberg, A., Hennig, C., Reich, T., Selenska-Pobell, S., 2005. Complexation of Uranium by Cells and S-Layer Sheets of *Bacillus sphaericus* JG-A12. Appl Environ Microbiol 71, 5532–5543. https://doi.org/10.1128/AEM.71.9.5532-5543.2005

Merroun, M.L., Selenska-Pobell, S., 2008. Bacterial interactions with uranium: An environmental perspective. Journal of Contaminant Hydrology 102, 285–295. https://doi.org/10.1016/j.jconhyd.2008.09.019

Millan, F., Izere, C., Breton, V., Voldoire, O., Biron, D.G., Wetzel, C.E., Miallier, D., Allain, E., Ector, L., Beauger, A., 2020. The effect of natural radioactivity on diatom communities in mineral springs. Botany Letters 167, 95–113. https://doi.org/10.1080/23818107.2019.1691051

Milligan, A.J., Morel, F.M.M., 2002. A Proton Buffering Role for Silica in Diatoms. Science 297, 1848–1850. https://doi.org/10.1126/science.1074958

Monteiro, C.M., Castro, P.M.L., Malcata, F.X., 2012. Metal uptake by microalgae: Underlying mechanisms and practical applications. Biotechnol Progress 28, 299–311. https://doi.org/10.1002/btpr.1504

Morelli, E., Scarano, G., 2001. Synthesis and stability of phytochelatins induced by cadmium and lead in the marine diatom *Phaeodactylum tricornutum*. Marine Environmental Research 52, 383–395. https://doi.org/10.1016/S0141-1136(01)00093-9

Müller, K., Foerstendorf, H., Steudtner, R., Tsushima, S., Kumke, M.U., Lefèvre, G., Rothe, J., Mason, H., Szabó, Z., Yang, P., Adam, C.K.R., André, R., Brennenstuhl, K., Chiorescu, I., Cho, H.M., Creff, G., Coppin, F., Dardenne, K., Den Auwer, C., Drobot, B., Eidner, S., Hess, N.J., Kaden, P., Kremleva, A., Kretzschmar, J., Krüger, S., Platts, J.A., Panak, P.J., Polly, R., Powell, B.A., Rabung, T., Redon, R., Reiller, P.E., Rösch, N., Rossberg, A., Scheinost, A.C., Schimmelpfennig, B., Schreckenbach, G., Skerencak-Frech, A., Sladkov, V., Solari, P.L., Wang, Z., Washton, N.M., Zhang, X., 2019. Interdisciplinary Round-Robin Test on Molecular Spectroscopy of the U(VI) Acetate System. ACS Omega 4, 8167–8177. https://doi.org/10.1021/acsomega.9b00164

Muturi, E.J., Donthu, R.K., Fields, C.J., Moise, I.K., Kim, C.-H., 2017. Effect of pesticides on microbial communities in container aquatic habitats. Sci Rep 7, 44565. https://doi.org/10.1038/srep44565

Nagel, K., Adelmeier, U., Voigt, J., 1996. Subcellular distribution of cadmium in the unicellular green alga *Chlamydomonas reinhardtii*. Journal of Plant Physiology 149, 86–90. https://doi.org/10.1016/S0176-1617(96)80178-7

Nakajima, A., Tsuruta, T., 2004. Competitive biosorption of thorium and uranium by *Micrococcus luteus*. Journal of Radioanalytical and Nuclear Chemistry 260, 13–18. https://doi.org/10.1023/B:JRNC.0000027055.16768.1e

Nassiri, Y., Mansot, J.L., Wéry, J., Ginsburger-Vogel, T., Amiard, J.C., 1997. Ultrastructural and Electron Energy Loss Spectroscopy Studies of Sequestration Mechanisms of Cd and Cu in the Marine Diatom *Skeletonema costatum*. Archives of Environmental Contamination and Toxicology 33, 147–155. https://doi.org/10.1007/s002449900236

Nathwani, J.S., Phillips, C.R., 1979. Adsorption of ^{226}Ra by soils (I). Chemosphere 8, 285–291. https://doi.org/10.1016/0045-6535(79)90111-5

Necchi Jr, O. (Ed.), 2016. River Algae. Springer International Publishing, Cham. https://doi.org/10.1007/978-3-319-31984-1

Nedelkova, M., Merroun, M.L., Rossberg, A., Hennig, C., Selenska-Pobell, S., 2007. Microbacterium isolates from the vicinity of a radioactive waste depository and their interactions with uranium: Isolates from the vicinity of a radioactive depository. FEMS Microbiology Ecology 59, 694–705. https://doi.org/10.1111/j.1574-6941.2006.00261.x

Nikaido, H., Saier, M.H., 1992. Transport Proteins in Bacteria: Common Themes in Their Design. Science 258, 936–942. https://doi.org/10.1126/science.1279804

Oliveira, R.C., Hammer, P., Guibal, E., Taulemesse, J.-M., Garcia, O., 2014. Characterization of metal–biomass interactions in the lanthanum(III) biosorption on *Sargassum* sp. using SEM/EDX, FTIR, and XPS: Preliminary studies. Chemical Engineering Journal 239, 381–391. https://doi.org/10.1016/j.cej.2013.11.042

Oremland, R.S., Steinberg, N.A., Maest, A.S., Miller, L.G., Hollibaugh, J.T., 1990. Measurement of in situ rates of selenate removal by dissimilatory bacterial reduction in sediments. Environ. Sci. Technol. 24, 1157–1164. https://doi.org/10.1021/es00078a001

Osuna-Cruz, C.M., Bilcke, G., Vancaester, E., De Decker, S., Bones, A.M., Winge, P., Poulsen, N., Bulankova, P., Verhelst, B., Audoor, S., Belisova, D., Pargana, A., Russo, M., Stock, F., Cirri, E., Brembu, T., Pohnert, G., Piganeau, G., Ferrante, M.I., Mock, T., Sterck, L., Sabbe, K., De Veylder, L., Vyverman, W., Vandepoele, K., 2020. The Seminavis robusta genome provides insights into the evolutionary adaptations of benthic diatoms. Nat Commun 11, 3320. https://doi.org/10.1038/s41467-020-17191-8

Panak, P., Raff, J., Selenska-Pobell, S., Geipel, G., Bernhard, G., Nitsche, H., 2000. Complex formation of U(VI) with *Bacillus*-isolates from a uranium mining waste pile. Radiochimica Acta 88, 71–76. https://doi.org/10.1524/ract.2000.88.2.071

Panak, P.J., Knopp, R., Booth, C.H., Nitsche, H., 2002. Spectroscopic studies on the interaction of U(VI) with *Bacillus sphaericus*. Radiochimica Acta 90, 779–783. https://doi.org/10.1524/ract.2002.90.9-11_2002.779

Pandey, L.K., Sharma, Y.C., Park, J., Choi, S., Lee, H., Lyu, J., Han, T., 2018. Evaluating features of periphytic diatom communities as biomonitoring tools in fresh, brackish and marine waters. Aquatic Toxicology 194, 67–77. https://doi.org/10.1016/j.aquatox.2017.11.003

Parr, J.F., Taffs, K.H., Lane, C.M., 2004. A microwave digestion technique for the extraction of fossil diatoms from coastal lake and swamp sediments. Journal of Paleolimnology 31, 383–390. https://doi.org/10.1023/B:JOPL.0000021857.32734.c6

Payne, R.B., Gentry, D.M., Rapp-Giles, B.J., Casalot, L., Wall, J.D., 2002. Uranium Reduction by *Desulfovibrio desulfuricans* Strain G20 and a Cytochrome c_3 Mutant. Appl Environ Microbiol 68, 3129–3132. https://doi.org/10.1128/AEM.68.6.3129-3132.2002

Perales-Vela, H.V., Peña-Castro, J.M., Cañizares-Villanueva, R.O., 2006. Heavy metal detoxification in eukaryotic microalgae. Chemosphere 64, 1–10. https://doi.org/10.1016/j.chemosphere.2005.11.024

Perpetuo, E.A., Souza, C.B., Nascimento, C.A.O., 2011. Engineering Bacteria for Bioremediation, Progress in Molecular and Environmental Bioengineering - From Analysis and Modeling to Technology Applications. InTech.

Perrein-Ettajani, H., Amiard, J.C., Haure, J., Renaud, C., 1999. Effets des métaux (Ag, Cd, Cu) sur la composition biochimique et compartimentation de ces métaux chez deux microalgues *Skeletonema costatum* et *Tetraselmis suecica*. Canadian Journal of Fisheries and Aquatic Sciences 56, 1757–1765. https://doi.org/10.1139/f99-102

Potapova, M., Hamilton, P.B., 2007. Morphological and ecological variation within *Achnathidium minutissimum* (Bacillariophyceae) species complex. Journal of Phycology 43, 561–575. https://doi.org/10.1111/j.1529-8817.2007.00332.x

Priyadarshanee, M., Das, S., 2021. Biosorption and removal of toxic heavy metals by metal tolerating bacteria for bioremediation of metal contamination: A comprehensive review. Journal of Environmental Chemical Engineering 9, 104686. https://doi.org/10.1016/j.jece.2020.104686

Pruesse, E., Quast, C., Knittel, K., Fuchs, B.M., Ludwig, W., Peplies, J., Glockner, F.O., 2007. SILVA: a comprehensive online resource for quality checked and aligned ribosomal RNA sequence data compatible with ARB. Nucleic Acids Research 35, 7188–7196. https://doi.org/10.1093/nar/gkm864

Rachkova, N.G., Shuktomova, I.I., Taskaev, A.I., 2010. The state of natural radionuclides of uranium, radium, and thorium in soils. Eurasian Soil Sc. 43, 651–658. https://doi.org/10.1134/S1064229310060050

Ragueneau, O., Schultes, S., Bidle, K., Claquin, P., Moriceau, B., 2006. Si and C interactions in the world ocean: Importance of ecological processes and implications for the role of diatoms in the biological pump. Global Biogeochem. Cycles 20, n/a-n/a. https://doi.org/10.1029/2006GB002688

Rajabi, F., Jessat, J., Garimella, J.N., Bok, F., Steudtner, R., Stumpf, T., Sachs, S., 2021.

Uranium(VI) toxicity in tobacco BY-2 cell suspension culture – A physiological study. Ecotoxicology and Environmental Safety 211, 111883. https://doi.org/10.1016/j.ecoenv.2020.111883

Rajagopal, M., Walker, S., 2015. Envelope Structures of Gram-Positive Bacteria, in: Bagnoli, F., Rappuoli, R. (Eds.), Protein and Sugar Export and Assembly in Gram-Positive Bacteria, Current Topics in Microbiology and Immunology. Springer International Publishing, Cham, pp. 1–44. https://doi.org/10.1007/82_2015_5021

Ran, Y., Wang, S., Zhao, Y., Li, J., Ran, X., Hao, Y., 2020. A review of biological effects and treatments of inhaled depleted uranium aerosol. Journal of Environmental Radioactivity 222, 106357. https://doi.org/10.1016/j.jenvrad.2020.106357

Rashid, M.I., Mujawar, L.H., Shahzad, T., Almeelbi, T., Ismail, I.M.I., Oves, M., 2016. Bacteria and fungi can contribute to nutrients bioavailability and aggregate formation in degraded soils. Microbiological Research 183, 26–41. https://doi.org/10.1016/j.micres.2015.11.007

Raven, J.A., 2010. Inorganic carbon acquisition by eukaryotic algae: four current questions. Photosynth Res 106, 123–134. https://doi.org/10.1007/s11120-010-9563-7

Reay, D.S., Nedwell, D.B., Priddle, J., Ellis-Evans, J.C., 1999. Temperature Dependence of Inorganic Nitrogen Uptake: Reduced Affinity for Nitrate at Suboptimal Temperatures in Both Algae and Bacteria. Appl Environ Microbiol 65, 2577–2584. https://doi.org/10.1128/AEM.65.6.2577-2584.1999

Regvar, M., Eichert, D., Kaulich, B., Gianoncelli, A., Pongrac, P., Vogel-Mikuš, K., 2013. Biochemical characterization of cell types within leaves of metal-hyperaccumulating *Noccaea praecox* (Brassicaceae). Plant Soil 373, 157–171. https://doi.org/10.1007/s11104-013-1768-z

Reimann, B.E.F., Lewin, J.C., Volcani, B.E., 1965. Studies on the Biochemistry and Fine Structure of Silica Shell Formation in Diatoms: I. The structure of the Cell Wall of *Cylindrotheca fusiformis*. The Journal of Cell Biology 24, 39–55. https://doi.org/10.1083/jcb.24.1.39

Renninger, N., Knopp, R., Nitsche, H., Clark, D.S., Keasling, J.D., 2004. Uranyl Precipitation by *Pseudomonas aeruginosa* via Controlled Polyphosphate Metabolism. Appl Environ Microbiol 70, 7404–7412. https://doi.org/10.1128/AEM.70.12.7404-7412.2004

Robertson, J., Gomersall, M., Gill, P., 1975. *Mycoplasma hominis*: Growth, Reproduction, and Isolation of Small Viable Cells. J Bacteriol 124, 1007–1018. https://doi.org/10.1128/jb.124.2.1007-1018.1975

Round, F.E., Crawford, R.M., Mann, D.G., 1990. Diatoms: biology and morphology of the genera. Cambridge university press.

Ruiz, F.A., Marchesini, N., Seufferheld, M., Govindjee, Docampo, R., 2001. The Polyphosphate Bodies of *Chlamydomonas reinhardtii* Possess a Proton-pumping Pyrophosphatase and Are Similar to Acidocalcisomes. Journal of Biological Chemistry 276, 46196–46203. https://doi.org/10.1074/jbc.M105268200

Sachs, S., Bernhard, G., 2011. Influence of humic acids on the actinide migration in the environment: suitable humic acid model substances and their application in studies with uranium—a review. J Radioanal Nucl Chem 290, 17–29. https://doi.org/10.1007/s10967-011-1084-0

Saito, T., Aoyagi, N., Kimura, T., 2015. Time-resolved laser-induced fluorescence spectroscopy combined with parallel factor analysis: a robust speciation technique for UO_2^{2+}. J Radioanal Nucl Chem 303, 1129–1132. https://doi.org/10.1007/s10967-014-3465-7

Sajih, M., Bryan, N.D., Livens, F.R., Vaughan, D.J., Descostes, M., Phrommavanh, V., Nos, J., Morris, K., 2014. Adsorption of radium and barium on goethite and ferrihydrite: A kinetic and surface complexation modelling study. Geochimica et Cosmochimica Acta 146, 150–163. https://doi.org/10.1016/j.gca.2014.10.008

Salomons, W., 1995. Environmental impact of metals derived from mining activities: Processes, predictions, prevention. Journal of Geochemical Exploration 52, 5–23. https://doi.org/10.1016/0375-6742(94)00039-E

Sánchez, C., Cristóbal, G., Bueno, G., 2019. Diatom identification including life cycle stages

through morphological and texture descriptors. PeerJ 7, e6770. https://doi.org/10.7717/peerj.6770

Sansom, B., Garner, R., 1966. The metabolism of radium in dairy cows. Biochemical Journal 99, 677–681. https://doi.org/10.1042/bj0990677

Sarthou, G., Timmermans, K.R., Blain, S., Tréguer, P., 2005. Growth physiology and fate of diatoms in the ocean: a review. Journal of Sea Research 53, 25–42. https://doi.org/10.1016/j.seares.2004.01.007

Sato, T., Murakami, T., Yanase, N., Isobe, H., Payne, T.E., Airey, P.L., 1997. Iron Nodules Scavenging Uranium from Groundwater. Environ. Sci. Technol. 31, 2854–2858. https://doi.org/10.1021/es970058m

Saxena, A., Tiwari, A., Kaushik, R., Iqbal, H.M.N., Parra-Saldívar, R., 2021. Diatoms recovery from wastewater: Overview from an ecological and economic perspective. Journal of Water Process Engineering 39, 101705. https://doi.org/10.1016/j.jwpe.2020.101705

Schleifer, K.H., 2009. Classification of Bacteria and Archaea: Past, present and future. Systematic and Applied Microbiology 32, 533–542. https://doi.org/10.1016/j.syapm.2009.09.002

Schmid, A.-M.M., Borowitzka, M.A., Volcani, B.E., 1981. Morphogenesis and Biochemistry of Diatom Cell Walls, in: Kiermayer, O. (Ed.), Cytomorphogenesis in Plants, Cell Biology Monographs. Springer Vienna, Vienna, pp. 63–97. https://doi.org/10.1007/978-3-7091-8602-2_3

Schnug, E., Lottermoser, B.G., 2013. Fertilizer-Derived Uranium and its Threat to Human Health. Environ. Sci. Technol. 47, 2433–2434. https://doi.org/10.1021/es4002357

Selenska-Pobell, S., Panak, P., Miteva, V., Boudakov, I., Bernhard, G., Nitsche, H., 1999. Selective accumulation of heavy metals by three indigenous *Bacillus* strains, *B. cereus*, *B. megaterium* and *B. sphaericus*, from drain waters of a uranium waste pile. FEMS Microbiology Ecology 29, 59–67. https://doi.org/10.1111/j.1574-6941.1999.tb00598.x

Seymour, J.R., Amin, S.A., Raina, J.-B., Stocker, R., 2017. Zooming in on the phycosphere: the ecological interface for phytoplankton–bacteria relationships. Nat Microbiol 2, 17065. https://doi.org/10.1038/nmicrobiol.2017.65

Shanab, S., Essa, A., Shalaby, E., 2012. Bioremoval capacity of three heavy metals by some microalgae species (Egyptian Isolates). Plant Signaling & Behavior 7, 392–399. https://doi.org/10.4161/psb.19173

Sharma, S.S., Dietz, K.-J., Mimura, T., 2016. Vacuolar compartmentalization as indispensable component of heavy metal detoxification in plants: Vacuolar functions in HM detoxification. Plant, Cell & Environment 39, 1112–1126. https://doi.org/10.1111/pce.12706

Shelobolina, E.S., Konishi, H., Xu, H., Roden, E.E., 2009. U(VI) Sequestration in Hydroxyapatite Produced by Microbial Glycerol 3-Phosphate Metabolism. Appl Environ Microbiol 75, 5773–5778. https://doi.org/10.1128/AEM.00628-09

Shelobolina, E.S., Sullivan, S.A., O'Neill, K.R., Nevin, K.P., Lovley, D.R., 2004. Isolation, Characterization, and U(VI)-Reducing Potential of a Facultatively Anaerobic, Acid-Resistant Bacterium from Low-pH, Nitrate- and U(VI)-Contaminated Subsurface Sediment and Description of *Salmonella subterranea* sp. nov. Appl Environ Microbiol 70, 2959–2965. https://doi.org/10.1128/AEM.70.5.2959-2965.2004

Shindo, D., Oikawa, T., 2002. Energy Dispersive X-ray Spectroscopy, in: Shindo, D., Oikawa, T. (Eds.), Analytical Electron Microscopy for Materials Science. Springer Japan, Tokyo, pp. 81–102. https://doi.org/10.1007/978-4-431-66988-3_4

Sirven, J.-B., Szenknect, S., Vors, E., Anzalone, E., Benarib, S., Sarr, P.-M., Reiller, P.E., Mesbah, A., Dacheux, N., Vercouter, T., Descostes, M., 2023. Time-resolved laser-induced fluorescence spectroscopy and chemometrics for fast identification of U(VI)-bearing minerals in a mining context. Spectrochimica Acta Part A: Molecular and Biomolecular Spectroscopy 296, 122671. https://doi.org/10.1016/j.saa.2023.122671

Sleytr, U.B., Bayley, H., Sára, M., Breitwieser, A., Küpcü, S., Mader, C., Weigert, S., Unger, F.M., Messner, P., Jahn-Schmid, B., Schuster, B., Pum, D., Douglas, K., Clark, N.A., Moore, J.T., Winningham, T.A., Levy, S., Frithsen, I., Pankovc, J., Beale, P., Gillis, H.P.,

Choutov, D.A., Martin, K.P., 1997. VI. Applications of S-layers. FEMS Microbiol Rev 20, 151–175. https://doi.org/10.1111/j.1574-6976.1997.tb00306.x

Sleytr, U.B., Schuster, B., Egelseer, E.-M., Pum, D., 2014. S-layers: principles and applications. FEMS Microbiol Rev 38, 823–864. https://doi.org/10.1111/1574-6976.12063

Smith, B.C., 2011. Fundamentals of Fourier Transform Infrared Spectroscopy, 2nd ed. CRC Press. https://doi.org/10.1201/b10777

Smith, H. (Ed.), 1995. Age-dependent doses to members of the public from intake of radionuclides. 4: Inhalation dose coefficients, Annals of the ICRP. Pergamon Press, Oxford.

Smith, W.L., Gadd, G.M., 2000. Reduction and precipitation of chromate by mixed culture sulphate-reducing bacterial biofilms. J Appl Microbiol 88, 983–991. https://doi.org/10.1046/j.1365-2672.2000.01066.x

Soldo, D., Hari, R., Sigg, L., Behra, R., 2005. Tolerance of *Oocystis nephrocytioides* to copper: intracellular distribution and extracellular complexation of copper. Aquatic Toxicology 71, 307–317. https://doi.org/10.1016/j.aquatox.2004.11.011

Sousa, T., Chung, A.-P., Pereira, A., Piedade, A.P., Morais, P.V., 2013. Aerobic uranium immobilization by *Rhodanobacter* A2-61 through formation of intracellular uranium–phosphate complexes. Metallomics 5, 390. https://doi.org/10.1039/c3mt00052d

Spencer, H., Osis, D., Fisenne, I.M., Perry, P.M., Harley, N.H., 1990. Measured Intake and Excretion Patterns of Naturally Occurring 234 U, 238 U, and Calcium in Humans. Radiation Research 124, 90. https://doi.org/10.2307/3577700

Sprynskyy, M., Kovalchuk, I., Buszewski, B., 2010. The separation of uranium ions by natural and modified diatomite from aqueous solution. Journal of Hazardous Materials 181, 700–707. https://doi.org/10.1016/j.jhazmat.2010.05.069

Sprynskyy, M., Kowalkowski, T., Tutu, H., Cukrowska, E.M., Buszewski, B., 2015. Ionic liquid modified diatomite as a new effective adsorbent for uranium ions removal from aqueous solution. Colloids and Surfaces A: Physicochemical and Engineering Aspects 465, 159–167. https://doi.org/10.1016/j.colsurfa.2014.10.042

Suresh Kumar, K., Dahms, H.-U., Won, E.-J., Lee, J.-S., Shin, K.-H., 2015. Microalgae – A promising tool for heavy metal remediation. Ecotoxicology and Environmental Safety 113, 329–352. https://doi.org/10.1016/j.ecoenv.2014.12.019

Sutcliffe, B., Chariton, A.A., Harford, A.J., Hose, G.C., Greenfield, P., Elbourne, L.D.H., Oytam, Y., Stephenson, S., Midgley, D.J., Paulsen, I.T., 2017. Effects of uranium concentration on microbial community structure and functional potential. Environmental Microbiology 19, 3323–3341. https://doi.org/10.1111/1462-2920.13839

Suzuki, Y., Kelly, S.D., Kemner, K.M., Banfield, J.F., 2005. Direct Microbial Reduction and Subsequent Preservation of Uranium in Natural Near-Surface Sediment. Appl Environ Microbiol 71, 1790–1797. https://doi.org/10.1128/AEM.71.4.1790-1797.2005

Suzuki, Y., Kelly, S.D., Kemner, K.M., Banfield, J.F., 2003. Microbial Populations Stimulated for Hexavalent Uranium Reduction in Uranium Mine Sediment. Appl Environ Microbiol 69, 1337–1346. https://doi.org/10.1128/AEM.69.3.1337-1346.2003

Swift, D.M., Wheeler, A.P., 1992. Evidence of an organic matrix from diatom biosilica. J Phycol 28, 202–209. https://doi.org/10.1111/j.0022-3646.1992.00202.x

Tang, Y.Z., Koch, F., Gobler, C.J., 2010. Most harmful algal bloom species are vitamin B_1 and B_{12} auxotrophs. Proc. Natl. Acad. Sci. U.S.A. 107, 20756–20761. https://doi.org/10.1073/pnas.1009566107

Taylor, D., Bligh, P., Duggan, M., 1962. The absorption of calcium, strontium, barium and radium from the gastrointestinal tract of the rat. Biochemical Journal 83, 25–29. https://doi.org/10.1042/bj0830025

Terrill, JG.Jr., Ingraham, S.C.II., Il, Moeller, DW., 1954. Radium in the Healing Arts and in Industry: Radiation Exposure in the United States. Public Health Rep (1896) 69, 255–262. https://doi.org/doi:10.2307/4588736

Thamatrakoln, K., Hildebrand, M., 2008. Silicon Uptake in Diatoms Revisited: A Model for Saturable and Nonsaturable Uptake Kinetics and the Role of Silicon Transporters. Plant

Physiol. 146, 1397–1407. https://doi.org/10.1104/pp.107.107094

Thingstad, T., Skjoldal, E., Bohne, R., 1993. Phosphorus cycling and algal-bacterial competition in Sandsfjord, western Norway. Mar. Ecol. Prog. Ser. 99, 239–259. https://doi.org/10.3354/meps099239

Tréguer, P., Bowler, C., Moriceau, B., Dutkiewicz, S., Gehlen, M., Aumont, O., Bittner, L., Dugdale, R., Finkel, Z., Iudicone, D., Jahn, O., Guidi, L., Lasbleiz, M., Leblanc, K., Levy, M., Pondaven, P., 2018. Influence of diatom diversity on the ocean biological carbon pump. Nature Geosci 11, 27–37. https://doi.org/10.1038/s41561-017-0028-x

Ullah, A., Heng, S., Munis, M.F.H., Fahad, S., Yang, X., 2015. Phytoremediation of heavy metals assisted by plant growth promoting (PGP) bacteria: A review. Environmental and Experimental Botany 117, 28–40. https://doi.org/10.1016/j.envexpbot.2015.05.001

Vandenhove, H., Van Hees, M., 2007. Predicting radium availability and uptake from soil properties. Chemosphere 69, 664–674. https://doi.org/10.1016/j.chemosphere.2007.02.054

Vernon-Parry, K.D., 2000. Scanning electron microscopy: an introduction. III-Vs Review 13, 40–44. https://doi.org/10.1016/S0961-1290(00)80006-X

Vidoudez, C., Pohnert, G., 2012. Comparative metabolomics of the diatom *Skeletonema marinoi* in different growth phases. Metabolomics 8, 654–669. https://doi.org/10.1007/s11306-011-0356-6

Vidoudez, C., Pohnert, G., 2008. Growth phase-specific release of polyunsaturated aldehydes by the diatom *Skeletonema marinoi*. Journal of Plankton Research 30, 1305–1313. https://doi.org/10.1093/plankt/fbn085

Virta, L., Gammal, J., Järnström, M., Bernard, G., Soininen, J., Norkko, J., Norkko, A., 2019. The diversity of benthic diatoms affects ecosystem productivity in heterogeneous coastal environments. Ecology 100. https://doi.org/10.1002/ecy.2765

Volland, S., Bayer, E., Baumgartner, V., Andosch, A., Lütz, C., Sima, E., Lütz-Meindl, U., 2014. Rescue of heavy metal effects on cell physiology of the algal model system *Micrasterias* by divalent ions. Journal of Plant Physiology 171, 154–163. https://doi.org/10.1016/j.jplph.2013.10.002

Vollmer, W., Blanot, D., De Pedro, M.A., 2008. Peptidoglycan structure and architecture. FEMS Microbiol Rev 32, 149–167. https://doi.org/10.1111/j.1574-6976.2007.00094.x

Walters, W., Hyde, E.R., Berg-Lyons, D., Ackermann, G., Humphrey, G., Parada, A., Gilbert, J.A., Jansson, J.K., Caporaso, J.G., Fuhrman, J.A., Apprill, A., Knight, R., 2016. Improved Bacterial 16S rRNA Gene (V4 and V4-5) and Fungal Internal Transcribed Spacer Marker Gene Primers for Microbial Community Surveys. mSystems 1, e00009-15. https://doi.org/10.1128/mSystems.00009-15

Wang, W.-X., Dei, R.C.H., 2006. Metal stoichiometry in predicting Cd and Cu toxicity to a freshwater green alga *Chlamydomonas reinhardtii*. Environmental Pollution 142, 303–312. https://doi.org/10.1016/j.envpol.2005.10.005

Wei, X., Fang, L., Cai, P., Huang, Q., Chen, H., Liang, W., Rong, X., 2011. Influence of extracellular polymeric substances (EPS) on Cd adsorption by bacteria. Environmental Pollution 159, 1369–1374. https://doi.org/10.1016/j.envpol.2011.01.006

Williams, D.B., Carter, C.B., 1996. The Transmission Electron Microscope, in: Williams, D.B., Carter, C.B. (Eds.), Transmission Electron Microscopy: A Textbook for Materials Science. Springer US, Boston, MA, pp. 3–17. https://doi.org/10.1007/978-1-4757-2519-3_1

Williams, D.M., 2020. Diatom Classifications: What Purpose Do They Serve?, in: Cristóbal, G., Blanco, S., Bueno, G. (Eds.), Modern Trends in Diatom Identification. Springer International Publishing, Cham, pp. 11–24. https://doi.org/10.1007/978-3-030-39212-3_2

Williams, D.M., Kociolek, J.P., 2011. An Overview of Diatom Classification with Some Prospects for the Future, in: Seckbach, J., Kociolek, P. (Eds.), The Diatom World, Cellular Origin, Life in Extreme Habitats and Astrobiology. Springer Netherlands, Dordrecht, pp. 47–91. https://doi.org/10.1007/978-94-007-1327-7_3

Wilschefski, S., Baxter, M., 2019. Inductively Coupled Plasma Mass Spectrometry:

Introduction to Analytical Aspects. CBR 40, 115–133. https://doi.org/10.33176/AACB-19-00024

Winey, M., Meehl, J.B., O'Toole, E.T., Giddings, T.H., 2014. Conventional transmission electron microscopy. MBoC 25, 319–323. https://doi.org/10.1091/mbc.e12-12-0863

Wong, D.M., Nguyen, T.T.N., Franz, A.K., 2014. Ethylenediaminetetraacetic acid (EDTA) enhances intracellular lipid staining with Nile red in microalgae *Tetraselmis suecica*. Algal Research 5, 158–163. https://doi.org/10.1016/j.algal.2014.08.002

Woolfolk, C.A., Whiteley, H.R., 1962. Reduction of inorganic compounds with molecular hydrogen by *Micrococcus lactilyticus*. I. Stoichiometry with compounds of arsenic, selenium, tellurium, transition and other elements. J. BACTERIOL. 84.

Wu, Q., Sanford, R.A., Löffler, F.E., 2006. Uranium(VI) Reduction by *Anaeromyxobacter dehalogenans* Strain 2CP-C. Appl Environ Microbiol 72, 3608–3614. https://doi.org/10.1128/AEM.72.5.3608-3614.2006

Yee, N., Fein, J.B., 2003. Quantifying Metal Adsorption onto Bacteria Mixtures: A Test and Application of the Surface Complexation Model. Geomicrobiology Journal 20, 43–60. https://doi.org/10.1080/01490450303887

Yin, H., Niu, J., Ren, Y., Cong, J., Zhang, Xiaoxia, Fan, F., Xiao, Y., Zhang, Xian, Deng, J., Xie, M., He, Z., Zhou, J., Liang, Y., Liu, X., 2015. An integrated insight into the response of sedimentary microbial communities to heavy metal contamination. Sci Rep 5, 14266. https://doi.org/10.1038/srep14266

Yool, A., Tyrrell, T., 2003. Role of diatoms in regulating the ocean's silicon cycle. Global Biogeochem. Cycles 17, n/a-n/a. https://doi.org/10.1029/2002GB002018

Zaghloul, A., Saber, M., Gadow, S., Awad, F., 2020. Biological indicators for pollution detection in terrestrial and aquatic ecosystems. Bull Natl Res Cent 44, 127. https://doi.org/10.1186/s42269-020-00385-x

Zakeri, F., Noghabi, K.A., Sadeghizadeh, M., Kardan, M.R., Masoomi, F., Farshidpour, M.R., Atarilar, A., 2010. *Serratia* sp. ZF03: An efficient radium biosorbent isolated from hot-spring waters in high background radiation areas. Bioresource Technology 101, 9163–9170. https://doi.org/10.1016/j.biortech.2010.07.032

Zakeri, F., Sadeghizadeh, M., Kardan, M.R., Shahbani Zahiri, H., Ahmadian, G., Masoumi, F., Sharafi, H., Rigi, G., Vali, H., Akbari Noghabi, K., 2012. Differential proteome analysis of a selected bacterial strain isolated from a high background radiation area in response to radium stress. Journal of Proteomics 75, 4820–4832. https://doi.org/10.1016/j.jprot.2012.05.020

Zechmeister, Harald G., Grodzińska, K., Szarek-Łukaszewska, G., 2003. Chapter 10 Bryophytes, in: Markert, B.A., Breure, A.M., Zechmeister, H.G. (Eds.), Trace Metals and Other Contaminants in the Environment. Elsevier, pp. 329–375. https://doi.org/10.1016/S0927-5215(03)80140-6

Zimmermann, J., Jahn, R., Gemeinholzer, B., 2011. Barcoding diatoms: evaluation of the V4 subregion on the 18S rRNA gene, including new primers and protocols. Org Divers Evol 11, 173–192. https://doi.org/10.1007/s13127-011-0050-6

Annex

Annex 1: Verification of the diatom taxonomy and the culture purity

Table A1-1: PCR setup and thermal cycle for V4 region of 18S rRNA genes.

PCR setup	Volume (µL)
Total DNA (0.9 ng/µL)	2.5
Forward primer 1 µmol/L	5
Reverse primer 1 µmol/L	5
2x KAPA HiFi HotStart ReadyMix (Roche)	12.5
Thermal cycle	
Temperature (°C)	Time
95	5 min.
30 cycles of	
95	30 sec.
55	30 sec.
72	30 sec.
72	5 min.

To verify the resulting PCR amplicons via electrophoresis, 1% of agarose gel (Biozym LE Agarose) was prepared in 1× TAE (Tris base-Acetic acid-EDTA) buffer. The detailed composition of the TAE buffer is provided in **Table A1-2**.

Table A1-2: Composition of the 10× TAE buffer.

10× TAE buffer solution (pH 8.2)	For 1 L
TRIS base (Carl Roth)	48.4 g
EDTA disodium salt dihydrate (Merck)	3.7 g
Acetic Acid 99.9% (Carl Roth)	11.6 mL

5 µL of the Midori Green Advanced DNA stain (Nippon Genetics Europe GmbH) were added per 100 mL of the agarose solution. Once the gel solidified in the mold, an aliquot of 3 µL of the PCR amplicon was mixed with 2 µL of the 1× loading buffer (composition is listed in **Table A1-3**) and pipetted into the well on the gel.

Table A1-3: Composition of the 3× loading buffer.

3× Loading buffer	For 100 mL
4mol/L Urea (Carl Roth)	24.024 g
Sucrose (Carl Roth)	50 g
50mmol/L Na_2-EDTA (Merck)	1.861 g
Bromphenol Blue sodium salt (Merck)	0.250 g
Xylencyanol FF (Merck)	0.250 g

GenRuler 1kb Plus DNA Ladder (Thermo Scientific, as ruler reference), positive control (*E. Coli* K12) and negative control (Milli-Q water) were also prepared in the same way. The electrophoresis was performed under a voltage of 100 V for 80 minutes. To evaluate the gel, UVP Gel Solo (Analytikjena) was used.

Annex 2: Medium used for the *Achnanthidium saprophilum* diatoms cultivation

The composition of the DM medium that was used for the cultivation of the diatoms is proposed by CCAP (accessible at https://www.ccap.ac.uk/wp-content/uploads/MR_DM.pdf) and is listed in **Table A2**.

Table A2: Composition of the DM medium

	Stock solution	Per 200 mL	
1	$Ca(NO_3)_2 \cdot 4H_2O$	4.00 g	> 99%, ACS reagent Sigma Aldrich
2	KH_2PO_4	2.48 g	≥ 99.0%, ACS reagent, Sigma Aldrich
3	$MgSO_4 \cdot 7H_2O$	5.00 g	> 99%, Thermo Fisher
4	$NaHCO_3$	3.18 g	> 99%, Sigma Aldrich
5	FeNaEDTA	0.45 g	Alfa Aesar
	Na_2EDTA	0.45 g	99.0-101.0%, Normapure, ACS reagent, VWR
6	H_3BO_3	0.496 g	> 99.5%, Thermo Scientific
	$MnCl_2 \cdot 4H_2O$	0.278 g	≥ 99%, ReagentPlus, Sigma Aldrich
	$(NH_4)_6Mo_7O_{24} \cdot 4H_2O$	0.20 g	> 99%, PanReac AppliChem
7	Cyanocobalamin	0.008 g	Vitamin B12, 96.0 - 102.0 %, PanReac AppliChem
	Thiamine HCl	0.008 g	≥ 99%, Reagent grade, Sigma Aldrich
	Biotin	0.008 g	D-(+)-Biotin, > 98%, Alfa Aesar
8	$Na_2SiO_3 \cdot 9H_2O$	11.4 g	$Na_2SiO_3 \cdot 5H_2O$, technical grade, Fisher Chemical
Reference: QF 09 Media Preparation Recipe Template, CCAP (Culture Collection of Algae and Protozoa), reviewed on 06th January 2023, accessible online (www.ccap.ac.uk)			

To prepare the DM medium, take 1 mL of the stock solution 1-8 mentioned in **Table A2** and make up to 1 L with deionized water. The pH of the prepared medium was adjusted to 6.9 and autoclaved at 120 °C for 15 minutes.

Annex 3: Bacterial strains isolation and taxonomy identification

The composition of the LB medium that was used during the bacterial strains isolation and cultivation is presented in **Table A3-1**.

Table A3-1: Composition of full lysogeny broth (LB) medium

Full LB medium	For 1 L
Bacto Yeast Extract (BD Biosciences)	5 g
Bacto Trytone (Gibco, Thermal Fisher Scientific)	10 g
NaCl (Carl Roth)	10 g

To identify the taxonomy of the isolated bacterial strains, the 16S rRNA genes of the bacteria were amplified via PCR and sequenced. Information concerning the PCR setup and the thermal cycles is provided in **Table A3-2**.

Table A3-2: PCR setup and thermal cycle for 16S rRNA genes.

PCR setup	Volume (µL)
DNA	5
Forward 7f primer 10 µmol/L (Eurofins Genomics)	2
Reserve 1513r primer 10 µmol/L (Eurofins Genomics)	2
$MgCl_2$ 25 mmol/L (Promega)	5
5X Colorless GoTaq® Flexi Buffer (Promega)	10
GoTaq® G2 Flexi DNA Polymerase (5u/µL) (Promega)	0.5
dNTPs 12.5 mmol/L (Thermo Scientific)	0.5
Milli-Q water (LiChrosolv®, LC-MS grade, Merck)	25
Thermal cycle	
Temperature (°C)	Time
95	3 min.
5 cycles of	
95	1.5 min.
59	40 sec.
72	1.5 min.
25 cycles of	
94	1 min.
55	40 sec.
72	1.5 min.
72	20 min.

Annex 4: Experimental conditions applied for the preparation of U-loaded diatoms and bacteria for various microscopic and spectroscopic investigations.

Table A4: Experimental conditions applied during the preparation of the U-loaded diatoms and bacterial isolates prior to the SEM, (S)TEM, FTIR and TRLFS measurements. Preparations were conducted at room temperature.

Experiment		Type of sample	Medium	pH	U exposure time	U(VI) exposure concentration (µmol/L)	Growth phase of the cells
SEM measurement		Diatoms	2 mmol/L NaCl + 3 mmol/L HEPES	7.0	45 minutes	500	Exponential growth phase
(S)TEM measurement		Diatoms	2 mmol/L NaCl + 3 mmol/L HEPES	7.0	45 minutes	10	Exponential growth phase
FTIR measurement	Standard analysis	Diatoms	2 mmol/L NaCl + 3 mmol/L HEPES	7.0	45 minutes	10	Exponential growth phase
	Flow-through experiment	I. Diatoms II. Frustules	0.1 mol/L NaCl		Adsorption process: 0~200 minutes Flushing process: 0~50 minutes	10	
TRLFS measurement		Diatoms	I. 2 mmol/L $NaNO_3$ + 3 mmol/L HEPES II. DM medium	I. 7.0 II. 7.3	I. 45 minutes II. 4, 11, 35 days	I. 0.8-20 II. 1	I. Exponential growth phase II. Exponential growth phase, late-exponential growth phase and stationary growth phase
		Bacterial isolates	2 mmol/L $NaNO_3$ + 3 mmol/L HEPES	7.0	45 minutes	2	Not specified

Annex 5: Diatom cell viability and activity test

The diatom cell viability and activity test was performed using the flow cytometry. Experiment was performed by collaborators from LMGE. The experimental data presented in **Figure A-1** are also credited to LMGE.

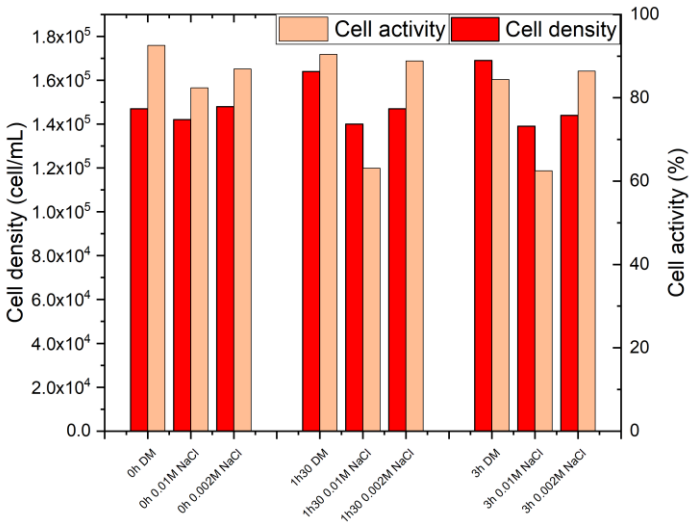

Figure A-1: The variation of the diatom cell viability and activity with increasing exposure time in the DM medium, 10 mmol/L of NaCl solution and 2 mmol/L of NaCl solution. The NaCl solution is buffered with 3 mmol/L of HEPES at pH 7.0.

As shown in the figure, the variation of the diatom cell density (represented by the red bars) in the three studied media during the test can be considered as insignificant in fact. Note that only viable cells were detected using the applied method. As a result, data suggested that the diatom cells remained viable within the time scale of the experiment (three hours). Besides, as represented by the orange bars, the cell activity in the 10 mmol/L of NaCl medium displayed an obvious decrease compared to that in the original DM medium, while the cell activity in the 2 mmol/L of NaCl medium stayed at comparable level as in the DM medium throughout the entire experiment.

This test shows that the solution consisting of 2 mmol/L of NaCl (buffered by 3 mmol/L of HEPES) has no negative impact on the diatom cells (within three hours) and thus can be used for the batch-type U/Ra bio-association experiments in this work. However, experiment should be limited within three hours.

COLLEGE DOCTORAL PAYS DE LA LOIRE
ED MATIERE,MOLECULES MATERIAUX ET GEOSCIENCES

IMT Atlantique
Bretagne-Pays de la Loire
École Mines-Télécom

Titre : Interaction des radioéléments (Ra, U) avec les diatomées

Mots clés : *Achnanthidium saprophilum*, uranium, radium, adsorption, accumulation, spéciation

Résumé : Les diatomées sont des microalgues unicellulaires omniprésentes sur Terre et utilisées comme bioindicateurs pour évaluer l'impact de contaminations sur les écosystèmes aquatiques. Elles font également l'objet d'une attention croissante en tant que matériel de décontamination de métaux lourds d'effluents contaminés ou à des fins de biorestauration in situ. Cependant, les interactions entre les diatomées et les radioéléments, notamment l'uranium (U) et le radium (Ra), restent peu documentées. Ce travail vise à étudier tant au niveau macroscopique que moléculaire, les interactions de U et du Ra avec une culture xénique de diatomées *Achnanthidium saprophilum*, dans laquelle une communauté bactérienne est naturellement associée de manière symbiotique. Des expériences de bio-association de U et du Ra sont faites en présence de diatomées afin d'évaluer les fractions en U/Ra adsorbées et incorporées. En parallèle, diverses techniques de microscopie et de spectroscopie sont appliquées pour étudier la localisation et la spéciation de U au niveau cellulaire. Les résultats démontrent une bio-association significative de U et du Ra avec les diatomées et soulignent le rôle important des groupes carboxyliques et phosphates dans l'interaction U-diatomées. Les deux mécanismes d'adsorption et d'incorporation ont pu être mis en évidence pour U et Ra, la répartition entre les fractions adsorbées et incorporées dépendant de la phase de croissance des diatomées et du temps de contact entre les micro-algues est les radioéléments. Ce travail met également en évidence la contribution significative des bactéries symbiotiquement associées aux diatomées aux interactions globales.

Title : Interaction of radioelements (Ra, U) with diatoms

Keywords : *Achnanthidium saprophilum*, uranium, radium, surface adsorption, intracellular accumulation, speciation

Abstract : Diatoms are ubiquitous unicellular microalgae that are commonly used as bioindicators to evaluate the impact of contaminations on the ecological health of aquatic ecosystems. In recent decades, diatoms have received increasing attention as a decontamination material for removing heavy metals from contaminated effluents or for in situ bioremediation purposes. However, the interactions between diatoms and radioelements, e.g., uranium (U) and radium (Ra), remain relatively unclear and poorly documented. Therefore, this work aims to study, at both the macroscopic and molecular level, the interaction of U and Ra with a xenic *Achnanthidium saprophilum* diatom culture in which a naturally occurring bacterial community is symbiotically associated to diatoms. Batch-type U and Ra bio-association experiments are performed to evaluate the adsorbed and incorporated fractions of U/Ra in the diatom culture. Besides, various microscopic and spectroscopic techniques are applied to investigate the localization and speciation of U at the cellular level. Results demonstrate the significant bio-association of U and Ra with the diatoms and highlight the important role of carboxylic and phosphate groups in the U-diatoms interaction. Both adsorption and incorporation are observed for U and Ra in the diatom culture, with their distribution depending on the diatom growth phase and on the contact time. This work contributes to a better understanding of the interaction of U and Ra with the xenic diatom culture and also highlights the contribution of the bacteria symbiotically associated with the diatoms to the overall interactions.